FLOW VISUALIZATION AND DYNAMICS OF HEAT EXCHANGER TUBE ARRAYS IN WATER CROSS-FLOW

by

AHMED ALI ABD-RABBO, B.Sc., M.A.Sc.

A Thesis
Submitted to the School of Graduate Studies
in Partial Fulfilment of the Requirements
for the Degree
Doctor of Philosophy

McMaster University

FLOW VISUALIZATION AND DYNAMICS OF HEAT EXCHANGER TUBE ARRAYS IN WATER CROSS-FLOW

by

AHMED ALI ABD-RABBO, B.Sc., M.A.Sc.

A Thesis
Submitted to the School of Graduate Studies
in Partial Fulfilment of the Requirements
for the Degree
Doctor of Philosophy

McMaster University

FLOW VISUALIZATION AND DYNAMICS OF HEAT EXCHANGER TUBE ARRAYS

IN THE NAME OF GOD

THE COMPASSIONATE

THE MERCIFUL

DOCTOR OF PHILOSOPHY (1984)
(Mechanical Engineering)

McMASTER UNIVERSITY
Hamilton, Ontario

TITLE: Flow Visualization and Dynamics of Heat Exchanger Tube Arrays in Water Cross-Flow

AUTHOR: Ahmed Ali Abd-Rabbo, B.Sc. (Ain-Shams University)

M.A.Sc. (University of Toronto)

SUPERVISOR: Dr. D. S. Weaver

NUMBER OF PAGES: (xviii), 284

ABSTRACT

A flow visualization technique has been developed to investigate the flow developments in tube arrays over a wide range of Reynolds numbers. The technique is non-obtrusive and permits observations deep inside a tube bundle where the flow is unaffected by free surface or boundary effects. The technique has been used to examine flow behaviour in a rigidly and flexibly mounted square in-line and rotated square arrays in a water cross-flow. The important case of a single flexible tube in an otherwise rigid bundle, which received considerable attention in the literature, has also been examined. Results pertinent to vortex shedding, turbulence and fluidelastic instability are given which include response curves and frequency spectra together with flow visualization films and photographs.

The results indicate that discrete alternate and symmetric vortex shedding can occur within the confinement of a tube bundle. Increased turbulence, as more rows are traversed by the flow, has a detrimental effect on the discrete vortex structures. Vorticity shedding and turbulence coexist as separate phenomena however, vorticity shedding is identified as the mechanism responsible for the observed resonance peaks in the response curves. Vortex shedding and the associated flow induced response in the square array is different from that

in the staggered rotated square array. Fluidelastic instability is associated with marked increase in the transverse response amplitude and significant flow redistribution although it appears random in a full flexible bundle. Finally, a single flexible tube in an otherwise rigid bundle will become unstable at essentially the same flow velocity as that when the surrounding tubes are free to move. The response is predominantly in a transverse direction with significant flow redistribution. The motion of the redistributed flow lags behind the tube motion.

ACKNOWLEDGEMENTS

The author wishes to thank and express his sincere gratitude to his supervisor, Dr. D. S. Weaver, for his kind advice and assistance throughout the course of this work, and whose teachings extend far beyond the scope of this thesis.

I would like also to express my gratefulness and deep appreciation to my wife Suzanne, my parents and my family for the inexhaustive support, encouragement and affections which are valued most of all.

Appreciation is extended to the departmental technicians, Mr. Frank Drieman and Mr. Dave Schick for their kind help and assistance. The careful and efficient typing of this manuscript by Ms. B. A. Bedell-Ryc is also gratefully acknowledged.

TABLE OF CONTENTS

LIST OF FIGURES

Page

LIST OF TABLES

NOMENCLATURE

A	Projected area of a tube
C_D	Drag coefficient
C_L	Alternating lift coefficient
C_m	Added mass coefficient
ΔC_p	Pressure drop coefficient
d	Tube diameter
d_p	Tracer particle diameter
f, f_s	Frequency of vortex shedding
f_a	Natural frequency in air
f_{ac}	Natural frequency of a standing wave
f_c	Calculated frequency of vortex shedding
f_{fp}	Frequency of flow periodicity
f_n	Natural frequency of a tube
f_w	Natural frequency of a tube in water
f_D	Drag force
F_L	Lift force
g	The gravitational acceleration
h	Width of a vortex street
h'	The distance between two neighbouring streets
K	Constant
ℓ	Length scale of turbulence
ℓ_1	Tube length
ℓ_2	Longitudinal spacing of vortices in a vortex column
L	Longitudinal tube spacing
m	Mass per unit length of a tube

n	Integer
n_1, n_2	Refractive indecies of Plexiglass and Water
P	Tube pitch
q	Turbulent velocity component in root mean square
R_p	Tracer particle's Reynolds Number
Re	Reynolds number
S	Strouhal number
t	Time
T	Lateral tube spacing
u_f, u_p	Fluid and tracer particle velocities
U	Mean gas velocity through a boiler
U_1	Mean gas velocity between adjacent tubes
U_R	Translation velocity of a vortex $= \frac{\Gamma}{2\ell_2}\left(\tanh\frac{\pi h}{\ell_2} - \tanh\frac{\pi h'}{\ell_2}\right)$
V	Free stream flow velocity
V_{cr}	Critical or threshold velocity
V_g	Velocity in the minimum gap between adjacent tubes
V_s	The sink velocity
V_T	Velocity in the gap between two tubes in the same row
V_u	Upstream flow velocity
x_ℓ	Longitudinal spacing ration $= \frac{L}{d}$
x_t	Transverse spacing ratio $= \frac{T}{d}$
β	Constant = 1.4 for an isolated cylinder
γ_t, γ_w	Specific gravities of tube and water
Γ	Intensity of a vortex

δ	Logarithmic decrement of damping
ε	Constant = 0.43 - 0.50 for an isolated cylinder
μ_f	Dynamic viscosity of the fluid
ν	Buffeting frequency
ρ, ρ_f	Density of the fluid
ρ_p	Density of the tracer particle
ϕ	Constant = $\frac{f}{U_R}$

CHAPTER 1

INTRODUCTION

Arrays of cylindrical structures exposed to external flow are common in conventional and nuclear industries. The cylindrical arrays can be found in heat exchangers such as steam generators, condensors and moderator coolers in the form of banks of tubes. In most nuclear reactors they can also be found in the form of clusters of fuel rods. In modern tube and shell heat exchangers, tubes are subjected to high flow velocities to satisfy heat transfer criteria associated with higher thermal efficiencies. Closely spaced tubes tend to be designed with smaller diameters either to achieve higher heat transfer rates or to minimize heavy water inventory as in the case of the CANDU nuclear steam generators. Utilization of modern high strength materials aggravates the problem by reducing tube stiffness. The decreased structural rigidity and higher flow rates have led inevitably to increased incidence of flow induced vibrations.

The ensuing long term and short term damages are due to fretting and fatigue failures at the tube supports, and mid-span leaks due to tube-to-tube clashing. Nelms and Segaser [1], Hartlen [2] and Shin and Wambsganss [3] reported field experiences where excessive vibrations have caused tube failures. The high cost of repairs and the lost revenue due

plant shut downs are quite impressive. Dueck [4] reported that in 1979 heat exchanger problems alone contributed 4.9% of the nuclear generating stations incapability factor while the value for all causes was 20.6%. Minor and major repairs in the nuclear industry have to be done in a hostile environment and may involve handling of radioactive materials. Tube failures can lead to pollution problems due to mixing of shell-side lake water and the expensive tube-side heavy water. Such high costs, lost revenue, and health hazards render tube failures unacceptable.

A number of conferences and symposia have been held [5-13] to discuss and expose flow induced vibration problems in the different fields where they were encountered. This resulted in better feedback from the field and helped to narrow the communication gap that existed between designers and researchers. This also helped advance the state of the art as an increasing number of researchers became involved and devoted their efforts to investigate these problems.

A number of reviews [14-20] have been published to clarify the state of knowledge and to identify important areas for future research. Paidoussis in his review [18] presented a compendium of 50 practical cases of flow induced vibration problems in heat exchangers and nuclear reactors. Such a compendium reflects the great technical, financial, and safety dimensions of flow induced vibration problems.

A relatively clear picture is emerging from the

voluminous published technical literature written on the subject. It is widely accepted that cross flow induced vibrations in tube banks are attributed to the following four basic mechanisms:

a - vortex shedding

b - turbulent buffeting

c - fluidelastic instability

d - acoustic resonance

Acoustic resonance as an excitation mechanism was the subject of many investigations [21-25] aimed at understanding its nature and finding ways to minimize its annoying and destructive effects. One of two situations may arise in the conduit containing the tube array. If the natural frequency of a standing wave in the cavity, f_a, coincides with the frequency of the flow periodicity, f_{fp}, acoustic resonance may occur and the resulting sound amplification may lead to high noise levels. If, however, $f_a = f_{fp} = f_n$, where f_n is a natural frequency of the tube array, the whole structure may be destroyed in a short period of time [19]. Acoustic resonance is associated mainly with gas flows and is not likely to occur in water flows where the values of f_{fp} and f_n are expected to be much lower than f_a. Thus, this mechanism will not be considered here any further.

Turbulent buffeting results from random pressure fluctuations in the turbulent flow inside a tube bundle. The response of a tube in the interior of the bundle is that

of a randomly forced oscillation, it is generally small and falls within acceptable amplitude limits. Nevertheless, long term damage may occur as a result of the relative motion between the tubes and tube supports. Owen [26] postulated that tube response amplitudes may exceed acceptable limits if it happens that the turbulent energy is concentrated at frequencies near the tube natural frequencies. Owen rejected Grotz and Arnold's approach to explain the buffeting problem [27] and stated that turbulent fluctuations give rise to a behaviour associated with a randomly forced, damped vibration in which the tube structure acts as a mechanical filter and selects for its response preponderantly that part of the force spectrum neighbouring on a natural frequency, hence a peak displacement appears at such a gas speed that the dominant frequency in the force spectrum coincides with a natural structural frequency.

The origin of flow periodicity inside a tube bundle is accepted by Chen [21] to be due to Karman vortex streets. The analysis advanced by Chen of the flow periodicity was based on certain important assumptions one of which is the existence of acoustic resonance. Chen later [28, 29] advanced the opinion that Karman vortex shedding is confined to tube banks of moderate to large tube spacing ratios. In tube banks of small tube spacings jet excitation mechanisms will be the excitation sources. Possible ways for vortex street formation and jet excitation mechanisms inside tube

bundles were then sketched by Chen in support of his arguments. These sketches however, remain unsubstantiated by experiments.

Paidoussis [18, 92] demonstrated that for a certain array pattern's layout and angle, a close agreement can be found between the vortex shedding Strouhal numbers of Chen and the dominant buffeting frequency Strouhal numbers of Owen. Paidoussis concluded that the models advanced by Chen and Owen represent two divergent schools of thought discussing the same phenomenon, but is inclined to lean towards Owen's model since Owen's work is based on sound physical reasoning. Furthermore, Paidoussis stated that Vortex shedding is difficult to visualize in closely spaced tube arrays where there is obviously insufficient room for the shear layers to roll up in the classical manner. Yet Paidoussis has still his doubts about the true mechanism underlying periodicity in the flow within the cylinder arrays.

The character of flow periodicity is even more complex than indicated above. Research to date has established that flow periodicity does not always arise nor it does necessarily occur throughout the tube bundle if it does arise [18, 92]. Resonance can be established under certain conditions and is related to the dimensionless parameters

$$\frac{V}{f_n d} \quad \text{and} \quad \frac{m\delta}{\rho d^2}$$

Grover and Weaver [30] reported discrete vortex shedding in

the first 15 rows of a parallel triangular array in cross flow of air at Reynolds numbers less than 1200. Further complications arise when water flows are considered. In water flows the added mass and fluid coupling effects are very important and cannot be neglected as in the case of gas flows. Experimental evidence suggests that vortex shedding resonance in water flows may be significant. Pettigrew et al. [31] reported that no significant wake shedding resonance has been observed for tubes deep inside a tube bundle in water and resonance is more likely in the first and second tube rows. Nevertheless, Pettigrew et al. [31] and Pettigrew and Gorman [32] repeatedly stated that what happens in closely packed bundles of tubes is not well understood. To add to the complexity of the problem, tentative generalizations such as "small", "moderate", "large" tube spacing ratios, "deep" inside a tube bundle, "the first few rows", and "the interior of a tube bundle" to mention a few were used by different researchers without being quantitatively specified. To make matters even worse, researchers have used different methods to determine the Strouhal numbers they reported. A great deal of scatter exists in the reported data and confusion reigns regarding the nature of the excitation mechanism.

The nature of the fluidelastic instability is not fully understood either. Connors' theory [33] for tube rows was based on a presupposed relative tube motion reported

by Livesey and Dye [34] and confirmed by Zdravkovich et al. [35]. Blevins [36, 37] using stability criteria, extended Connors' theory to tube arrays. His theory predicted that detuning the tubes stabilises the array. The experimental investigations of Weaver and Lever [38], Weaver and Groner [39], Weaver and Koroyannakis [40], Zdravkovich [41] and Gorman [42] have demonstrated that a relative motion at the same frequency between a given tube and its neighbors, is not necessary for instability. A flexible tube in a rigid array can become unstable at essentially the same flow velocity if the rigid tubes were replaced by flexibly mounted ones [40]. Chen [43] introduced a theory based on the same mode of relative motion between a tube and its two closest neighbors as Connors did. However, Chen used a vortex model of symmetrical vortex pair trains behind the tubes vibrating in the streamwise direction and the Karman vortex streets behind the tubes vibrating in the transverse direction. The coupling between the two groups of vortex systems excites tube arrays to perform this fluidelastic vibration. The variation in the separation point's position leads to jet switch which maintains the fluidelastic vibrations.

Recently Connors [44] remarked that a number of vibrational patterns have been observed experimentally for the tubes of square arrays experiencing fluidelastic excitation. The patterns range from orbital whirling motions, to ones in which all the tubes vibrate primarily in the transverse

direction or primarily in the streamwise direction. Tanaka and Takahara [45, 46] are of the view that many kinds of unsteady fluid dynamic forces and vibration modes, in addition to those adopted by Connors [33] and Blevins [36, 37] exist. Vibrations of the type that cannot be explained by Connors' equation [33] may be caused by the component of unsteady fluid dynamic forces and vibration modes of cylinders that were not taken into account in deriving Connors' equation.

Zdravkovich and Namork [47] divide the mechanisms involved into excitation and amplification mechanisms. Buffeting, not vortex shedding in their opinion, excites tube banks to vibrate with low amplitude. The fluidelastic displacement, jet-switch, wake-switch and other related phenomena can amplify, build-up and maintain large amplitude vibration. Therefore, pressure fluctuations around stationary tubes excite vibration and time averaged force on variously displaced tubes amplifies and maintains large amplitude vibration.

The fluidelastic stability behaviour of tube arrays in gas flows is relatively well defined. However, critical flow velocities for fluidelastic instability of tube arrays in heavy fluids are difficult to determine with certainty. The lack of a consistent definition for the threshold velocities and the possible coincidence of vortex shedding resonant peaks in the response amplitude curves with the stability thresholds are two reasons for the difficulty encountered with the accurate determination of the critical

velocity. A third reason is the irregular amplitude response behaviour in the post stable region due to closely spaced band of fluid coupled natural tube frequencies.

In view of this discussion it is clear that the state of knowledge of excitation mechanisms of tube arrays in cross-flow is far from satisfactory. Flow development with increasing flow velocity inside tube banks is virtually unknown and detailed investigations of this type cannot be found in the technical literature. Beyond the observation that some periodicity exists in the flow, as indicated by fluid velocity, pressure, and tube response spectra, information about the flow structure is very sketchy and cannot be asserted with any degree of certainty. Although some researchers, notably Zdravkovich and Namork [48, 49], have tried to gain some insight into the structure of the interstitial flow, the information obtained is very limited.

The purpose of the present investigation is two-fold.

i) to develop an experimental technique capable of investigating flow development in a tube array over a wide range of Reynolds numbers. The technique should be non-obtrusive and permit observations deep inside a tube bundle where the flow is unaffected by free surface or boundary effects.

ii) to use this experimental technique to improve our understanding of flow development in tube arrays in cross-flow. In particular, it is intended to examine

the nature of the excitation mechanisms associated with the so-called vortex shedding and fluidelastic vibrations.

Experiments were conducted on identical rigid and flexible arrays so that the effect of tube motion could be studied. In addition, results were obtained for two different array geometries of practical interest in order to provide some indication of the degree of generality of the phenomena observed. Simultaneously with detailed flow observations, tube response data were obtained so that they could be related directly with the fluid excitation phenomena.

The plan of this thesis can be summarized briefly as follows. In Chapter 2, an overview of the relevant research conducted in the area of flow induced vibrations is given which outlines the positions taken by the major contributors to the present state of knowledge. In Chapter 3, the experimental facility, the instrumentation used and, the experimental procedure followed are described. Chapter 4 provides a background on the available flow visualization techniques and outlines the development of the flow visualization method and procedure used in the present investigation. Chapters 5 and 6 deal with the experimental results obtained in investigating a square in-line and a rotated square arrays respectively. The results are discussed and compared with the pertinent results found in the technical literature. The conclusions arrived at and the contributions of the

present study to the state of knowledge as well as recommendations for future investigations are included in Chapter 7.

CHAPTER 2

FLOW INDUCED VIBRATIONS

2.1 Brief Review

2.1.1 Historical Background

Aeroelasticity is a discipline which owes it development and maturity to over half a century of experience and studies in design of modern airplane components and structures. It denotes the phenomena involving mutual interaction among aerodynamic, inertial and elastic forces. Collar [50] developed his aeroelastic triangle to give an overview of the field. Numerous texts and papers have been written on the subject see for example, [51-53]. Heller and Abramson [54] coined by analogy to aeroelasticity the term "hydroelasticity" to denote the phenomena involving mutual interaction between hydrodynamic, inertial, and elastic forces. In recognition of the similarities and differences between the old and the new developing discipline, the authors drew upon aeroelasticity to define the scope and limitation of hydroelasticity lest experience in the former be used in the latter without regard for validity. The differences between aero and hydroelasticity and their implications were later outlined and discussed by Heller [55]. Abramson [56] stated that were it not for three major differences, virtually all that is known of aeroelasticity would be applicable in hydro-

elastic problems. The three major differences are,

1 - the existence of a liquid free surface

2 - cavitation

3 - the relative masses of the dynamic structure and the immediately surrounding fluid.

Toebes [57] is of the view that it is preferable to designate both fields by the term "fluidelasticity" thus permitting coherence of thought in the examination of the analytical and physical characteristics of flow induced vibrations. The main classification in fluidelasticity does not derive from fluid properties, rather, it should be based on the shape of the structure in question.

2.1.2 Classification of Flow Induced Vibration

Weaver [58, 59] classified flow induced vibrations into forced, self-controlled and self-excited vibrations. Forced vibrations are induced by turbulence in the flow and the fluid forces are not appreciably affected by the resulting small amplitude random motion of the structure. These are, mathematically, equilibrium problems for which the steady state response configurations are to be determined. In this class of problems, some response is unavoidable and the emphasis is on trying to minimize this response by increasing damping and/or stiffness. Examples of forced vibration problems are the response of tall buildings to atmospheric boundary layer turbulence and the response of an aircraft to gusty winds.

Self-controlled vibrations are excited if the periodicity in the flow coincides with one of the natural frequencies of the structure. The amplitude of vibration builds up to the point where the magnitude and frequency of fluid forces are controlled by the motion of the structure and a feedback mechanism develops. Increasing stiffness or damping may prevent such oscillations as well as some geometry change which destroys periodicity in the flow. A good example of self-controlled type of vibration is the oscillation of a cylindrical structure in a fluid flow. The periodicity in the flow is provided by alternate vortex shedding resulting from rolling up of the unstable shear layers into discrete vortices. The fixed body Strouhal number

$$S = \frac{f_s d}{V}$$

defines the linear relationship between the frequency of vortex shedding, f_s, and the free stream flow velocity, V. If f_s does not coincide with the natural frequency of the structure, f_n, the ensuing response is generally very small.

Self-excited vibrations develop when the oscillations of the structure result in periodic forces which amplify the structure's motion. The distinguishing feature of this class of problems from the previous one is that the periodic forces disappear in the absence of structural motion. Self-excied vibrations are, mathematically, stability or eigenvalue

problems in which critical values of certain parameters are to be determined in addition to the corresponding steady state configurations. The most effective remedy for these problems is often a change in the geometry of the structure since increasing stiffness or damping may be detrimental.

Self-controlled and self-excited vibrations are referred to as fluidelastic vibrations where a mutual interaction of inertial and elastic forces of the structure with the fluid forces is an essential feature. A necessary condition for such a designation is that the structural motion alter or modify the fluid forces acting on the structure. Fluidelastic problems are associated with the transfer of energy from the fluid to the structure. Weaver [58] stated that this energy transfer is the result of nonconservative hydrodynamic forces which manifest themselves in the form of non-self adjoint operators in the differential equations of motion. It follows that this special class of mathematical problems must be solved using the appropriate methods, whose mathematics continue to be developed [60, 61] and that the solutions exhibit unique behavioral characteristics. In particular, such equations admit complex eigenvalues, or in physical terms, oscillatory types of instability. In addition, the eigenvectors or unstable mode shapes are generally not the normal modes of free vibration but coupled modes which do not satisfy the usual orthogonality conditions. Thus regardless of the specific mechanism involved, hydroelastic problems form a class which is distinct from free

vibration, dynamic response and conservative stability problems.

2.1.3 Theoretical and Experimental Considerations

The formulation of the equation of motion pertaining to a fluidelastic problem requires certain simplifying assumptions to be made. The adequacy of such assumptions depend on how well and to what degree the mechanisms of excitation are perceived and understood. The formulation of the equation of motion involves the determination of the inertial, the structural and the fluid-dynamic operators of the system. For small structural motions in the elastic range, the linearity of the inertial and the structural operators is usually assured. The major difficulty of the fluidelastic problem centers around the fluid-dynamic operators because of their nonlinear and possibly stochastic nature. The difficulty is influenced to a degree by the structural characteristics of which the geometric shape is the most important. For streamlined bodies at a small angle of attack, flow separation does not occur and the potential flow theory can be used to determine the flow field. Linearization of the nonlinear fluid-dynamic operators is then feasible. With bluff bodies in the flow field, flow separation cannot be avoided and nonlinearities related to the free shear layer characteristics have to be accounted for. The potential flow theory cannot be used to analyze unsteady separated flows and the determina-

tion of the fluid-dynamic operators rely heavily on experimental information. This places greater demands on the theories of boundary layers, turbulence, wake mechanics and cavitation in obtaining and interpreting such information. Indeed, fluidelastic phenomena seldom yield to analytical methods and the only option available is to use experimental methods for their solution. The needed experimental information is usually in the form of amplitude-frequency spectra of oscillations; intensity-scale spectra of turbulence, noise spectra, vortex shedding frequencies, stability thresholds, velocity profiles, pressure distributions, fluid-dynamic coefficients, etc. Flow visualization is a very rapidly developing and promising experimental tool which renders certain properties of the fluid-structure system directly accessible to visual perception thereby yielding a great deal of valuable information. Experiments are usually conducted in wind and water-tunnels, water-loops, and two-phase flow loops to study the stability and response of a wide variety of models.

Preliminary analysis of complex phenomena is made possible by dimensional analysis which yields a system of non-dimensional parameters that are of great help in setting up and minimizing the number of experiments required. Experiments are conducted on models constructed according to similarity principles in order to obtain information that can be used to predict accurately the performance of a physical

system (prototype) in the desired respect. Modelling the dynamic interaction between a flexible structure and a fluid is not an easy task in view of the complexities and difficulties involved. Baker et al. [62] state that the modelling problems of the flow induced vibrations of heat exchangers and nuclear reactors are particularly complicated and have to this day defied complete analysis and accurate modelling. In their words, the model laws that arise in fluid-structure interactions impose stringent scaling requirements. To obtain a feasible model it is usually necessary to allow several of the dimensionless parameters to be distorted. This can only be done with confidence when the physics of the problem is well understood. The modeller must know, for example what kind of prototype responses are really important and what kinds can be neglected, for otherwise modelling may be impossible.

2.2 Flow Past An Isolated Circular Cylinder

2.2.1 Flow Regimes

The wake development behind an isolated rigid circular cylinder exposed to a uniform cross flow received the attention of many researchers in the past. Marris [63] presented a synopsis of the somewhat scattered information to correlate the results of the theoretical and experimental work done into a picture of the state of knowledge on the problem. Shin and Wambsganss [3], based on the work of Marris, summarized

the major regimes of the wake development, an account of which is given here as they appear in figure 2.1.

In the Reynolds number range Re<5, a regime of unseparated flow develops where the flow streamlines close behind the cylinder, figure 2.1a. As the Reynolds number is increased the streamlines widen and a pair of Foppl vortices are formed behind the cylinder at a Reynolds number of approximately 5-15. The mechanism by which such vortices are formed is not clear. A plausible explanation may be that with increasing Reynolds number the convection of vorticity overcomes its diffusion and more vorticity is carried round to the rear of the cylinder. The accumulated vorticity induces a backward flow near the surface which counters the forward moving fluid and deflects it away from the rear of the cylinder. This in turn tends to strengthen the rotational motion in the standing vortices [64]. In the range 5-15<Re<40, the vortices elongate in the streamwise direction and remain separated from the main body of the fluid by the vortex layers which are continuations of the laminar boundary layer of the cylinder after its separation, figure 2.1b. The layers join together again below the vortex pair to form a line wake. Kovasznay [65] and Tritton [66] showed that the line wake behind the vortex pair becomes unstable at Re>40. Tritton's opinion is that the wake instability gives rise to a periodic motion rather than turbulence and his investigation indicates that the vortex street resulting from this instability has a

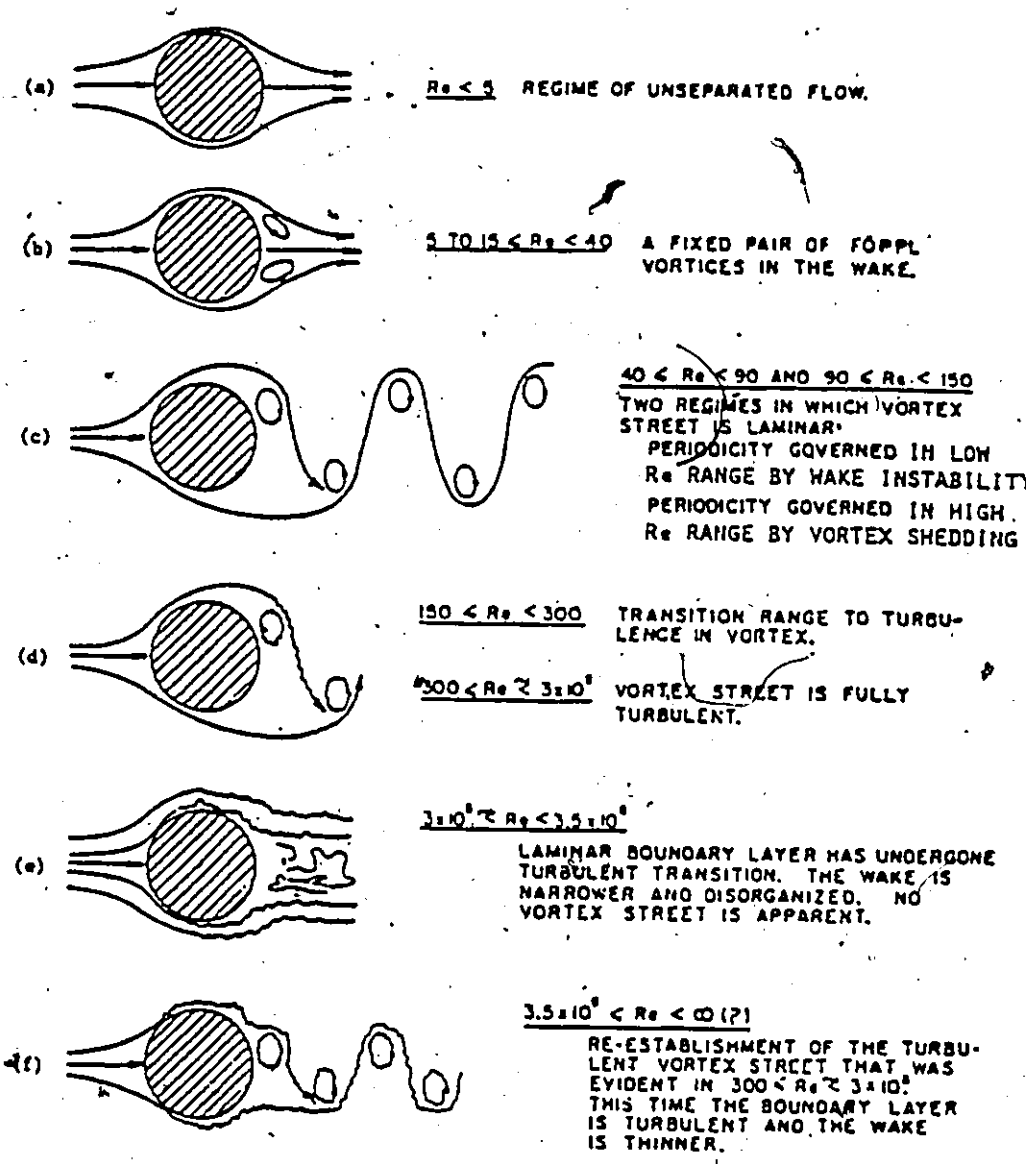

Figure 2.1 Regimes of fluid flow across a circular cylinder (from ref. 3)

different longitudinal spacing from the vortex street generated due to vortex shedding. The instability appears at some distance downstream from the cylinder and gives rise to slow oscillation of the wake, nearly sinusoidal in both time and streamwise distance with an amplitude which increases with the distance downstream. As the Reynolds number increases, the oscillations of the wake moves closer to the cylinder and the two standing vortices oscillate together in lateral position. At a Reynolds number of about 90, one of the Foppl vortices breaks away from the cylinder which causes a wake-pressure asymmetry and then the other leaves. The process repeats itself and a state of alternating vortex shedding is established. In the Reynolds number range $90<Re<150$, Roshko's observations [67] indicate that the free vortex layers roll up into viscous vortices and the fluid in these vortices is laminar figure 2.1c. In the range $150<Re<300$ a laminar-to-turbulent transition begins in the shear layers prior to their rolling up into vortices. The position of the transition point depends on the free stream turbulence. The formed vortices consist of turbulent fluid and soon diffuse as they move downstream. In the range $300<Re<3x10^5$ the vortices are fully turbulent, figure 2.1d. In the Reynolds number range $3x10^5<Re<3.5x10^6$, the laminar boundary layer on the cylinder undergoes turbulent transition, the wake is narrower and disorganized and no vortex street is apparent in the wake, figure 2.1e. Beyond the Reynolds number of $3.5x10^6$ the

the turbulent vortex street is reestablished and the wake becomes thinner as figure 2.5f shows.

2.2.2 Drag and Lift Forces

Because the eddies in the wake of a cylinder cannot convert their kinetic energy of rotation into an increased pressure, as the ideal fluid theory would dictate, the pressure within the wake remains close to that at the separation point. Since this is always less than the pressure at the front stagnation point, there results a net pressure difference tending to move the body with the flow. The resulting steady force is called pressure or form drag and it is the resultant of the forces normal to the surface. The skin friction is the resultant of the forces tangential to the surface and depends on the surface roughness. The total or the profile drag is the sum of the form drag and the skin friction. The total drag is expressed in terms of a dimensionless drag coefficient C_D defined as

$$C_D = \text{Total drag force}/\tfrac{1}{2}\rho V^2 A$$

Being a ratio of two forces, the drag coefficient is the same for two dynamically similar flows; it is independent of the size of the body but not of its shape, and it is a function of Reynolds number. The skin friction component is negligible in comparison with the form drag for Reynolds numbers exceeding about 100. In the Reynolds number range $100<Re<3.5\times10^5$, the drag coefficient has an approximately constant value of 1.2.

As transition to turbulence takes place in the boundary layer and the wake narrows, the drag coefficient reaches a minimum of $C_D \approx 0.3$. At very high Reynolds numbers exceeding $Re \approx 10^6$ the drag coefficient increases and reaches a value of $C_D \approx 0.55$ at $Re \approx 10^7$. The transition Reynolds number depends on cylinder roughness and ambient turbulence.

Periodic forces are generated as the vortices are alternately shed from each side of the cylinder [68]. The oscillating pressure field gives rise to unsteady lift and drag forces in the transverse and streamwise directions on the cylinder due to the changing circulation and wake asymmetries as each vortex is shed. The results of Bishop and Hassan [69] showed that the frequency of the unsteady lift force, F_L, is given by the vortex shedding frequency, f_s, and the frequency of the unsteady drag force, F_D, is twice that of the vortex shedding frequency. Furthermore, the unsteady lift force is approximately one order of magnitude greater than the unsteady drag force. Surry's results [70] showed that the unsteady drag force is reduced and the unsteady lift force is increased with increasing turbulence level. The unsteady lift force, F_L, associated with alternate vortex shedding from a stationary cylinder is expressed as

$$F_L = C_L \frac{1}{2}\rho V^2 d\ell_1 \sin(2\pi f_s t)$$

where C_L is the alternating lift coefficient

$\frac{1}{2}\rho V^2$ is the dynamic pressure

ℓ_1 is the cylinder length

t is the time

Bishop and Hassan [69] reviewed and plotted the experimentally determined data on the drag coefficients over a wide range of Reynolds numbers. Chen [71] compiled the available data on the mean oscillatory lift coefficients in the range $10^4 < Re < 10^6$. The scatter in the data is large and the values vary from 0.1 to 1.5. Despite the fact that vortex shedding occurs at a discrete frequency, the alternating force acting on the cylinder is randomly modulated. Keefe [72] showed that the flow over a circular cylinder is three-dimensional rather than two-dimensional even at Reynolds number of about 300. This means that at a given instant the local forces along the cylinder span may or may not be acting in phase. The lift coefficient is therefore determined as an RMS value using a suitable frequency measuring device.

For a rigid circular cylinder a linear relationship exists between the frequency of vortex shedding and the flow velocity. Such a relationship is expressed as

$$S = \frac{f_s d}{V}$$

where S is the Strouhal number as was discussed in section 2.1.2. The Strouhal number varies with the Reynolds number, however, in the Reynolds number range $300 < Re < 2x10^5$ the Strouhal number has a constant value of approximately 0.2. In the

transition range, $Re>3.5x10^5$ no clear Strouhal number is found as a spectrum of frequencies is seen in the wake. With the reestablishment of the vortex street for $Re>3.5x10^6$, the Strouhal number is about 0.3. Chen [71] reviewed and plotted the data of several researchers and Lienhard [73] proposed a reasonable envelope within $\pm$ 5% accuracy over a wide range of Reynolds numbers.

2.2.3 Effect of Cylinder Motion

If the frequency of vortex shedding coincides with the natural frequency of the cylinder, a self-controlled type of vibration can develop as was outlined in section 2.1.2. The developing large amplitudes are attributed to

1 - the reduction of the vortex formation region length [74, 75].
2 - an increase in the correlation length [76, 77].
3 - an increased period of vortex shedding [78] which is associated with an increased circulation in the vortices.

Vortex induced oscillations, the correlating parameters involved, the reduced velocity ranges of their occurrence, the associated Strouhal numbers and some related research in this area [80-84] were thoroughly reviewed by King [79]. Methods of alleviation of vortex induced motion were discussed in detail by Walshe and Wootton [85] as applied to prevent wind induced oscillations. Several mathematical models have been proposed for estimating the amplitude of resonant vortex

induced vibrations of circular cylinders [69, 86-91, 93]. Paidoussis in his review [92] showed that the models [86, 89, 90, 93] give similar answers and correctly predict the self-limiting vortex induced vibrations at large amplitudes.

2.2.4 Closing Remarks

The extensive literature on the different parameters involved in vortex induced oscillations of isolated circular cylinders cannot adequately be covered in the span of one chapter. Not reviewed here for example are the harmonic and subharmonic resonances which were observed as well as streamwise oscillations at twice the vortex shedding frequency. Important work has been done on the effect of confinement, end conditions, aspect ratios, mass ratios, upstream turbulence, surface roughness, and phase composition of the fluid. Paidoussis [92] stated that such parameters constitute a complex multi-dimensional space affecting vortex shedding excited vibrations both quantitatively and qualitatively. Vibrations induced by turbulent buffeting were the subject of some important investigations notably by Savkar and So [94, 95] which yielded some interesting results. The recent review of Paidoussis [92] cover those works in some detail and provides a list of references on the subjects.

Many studies have also been undertaken to investigate the dynamical behaviour, the flow pattern and the interference effects of two cylinders positioned at various distances

apart and arranged in tandem, side-by-side or in stagger [96-98]. Savkar [14] and recently Zdravkovich [99] gave excellent reviews of the work done in this area. In this chapter, attention will be focussed on tube arrays of many cylinders arranged in recognizable geometric patterns. Of particular interest are those works devoted to study the interstitial flow structure in the interior of such arrays probing the origin of flow periodicity and contributing to understanding its nature.

2.3 Flow Periodicty in Tube Banks

2.3.1 Early Studies of Flow Periodicity

The early studies attributed the periodicity in the flow to vortex shedding. In 1959, Putnam [100] stated that with increasing emphasis on more compact heat exchangers and higher flow velocities, the problems associated with vortex shedding can be expected to become more common and more acute. Putnam [100, 101] outlined the lock-in phenomenon as it occurs between the vortex shedding frequency and the natural frequency of heat exchanger tubes. The emphasis was then placed on determining Strouhal numbers for various array pitches and patterns to help designers avoid resonance under operating conditions. Buffeting excitation of tubes was recognized to give rise to vibrations of very small amplitudes and hence less destructive than vibrations produced by vortex shedding resonance. This was the case until 1964 when Owen published

his work on buffeting excitation of boiler tube vibration [26].

2.3.2 Models of Owen and Chen

The problem Owen studied [26] is the origin of the vibration, generated within an extensive bank of tubes that run transverse to the direction of gas flow through a boiler shell, whose movement is small enough in amplitude to have no perceptible effect on the motion of the gas. To develop his model which applies equally to staggered and in-line arrangements Owen assumed that

1 - the tubes are rigidly placed.

2 - the Reynolds number is high enough for the large scale components of the flow to be free from the influence of viscosity.

3 - the transverse spacing $\frac{T}{d}$ is appreciably greater than unity so that in its effect locally on the gas flow a tube preserves some of the features peculiar to a cylinder in isolation, but not so large that these features predominate.

4 - there is a periodic replenishment of turbulent energy, the spatial periodicity being L.

5 - turbulent energy is nearly homogeneous with respect to the direction of the mean flow and has a vigorous energy content.

The first assumption is a pivotal one which implies that

tube motion is nonexistent or if it exists, it is very small that it has no organizing effect on the flow. The conditions within a box of gas lying between two rows of tubes having unit breadth perpendicular to the flow and the tube axis with a width T and length L were then considered. Owen stated that turbulent energy is increased at each row of tubes, between rows it suffers dissipation by viscosity. After a sufficient number of rows has been traversed by the gas, energy equilibrium exists where the turbulent energy generated is balanced by that dissipated by viscosity. It follows from the assumption of energy equilibrium that

$$\Delta C_p \frac{1}{2}\rho U^3 T = 3\rho q^3 L T / 2 \ell . \qquad (2.1)$$

The left hand side term in this relation expresses the approximate rate at which turbulent energy is convected and the right hand side term expresses the rate at which turbulence suffers decay in the box.

where

ΔC_p	Pressure drop coefficient
U	Mean gas velocity through the boiler
ρ	Gas density
q	Turbulent velocity component in root mean square
L	Distance between successive tube rows
ℓ	Length scale of the turbulence

Owen, based on the suggestion of Wieghardt [102], expressed

ΔC_p as

$$\Delta C_p = C_D \frac{d}{T} (1 - \frac{d}{T})^2 \tag{2.2}$$

where

C_D	Drag coefficient for a tube
T	Lateral tube spacing
d	Tube diameter

and used the substitutions

$$U_1 = U (1 - \frac{d}{T})^{-1}, \quad \nu = U/\ell \tag{2.3}$$

where

U_1	Mean gas velocity between adjacent tubes,

into equations (2.1) and (2.2) to arrive at

$$\frac{\nu L}{U_1} \frac{T}{d} = \frac{1}{3} C_D (\frac{U_1}{q})^3 (1 - \frac{d}{T})^2 \tag{2.4}$$

Owen then drew the attention to the slender numerical foundation on which his equation (2.4) rests and showed that any predicted numerical value for the quantity $\frac{1}{3} C_D (\frac{U_1}{q})^3$ on the right hand side of equation (2.4) is of doubtful significance. Therefore equation (2.4) was rewritten as

$$\frac{\nu L}{U_1} \frac{T}{d} = K (1 - \frac{d}{T})^2 \tag{2.5}$$

where the constant K is to be determined from available experimental results. The data of Grotz and Arnold [27], although known to be marred by possible measurement errors up to 30% and recorded under conditions of acoustic resonance, were considered by Owen. Hill and Armstrong's data [103] for a staggered arrangement of three rows with a fixed spacing between the first two rows and a variable spacing between the second and third rows were also considered by Owen despite the fact that these data may not be representative of full arrays and recorded under conditions of acoustic resonance. Owen stated that consistent with the buffeting explanation, incident turbulent eddies impose forces on the tubes which provide a fluctuating momentum flux equivalent in its effect to an acoustic dipole. When the frequency ν of the acoustic dipole radiation due to the fluctuating forces on the tubes happen to coincide with a natural acoustic frequency of the duct, resonance is established. The pattern of gas flow then is likely to be affected and the model that he has described ceases to be valid. But it should still serve to predict the approach to resonance and in particular the gas speed at which it occurs. The production of such acoustic waves by such forces does not require any movement on the part of the tube. The dominant frequency of the turbulent fluctuations, identifiable with the dominant frequency of the fluctuating forces on the tubes is proportional to the average gas speed through the bank. However, faced with the dilemma that the

results of Hill and Armstrong [103] would hardly be expected to fall within the scope of his theory yet they do, Owen attributed that to coincidence. Finally some results of his own, one of which he depicted in his figure 5, reproduced here in figure 2.2 were considered in search for an experimentally determined value of K. The equation

$$\frac{\nu L}{U_1}\frac{T}{d} = 3.05\ (1 - (\frac{d}{T}))^2 + 0.28 \qquad (2.6)$$

was then developed where K = 3.05.

The particular result given in Owen's figure 2.2 indicates that the value of

$$(\frac{\nu L}{U_1})\ (\frac{T}{d})$$

at which the peak in the normalized spectral density is equal to 0.4. The figure was given to illustrate that the size of the energetic turbulent eddies in the direction of the mean motion is comparable with the longitudinal tube spacing L. Hence for an array with $\frac{T}{d} = 1.5$ and $\frac{L}{d} = 1.3$

$$(\frac{\nu L}{U_1})\ (\frac{T}{d}) = 0.4$$

substituting $\nu = \frac{U}{\ell}$ in the above relation we get

$$\frac{U}{U_1}\frac{L}{\ell}\frac{T}{d} = 0.4, \text{ or}$$

$$\ell = \frac{U}{U_1}\frac{L}{0.4}\frac{T}{d}$$

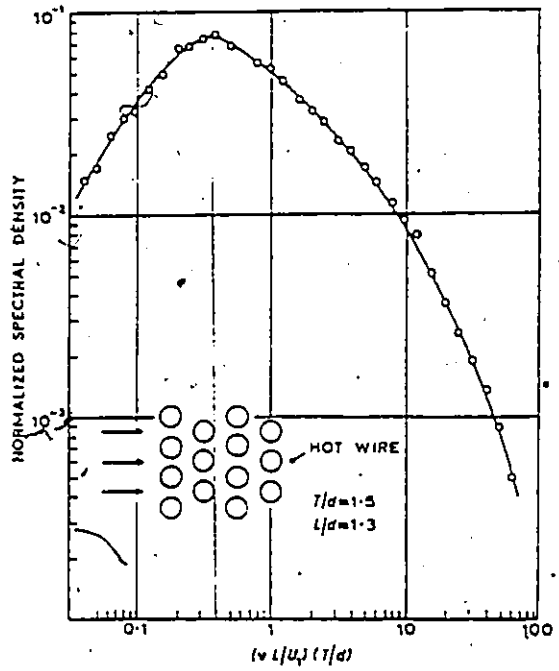

Figure 2.2 A typical one-dimensional turbulent energy spectrum found experimentally (from ref. 26)

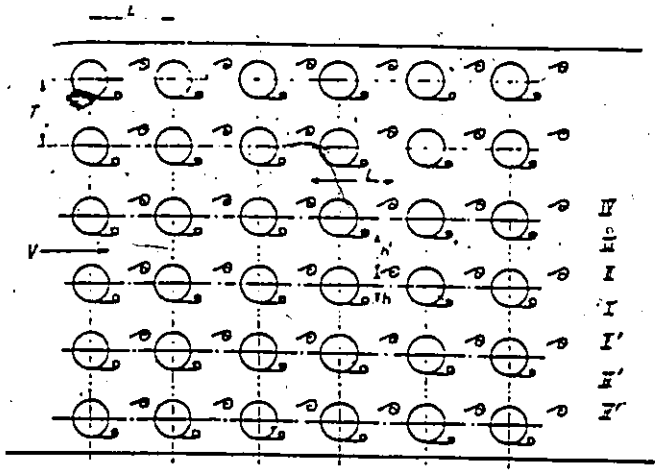

Figure 2.3 Von Karman vortex streets in an in-line tube bank arranged in a rectangular duct (heat exchanger) (from ref. 21)

for this tube arrangement $\frac{U}{U_1} = \frac{1}{3}$

$$\ell = \frac{1}{3}\,\frac{L}{0.4}\;1.5$$

$$\ell = \frac{0.5}{0.4}\,L = 1.25\,L$$

Strangely enough Owen's equation (2.6) predicts that for this particular array

$$\left(\frac{\nu L}{U_1}\right)\left(\frac{T}{d}\right) \approx 0.60$$

which is exactly 1.5 times the value of

$$\left(\frac{\nu L}{U_1}\right)\left(\frac{T}{d}\right)$$

at which the peak of the normalized spectral density appear in Owen's figure 2.2. The following table shows the calculated

$$\left(\frac{\nu L}{U_1}\right)\left(\frac{T}{d}\right)$$

parameter and length scale ℓ in both cases.

	Experiment	Calculated from equation (2.6)
$\left(\frac{\nu L}{U_1}\right)\left(\frac{T}{d}\right) = \phi$	0.4	0.6
$\ell = \frac{0.5}{\phi}\,L$	1.25 L	0.8 L

However, in view of the fact that $L = 1.3$ d, then the size ℓ of the energetic turbulent eddies, suggested by Owen's experiment, is

$$\ell = 1.25 \times 1.3\ d = 1.6\ d.$$

Owen, in assessing the impact of the eddies' size on the fluctuating force by which a tube would respond, decided that the influence of eddies significantly smaller or significantly larger in the direction of the flow than a tube diameter will be small and an attenuation in the ability of the eddies to produce a resultant force is to be expected. Owen then deduced that a tube is aerodynamically selective and responds by means of a force principally to that group of eddies whose dimensions are comparable with the tube diameter, and inferred that the most vigorous turbulent eddies are only a little larger in scale than a tube diameter. Whether or not this value of ℓ (= 1.6 d) is comparable with the tube diameter is questionable in view of the closeness of values of ℓ Owen gave in his table 1 to unity. Incidentally, the value of ℓ for

$$\left(\frac{\nu L}{U_1}\right)\left(\frac{T}{d}\right) = 0.6$$

calculated from Owen's equation (2.6) is equal to d. Furthermore from the table considered above

$$\left(\frac{\nu L}{U_1}\ \frac{T}{d}\right)_{\text{calculated}} = 1.5 \left(\frac{\nu L}{U_1}\ \frac{T}{d}\right)_{\text{experiment}}$$

which suggests that

$$\nu_{\text{cal.}} = 1.5\ \nu_{\text{experiment.}}$$

for the same array. This implies that Owen's equation (2.6)

predicted frequency value which is 1.5 times greater than the dominant frequency indicated by the experiment.

Owen added that additional to the aerodynamic filter, mechanical and acoustic filters, in effect, serve to sharpen any resonances that may occur, since the response of a dynamical system to random excitation is highly discriminating if that system is lightly damped and its normal modes are distinct and centers the vibrations upon natural frequencies. In his final remark, however, Owen mentioned that the effectivensss of the fluctuating forces in sustaining mechanical vibrations, although troublesome enough in practice, is severely impaired by the lack of coherence in the distribution of phase across the span of the tubes. The fact that vibrations of appreciable amplitude are observed under resonant conditions is due to the non-trivial magnitude of the fluctuating force per unit of span, $O(\rho U^2 d)$ and the small structural damping in the system.

Owen's work generated interest and was subjected to close scrutiny by several researchers in the area. Weaver and Grover [39] showed that, for a parallel triangular array of pitch to diameter ratio of 1.375 in air flow, Owen's equation (2.6) predicted the peak frequency observed in their experiments reasonably well provided that the velocity V_G in the minimum gap between adjacent tubes in the array was used rather than the velocity V_T in the gap between two tubes in the same row as Owen's model require. The authors also stated that as long as the minimum gap velocity V_G is used in computations,

the requirement given by Owen that $\frac{d}{T}$ be much less than unity is needlessly restrictive. The authors showed that if V_T is used as given in Owen's paper, the predictions are badly in error but agree surprisingly well with those of Hill and Armstrong. Weaver and Grover [39] added that Owen's equation (2.6) did not predict the discrete vortex shedding frequency observed in their experiment at low Reynolds number. Savkar [14] noted that the data discussed by Owen, having been measured downstream from the array, is strongly dominated by a free wake signature of the last row and is certainly not indicative of the bulk of the array. To arrive at his equation (2.5), Owen assumed that the eddies of scale ℓ are convected through the box of gas lying between two rows of tubes with the mean velocity U. In view of the 4 rows array considered by Owen, this assumption can be made if the streamwise spacing L is comparatively large with respect to the tube diameter. If L is comparable with the tube diameter, the mean velocity by which the eddies are convected through the box should be U_1 instead of U.

However, it is very important to recognize the fact that Owen investigated the origin of flow periodicity by considering rigidly mounted tubes in a bank. Owen admitted the possibility of vortex shedding in tube bundles under other circumstances that are different from those he considered. As was discussed earlier, Owen recognized the limitations of his model and stated that once acoustic resonance is established

his model is no longer valid. Also in the case when $\frac{d}{T}$ is in the neighborhood of unity Owen stated that a regularity in the flow pattern emerges and the detailed effects of geometry cease to be blurred by the randomness of the flow.

Chen [104] on the other hand accepted the position of many researchers that vortex shedding does exist in tube bundles. Nevertheless he also recognized the presence of turbulence components in the flow. Chen stated that his measurement on a finned tube bank for the power spectra of the wake formed behind the tube by the flow reveals that up to a Reynolds number of about 1.5×10^4 there still exist intense vortices in the wake with a very pronounced energy while the turbulence components accompanying it remain moderate. He added that as the Reynolds number reaches 6×10^4 the excess energy of the vortex over the broad turbulence spectrum diminishes to a negligible amount. In this paper, Chen correlated his results with those of Livesey and Dye [34] and Grotz and Arnold [27], obtained under the conditions of acoustic resonance, into a curve group of his own for in-line tube banks. The Strouhal number and the transverse spacing ratio $x_\ell = \frac{T}{d}$ were taken as the coordinates of the diagram with the longitudinal spacing ratio $x_\ell = \frac{L}{d}$ as a parameter.

Chen [21] proceeded to further analyze the problem on a theoretical basis. His assumptions were

1 - when the shedding frequency of the vortex formed in the wake of the flow behind the individual tubes

happen to be near the natural frequency of the gas column perpendicular to the flow and the tube axis, strong transverse acoustic oscillations will be excited. Under the influence of this gas column oscillation, the shedding of the vortices from all individual tube surfaces will be kept in phase as shown in figure 2.3, reproduced here from his paper for an in-line tube bank.

2 - a vortex, for example V_{n-1} shedding from the tube n-1, travels just so far down the stream that its pressure field starts to disturb effectively the flow field around the tube n, so that a vortex V_n begins to form from this due to the roll of the separated boundary layer. The more the vortex V_{n-1} sweeps the tube n the more its size will be diminished. At the same time the vortex V_n will grow at the same rate. The vortex V_{n-1} which was born at tube n-1 will after diminuation in front of the tube n start a new life behind it again. The vortex V_n can therefore be considered as the sequel to the one V_{n-1}. This assumption implies that the vortex spacing ℓ is equal to the longitudinal spacing L.

3 - $\frac{T}{d} > 2\text{-}3$.

4 - tube columns and tube rows are infinitely long. This assumption is necessary because a finite number of

parallel vortex streets cannot be stable as pointed out by Tung [105]

5 - the existence of the tubes does not prevent the influence of the vortices on each other.

6 - the vortex columns existing at a great distance from a considered vortex has no significant influence on it.

Based on these assumptions, Chen was able to establish a relationship between the vortex shedding frequency, the flow velocity, and the tube spacing as given by his equation (5) in the form

$$f^2 = \frac{\varepsilon \phi \beta^2 V^2}{4 \ell_2} \left[\tanh \frac{\pi h}{\ell_2} - \tanh \frac{\pi h'}{\ell_2}\right] \qquad (2.7)$$

where

ε = 0.43 - 0.5 for an isolated cylinder

β = 1.4 for an isolated cylinder

V free stream velocity

ϕ constant $= \frac{f}{U_R}$

f vortex shedding frequency

U_R translation velocity of the vortex

$$= \frac{\Gamma}{2\ell_2} \left[\tanh \frac{\pi h}{\ell_2} - \tanh \frac{\pi h'}{\ell_2}\right].$$

Γ intensity of one vortex

ℓ_2 longitudinal spacing of the vortices

It can be seen from this equation that the vortex shedding

frequency f is linearly proportional to the flow velocity V. It is always smaller for a number of existing vortex streets in a tube bank than for a single one with single tube column.

The pattern of vortex shedding in a staggered tube bank as envisaged by Chen was divided into two groups of large and small transverse spacing ratios reproduced here in figures 2.4 and 2.5. For the large one with normal longitudinal spacing ratio, figure 2.4a, the flow direction does not change. In each tube column an independent vortex street forms and the vortices from the tubes of each subsequent row will always change their rotation direction. Two vortex streets exist in the width of the transverse spacing T. When the longitudinal spacing ratio is large, figure 2.4b, the vortices from all tubes may be in phase. In this case the longitudinal spacing ℓ_2 of the vortices will be equal to $\frac{L}{n}$ with n - an integer. For the small transverse spacing ratio, figure 2.5 the flow may follow the gaps between two neighboring tubes of the row. Both the flow and the vortex streets will take an S shaped path and one vortex street exists in the width of the transverse spacing T. Chen added that transition condition can be expected at a certain transverse spacing ratio whereby the flow may change its path between the two patterns shown in figures 2.4a and 2.5. The vortex shedding frequency may then vary accordingly between two values. In his paper [104] published in 1967, Chen stated that the jets after the gaps between two neighboring tubes of a row can become unstable and oscillate

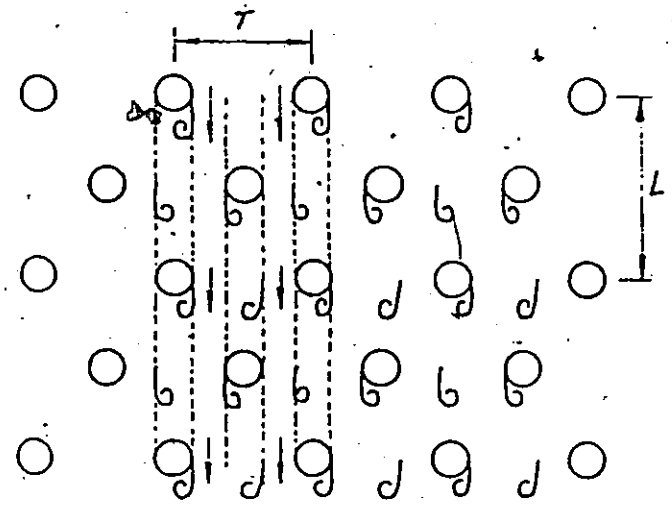

(a) Normal x_1

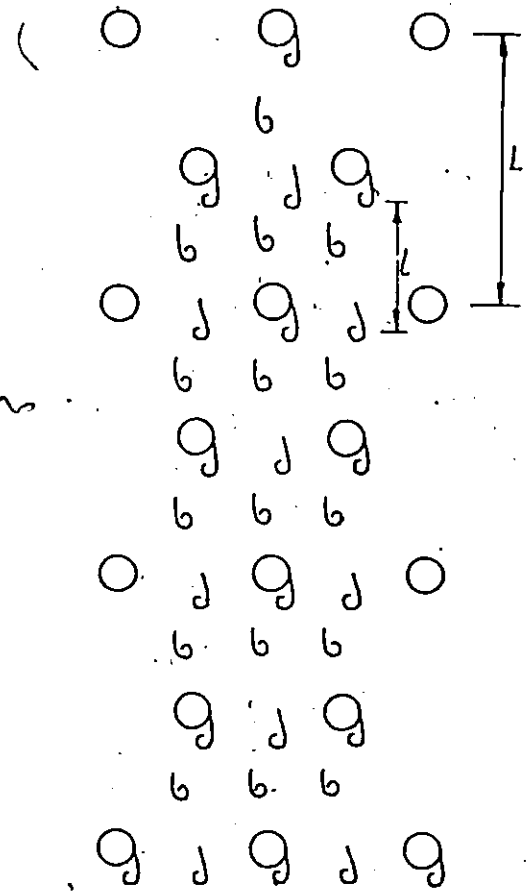

(b) Large x_1

Figure 2.4 Pattern of vortex shedding in staggered tube banks with large x_t (from ref. 21)

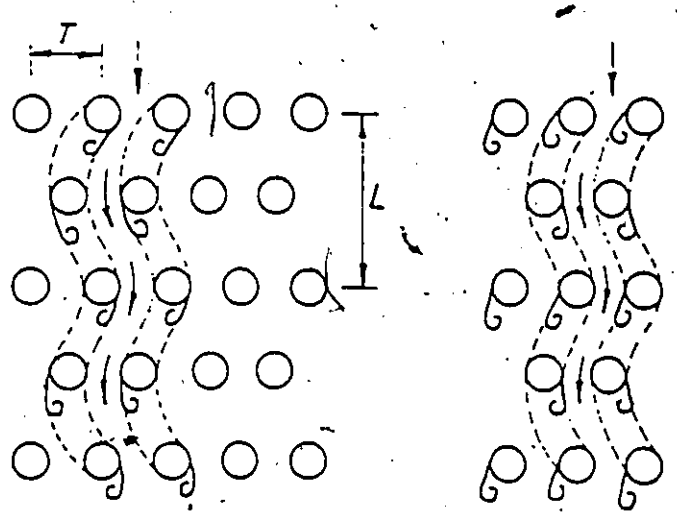

Figure 2.5 Pattern of vortex shedding in staggered tube banks with small x_t (from ref. 21)

from one side to the other. Especially in a staggered tube bank, the main flow may interchange its pattern between a parallel one and one in random directions. It is reasonable to expect that for this case, the Strouhal number of the vortices will vary simultaneously too. Chen added that two alternative Strouhal numbers and change between each at random was experienced in staggered tube banks with large longitudinal and transverse spacing ratios.

In his paper [21], Chen reported results of some experiments conducted in his small wind tunnel in the range $1.5 \times 10^4 < Re < 6 \times 10^4$ using staggered tube arrays. Finned and unfinned tubes of 38 mm diameter were considered. Two hot wire probes were arranged behind a monitored tube at two different positions along the tube span to measure the phase relation of the vortex sheet along the span and the vortex sheet along the span and the vortex shedding frequency. Strain gauges were gummed on the tube to measure the vibrational response of the tube. A record of the output of the two anemometers at a frequency of 95 Hz of the vortex near the first mode of the tube flexible vibration is given. From this record it could be seen that the phase shift of the vortices on both sides of the tube deviate scarcely from π. In other words, the vortex sheet of the same tube side is practically in phase along the tube axis. It is clear that the Reynolds number range in Chen's experiments is large enough as required by Owen's model. However, the shedding does occur uniformly

from all parts of the tube span and the elements of randomness envisaged by Owen disappeared. The observed large correlation length and organized flow is no doubt brought about by the near coincidence of the tube natural frequency and the shedding frequency. This certainly lends support to Owen's suggested distinction between periodic flow fluctuations and turbulence and proves that under some specific conditions such periodic gaseous fluctuations do exist as suggested by Chen.

Chen also showed by means of a sample diagram that the vibration of a finned tube always possesses a character of a beat of two components. One of them has the main frequency of the vortex recorded by the hot-wire anemometer behind the tube and the other has one of the natural flexible frequencies of the tube. Chen stated that the natural flexible vibration of the tube must be excited by the wake in which there should exist not only the regular Von Karman vortices but also a broad band of turbulence. Yet only the frequency in the turbulence coinciding with the natural flexible frequency of the tube can be picked up and amplified by his rig, while all other frequencies will scarcely leave any trace in the output of the strain gauges mentioned. Since the tube vibrates above the flow velocity at which synchronization between the vortex shedding frequency and tube natural frequency is supposed to take place with both the vortex frequency and its natural frequency, Chen concluded that it must be the

energy in the turbulence of the wake that excited the tube to vibrate at its natural frequency.

The investigation of staggered tube banks with finned tubes was carried in much more detail than of staggered banks with unfinned tubes. As the courses of the two kinds of curve groups are expected to be similar, the curve group for the unfinned tubes was constructed through few points with reference to the form of the group for the unfinned ones. Chen stated that the ratio of the Strouhal number for the two kinds of curve groups of an equal longitudinal spacing ratio is not uniform for the different transverse spacing ratios. The curves for the finned tubes at small longitudinal spacing ratios lie above but, at large ratios lie below the curves for the unfinned tubes. The curve group for staggered and in-line tube banks is given in figure 2.6. Chen stated that the accuracy of these curves may be about ± 10%.

In a following paper [71] Chen published sketches showing the flow path in staggered and in-line tube banks. These sketches are reproduced here in figure 2.7. Chen suggested that the guidance of the flow in the staggered tubes is quite different from that in the in-line tubes. The flow in the former will always stream between a tube surface on one side and a vortex on the other, figure 2.7a. As the vortex grows and decays periodically, the flow velocity will fluctuate in the same rhythm. The consequence of this is that

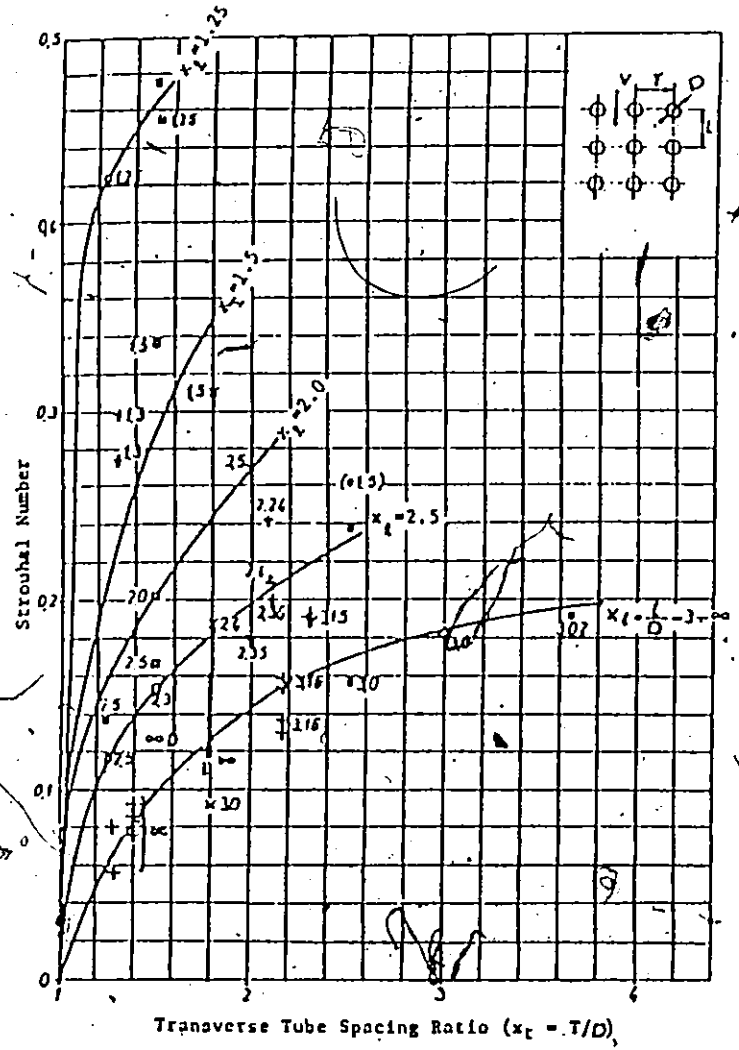

(a) For in-line tube banks

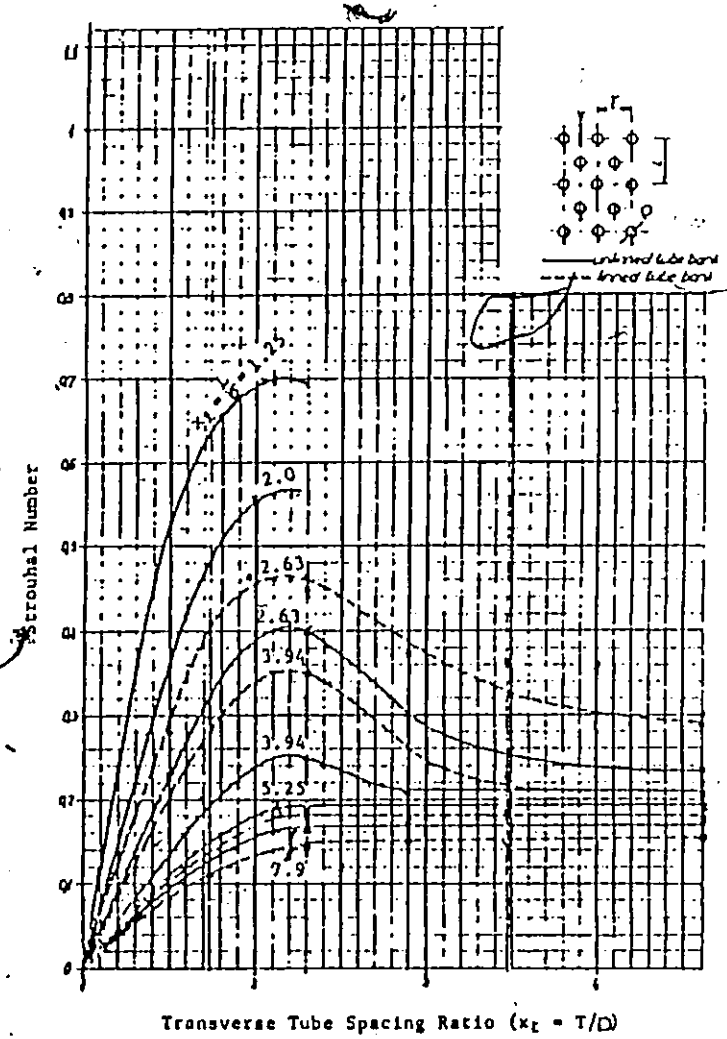

(b) For staggered tube banks

Figure 2.6 Strouhal number vs. transverse tube-spacing ratio with longitudinal tube-spacing ratio (x_l = L/d) (from ref. 21)

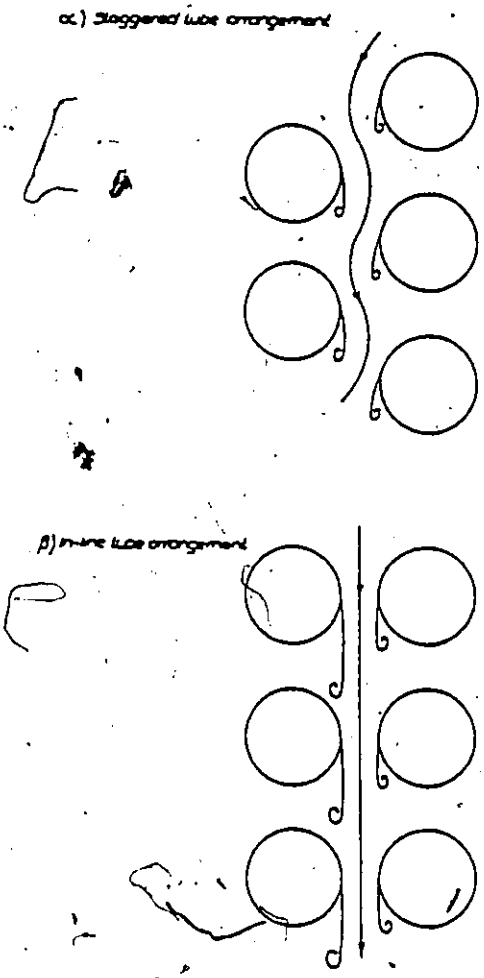

Figure 2.7 The flow path in the tube bank
a) Staggered tube arrangement
b) In-line tube arrangement
(from ref. 71)

fluctuations will influence the separation of the vortex itself. This feedback process induces a very strong vortex formation.

In the in-line tube bank the flow will be guided by the surface of the neighboring tubes themselves, figure 2.7b. The formation of the vortex will have a negligible influence on the flow velocity. The strong feedback effect just described will not appear to any great extent here. A strong vortex formation as occurring in the case of a staggered tube bundle therefore cannot be expected in the in-line case.

Further consideration was given to three in-line arrays with the different spacing ratios outlined below [106]

	case a	case b	case c
$\frac{x_t}{x_\ell}$	2.4/2.8	1.2/1.4	1.2/2.8

These arrays are depicted here in figure 2.8, together with the velocity amplitude of vibration curves and the Strouhal number values obtained. Chen stated that the cases a,b,c exhibit quite different properties. The vortex possesses a practically sinusoidal characteristic with great intensity only for large tube spacing, case a. It will be very weak and associated with broad turbulence when the tube spacing x_t/x_ℓ reduces to small values like 1.2/1.4, case b, or less. For the intermediate case c with small x_t (1.2) and normal x_ℓ (2.8) the vortex becomes stronger but remains still very turbulent. It possesses, therefore, an intense second harmonic.

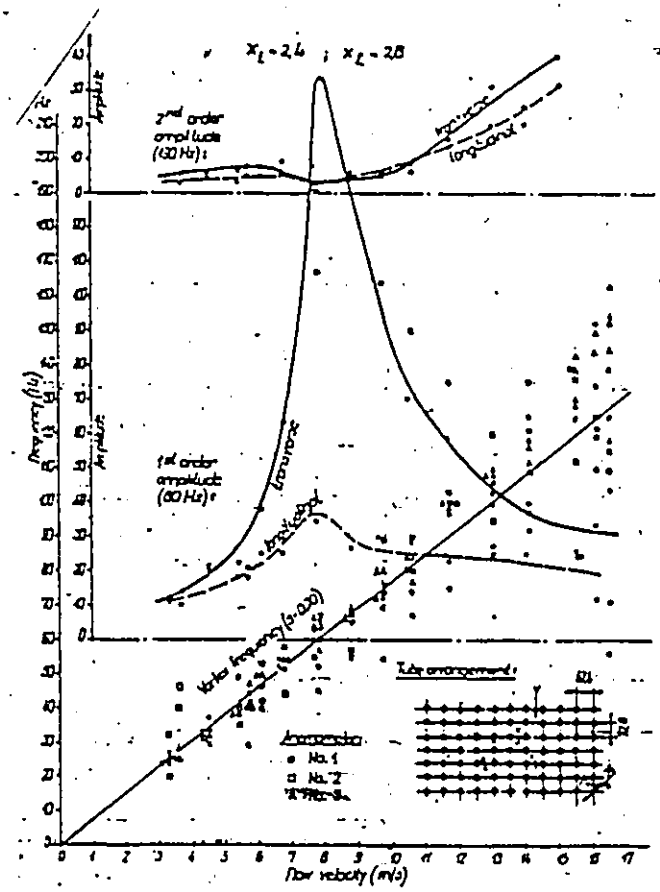

Figure 2.8(a) Vibration amplitude of the measuring tube (measured by strain gauges) and vortex frequency (measured by anemometers) for a tube bundle with an in-line arrangement of $x_t = 62.4/26 = 2.4$; $x_l = 72.8/26 = 2.8$. (from ref. 106)

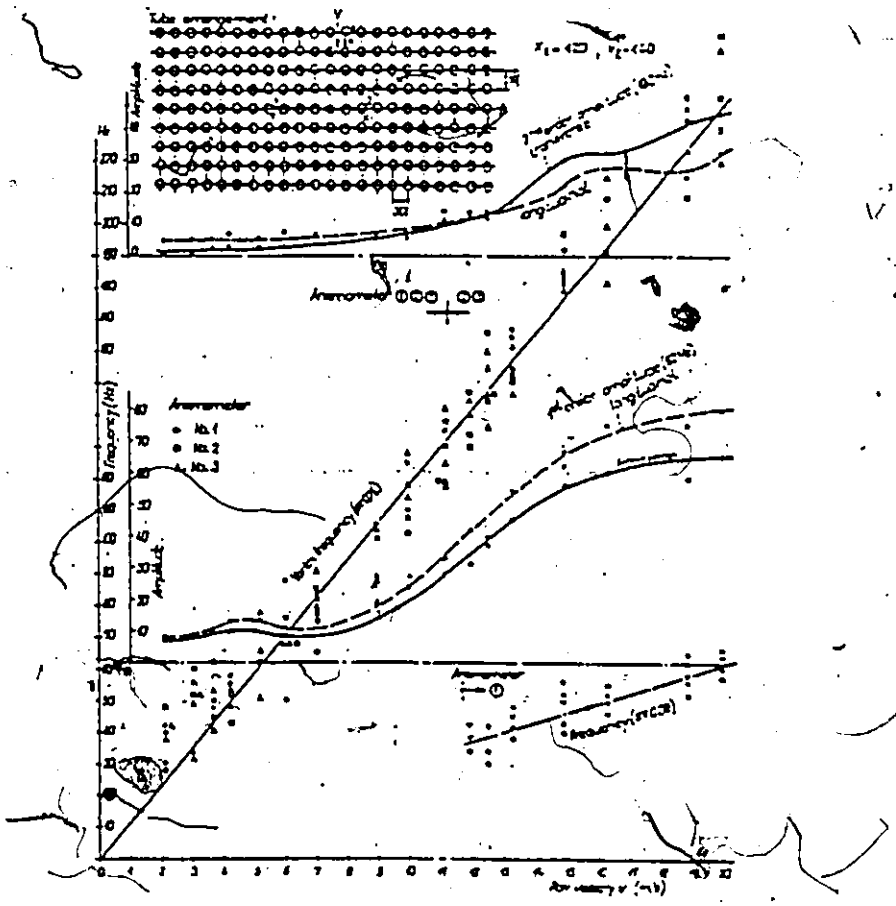

Figure 2.8(b) Vibration amplitude of the measuring tube (measured by strain gauges) and vortex frequency (measured by anemometers) for a tube bundle with an in-line arrangement of $x_t = 1.20$; $x_l = 1.40$. (from ref. 106)

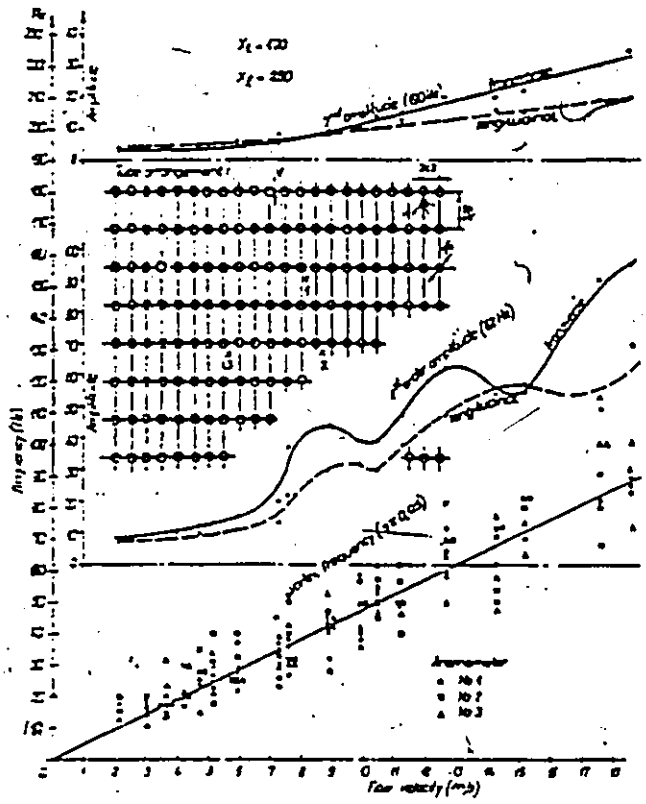

Figure 2.8(c) Vibration amplitude of the measuring tube (measured by strain gauges) and vortex frequency (measured by anemometers) for a tube bundle with an in-line arrangement of $x_t = 1.20$; $x_l = 2.80$. (from ref. 106)

Figure 2.8 Response curves for in-line tube bundles with three different tube spacings

Chen added that the difference in the properties of the three cases can be intuitively explained by the flow pattern reproduced here in figure 2.9. The free flow width between two neighboring tubes for case b is very narrow, so that the main flow consists nearly of only the vortex motion. The consequence of this is the high turbulence in the main flow. As the longitudinal tube spacing is very small also, no reasonable vortex can be formed. However for case c with the same narrow flow gap as case b, yet with a much larger longitudinal tube spacing, there will be enough space for the formation of the vortex again. More intensive vortices can be built, but the main vortex is still very turbulent due to the small free flow width. Therefore the vortex possesses a strong second harmonic. The free flow width for case a is very broad. The main flow thus has a smooth core. This explains why the vortex has a great intensity and a good sinusoidal characteristic.

In the same paper Chen demonstrated that once the vortex shedding frequency coincides with the natural frequency of the transverse gas column in the channel, the gas column will be excited to vibrate in resonance. As soon as this occurs, the gas vibration will bring about the vortex shedding in its own rhythm, so that the vortex shedding frequency will no longer follow the relationship of $f = SV/d$. The graph showing this coupling phenomenon is reproduced here in figure 2.10. A staggered tube bundle with $x_t/x_\ell = 2.84/1.46$ having

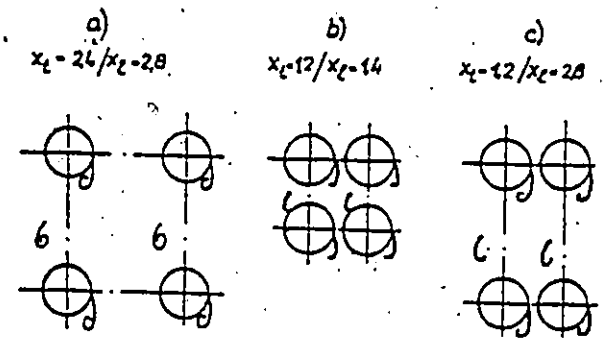

Figure 2.9 Flow pattern in the in-line tube bundles with the three different tube spacings (from ref. 106)

Case (a) Normal spacings ($x_t/x_l = 2.4/2.8$) with strong and practically sinusoidal vortices (cf. Fig. 2.8(a))

Case (b) Small spacings ($x_t/x_l = 1.20/1.40$) with weak vortices, associated by broad frequency-band turbulence (cf. Fig. 2.8(b))

Case (c) Mixed spacings of small x_t and normal x_l $x_t/x_l = 1.2/2.8$ with stronger vortices, associated with broad frequency bank turbulence. The vortices possess an intense second harmonic (cf. Fig. 2.8(c))

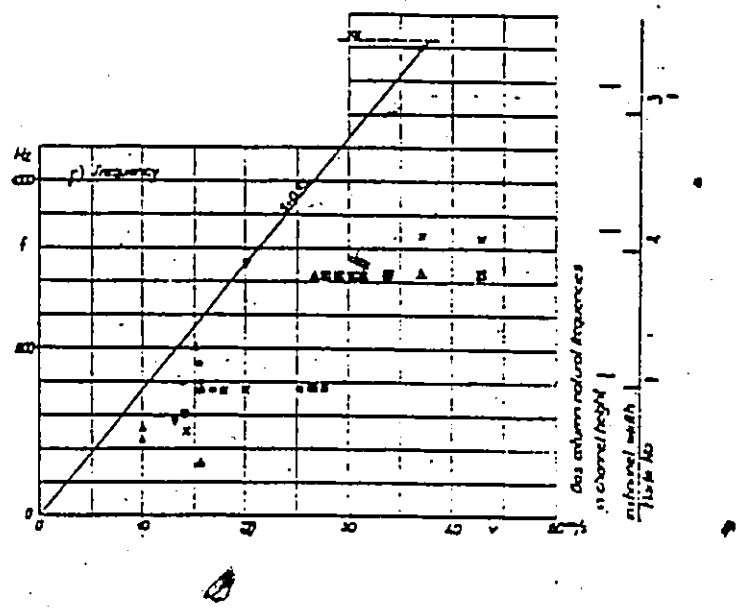

Figure 2.10 Frequency f and amplitude A of the vortex and the channel wall as function of gas flow velocity V for a staggered tube bundle model with mixed spacing ratios of normal x_t and small x_l (x_t/x_l = 2.84/1.46) (from ref. 106)

12 columns and 15 rows was used. Three hot wire probes were positioned within the tube bundle at different locations to measure the shedding frequency. Chen commented that all the signals up to the veloxity of V = 14 m/s are rather irregular from which it follows that Karman vortex streets are strongly turbulent. Only above this velocity do the very regular sinusoidal signals commence. Their frequency does not increase as the velocity increases, but remains constant at about 375 Hz up to the flow velocity V = 27.5 m/s. Afterwards it jumps to 720 Hz and remains so up to the highest velocity range measured.

Chen [29] in later publication introduced a working chart for staggered tube banks reproduced here in figure 2.11 showing the Strouhal numbers of the various excitation sources for acoustic resonance. It was suggested that Karman vortex shedding applies only for moderate to large spacing x_t and x_ℓ. If x_ℓ decreases below a certain limit Karman vortex ceases to exist. Instead, the wake can only swing as a pendulum associated with a secondary jet switch. If in addition x_t is also small, instability of ~~the~~ jet emanating from the gap of two adjacent tubes will take over the role of the excitation sources. Either primary jet switch or instability of the strongly sinusoidal jet path associated with formation of small eddies will arise. The intensity of acoustic resonance is strongest for the border region between Karman vortex shedding and primary jet switch. A working chart

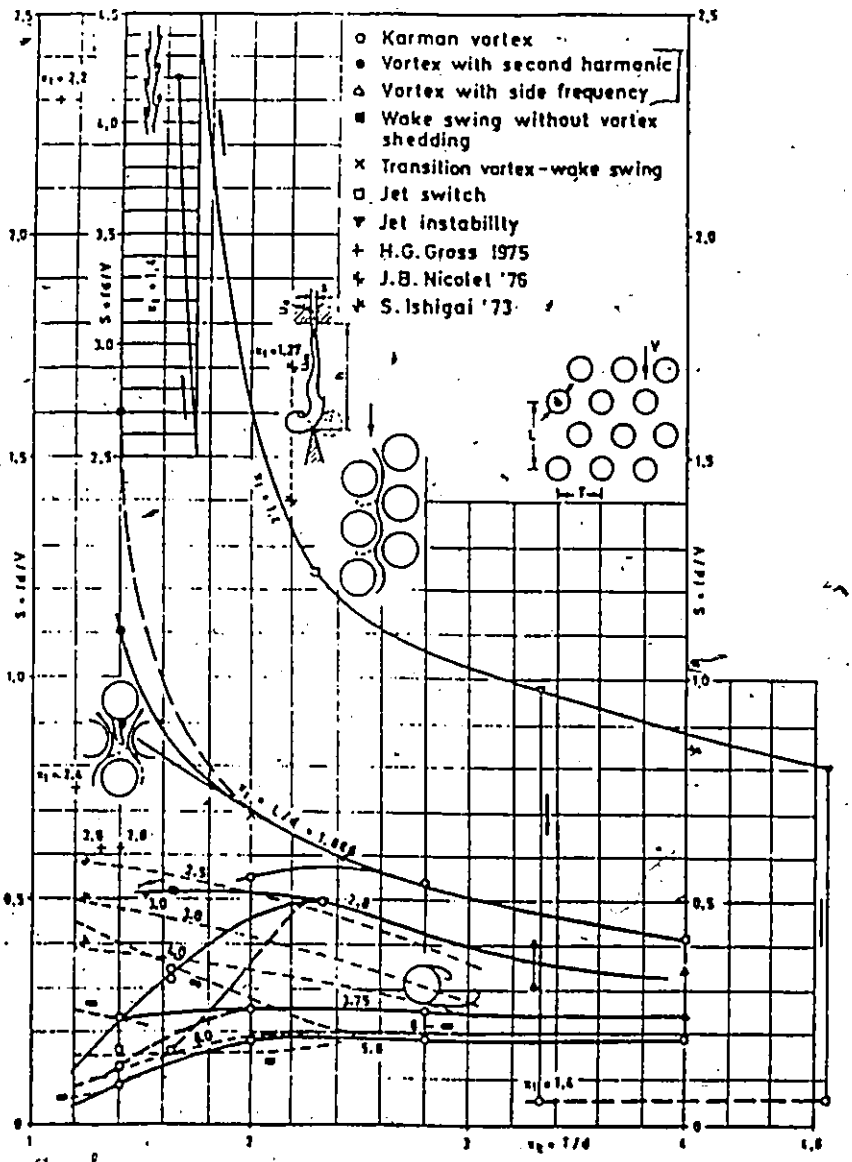

Figure 2.11 Strouhal number S=fd/V versus transverse spacing ratio x_t= T/d with longitudinal spacing ratio x_l= L/d as parameter for staggered tube bank (from ref. 29)

showing the various excitation sources in the different tube spacing regions of the staggered tube banks is reproduced here in figure 2.12. Wake swing, jet switch and jet instability were termed as jet excitation mechanisms to distinguish them from Karman vortex excitation.

The effects of jet excitation mechanisms with regard to the excitation of mechanical tube vibration are expected to be weak compared to that of Karman vortex shedding, owing to the small size of the eddies formed on the jet. These eddies will not be able to induce any noticeable counter-circulation, nor therefore any strong dynamic force on the tube contrary to the large sized Karman vortex, which will induce strong tube vibrations. Consequently, tube banks with small spacing ratios can be operated to a high flow velocity until fluidelastic instability arises.

To illustrate how fluidelastic instability is initiated, the investigation of Gross [107] on in-line ($x_\ell \leq 1.5$ and $x_t \leq 1.5$) and staggered ($x_\ell \leq 3$ and $x_t \leq 1.5$) tube banks were considered. Chen [29] stated that the measurements taken by Gross showed that fluidelastic instability of the tubes is initiated by movement of one tube row in the direction perpendicular to flow while its two close neighbouring rows move in the opposite direction. The tubes in the same row move essentially in the same phase so that each row behaves as a whole. Only after this relatively orderly movement between adjacent rows is initiated can the orbital movements of the

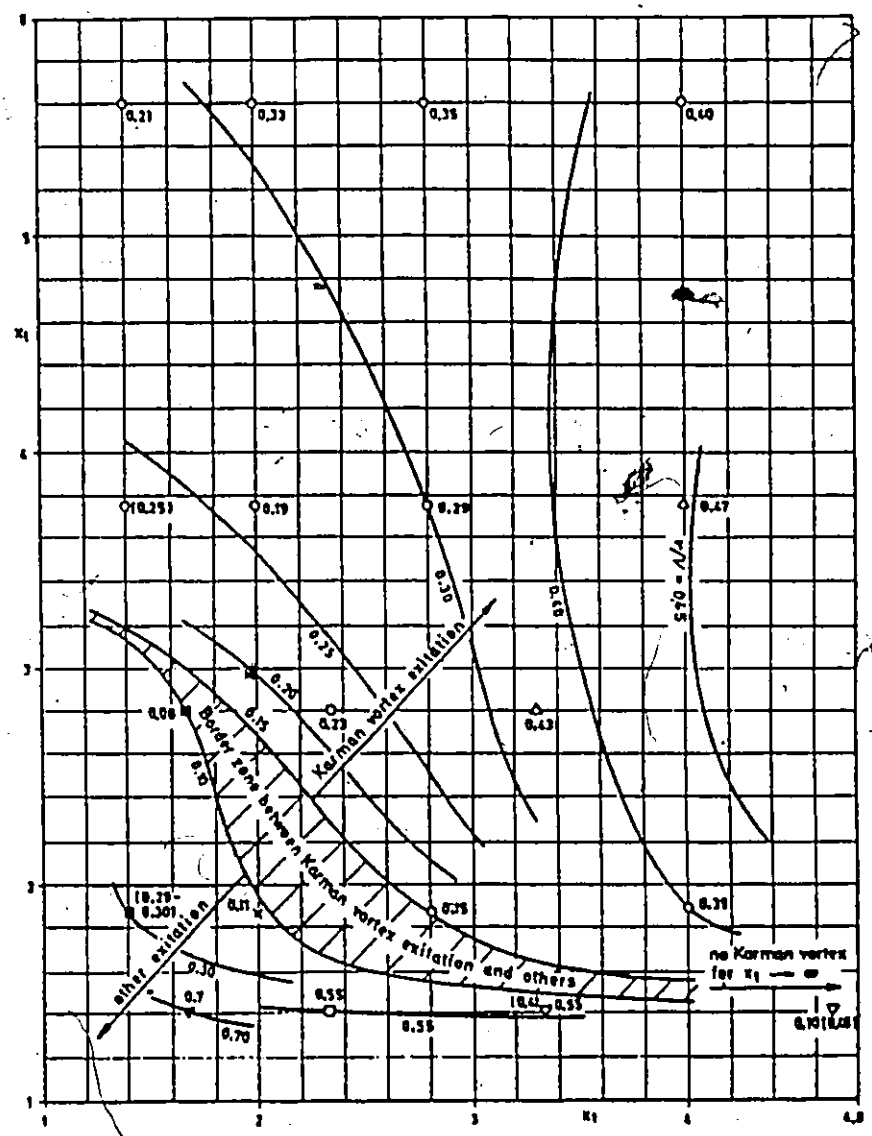

Figure 2.12 Equal value curve for dimensionless fluctuating velocity v/V in middle row of staggered tube bank (from ref. 29) .

tubes in elliptical paths with their main axes lying in nonunified directions occur as the flow rate is further increased. The orderly movement of the tube rows against each other appear to be connected with the onset of shedding of vortices of the same phase in the same row, while the vortices of the adjacent rows stay in antiphase.

Chen then proceeded to draw some sketches which are reproduced here in figure 2.13, to illustrate the above mentioned argument. A normal Flow Pattern, i.e., outside the lock-in region in a staggered tube bank at low Reynolds numbers is given in figure. 2.13a. Chen stated that the flow path is symmetric around each tube. No essential dynamic force can be affected by the flow on the tube. However, when the critical Reynolds number is reached, the separation point of the flow travels upstream along the tube surface, so that large vortices are formed as a result of the broadening of the wake. These vortices will soon show an asymmetric pattern due to instability. They are expected to be formed alternately on the left and the right sides of the tubes of adjacent rows, as suggested in figure 2.13b for a certain instant. The vortices narrow the flow path on the respective sides of the tube so that the main flow will be forced to stream along the other side of the tube. This curved, one-sided flow will exert a centrifugal force on the adjacent tube, supported by the dynamic force of the same phase induced by the formation of the vortex. Since the flow

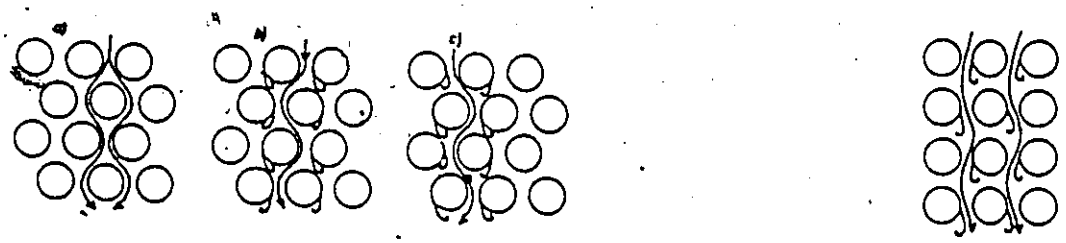

(a, b, c) in staggered tube bank (d) in in-line tube bank

Figure 2.13 Formation of alternate vortices behind adjacent tube rows as the initiating mechanism for fluid-elastic instability (from ref. 29)

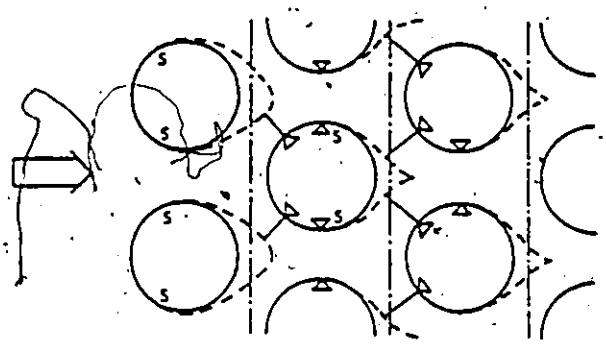

Figure 2.14 Inferred flow pattern; --- tentative wakes -.- hot-wire traverse, s-separation point, -minimum pressure (from ref. 49)

pattern has alternate hills and valleys in the following tube rows and the vortex is forming alternately on the left and right sides of the tubes of the following rows, the centrifugal and vortex dynamic forces change sign from one row to the next, inducing the anti-phase movements between adjacent rows. Figure 2.13c incorporate the flow pattern for the instant of half a period later. The flow pattern for an in-line tube bank at Reynolds numbers above the critical value is given in figure 2.13d as suggested by Chen using the argument for the staggered tube arrangement outlined in figure 2.13a-c.

Chen added that, the blocking effect on the flow of the vortices mentioned previously will apparently diminish, and the initiation of fluidelastic instability will be postponed accordingly if there is a strong turbulence in the incident flow as shown by Gross measurements [107]. The reason appears to lie in the fact that the turbulence cells will cause the vortex to form at different angles of the circular tube surface along the axial direction and thus at different depths of the gap between adjacent tubes. A poor blocking effect will result.

2.3.3 Recent Developments

Zdravkovich and Namork [48] are of the view that vortex shedding modified by the proximity of adjacent tubes as described by Chen [104] may excite vibrations at all speeds.

The amplification of such vibrations occurs only within the synchronization range (vortex shedding follows the tube natural frequency). Buffeting produced by the turbulence generated within the tube bank with a 'frequency-content' characteristic for the particular arrangement of the tubes as described by Owen [26] may excite vibrations only when the fluctuating dynamic pressure is above a certain threshold level which depends on the stiffness of the tubes.

Zdravkovich and Namork [48] conducted some experiments to study the flow structure within both stationary and vibrating two-row deep staggered tube bank having $x_t = 1.375$ and $x_\ell = 1.1875$. Time average and fluctuating pressure distributions were measured around a stationary measuring tube positioned either in the first or second row within both stationary and vibrating tube banks. The amplitude-frequency spectra of pressure fluctuations were computed for signals taken at various circumferential locations around the measuring tube at a Reynolds number Re_T of 7×10^4 and a reduced velocity $\frac{V_T}{f_n d} = 22.5$. The fluctuating and time-average pressure distributions were typical of the subcritical and critical regimes in the first and second rows respectively. The presence of a critical regime of flow and thus narrow wakes behind the second row tubes, despite the fact that the tubes were free to form the wakes without the interference of subsequent non-existing rows, was puzzling. The authors explained that the subcritical flow around tubes in the first row would normally

lead to the expectation of wide wakes. The proximity of the second row tubes prevented the formation of the wide wakes behind the first row tubes. The turbulent shear layers emanating from the first row tube shoulders collided with the tubes in the second row and triggered the transition of their boundary layers to turbulence. This caused a delay of final separation and resulted in a narrow wake behind the second row tubes. The authors concluded that the critical regime of flow observed in the second row is an intrinsic feature and whether more rows are added is irrelevant. The authors then compared their results with those available in the technical literature. Achenbach [108] found that for a five-row deep staggered tube bank, with $x_t = 2$ and $x_\ell = 1.4$, the critical flow in the second row started only when $Re = 1.4 \times 10^5$ was reached. Batham [109] found that for an in-line arrangement with $x_t = 2$ and $x_\ell = 2$, only the last 9th row produced a subcritical pressure distribution at $Re = 9.8 \times 10^4$. In view of these results Zdravkovich and Namork stated that it might be inferred that the observed change of the flow regime in their second row occurred simply because of sufficient proximity of the tubes. Nevertheless they concluded that the flow structures within the first and second row of the tested, closely packed tube bank were found to be entirely different.

In a subsequent paper [49] the time averaged and fluctuating (rms) pressures were measured around a tube

positioned sequentially in each row of a six-row deep bank at a Reynolds number $Re = 1.1 \times 10^5$. From the time averaged pressure curves the flow pattern was inferred and sketches of tentative wakes were drawn behind tubes in the first three rows. These are reproduced here in figure 2.14. Information obtained from time averaged and fluctuating pressure curves were used to infer the location of the separation points in the second and the third rows. Zdravkovich and Namork concluded from their sketches that wide wakes were formed behind the first row, narrow wakes were formed behind the second and third rows. They stated that pressure distribution curves similar to these found in the third row were obtained for all subsequent rows with minor variations of magnitude of pressure fluctuation peaks. This indicated that wakes similar in size and shape were formed in all subsequent rows. The authors however indicated that the fluctuating pressure curves exhibited a puzzling feature. The separation point peak becomes more distinct and prominant in the curves of the fourth, fifth and sixth rows. They also stated that one unexpected variation of the magnitude of base pressure fluctuations was found in even and odd rows. The base pressure fluctuations were almost identical to each other in all even rows, and were equal to one another in the third and fifth row but almost 25% below the level measured in even rows. The cause for this consistent discrepancy was not investigated further by the authors.

The time averaged velocity and intensity of turbulence were measured sequentially behind all rows by traversing a hot wire across the bank. Behind a tube located in the first row, very low velocity and high turbulence intensity were found within the wake which was squeezed to 0.64 of the tube diameter figure 2.15. The velocity peaks were not found behind the gaps but they appeared adjacent to separated shear layer. The minimum velocity behind the gap centre was caused by the proximity of the stagnation region in front of the tubes in the second row. The latter did not affect the turbulence intensity which remained low and constant. Behind a tube located in the second row the low velocity and high turbulence showed again the position and width of the wake. The wake was narrower from that found behind the first row tube and its width was only about 0.43 of tube diameter. Both velocity peaks were significantly lower when compared with the corresponding peaks behind the first row of tubes. This reduction was in direct proportion to the wake narrowing. The time-average velocity peaks coincided with the minima of intensity of turbulence. The minimum velocity behind the gap centre is now coupled with the maximum turbulence intensity so that one profile appeared as the mirror image of the other. This feature remained typical for all subsequent rows.

The authors concluded that a first row tube of their bank was subject to direct interference of the adjacent tubes. The tube in the second row was strongly affected by the shape

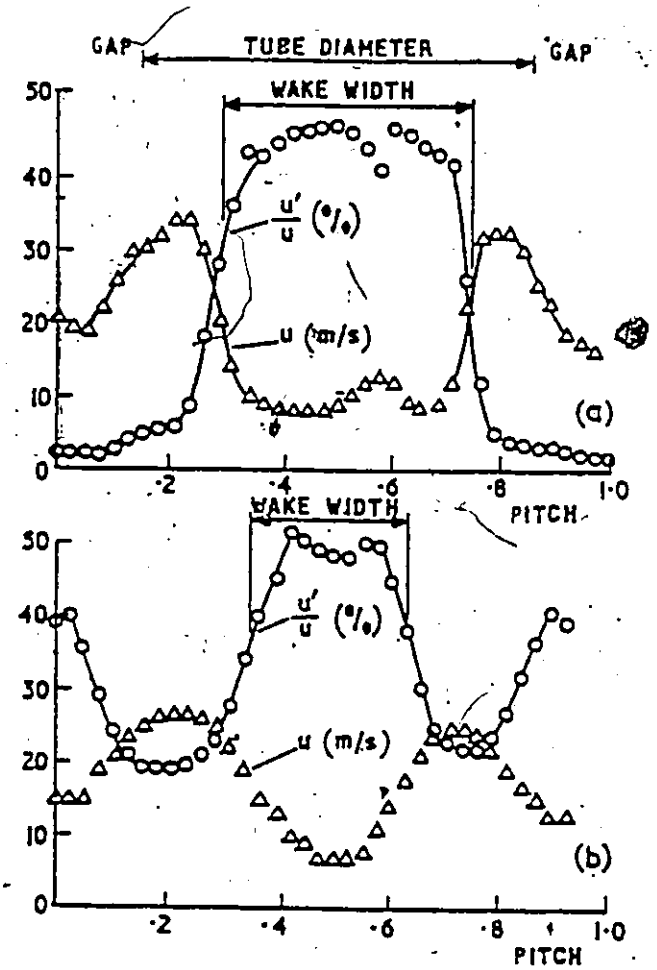

Figure 2.15 Velocity and turbulence profiles between rows along one pitch (from ref. 49)
a) behind first row b) behind second row

of the wide wakes behind the first row. The tube in the third row was affected not only by the narrow wakes behind the second row but also by the turbulence generated in the wide wake behind the first row. The authors added that tubes in the second row, where highest pressure fluctuations were found, were always excited first by buffeting vibration and produced maximum amplitude of vibration when fluidelastic mechanism took over. They argued that the practical aspect of their findings refers to the importance of the peaks in fluctuating pressure around the tubes. Their magnitude seems to be a primary factor in exciting buffeting rather than the resonance produced by the frequency content in them close to the natural frequency of tubes.

Pettigrew [20] stated that what happens in closely packed bundles of cylinders is not as well understood as in the case of an isolated circular cylinder. Three mechanisms of periodic wake shedding which could lead to periodic forces may be postulated as shown in figure 2.16 reproduced from his paper.

1) Vortex shedding as described by Chen [106, 110, 111]. The formation of vortices should however be much affected by the close proximity of adjacent and particularly downstream tubes.

2) Buffeting. Periodic forces may arise on a given cylinder as it is being subjected to the vortices generated by the upstream cylinder.

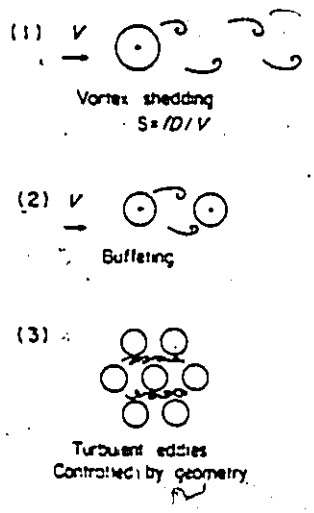

Figure 2.16 Postulated mechanisms for periodic wake shedding excitation (from ref. 20)

3) Turbulent theory of Owen [26], where the argument is that the scale of turbulence is controlled by the geometry of the cylinder bundle configuration. For a given flow velocity, some scale turbulence leads to narrow band turbulent forces and to some degree of periodicity.

Pettigrew added that whatever the mechanism, periodic wake shedding forces could result in a resonance problem if their frequencies coincide with one of the natural frequencies of the cylinders. Pettigrew and Gorman [32] stated that periodic wake shedding resonances are more likely to occur in upstream tubes.

Grover and Weaver [30] investigated cross flow induced vibrations in a parallel triangular array having a pitch to diameter ratio of 1.375. They reported that discrete vortex shedding at a Strouhal number of approximately 0.83 has been observed in the first 15 rows of a tube array for Reynolds numbers based on minimum gap velocity up to about 1200. As the Reynolds number is increased beyond this value, the discrete vorticity is suppressed by random turbulence. The Reynolds number at which this occurs appears to decrease as the number of tube rows increases. Even when the flow velocity was carefully tuned to synchronize vortex shedding and tube natural frequencies the resonant response was very small. This suggested that vortex shedding will not cause dangerous vibrations of tube arrays of the type studied and hence may be

neglected at least when the shell side fluid is a gas. The maximum tube response due to vortex shedding occurs in the early rows of tubes and no resonant response was observed after about the 15th row. Weaver and Grover [39] reported that as the flow velocity is increased beyond that at which discrete vortex shedding occurs, random turbulence develops. The turbulence spectra have a peak which apparently coincides with a Strouhal number, based on the minimum gap velocity, of 0.21. The strength of this peak may be dependent on the geometry of the array and in some cases could be responsible for acoustic resonance in tube banks. In the experiments conducted no excessive vibrations were observed even when the peak in the turbulence spectrum coincided with the tube natural frequency.

CHAPTER 3

EXPERIMENTAL FACILITY AND PROCEDURE

In this chapter, the essential details of the experimental facility will be described. Tube bundle configurations as well as the instrumentation used in the course of the investigation will be outlined. The experimental procedure and some preliminary test results will be given.

3.1 The Experimental Facility

The experiments were conducted in the McMaster University water tunnel, designed to provide low turbulence flow with a flat velocity profile. A schematic of the water tunnel is shown in figure 3.1. The power requirements are provided by a V8, 5.6 litres 190 HP Chrysler internal combustion engine fitted with an automatic transmission and marine manifolds. The pump, P, is a double suction Babcox and Wilcox centrifugal pump, delivering 0.4 m^3/s at 33 m head which far exceeds the requirements of the present study.

To the exit side of the pump, the main line is equipped with a 0.304 m diameter gate valve, V1, to control the test-section flow rate over the range 0.4 m/s to 4 m/s. A parallel by-pass line was designed and equipped with 0.152 m diameter gate valve, V2, to control the flow over the range 0.07 m/s

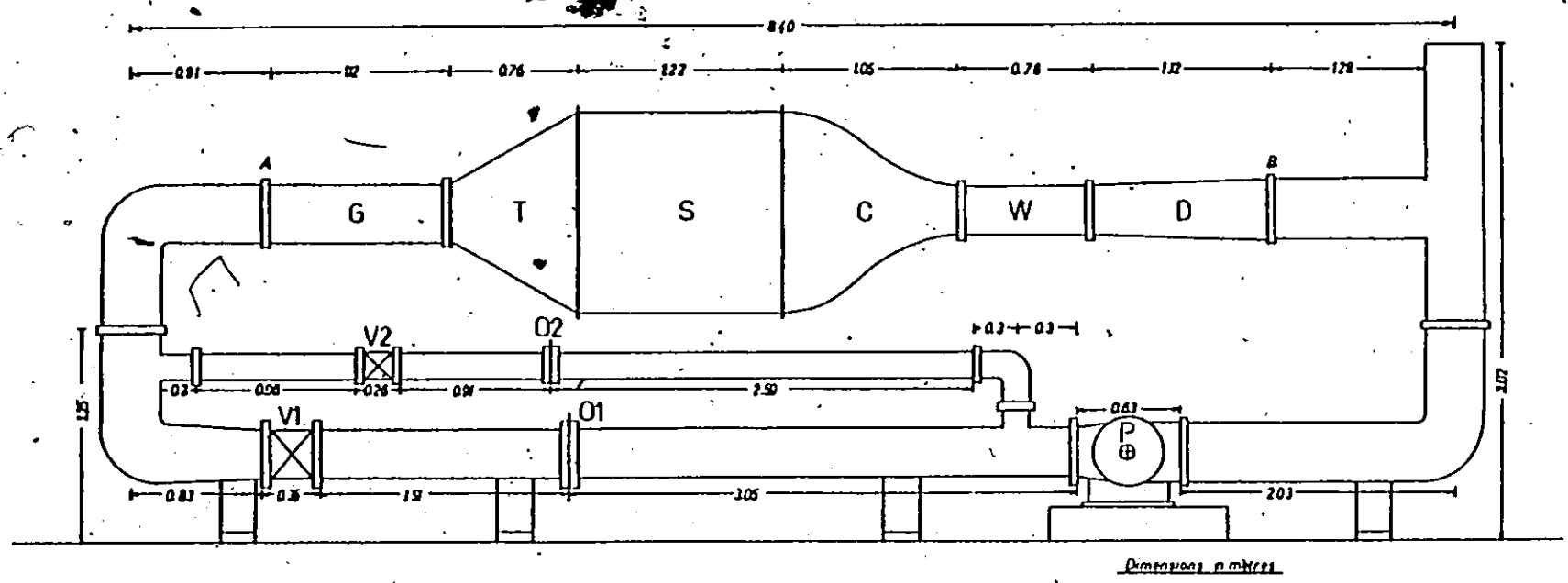

Figure 3.1 Schematic of the water tunnel
(from ref. 113)

to a maximum of 0.8 m/s. In the present investigation the parallel by-pass line was used since the maximum flow velocity attained is well below the maximum flow velocity this by-pass line provided.

On each line, a restriction orifice plate and a by-pass Brooks full view rotameter type 1110-08-C1A was used for flow measurements. The specification of the orifice plates, their installation and the piping between the rotameters and orifice flanges satisfied the requirements specified by the Institute of Hydraulics handbook [112] and the manufacturer's requirements. The rotameter on the main line and the by-pass line has the range of 100-1700 USGPM and 500-6500 USGPM respectively. Proper installation of these rotameters ensured correct flow rates within 2 percent of maximum flow of their designed ranges.

The four elbows of the water tunnel are equipped with turning vanes to minimize disturbances and losses. Following the second elbow, the flow enters a 30° half angle transition, T, from the straight section of pipe, G. In the wide angle transition section, the kinetic energy of the flow is converted to pressure energy and the flow is decelerated. At the half-way and exit planes of this section, 40% open screens are placed to aid the reattachment of the flow to the section walls and to reduce flow velocity variations.

Installed in the settling chamber, S, is a set of straightening aluminum tubes to reduce the large lateral flow

nonuniformities and to breakdown any large scale vorticity in the flow. The set of aluminum tubes is followed by a 60% open screen which further helps to produce a uniform velocity profile. The settling chamber is equipped with an observation window made of acrylic and designed to be flush with the inside surface of the chamber in order not to disturb the flow.

The conditioned flow then enters the two dimensional contraction C where it accelerates. Acceleration due to contraction reduces the relative turbulence levels in the flow and produces a flat velocity profile at the entrance of the test section. The test section, W, is a leak proof enclosure constructed of 19 mm thick acrylic plate which houses the tube bundles. The transparency of the test section is an essential requirement for the successful utilization of the flow visualization technique. The flow then enters a square to circular transition piece, D, and is directed back to the pump through the third and fourth elbows of the closed loop.

The performance of the water tunnel was examined [113] by measuring the local flow velocity at a distance of 0.2 m downstream from the contraction exit using a pitot-static probe. It is reported that the flow approaching the test section has a flat velocity profile outside the boundary layers within 1 percent and low turbulence intensity of about 1/2 percent. The normalized velocity distribution at an

upstream velocity of 1.15 m/s is given in figure 3.2. Investigated also were the noise in the flow and the vibration levels of the water tunnel. It was reported [113] that no predominant frequencies occurred except from the expected turbulent power spectrum of the flow and that structural vibration levels were negligible in the frequency range 0-100 Hz. At a higher range of frequencies, 150-500 Hz, very small levels of vibrations were reported but due to the adequate frequency separation, these levels of vibration will not contribute to the excitation of the tube bundles in the present investigation. More information about the design principles, the limitations and description of the water tunnel can be found in reference [113].

3.2 The Tube Bundles

With the advent of the successful development of the flow visualization technique discussed in the next chapter, long and short term goals were developed. The long term plan was to use the flow visualization technique to investigate the different array patterns with varying pitch ratios. Significant insight into the structure of the interstitial flow as related to the excitation mechanisms and the way in which the energy is transferred from the flow to the bundle tubes can be gained. The effect of various pitches and patterns on these parameters with regard to the susceptibility of such arrays to flow induced vibration can also be investi-

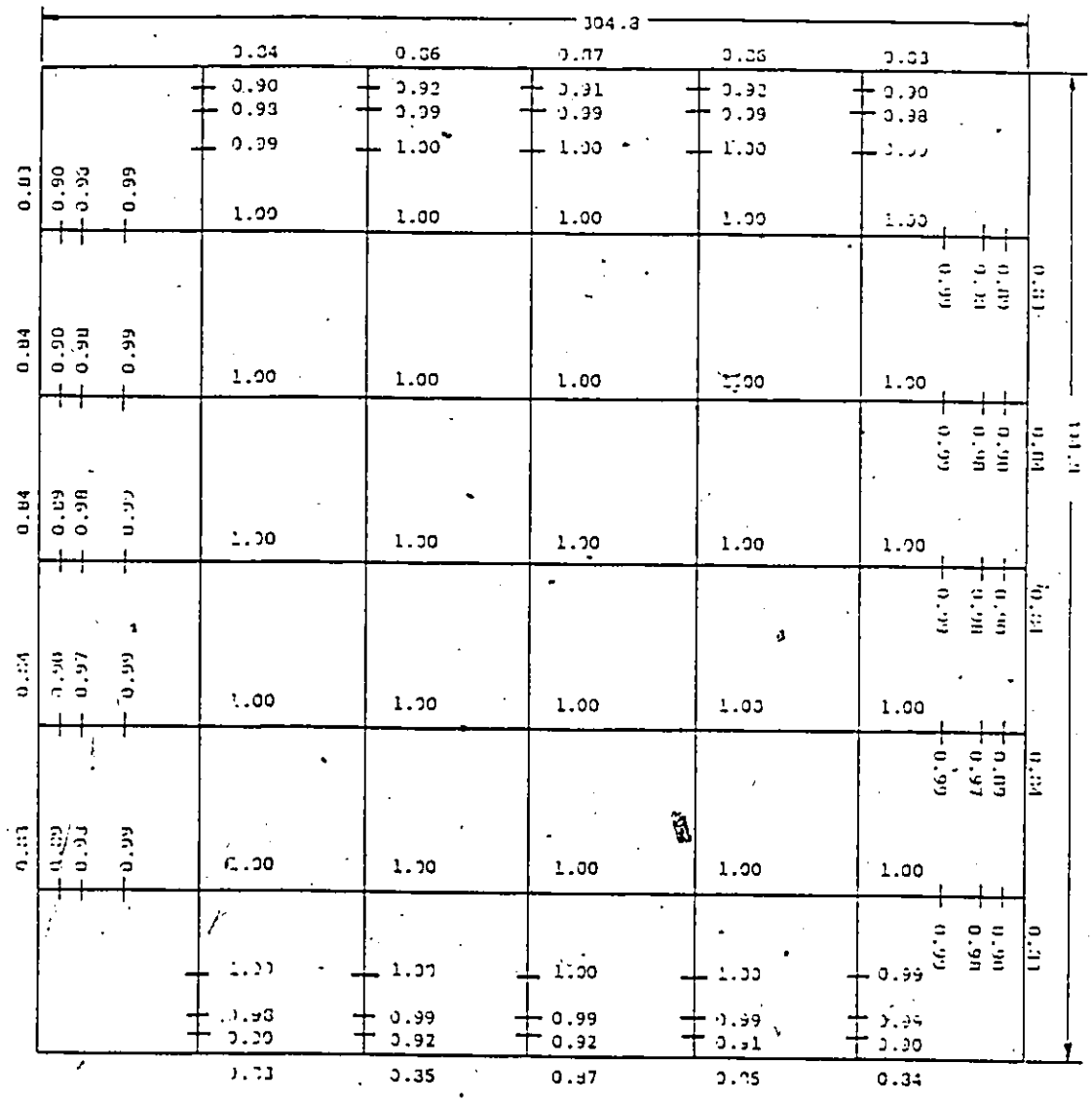

CENTRE VELOCITY 1.15 m/s

Figure 3.2 Normalized velocity distribution
(from ref. 113)

gated. Indeed, adequate understanding of the nature of the excitation mechanisms is very important and cannot be overemphasized.

The short term plan was to examine a square in-line array and a rotated square array with moderate pitch ratios. The work done in the past on square in-line arrays yielded some unexplained results. Weaver and Yeung [114, 115] reported that their frequency spectra showed no evidence of constant Strouhal number vorticity excitation yet all amplitude response curves show significant peaks at or just below their respective stability thresholds. This was rather surprising in view of previous predictions [21, 26, 116, 117] of Strouhal periodicity. Chen and Weber [71] reported that in a square in-line array with longitudinal and transverse pitch ratios of 1.4 and 2.4 respectively, periodicity in the flow due to vortex shedding was absent. Hartlen [118] on the other hand noted that the rotated square pattern, of the four patterns he tested in air, had a very sharp threshold, i.e. steep increase of vibration amplitude with flow velocity. His observations indicated that often the rotated square array changed its mode from "no-vibration" to "tube-to-tube contact" with a velocity increase of the order of 10 percent. However, Weaver and Yeung [114] reported that the square in-line array is slightly less stable than the rotated square array. Such interesting results influenced the decision to choose the above mentioned tube patterns to investigate in the short term plan.

The square in-line array consisted of 28 plexiglass tubes arranged in four rows deep, each row of seven tubes, with a pitch to diameter ratio of 1.5 as shown in figure 3.3. The twelve numbered tubes are flexibly mounted while the rest of the tubes are essentially rigid. Tubes no. 5 and no. 8 in the second and the third rows respectively were the monitored tubes.

The rotated square array, shown in figure 3.4, had 30 plexiglass tubes arranged in five rows deep, each row of six tubes with a pitch to diameter ratio of 1.414. Twelve tubes were flexibly mounted, as shown in figure 3.4, while the rest of the tubes are essentially rigid. The monitored tubes, no. 4 and no. 6, were located in the second and the third rows respectively.

The response of the monitored tubes, positioned in the second and third rows of both arrays, is not typical of tubes deep inside similar arrays. Nevertheless, it was reported [119] that the early rows are critical in terms of fluidelastic instability, and will have slightly lower stability thresholds. It was also reported [120] that tubes deep inside tube bundles did not experience vortex shedding resonance.

The flexibly mounted tubes are 300 mm long and 25.4 mm in diameter. Flexibility was achieved by attaching the tubes to one end of a stainless steel threaded rod support 7.95 mm in diameter. The other end of the threaded rod was screwed and locked into a heavy steel base plate fixed in the base

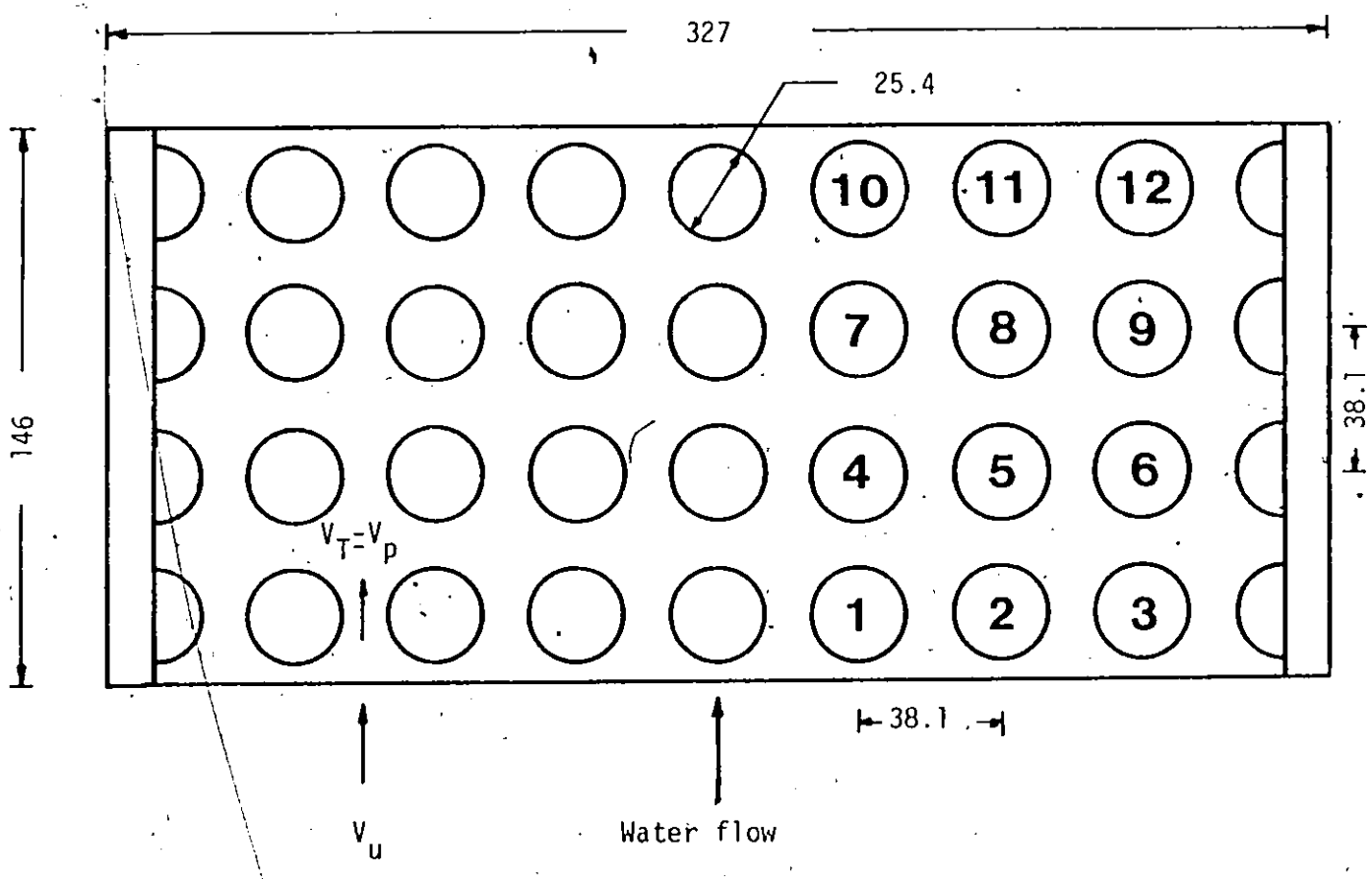

Figure 3.3 Cross section of the square in-line tube array

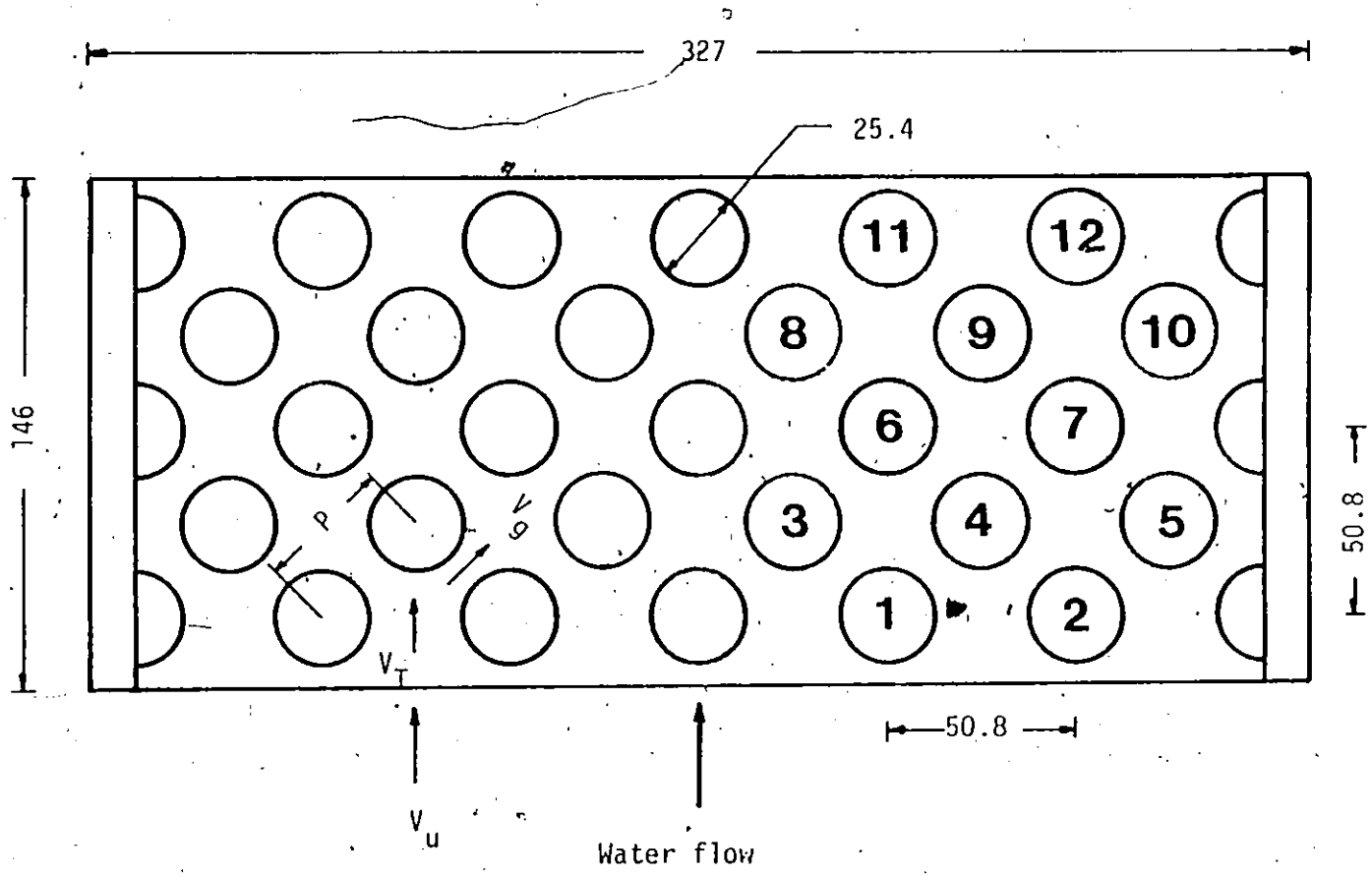

Figure 3.4 Cross section section of the rotated square array

assembly of the bundle, as shown in the photograph of figure 3.5. The natural frequency of the tube-rod assembly was controlled by varying the length of the threaded rod which acted as a cantilever spring. When the tube bundle was assembled, the acrylic portion of the tubes only was exposed to the flow, while the base assembly and the support rods below the test section were in quiescent fluid. They were isolated from the flow by an acrylic false bottom to the test section into which clearance holes allowed the passage of the flexibly mounted tubes. The cantilevered tube model concept has been used in previous investigations [114, 115, 121] to simulate the mid span vibrational characteristics of a real tube in heat exchangers. The performance characteristics of this tube model was reported to be satisfactory [115]. Rigid tubes were 25.4 mm in diameter and made of acrylic rods. Half tubes were installed along the walls of the tube bundle to minimize the edge effects. A full view of the two tube bundles are shown in the photographs of figure 3.6.

3.3 Instrumentation for Dynamic Measurements

The motions in the streamwise and the transverse direction of the monitored tubes were monitored using two pairs of precision strain gauges type CEA-06-032UW-120 attached to the base of the tube's support rod. The strain gauges were wired in a half bridge mode and their signals were filtered and amplified using a Vishay 2310 signal conditioner and

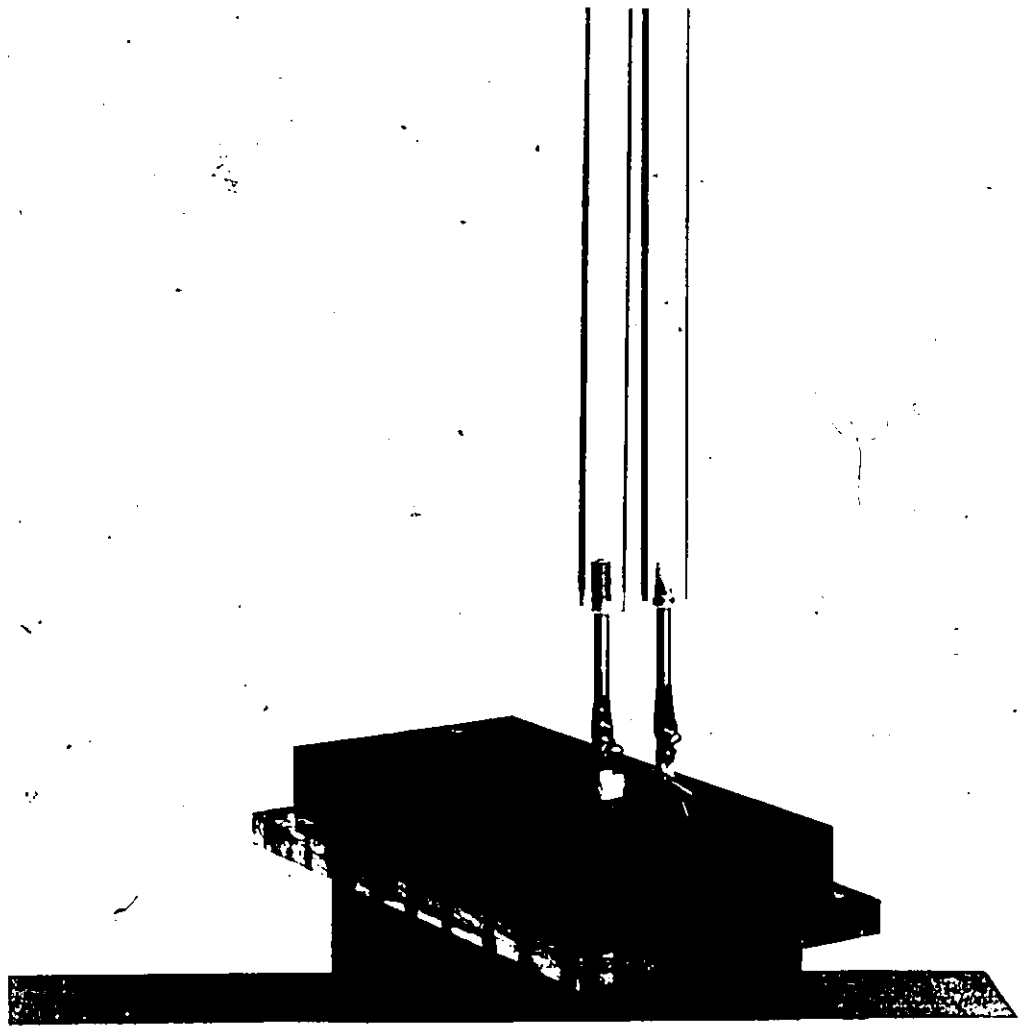

Figure 3.5 Flexible tubes and base plate assembly

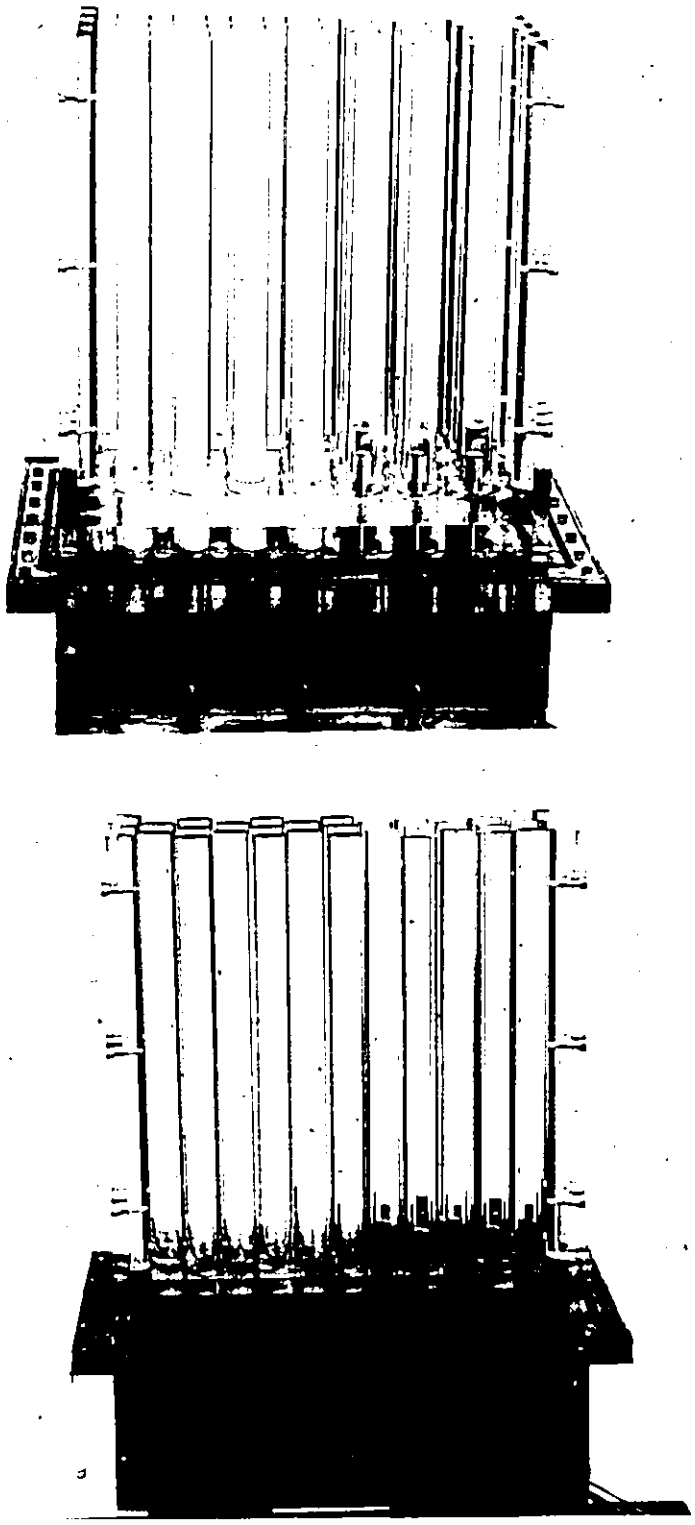

Figure 3.6 Full view of the two tube bundles

amplifier. The output of the amplifier was calibrated and found to vary linearly with tube tip deflections up to values in excess of those required to cause tube-to-tube clashing. This ensured the reliability of the tube response data. Information pertinent to the strain gauges, and their calibration are contained in Appendix A. The frequency spectra and the RMS response amplitudes in the streamwise and transverse directions were obtained using a Spectral Dynamics SD375 frequency analyzer. The frequency spectra of tube motion were recorded using a Hewlett Packard 7004B X-Y recorder. The tube mode shapes were observed and recorded whenever appropriate for further study using a Tektronix type 564B dual trace oscilloscope and a Polaroid Land camera.

These instruments were also used to tune the monitored tubes to the required natural frequency. Tuning of the non-instrumented tubes was accomplished using an MTI type ASP 10 non-contacting capacitance displacement probe in connection with MTI Accumeasure 1000 Bridge, together with the Spectral Dynamics SD 375 frequency analyzer. Hard copies of the frequency spectra were obtained using a SD 422 video printer.

A Honeywell 2106 visicorder and a Honeywell Accudata 6-channel amplifier were used to obtain tube amplitude decay traces from which the logarithmic decrement of damping was computed. A schematic layout of the experimental equipment used is shown in figure 3.7.

The Brooks full-view rotameters type 1110-08-2 C1A

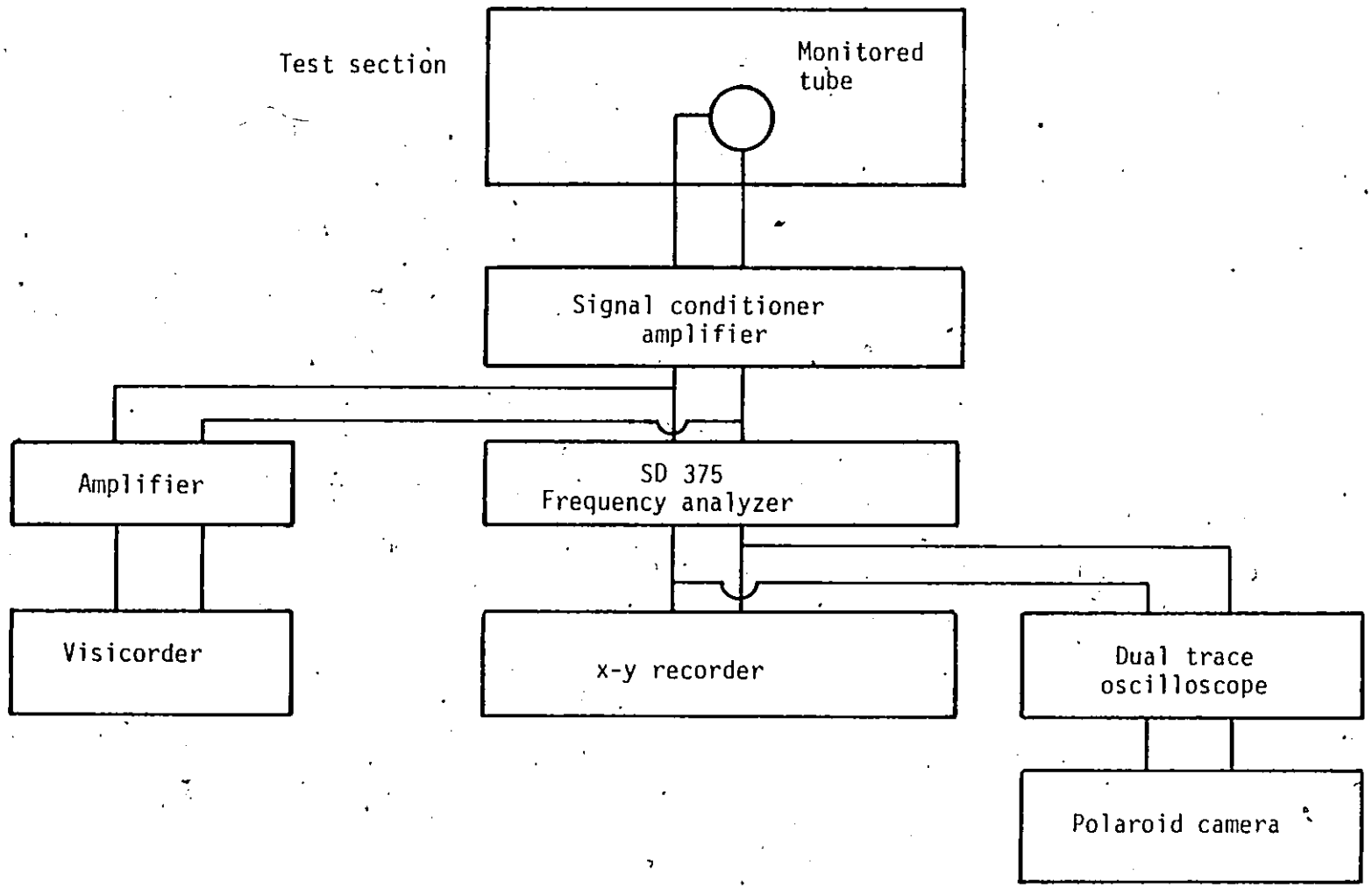

Figure 3.7 Experimental equipment for dynamic measurements

installed on the main and by-pass lines, with ranges from 500 to 6500 USGPM and 100 to 1700 USGPM respectively, were calibrated in a previous study [113]. The calibration was done by measuring the upstream flow velocity using a Pitot-static probe and a micro-manometer with carbon tetrachloride as the working fluid. The by-pass line rotameter was calibrated again in the present investigation by measuring the upstream flow velocity using aluminum tracer particles in the flow and the LOCAM model 51 high speed motion picture camera, as will be described in the next chapter. Agreement between the two calibration curves was found to be within 6%.

3.4 Experimental Procedure

The twelve flexibly mounted tubes of both arrays were finely tuned in air to a reference frequency. The reference frequency was 25.5 Hz for the square in-line arrangement and 28 Hz for the rotated square configurations. The frequency variation between tubes was within 0.25 Hz which amounts to less than 1 percent variation. Fine tuning was accomplished by adjusting the length of the support rods which were screwed into the base plate, and the plexiglass rods on their supports. Lock nuts were used on each support rod to ensure that its length did not change in the course of the investigation.

The rotated square array was used extensively over a long period of time to develop the flow visualization

technique and to conduct several preliminary runs of an exploratory nature. Following the establishment of a sound experimental procedure and verification that the flow visualization technique was satisfactorily developed, the experimental investigation and the flow visualization studies were carried out. This lasted for another extended period of time. As the investigation of the rotated square array ended a frequency check was done. The natural frequency in air of the monitored tubes, no. 4 and no. 6 were found to be 27.75 and 27.50 Hz respectively. The change in the natural frequency was not appreciable and the frequency variation between tubes was still within 1 percent. This was considered satisfactory and the calculations in the following chapters are based on these frequencies. The investigation into the square in-line array was concluded in a relatively shorter time. Frequency checks done on the square in-line arrangement, after the investigation was concluded, showed that the natural frequency did not change.

The next step was to determine damping in air for the monitored tubes. The monitored tube considered was lightly plucked and the amplitude decay traces were recorded using the Visicorder. Ten such records in two orthogonal directions permitted the calculation of an average value of the logarithmic decrement of damping. The standard deviation was less than 10 percent of this average value.

Previous experience [115, 122] with tubes vibrating in quiescent water have shown that well-defined frequency response and amplitude decay traces free from modulations can be obtained if all flexible tubes, except the one being monitored were restrained. The significant fluid coupling in water accompanied by possible mechanical coupling through the base plate results in broadened frequency spectra and modulated damping records if this procedure is not followed, as the energy is transferred back and forth between tubes. However artificial the procedure is, it was followed here in order to obtain more consistent results, since the data so obtained are used for reference purposes only. Consequently, all the data pertaining to the frequency and damping in quiescent water for the monitored tubes were obtained in this way. The recorded data are given in table 3.1.

The tube bundle was then inserted into the test section and the experiments commenced. Data recording started at the lowest flow velocity indicated by the calibrated bypass flow meter. The flow velocity was then increased in small increments and at a given flow velocity, a waiting period of at least ten minutes was allowed before any measurements were taken to ensure that a new steady state operating condition was attained. The frequency response spectra in the streamwise and transverse directions and the overall RMS response amplitude were recorded for the monitored tubes. The same procedure was repeated at all the flow velocities

Table 3.1

Preliminary experimental results

Monitored tubes	Rotated square array		Square in-line array	
	No. 4	No. 6	No. 5	No. 8
Natural frequency in air Hz	27.75	27.50	25.50	25.50
Natural frequency in water Hz	19.50	19.50	18.50	18.50
Damping in air	0.015	0.015	0.014	0.014
Damping in water	0.039	0.038	0.039	0.035

considered, until very large tube response amplitudes were developed and tube-to-tube clashing was imminent. Only then were the experiments terminated.

The RMS response amplitudes and the frequency response spectra recorded for the rotated square array were the result of 100 sample averages which yielded repeatable results. Previous investigations [113, 115] reported that 64 sample averages were found sufficient to achieve a steady state. Fitzpatrick and Donaldson [123] suggested that submerged spikes in the response spectra may become evident if the number of sample averages was increased. A comparative study with 100 and 200 sample averages in recording the data of the square in-line array at selected flow velocities showed that no essential differences were found in the results of both cases. However, it was decided to use 200 sample averages in investigating the square in-line array since the time involved in obtaining the data was not excessively prolonged.

When the experiments were completed, the data collected were carefully analyzed and studied to develop an understanding of the bundle behaviour and the phenomena involved. The results were compared with the available data and information found in the published technical literature. Such a process is of vital importance to the flow visualization study to be launched afterwards. Based on the understanding of the flow phenomena involved, filming and photographing of the tube bundle and the related factors such as the flow velocities,

the framing rates, the bundle areas of interest, and the magnification were then decided. The details of the flow visualization study are outlined in Chapter 4.

CHAPTER 4

FLOW VISUALIZATION TECHNIQUES

4.1 Introduction

Wind and water tunnels are used extensively to test a great variety of models covering a wide range of research work. Air and water are transparent working fluids whose motions remain invisible during direct visual observation. Observing fluid flow patterns, whether stationary or time dependent, greatly enhance the understanding of the phenomena involved in a physical process. In order to be able to "see" the flow patterns, certain flow visualization techniques have been developed.

From the visible picture of the flow, qualitative as well as quantitative data can be derived. The techniques differ from other experimental methods in that they provide information about the whole flow field while minimizing the physical interference with the fluid flow. They help investigators to select more strategic locations for single flow-measuring instruments, such as the hot wire anemometer and reduce the guess work inyolved in interpreting their results.

Today, the existence of a wide variety of flow visualization techniques, testifies to the popularity of these methods and the instructive results obtained by their applica-

tion. Technical information about these methods can be found in books, journals, and official reports. Films distributed by the National Committee for Fluid Mechanics and the National Aeronautics and Space Administration (NASA), are another important source of information.

Merzkirch [124] in his book, classifies flow visualization methods into three groups by outlining the physical principles on which each is based. The first group is suited for incompressible flows that might be liquid or gaseous. In these techniques, a visible foreign material is added to the flowing fluid and the motion of the foreign material is observed instead of the fluid itself. The smaller the size of the particles of the foreign material and the closer its density to that of the fluid, the smaller the difference between their motions will be.

The second group is suited for compressible flow fields which display fluid density variations, and hence variations in the refractive index of the working fluid. A light beam transmitted through the flow field is affected with respect to its optical phase, while the amplitude and intensity of the beam remain unchanged. The phase changes result in a nonuniform illumination that can be recorded by an optical device positioned behind the compressible flow field. From the recorded pattern, conclusions can be drawn regarding the density variations in the flow field. Schlieren method is the most frequently applied one of this group in aerodynamic

and thermodynamic laboratories since it combines a relatively simple optical arrangement with a high degree of resolution. Although the method is suited for compressible flow fields the method may be adopted for use with water where density gradients may be introduced by non-uniform heating.

The third group of visualization techniques is often applied to flows with low average density level such as rarefied gas flows. The foreign substance introduced into the flow field is energy in the form of heat or electric discharge. Fluid elements marked by their increased energy level can be discriminated from the rest of the fluid by optical methods. In some instances, the fluid elements become self-luminous and can be directly observed.

Of particular interest therefore, from the point of view of the present investigation is the first group of flow visualization techniques. Clayton and Massey [125] further classify the methods of indicating flow patterns into static and kinetic methods. Static methods involve the deposition of solids or liquids on boundary surfaces to illustrate the velocity gradient pattern and therefore the pattern of shear stress at a solid boundary. These methods may be used to detect boundary layer separation and transition. Such methods involve attaching tufts to the solid boundary, coating the surface with water-soluble coatings or allowing a dye to ooze from the forward part of the boundary and to flow downstream over the surface.

Kinetic methods on the other hand involve injecting tracer particles in the fluid itself, either in the free stream or in the boundary layer. Such kinetic methods must be used if the characteristics of time dependent flows are to be deduced or when quantitative results are required. Aluminum or lycopodium powder [126], Bakelite powder and air bubbles [127], small spheres of polystyrene [128, 129] and hydrogen bubbles [130, 131] have been used as tracer particles in water flows. Each of these methods has some advantages which render the method suitable for particular applications and some drawbacks which render the method unsuitable for other applications. In what follows only the aluminum tracer method will be considered. The other methods, their advantages and drawbacks are discussed in great detail in references [124, 125].

It was reported [132, 133] that the use of aluminum powder as tracer particles served the purpose admirably and yielded excellent results. Clutter et al. [131] scattered aluminum powder on the surface of water to study the separation of a steady boundary layer at the rear surface of a body of revolution and to visualize the vortex street in the wake of a steadily moving circular cylinder. The same method was used by Prandtl and Tietjens [134] to study flow in channels, past single air foils and isolated cylinders. The method was also used by Wallis and White [135] and Wallis [136] to study flow development in staggered and in-line arrays at the low

flow velocity of about 3 cm/sec. Chester, Halliday and Howes [127] reported that the angle of optimum reflection of the aluminum tracer particles is about 90° to the incident light. This property can be used to an advantage in a channel of rectangular cross section. If the incident light is horizontal, the tracers may be viewed from the top of the channel without significant distortion due to optical refraction of light.

The method is well suited to photography which has become accepted as an important instrument for the scientific researcher. In motion studies, several characteristics of vision limit the usefulness and the effectiveness of the human eye as an optical recording device. Rapid changes in fluids subjected to violent disturbances necessitate the use of photography as a means to "slow down" or to "still" the motion so that it can be analyzed and studied. Aside from making actions appear slower on the screen, permanent records of the events may be stored, duplicated or transmitted and documented for comparison or reference purposes.

4.2 The Flow Visualization Technique

Since one of the main objectives of the present investigation was to study the flow development over a wide range of Reynolds numbers, certain factors had to be considered in the development of the visualization technique. Consideration had to be given to whether or not to conduct the experiments in the presence of a free surface and to other advantages of

using the aluminum powder as tracer particles. Difficulties associated with a free surface has limited the flow velocity in previous investigations [135, 136] to a maximum of 4 cm/sec. Such difficulties are the formation of capillary and gravity surface waves at quite low flow velocities [137]. The problems can be avoided by conducting the experiments in the water tunnel in the absence of a free surface.

Aside from the high degree of light reflectivity of the aluminum powder and its optimum reflection angle of 90°, which can be used to advantage in the rectangular working section of the water tunnel, it has also some other attractive features. Aluminum flakes A9432 produced by Canbro Division of International Bronze Powders Ltd., is specified to give a 20 percent retention on a Tyler 325 mesh, i.e. the particle size is about 0.043 mm. It is relatively easy to inject these aluminum tracers into the water tunnel and to control particle density to keep the quality of the cine-photography constant during tests. Aluminum tracer injection was the least expensive and in preliminary tests no short term difficulties were encountered with aluminum particles adhering to the tubes' surfaces or staining the walls of the plexi-glass test section. The use of aluminum powder as a tracer was found to be the most appropriate in view of the turbulence and unsteady flow conditions [133].

Flow velocity measurements with tracer particles involve the important assumption that the velocity of the

particle and that of the fluid are the same. This is not the case. However, the difference between the particle and the fluid velocity can be reduced and reasonable experimental results can be obtained. The velocity of a tracer particle in a fluid is given by the relation [124]

$$u_p = u_f (1 - e^{-Kt})$$

where

u_p is the particle velocity

u_f is the fluid velocity

t is the time

and

$$K = 18 \mu_f/\rho_p d_p^2$$

μ_f is the dynamic viscosity of the fluid $= 1.005 \times 10^{-3}$ N S/m^2 for water

ρ_p is the particle density = 2699 Kg/m^3 for aluminum

d_p is the particle diameter

The foregoing relation postulates that the particle velocity approaches exponentially the fluid velocity. The smaller the density and the size of the particle, the faster is this approach [124]. According to this relation, an aluminum tracer particle released in a water flow will reach 99% of the flow velocity in 0.0013 sec. It is to be noticed

that the form of the drag coefficient used to arrive at the above relation requires that the particle density be larger than the fluid density and that the particle Reynolds number, given by

$$R_p = \rho_p (u_f - u_p) d_p/\mu_f$$

does not exceed the value of 1 [138]. However, Chen and Emrich [139] have found that the velocity of the particle will approach that of the flow even faster in the case where $R_p > 1$. It is to be also noticed that the above relation describes the particle motion in one coordinate direction only. Cases where particle trajectories are to be determined in two dimensional and three dimensional flow fields or where the particle is entrained in a flow regime exhibiting a velocity gradient are described in some detail by Merzkirch [124] and Somerscales [140].

The sink velocity, or the terminal velocity for a spherical particle dropping through a fluid that is otherwise at rest, is an important parameter to be considered in the selection of the tracer particle's material. It is desirable to keep the tracer particles suspended in the flow during the observation and recording times. The sink velocity as caused by gravity is derived from Stoke's law and is given by

$$V_s = (\rho_p - \rho_f) g d_p^2/18 \mu_f$$

where

V_s	is the sink velocity
ρ_p	is the density of the tracer particle
ρ_f	is the density of the fluid
	$= 998.2\ Kg/m^3$ for water
g	is the gravitational acceleration
d_p	is the diameter of the particle

Having chosen water as the fluid working medium for conducting the experiments, the sink velocity of the tracer particle depends solely on the size of the particle and its material. As was mentioned earlier, the aluminum particles can be manufactured with a diameter of about 0.043 mm which effectively reduces to a great extent the sink velocity and its disturbing influence. Using the above relation, the sink velocity of an aluminum tracer particle in water is found to be 0.0017 m/s.

An effective flow visualization technique for the present study was therefore thought to consist of injecting aluminum tracer particles into the closed water tunnel loop and illuminating a narrow slit in the side of the test section parallel to the main flow. Still and motion picture cameras could then be mounted on a stand on the top of the test section so that still photographs and cine-films could be taken. In what follows, the details of this technique as it was developed and the experimental equipment used will be fully described and discussed.

4.2.1 Tracer Injection Method

About 200 millilitres of aluminum powder were wetted with methyl alcohol and the mixture was vigorously stirred before transferring it to the injection tank. The mixture was then made into an aqueous solution by adding about two and one half litres of water to the tank. The water-alcohol mixture facilitates the injection of the tracer particles and prevents the powder from staining the sides of the transparent plexiglass test section. Immediately before injecting the tracer particles into the test section, the aqueous solution was vigorously stirred again.

The injection tank was made from perspex piping of 152 mm diameter and can safely withstand up to about 400 N/m^2 pressure without rupturing. The tank was fitted with a Bourdon gauge to indicate the inside pressure. A pressure of about 70 N/m^2 was found sufficient to operate the system satisfactorily. The transparency of the tank allowed the aqueous solution level to be visually monitored during the experiments.

When tracer injection is required, the tank is pressurized and a valve used to control the injection rate is opened. The tracers are injected into the test section through a stainless steel dispenser tube, 3.2 mm O.D. and 1.6 mm I.D., positioned 100 mm upstream from the first row of the tube bundle and 50 mm below the upper surface of the test section. The dispenser tube can be moved horizontally inside the test section and can be held stationary at any required

location in its horizontal plane. It can be used as such to direct a stream of tracer particles towards any target region to be further investigated.

4.2.2 The Optical Arrangement

A narrow sheet of light is required over an interior plane normal to the tube axis. A market survey showed that some very expensive illumination systems are available. One of the least expensive is La Tranche Lumineuse manufactured by Techniques des Fluides, a division of Techniques Industrielle de Sogreah in France ~~with~~ an estimated price of $4,000. However, in view of the special requirements of the present study, the decision was made to design a custom lighting system which would be both simple and inexpensive.

A light box 8.25 x 600 x 165 mm was constructed of wood and an asbestos plate 8 mm thick lined its base. The light box housed the light source and the optical arrangement. Its interior was painted flat black to minimize light reflection. The light source was an arrangement of nine Sylvania ELH Tungsten Halogen Projector lamps, rated at 300 watts each and equipped with a polished glass reflector. The lamps can be switched on and off individually through a switch box to control the intensity of illumination as required for proper film exposure.

A plano-convex cylindrical collimating lens machined from 127 mm diameter cast acrylic rod was used in the beginning of the investigation. It provided a thin horizontal sheet of

light needed to illuminate the plane interior of the tube bundle. This lens proved to be quite adequate. However, despite all precautions, the lens failed under the intense heat from the light source. The lens was then replaced by three cylindrical lenses, type PCX, each of 86 mm focal length and 57 x 200 mm in size. They spanned the front end of the light box behind a 10 mm wide slit facing another slit of the same width created on the side of the test section using black scotch tape. A schematic of the light and optical arrangements is shown in figure 4.1. Heat resistant glass plates 6.5 mm thick were placed between the lenses and the projector lamps to protect them from the excessive heat. Four perforated pipes were connected to 690 N/m^2 laboratory air supply to distribute cooling air over the entire length of the test section slit, the lenses and the projector lamps. Furthermore, lights were turned on only when required for the shortest possible period of time in order to minimize the amount of heat generated.

The light sheet's horizontal plane was located 50 mm below the upper interior surface of the water tunnel working section. The normalized upstream velocity obtained in a previous investigation [113], reproduced in figure 3.2, indicated that the boundary layer thickness was less than 25 mm at an upstream flow velocity of 1.15 m/s. Therefore, the illuminated interior horizontal plane of the tube bundle was outside the boundary layer and was not affected by it. The plane thus

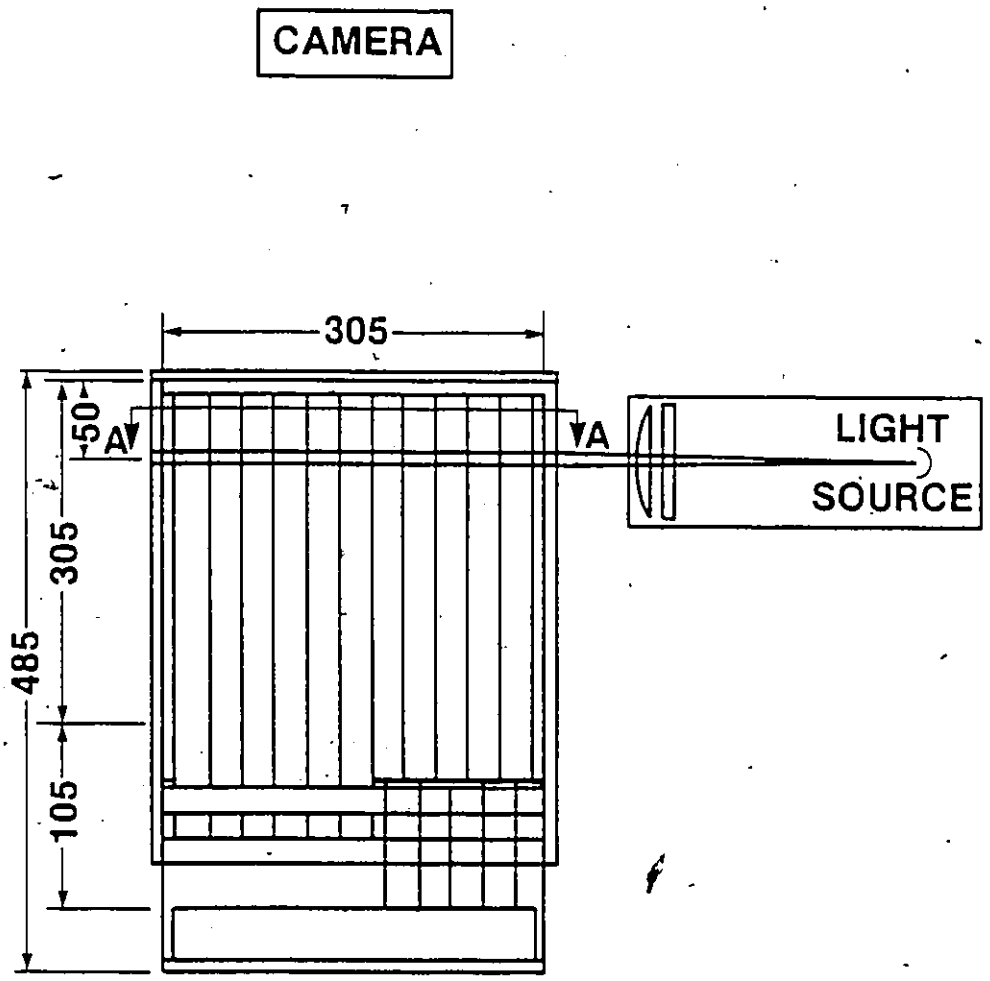

SCHEMATIC
OF TEST SECTION

Figure 4.1 Schematic of the test section and the flow visualization arrangement

located was not too far from the cameras, mounted on the top of the test section, so that the reflected light reaching the film was enough to produce excellent photographic records.

The individual lamps were first arranged in a straight line parallel to the lenses and the test section. This arrangement of lamps resulted in the formation of dark regions between tubes which greatly affected the quality of the photographic records to the extent that the details of the flow in these regions were indistinguishable. The dark regions were a consequence of the total internal reflection of the light rays inside the plexiglass tubes as the angle of incidence exceeds the critical angle. This is illustrated in figure 4.2 using a half tube attached to the wall of the tube bundle. The critical angle or the limiting angle of incidence in the plexiglass denser medium, which results in a 90° angle of refraction in water, the less dense medium, can be calculated from Snell's law

$$n_1 \sin \theta_1 = n_2 \sin \theta_2 = n_2 \sin 90 = n_2$$

where,

n_1 is the refractive index of the plexiglass = 1.49

n_2 is the refractive index of the water = 1.33

therefore,

$$\sin \theta_1 = \frac{n_2}{n_1} = \frac{1.33}{1.49} = 0.89$$

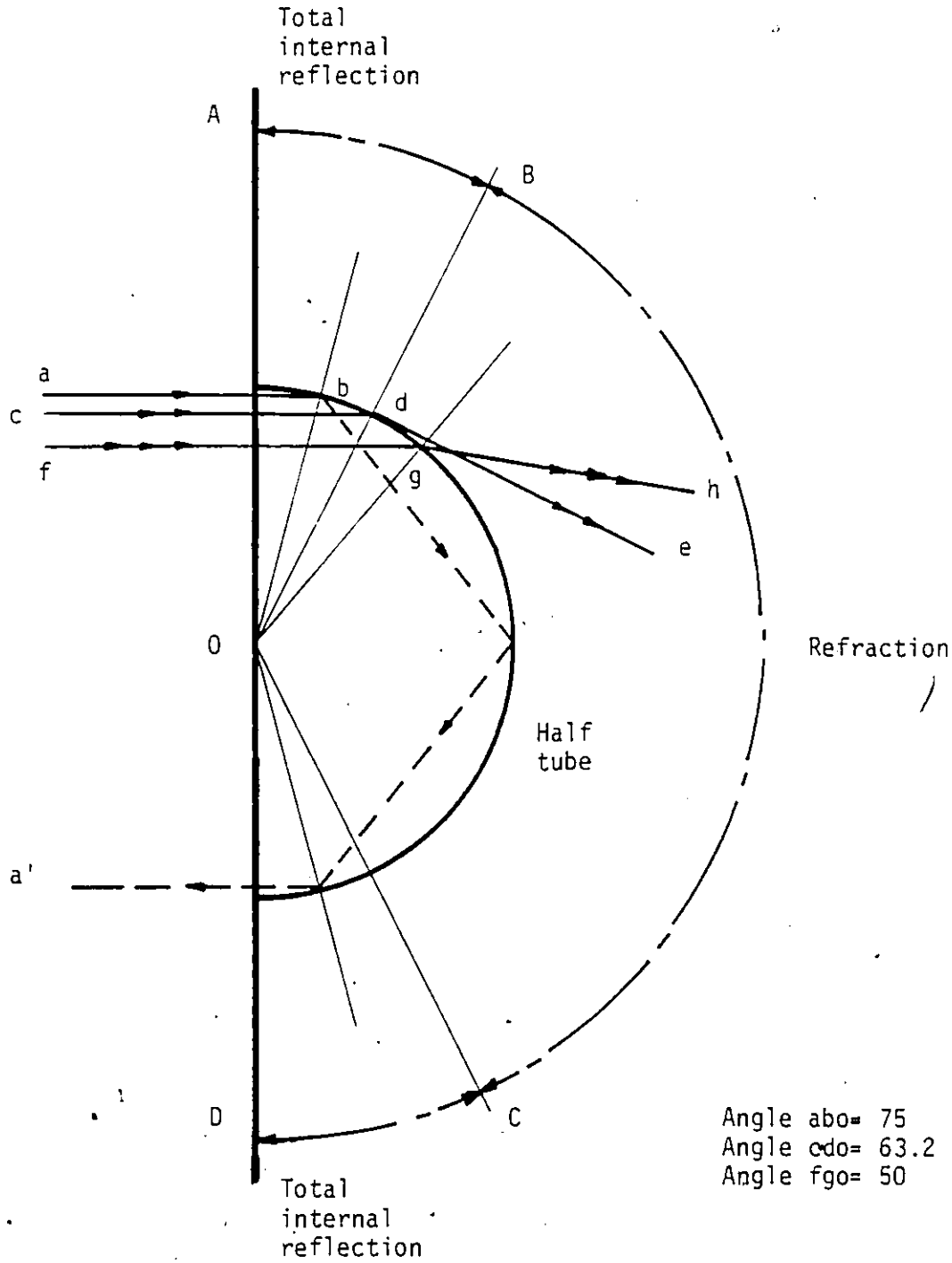

Figure 4.2 Reflection and refraction of incident light

The critical angle $\theta_1 = 63.2^{\circ}$.

Consequently, as shown in figure 4.2, the regions AB and CD are regions of total internal reflection corresponding to the dark regions mentioned above. In the region BC the incident light will be refracted in the water and refracted again as it becomes an incident light on another plexiglass tube. Hence, one can see the pattern of dark and bright regions developing around the individual tubes. As the bundle vibrates and the flexible tubes change their position the pattern is altered, however, these dark and bright regions persist. The problem was alleviated by moving the individual lamps around until the dark regions disappeared and a homogeneously illuminated flow field inside the bundle was achieved. The position of the individual lamps had to be adjusted when the second bundle configuration was used.

4.2.3 Still and High-Speed Photography

It was stated earlier that the aluminum tracer particles reflect the incident light at a 90° angle and that that property can be used to advantage in the rectangular working section of the water tunnel. Accordingly, still and movie cameras used for image recording were securely bolted to a cantilevered arm of a specially built rigid stand over the test section. The cantilevered arm can be raised and lowered in a vertical plane thereby allowing different degrees of magnification to be achieved. It can also swing in a horizontal plane, thus specific regions of interest can be photographed.

The cine-films were taken using LOCAM model 51 high speed motion picture camera equipped with 25 mm f 1.1 wide angle lens. The camera is capable of speeds up to 500 frames per second and is furnished with a double disc variable shutter adjustable from 0 to 160 degrees. The high image frequency required to resolve the fast motion of the flow and the tubes was therefore readily available and the short exposure time of each single image required to avoid blurring of the recorded image can be chosen. Before any films were taken, the camera was checked and certified by an authorized dealer to ensure that the camera was in good working order and that it met the manufacturer's specifications with regard to the accuracy of the shutter speeds and the precision of the framing rates.

Cine-film photography was accomplished using Kodak Plus-X negative film type 7231 having a speed rating of 64 ASA in sunlight. Its adequate speed and fine-grain negative material made the film well suited to interior photography and to exterior photography under average lighting conditions.

Still photography was done using a Graflex camera equipped with 135 mm, f 1: 4.7 lens, capable of up to 0.002 sec exposure time. Still photographs were taken using plus-X pan, 4 x 5 negatives which combine fine-grain, high resolving power and excellent sharpness in enlargement characteristics. Tri-X pan 4 x 5 negatives were also used in the course of the experiments, and excellent results were obtained using both types.

An overall view of the water tunnel and the photographic arrangement is given in figure 4.3.

4.3 Experimental Procedure and Results

4.3.1 Velocity Measurement

The first step in the experimental procedure followed here was to calibrate the by-pass line rotameter using the flow visualization technique. A good agreement between the calibration curve thus obtained and a calibration curve done in a previous study [113] using a pitot static probe will lend credibility to the new method. The established method can then be applied with confidence to measure the flow velocity in the range 0-100 GPM where the rotameter is not graduated. With the rotated square array assembled in the test section, tracer particles were released into the water stream. The ciné-camera was mounted on the top of the test section to photograph the tracer particles at a point 100 mm upstream from the tube bundle. For each discharge setting of the rotameter tried, at least one hundred randomly chosen streaks were measured and averaged to arrive at the corresponding mean flow velocity. The calibration curve obtained using this method is given in figure 4.4 together with that done in the previous investigation [113]. The agreement between the two curves is reasonable as the percentage difference between the velocities obtained from the two curves at the maximum flow rate attained in the present investigation is about 6%. This indicates that the new method can be used successfully to obtain an

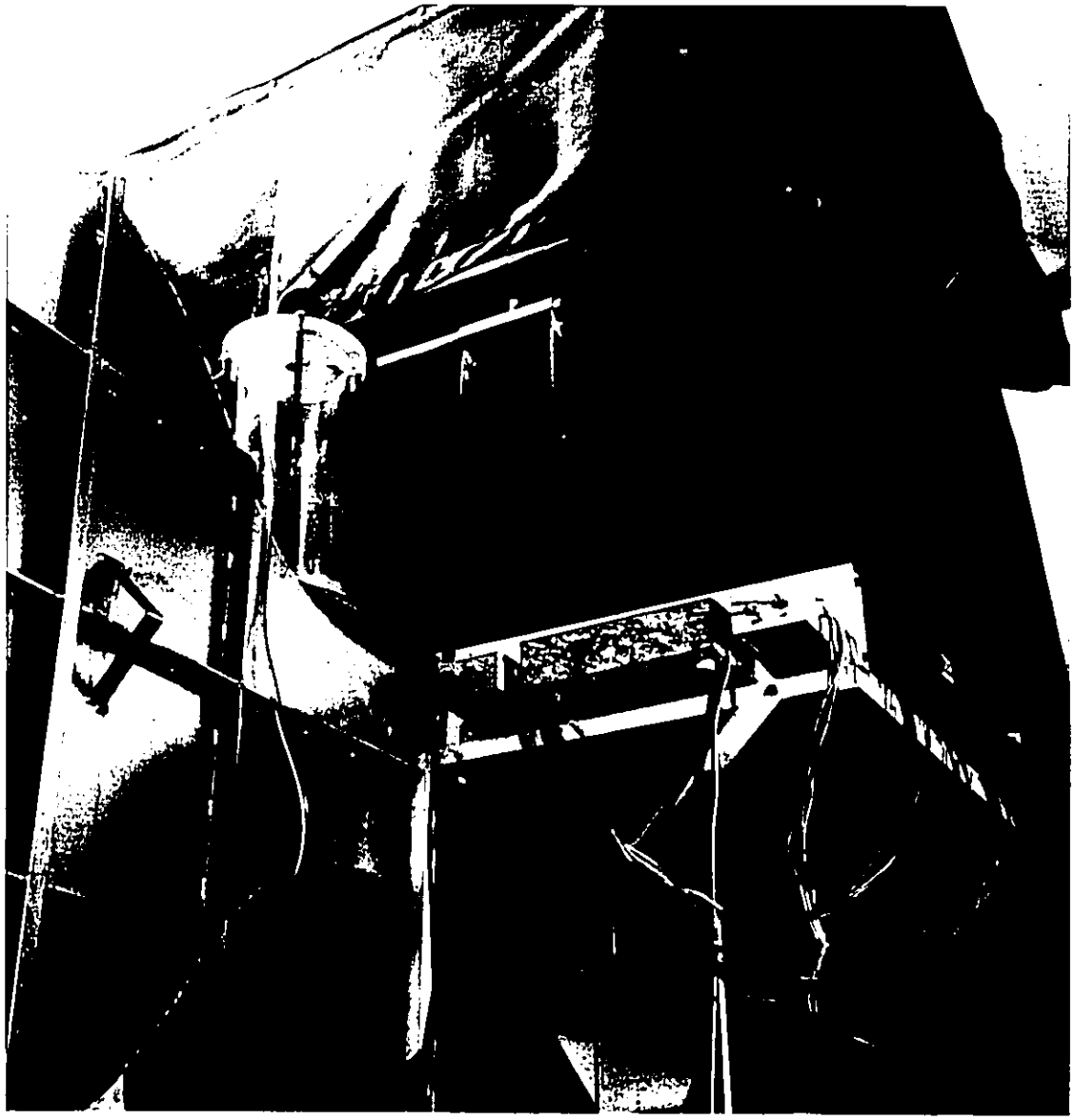

Figure 4.3(a)

Figure 4.3(b)

Figure 4.3 An overall view of the water tunnel and the photographic arrangement

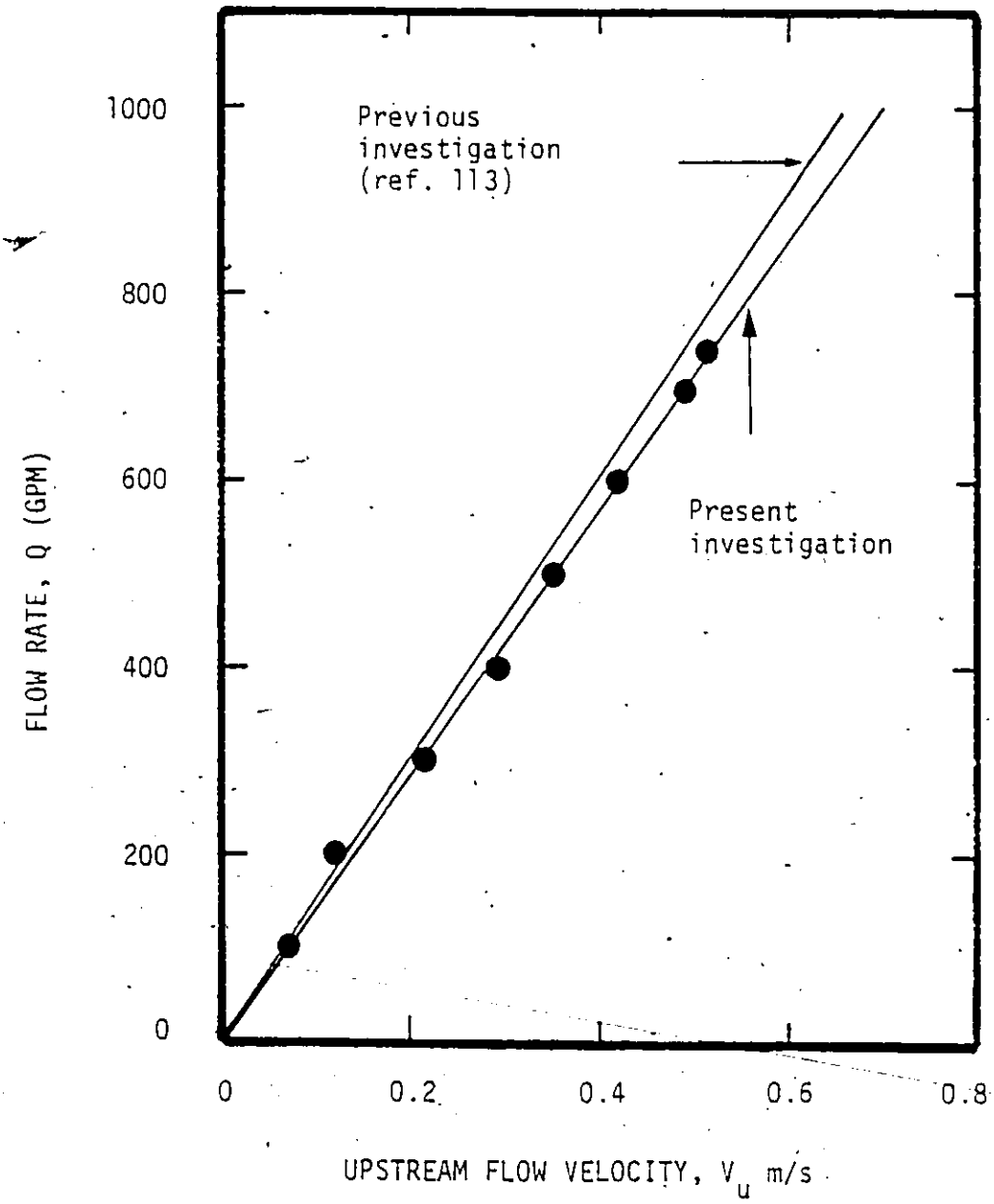

Figure 4.4 Calibration curves of the by-pass line flow meter

average value for the upstream flow velocity.

It is not a simple task to measure the upstream flow velocity accurately in the test section. Some researchers have found it difficult to do so as the velocity distribution over the test section is not uniform [21, 101, 104]. In the present investigation while preparing to measure the upstream flow velocity by photographing the tracer particles in the test section upstream from the tube bundle in the flow velocity range $V_u < 0.07$ m/s, it was visually observed that the tracer particles' velocities were not constant. The particles speed up and slow down as they advance towards the tube bundle. Films taken in this velocity range were projected onto a screen and viewed frame by frame. With the proper framing rate, a particle tracer is seen as a streak and the particle velocity can be computed from the measured streak length, and known framing rate. If the streaks of a series of particles are traced on the screen from a number of successive frames, the particles' trajectories can be seen as well as the fluctuations in their velocities. Measurements of the streaks in the respective parallel paths have shown that the individual particles advanced into the test section with practically the same speed. However, calculations have shown that the speed of an individual particle is not constant along its path but varies with time. Such variations in the speed of a particle are depicted in figure 4.5 at a flow rate where discrete vortex structures were formed and shed in the interior of the rotated square array. The uncertainty in measuring the

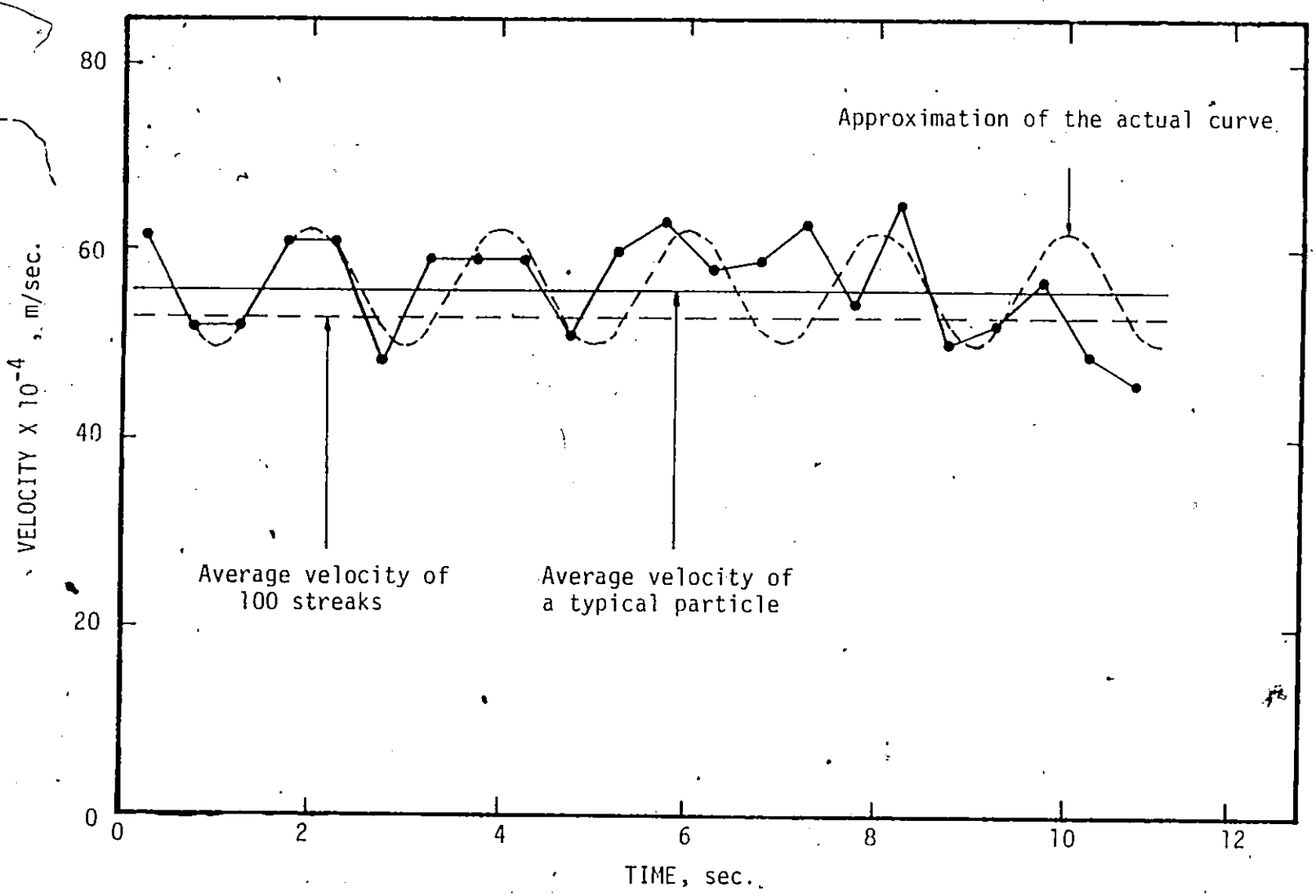

Figure 4.5 Variations in the speed of a tracer particle

streak lengths is about 3%. By following several particles at different flow rates, it was found that the maximum difference between the average particle velocity and the average flow velocity was about 6%. This difference is attributed to the relatively short period of time over which a particle was followed and traced. The average flow velocity was calculated by measuring at least 100 streaks chosen at random as was discussed earlier. The idealized speed curve of the tracer particle given in figure 4.5 is sinusoidal and indicate that the frequency of speed variation is about 0.5 Hz.

The velocity fluctuations of the tracer particles caused some concern and it was decided to further investigate the origin of these fluctuations. It was considered especially desirable to demonstrate that the fluctuations were not induced by extraneous excitation in the flow loop as this could adversely affect the flow behaviour in the test section. The pump impeller has six blades and the pump shaft was rotating at about 428 RPM at the time of the test. Therefore, the frequency of oscillations the pump would impart to the flow is about (428 x 6)/600 = 42 Hz. Since the frequency of velocity fluctuations indicated by the idealized curve was 0.5 Hz, the pump cannot be considered as a source of such fluctuations. The rotated square array was then removed from the test section to see whether or not the velocity fluctuations will persist. Visual observations revealed that the motion of the tracer

particles was smooth and that the periodic velocity fluctuations of the particles as they advanced in the test section had completely disappeared. Furthermore, when the square in-line array was assembled into the test section, visual observations revealed that such oscillatory motion of tracer particles upstream from the bundle was nonexistent. It should be mentioned that the formation and shedding of discrete vortex structures at such low flow velocities in the main stream flow is intense in the rotated square array while no coherent vortex shedding was observed in the square in-line array as is evident from the results that will be presented in Chapters 5 and 6.

The speed of a tracer particle, given in figure 4.5, corresponds to the photograph of figure 6.4 taken at the Reynolds number $Re_g = 320$. It also corresponds to point (A) in figure 6.10 where the calculated frequency of vortex shedding inside the tube bundle as determined from a cine film is $f_c = 0.46$ Hz. It can be seen from figure 4.5 that the frequency of velocity fluctuations is about 0.5 Hz which agrees well with the value of $f_c = 0.46$ Hz. The close agreement suggests that the velocity fluctuations upstream of the test section are caused by the vortex shedding in the tube bundle. Furthermore, these periodic velocity fluctuations in the upstream flow were no longer observed at Reynolds numbers above about $Re_g = 1000$ where discrete vorticity in the tube bundle ceases to exist.

4.3.2 Practical Considerations

The key to successful utilization of the photographic technique to analyze motion is to decide what information is required? The answer to this question comes mainly from analyzing the data obtained from the spectral records of tube motion and the phenomena that characterize the velocity amplitude curves. However, more often than not, critical visual observations of the developing flow regimes at different flow velocities also reveal some interesting and sometimes unexpected developments in the flow field. A case in point is the detection of a laminar separation bubble at low Reynolds number in the interior of the rotated square array as will be shown in Chapter 6. Without such visual observations, the flow regimes developed at low Reynolds numbers in both arrays tested here, could have never been detected and recorded.

Once the phenomena to be photographed and the corresponding flow velocities are selected, the exposure times and the shutter speeds of still and cine-cameras can be determined. The regions of interest inside the tube bundles can be targeted and the degree of magnification of these regions can be decided upon. The effective photographic analysis of the vibrational motions of the tubes or the periodic phenomenon of vortex shedding depends greatly on the picture-frequency chosen to record these events. To ensure an accurate photographic record of such cyclic phenomena, the picture-frequency should exceed the frequency of these events by a factor of

3 to 10 depending on the sensitivity requirements of the ensuing analysis [141].

4.3.3 Photography

Whenever photography was contemplated, the dispenser tube was extended into the test section and the aluminum tracer particles were injected into the water flow. A SIXTOMAT electronic exposure meter was used to monitor the light reflected from the aluminum particles. Experience has shown that the best photographic results were obtained when the light meter reading was between 11.5 and 12.5. Before photography was attempted, the dispenser tube was retracted to the wall of the test section and a waiting period of about five minutes was allowed for any extraneous disturbances to subside and to arrive at a steady state. The light meter reading was then taken for the selection of a suitable exposure combination of apertures and shutter speeds. Guides for the photographic methods of taking still photographs and cine-films are included in the appendices B and C.

Photography was done in the absence of light from any source except the light box. To prevent any extraneous light from reaching the test section, a specially tailored black curtain surrounded the working area during photography. This greatly enhanced the quality of the still photographs and the cine-films thus obtained. The 4 x 5 negatives of the still camera were processed in the darkroom using Kodak developer D-76 and Kodak fixer with an average developing time of about

8-9 minutes. The still photographs were then printed as specified by Kodak for an average contrast.

CHAPTER 5

THE SQUARE IN-LINE ARRAY RESPONSE

5.1 Introduction

In this chapter, the results obtained in investigating the square in-line array will be presented, discussed and compared with the results of other similar arrays available from the literature. The overall RMS amplitude response curves of tube no. 5 and tube no. 8 are given in figure 5.12. With reference to this figure, the presentation of the results is divided into four sections based on an identification of four different flow regimes. In section 5.2, the interstitial flow structure in the flow velocity range $V_u < 0.07$ m/s, part OA of the curves is examined. Tube response in this flow velocity range is negligible, hence the RMS amplitude responses were not measured. The flow characteristics which were observed in this Reynolds number range are identified and compared with those of an isolated circular cylinder in a cross flow. Section 5.3 deals with the turbulent response of the monitored tubes, in the flow velocity range 0.07 m/s $< V_u <$ 0.15 m/s, part AB of the response curves. Vorticity response of both monitored tubes in the flow velocity range 0.15 m/s $<$ $V_u < 0.35$ m/s, part BC of the response curves, is presented and discussed in section 5.4. In section 5.5, the fluidelastic response in the flow velocity range 0.35 m/s $< V_u < 0.44$ m/s,

part CD of the response curves, is dealt with.

The interstitial flow structure in a fully rigid bundle is also investigated using the flow visualization technique, in the flow velocity range 0.15 m/s $< V_u <$ 0.44 m/s. A comparison between the interstitial flow structure of the flexibly mounted bundle and the fully rigid one is given in sections 5.4 and 5.5. The comparison illustrates the important effects of the relative motion between tubes.

In this array, the flow velocity between two tubes in the first row, V_T, is equal to the pitch velocity, V_p. Both are related to the upstream flow velocity, V_u, as shown in figure 5.3 by:

$$V_T = V_p = \frac{P}{P-d} V_u$$

where,

the tube pitch $P = 38.1$ mm

the tube diameter $d = 25.4$ mm

Accordingly,

$$V_T = V_p = 3V_u$$

5.2 Flow Developments at Low Reynolds Numbers

Very few studies have been devoted to investigating the interstitial flow structure in tube bundles at low Reynolds numbers. Tube bundle dynamics rather than fluid flow dynamics have received the attention of most researchers in this field. The important aspect of most investigations has been to

develop the much needed criteria for vorticity and fluid-elastic response at higher Reynolds numbers, to help heat exchanger designers with their task. Tube response at low Reynolds numbers is negligible. Therefore, from the viewpoint of tube bundle dynamics, such an investigation is not warranted. However, from the point of view of understanding the flow development in heat exchanger tube bundles and hence the nature of the tube excitation mechanisms, a study of low Reynolds number flows becomes worthwile. Such a study also allows comparison between flow development in a tube bundle and that around an isolated cylinder. The latter has received a lot of attention in the technical literature.

Consequently, with the tube bundle mounted in the test section, the flow velocity was gradually increased from zero. Changes that occurred in the structure of the interstitial flow were observed from the top of the transparent test section as described in Chapter 3. It was found that a number of flow regimes could be distinguished as a function of Reynolds number in this Reynolds number range. The upper and lower limits of each regime were not well defined and therefore, the transition Reynolds numbers separating the different flow regimes should be considered approximate. Within a range of Reynolds numbers that define a flow regime, several observations were made at different flow velocities. Whenever it was considered instructive, the flow behaviour was photographed and the films and photographs were later studied. In what follows

an account of these flow regimes and the corresponding approximate Reynolds number ranges in which they developed will be given. Whenever it is considered illustrative, photographs will be included to show the features of the different regimes.

Up to a Reynolds number, based on the pitch velocity, of $Re_p \approx 120$, a regime of separated flow with almost stagnant wakes developed. The approaching flow accelerates as it streams around the first row of tubes and enters the tube bundle. Well defined straight flow lanes were formed as the accelerated laminar flow travelled deep into the bundle. Shear layers separated from the shoulders of the tubes in the successive rows and reattached nearly tangentially to the shoulders of the downstream tubes. Wide wakes developed between the successive tube rows with little entrainment of flow into them. The width of each of these wakes is about a tube diameter. The shear layers at the edges of the flow lanes appear reasonably stable. The photograph of figure 5.1, taken at a flow velocity corresponding to a Reynolds number $Re_p \approx 105$, illustrates the essential features of this flow regime. The first three rows of the bundle appear in this photograph and in the photographs which follow. The main stream flow in the flow lanes is moving from left to right.

A regime of unseparated flow which develops behind an isolated cylinder in the Reynolds number range $Re < 5$ was not observed in this tube bundle. It appears that the

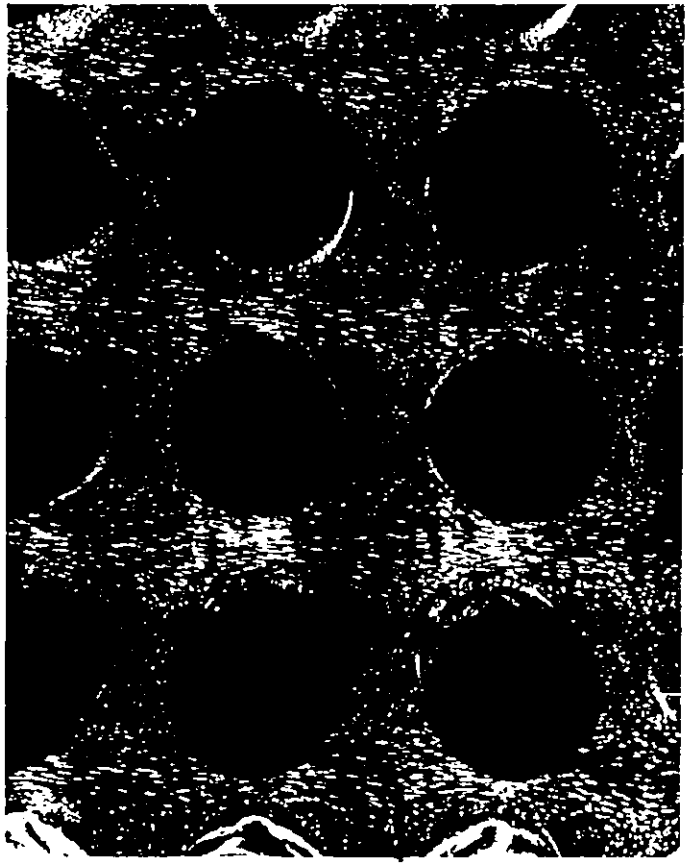

Figure 5.1 Flow Visualization at $Re_p = 105$

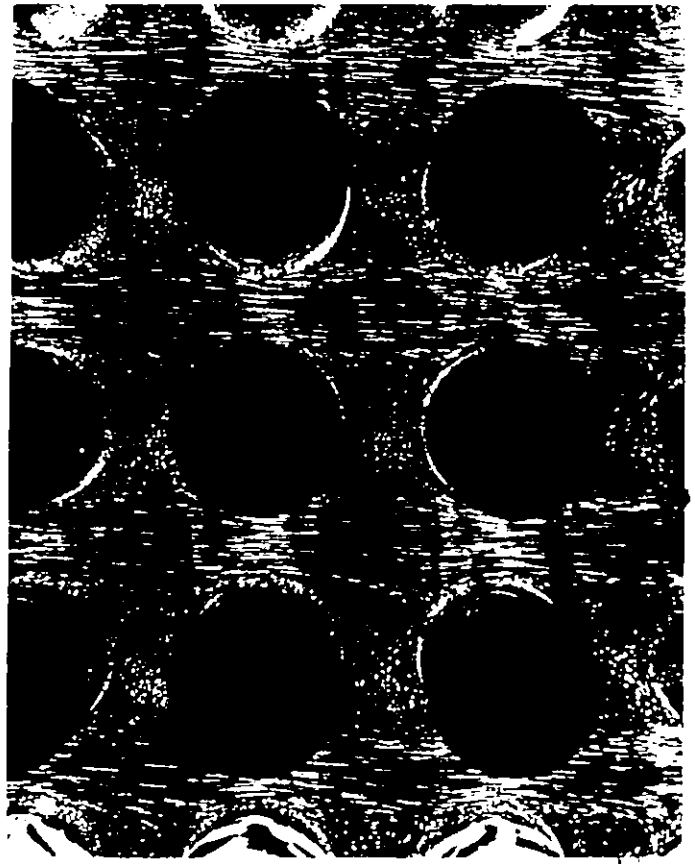

Figure 5.2 Flow Visualization at $Re_p = 135$

proximity of the downstream rows as well as the square pattern of the tube arrangement, have prevented the formation of such an "ideal" flow regime. Information about the regimes pertient to an isolated circular cylinder were derived from reference [3] and presented in Chapter 2. A comparison between the flow regimes found in the square in-line array and those formed in the wake of an isolated circular cylinder is given in figure 5.9.

In the Reynolds number range $120 < Re_p < 400$ a pair of stable vortices similar to the Foppl vortices found behind an isolated cylinder was seen to develop in the wakes of the tubes. The photographs of figures 5.2 and 5.3, taken at flow velocities corresponding to Reynolds numbers $Re_p = 135$ and $Re_p = 330$, illustrate the development of these vortices. In the photograph of figure 5.2, the pattern of the two standing vortices can be barely detected. In the photograph of figure 5.3 the two standing vortices are clearly visible. This is due to increased circulation which resulted in a larger size and more coherent vortex structure. The circulation in the upper vortex behind a cylinder is in the clockwise direction while that in the lower vortex is in the counter clockwise direction.

For an isolated cylinder in a cross flow a pair of Foppl vortices is found in the wake of the cylinder in the Reynolds number range $5 < Re < 40$. It can be concluded that the proximity of the downstream tube rows as well as the square

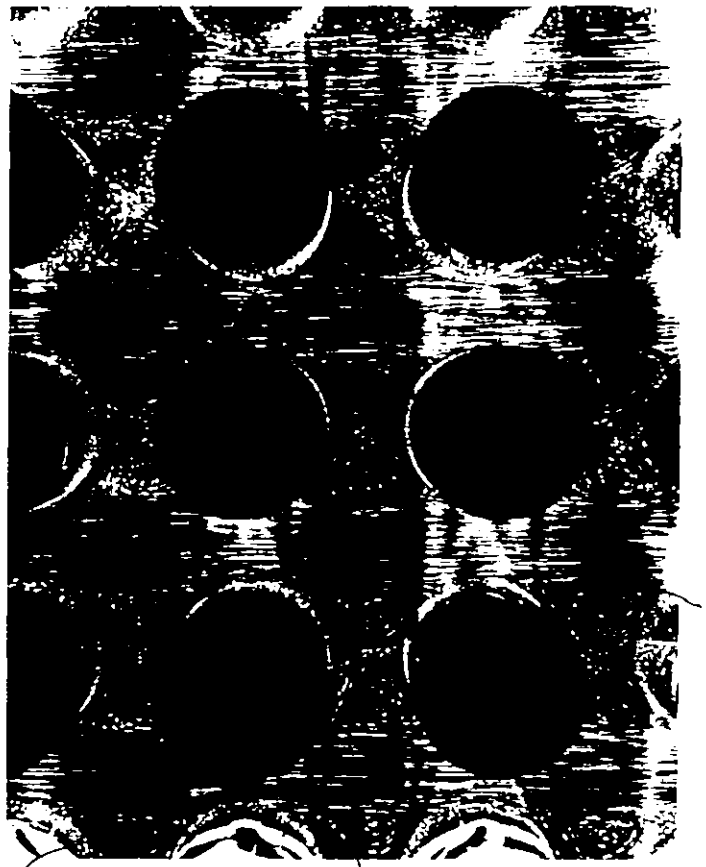

Figure 5.3 Flow Visualization at $Re_p = 330$

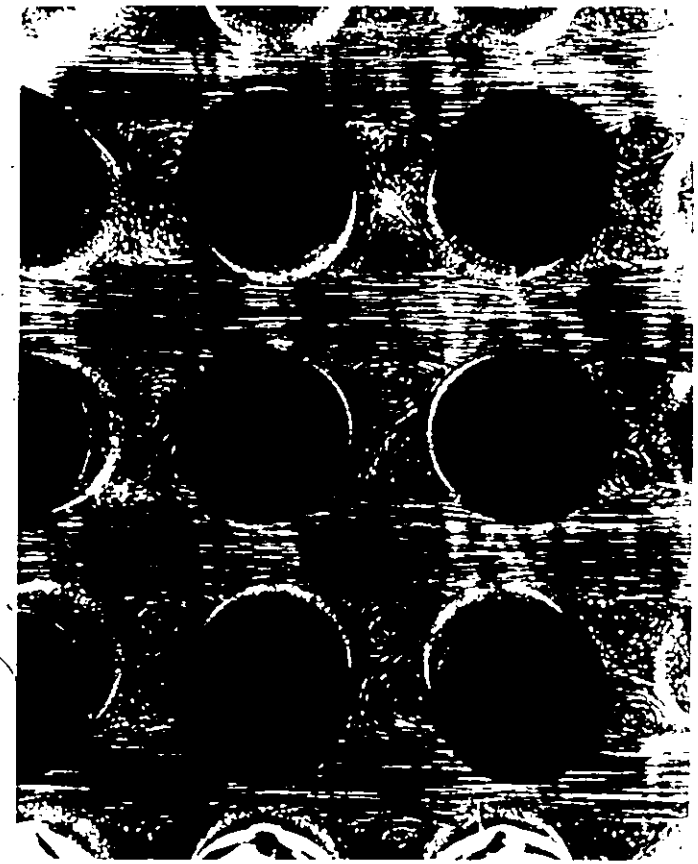

Figure 5.4 Flow Visualization at $Re_p = 550$

pattern of the tube arrangement, caused not only a delay in forming the standing vortices, but also stretched the range of Reynolds numbers over which this regime persisted. The laminar alternate vortex street formed behind an isolated circular cylinder in the Reynolds number range $40 < Re < 150$ was not observed in the tube bundle, undoubtedly due to the proximity of the downstream tube rows.

In the Reynolds number range $400 < Re_p < 550$, the standing vortices in the wakes of the tubes become unstable, and the wakes become turbulent. The photograph of figure 5.4, taken at a flow velocity corresponding to a Reynolds number $Re_p = 550$, illustrates such development. The upper vortices behind tubes no. 2, 3, 5 and 6 entrain more flow from the adjacent main stream. The additional flow travels across the wake and leaves the wake region tangentially to the neighboring flow lanes. Some of these vortices are drawn randomly into the main stream with the result that the vortices in the wake of a tube are generally not of the same size. However, the main stream flow in the flow lanes appears practically unaffected by such activities taking place in the wakes of the tubes.

For an isolated circular cylinder, transition to turbulence in the free shear layer takes place before rolling up into turbulent vortices in the Reynolds number range $150 < Re < 300$. Thus the formed vortices are turbulent from their creation. It appears that a transition to turbulence within the confinement of the tube bundle is delayed somewhat

in comparison with that for an isolated cylinder.

In the Reynolds number range $550 < Re_p < 1000$, well developed turbulent vortices continue to be found in the wake of the tubes. However, random ingestion of these vortices into the flow lanes causes the main stream flow to separate from the shoulders of the tubes. It reattaches again when the turbulent eddies have passed the tubes. The main stream flow in the flow lanes is increasingly influenced by such random injection of turbulent eddies. With increasing flow velocity in this Reynolds number range, the main stream flow becomes irregular, having a random undulating form whenever it passes the wake regions. Such developments are illustrated by the photographs of figures 5.5 and 5.6 taken at flow velocities corresponding to the Reynolds numbers $Re_p = 660$ and $Re_p = 870$.

Above the Reynolds number $Re_p = 1000$, a coherent vortex structure ceases to exist in the wakes of the tubes. The wakes are fully turbulent as can be seen in the photograph of figure 5.7. Wake flows, upon leaving the wake regions, deflect the neighbouring main stream flows towards the next tube column as can be seen, for example, behind tube no. 5. The wake flow escapes through the gap created between the deflected main stream flow and tube no. 8. Some of the escaping flow will find its way to the wake of this tube. The deflected main stream flow collides with the upstream side of tube no. 7, thereby forcing some of the main stream flow into the wake of tube no. 4. Again no regular pattern for the

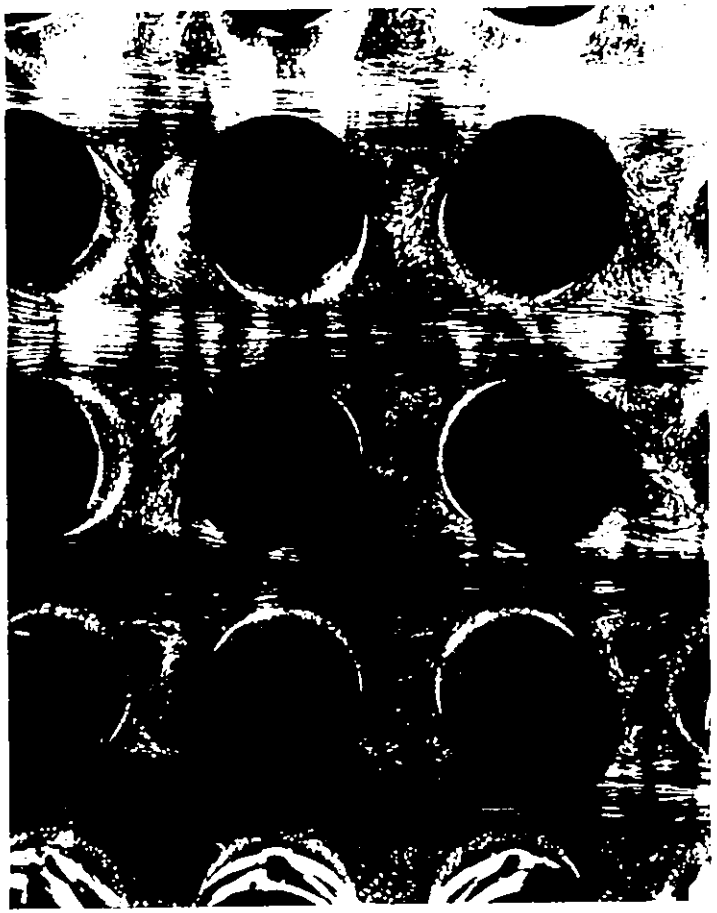

Figure 5.5 Flow Visualization at $Re_p = 660$

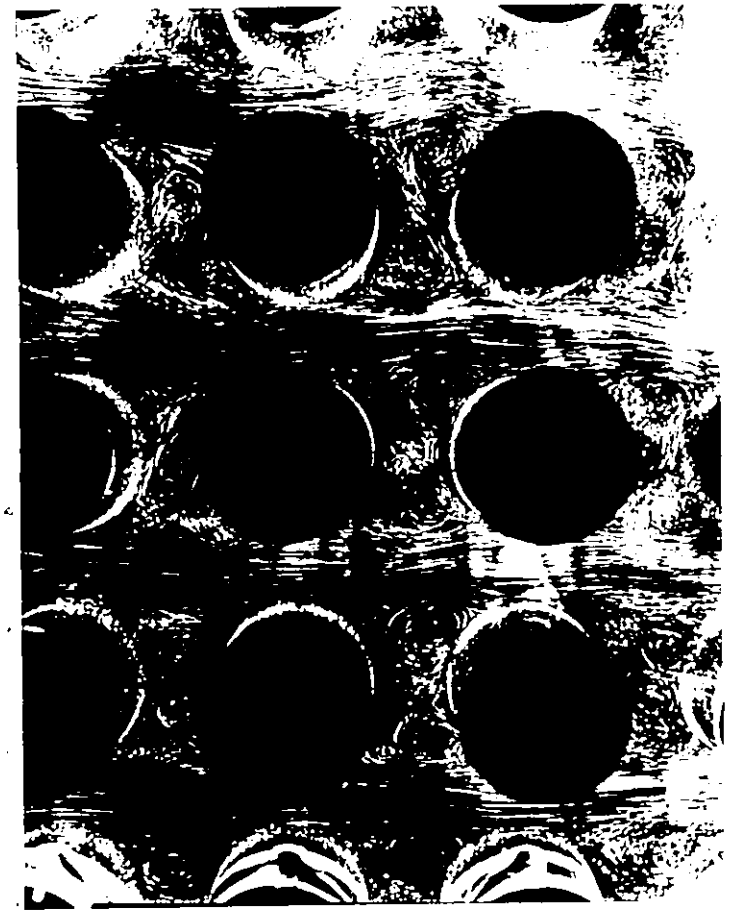

Figure 5.6 Flow Visualization at $Re_D = 870$

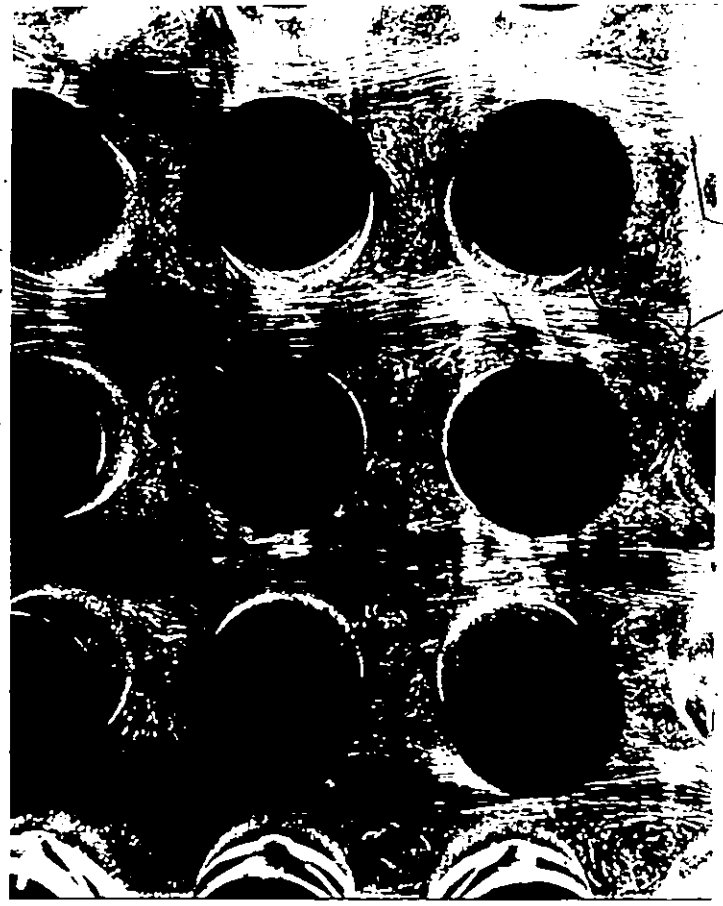

Figure 5.7 Flow Visualization at $Re_p = 1470$

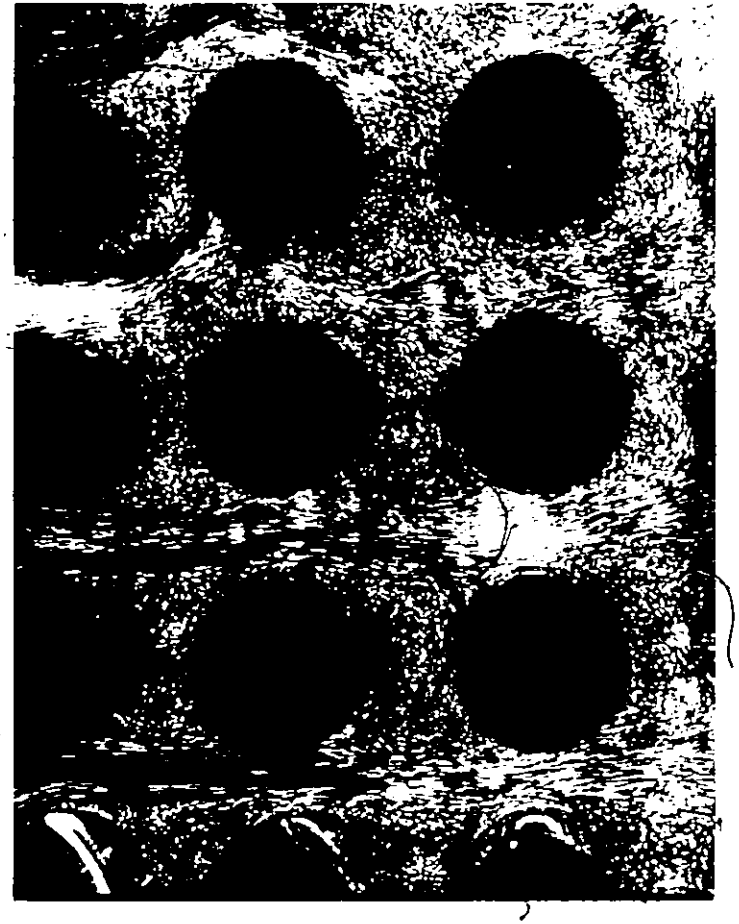

Figure 5.8 Flow Visualization at $Re_n = 5.23 \times 10^3$

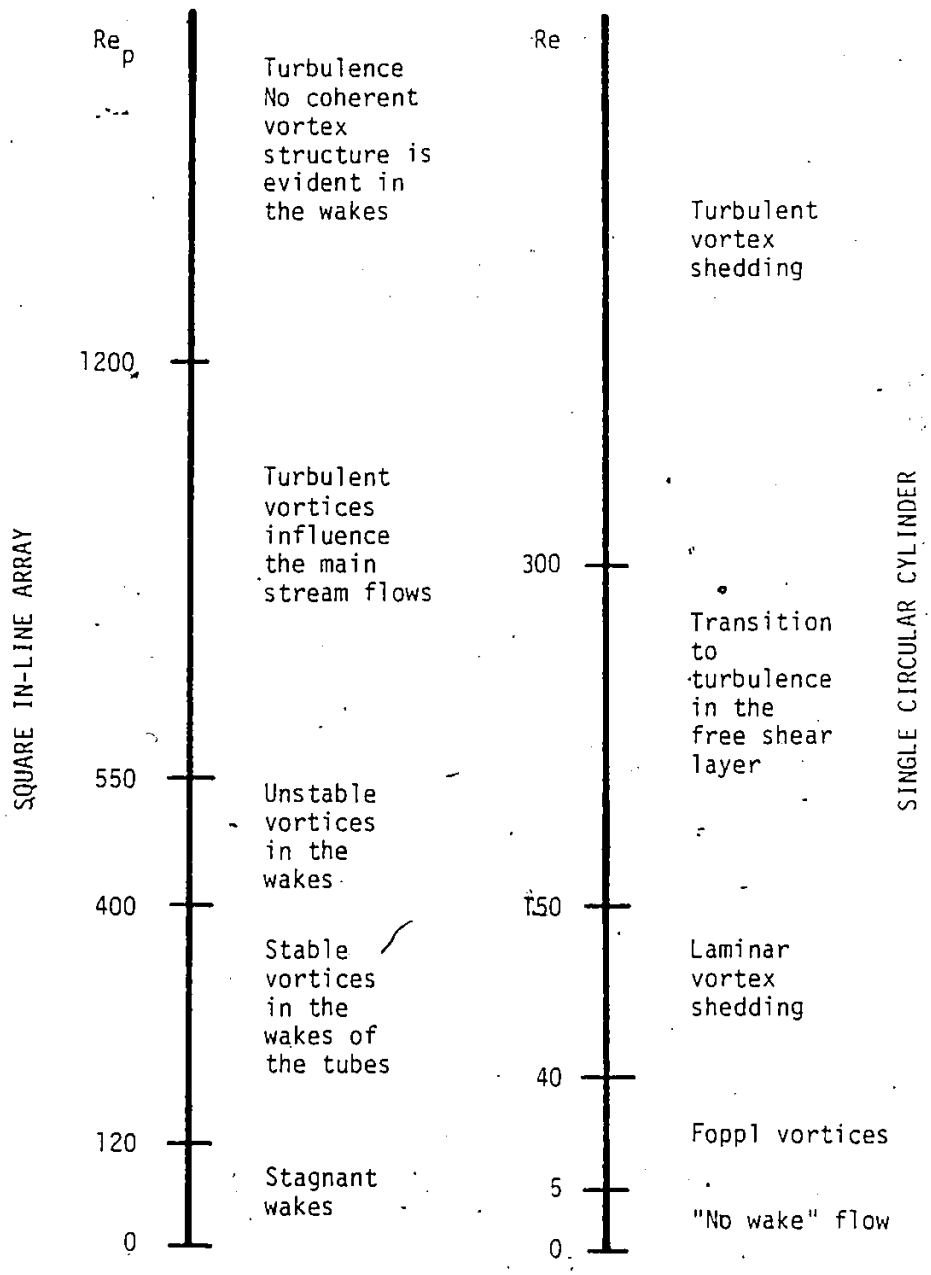

Figure 5.9 Comparison between the flow regimes behind an isolated cylinder and those found in the square in-line array

occurrence of this process can be identified, the process being random in nature. Increasing the flow velocity brings about increased turbulence in the main stream and the wake flows as they interact. This is documented in a cine-film and clearly seen in the photograph of figure 5.8 taken at a flow velocity corresponding to the Reynolds number $Re_p = 5.2 \times 10^3$. The main stream flow emerging from the gap between tube no. 1 and tube no. 2 in this figure, is deflected by the turbulent wake flow behind tube no. 2. As a consequence, the main stream flow impinges on the upstream side of tube no. 4 and more of the main stream flow is ingested into the wake of tube no. 1. This transverse flow deflects the main stream flow on the other side of tube no. 4. Much of that flow is recirculated in the wake of this tube. A great deal of this type of transverse flow occurs randomly at these high Reynolds numbers such that the well defined main stream flows seen at lower Reynolds numbers, practically cease to exist.

In the Reynolds number range $300 < Re < 3 \times 10^5$, a regular turbulent alternating vortex street is formed behind an isolated circular cylinder. It would appear that the proximity of the downstream tube rows in the square in-line arrangement has prevented the formation of such turbulent vortex streets inside this tube array.

5.3 Response of the Monitored Tubes to Turbulence

The response of both monitored tubes to flow excitation

were essentially the same. Consequently, the results pertaining to both monitored tubes will be presented simultaneously.

The response amplitudes in the streamwise and transverse directions are drawn against the upstream flow velocity for tube no. 5 in figure 5.10, and for tube no. 8 in figure 5.11. The overall RMS amplitude, calculated as the square root of the sum of the squares of the response amplitudes in both directions, is drawn against the upstream flow velocity for tube no. 5 and tube no. 8 in figure 5.12. The lowest data points do not show increasing tendency with flow velocity suggesting that it is mostly signal noise. Hence the lines have been extended to zero ignoring these points.

In the flow velocity range 0.07 m/s < V_u < 0.15 m/s, both monitored tubes respond randomly to turbulence in the wakes and in the main stream flow of the flow lanes surrounding them. The amplitude response is small and primarily in the streamwise direction. The spectra of figures 5.13, recorded at V_u = 0.15 m/s, show the range of the fluid coupled natural frequencies induced by turbulence in the response of tube no. 5. The natural frequency range extends approximately from 14.5 Hz to 21.3 Hz. For tube no. 8, similar frequency spectra recorded at the same flow velocity show that the frequency range extends from 14.6 Hz to 21.4 Hz. The response spectra in this flow velocity range do not show any obvious vorticity generated spikes in the frequency range below the fluid coupled natural

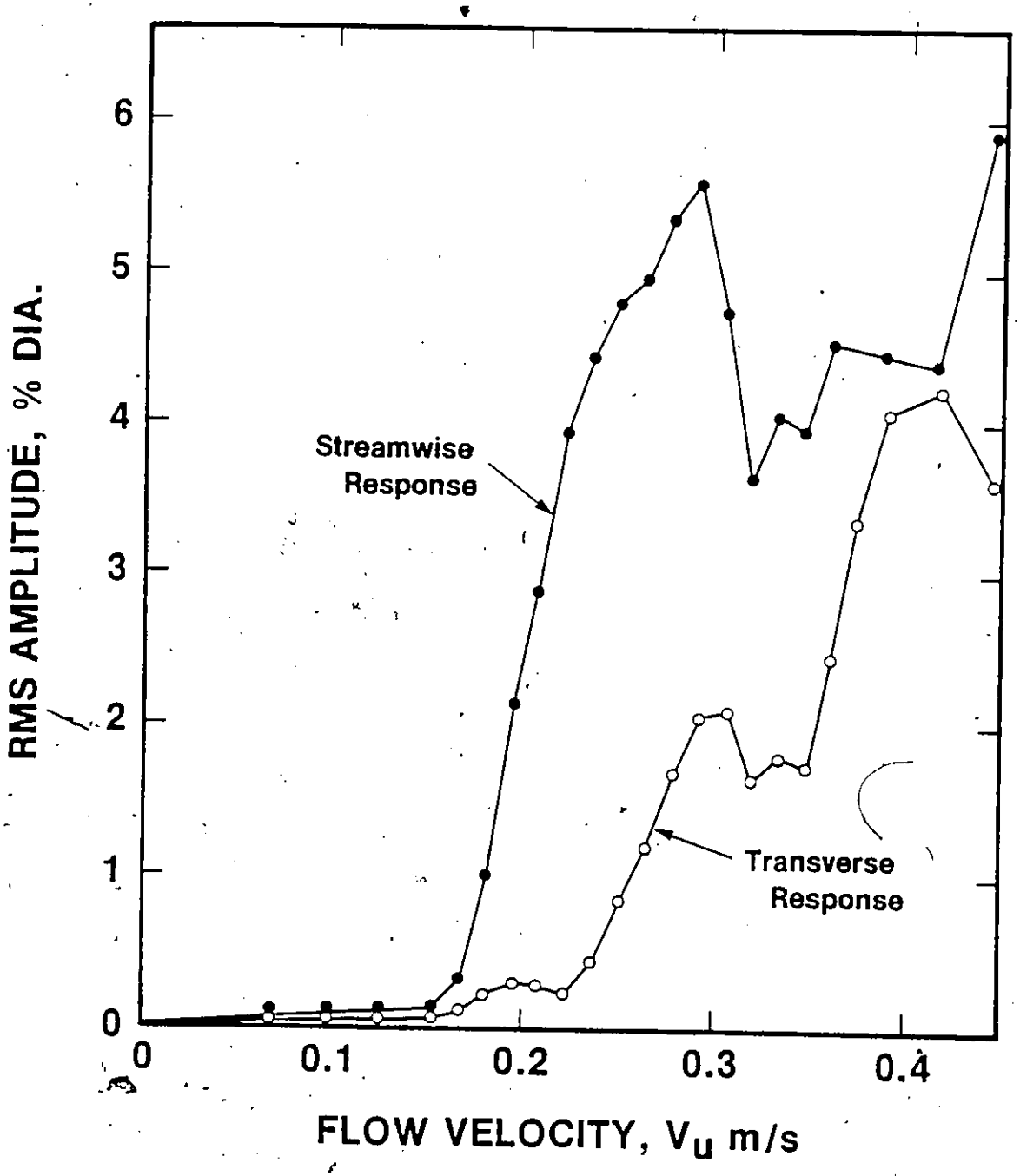

Figure 5.10 Response of tube no.5 in the second row

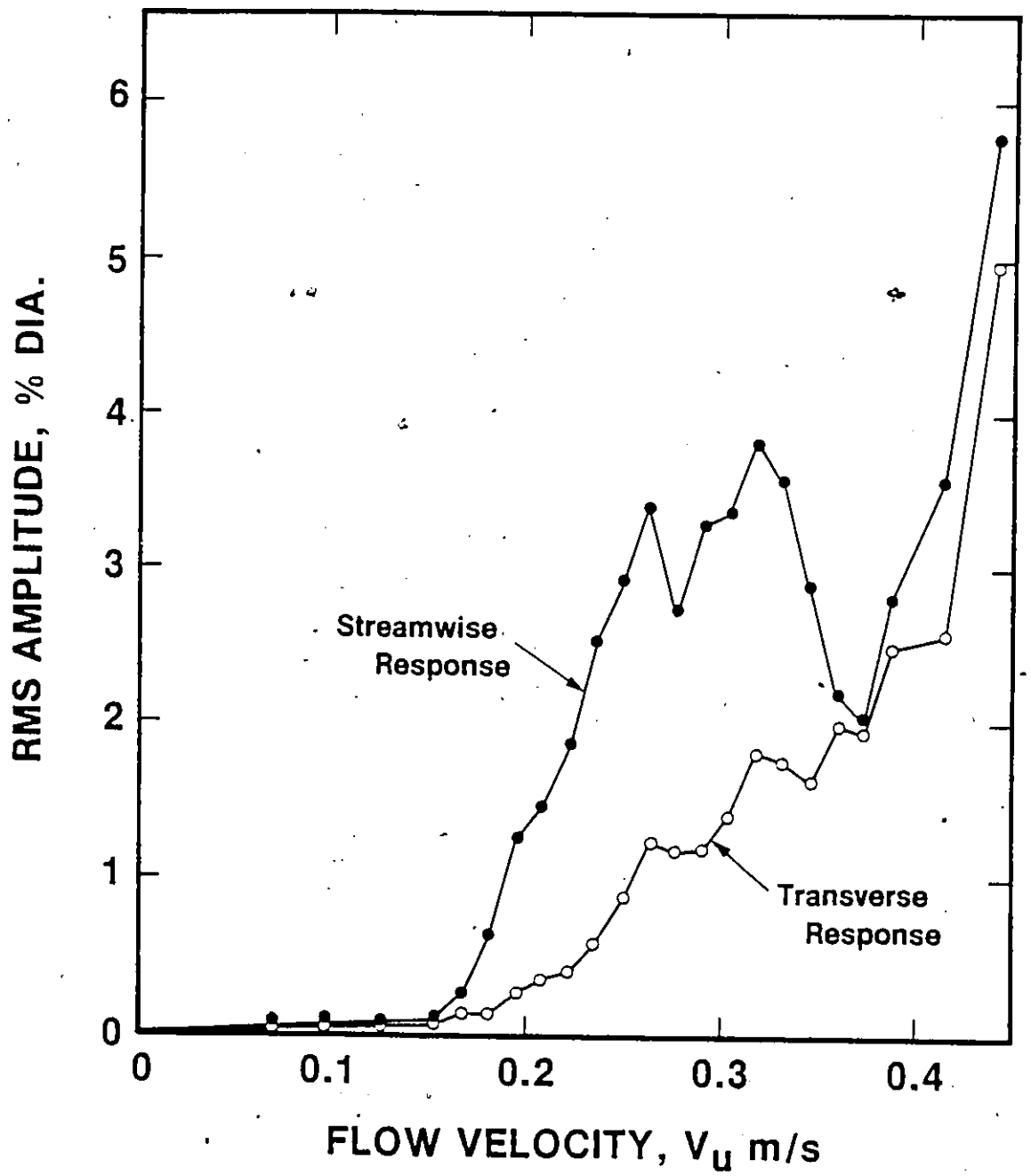

Figure 5.11 Response of tube no.8 in the third row

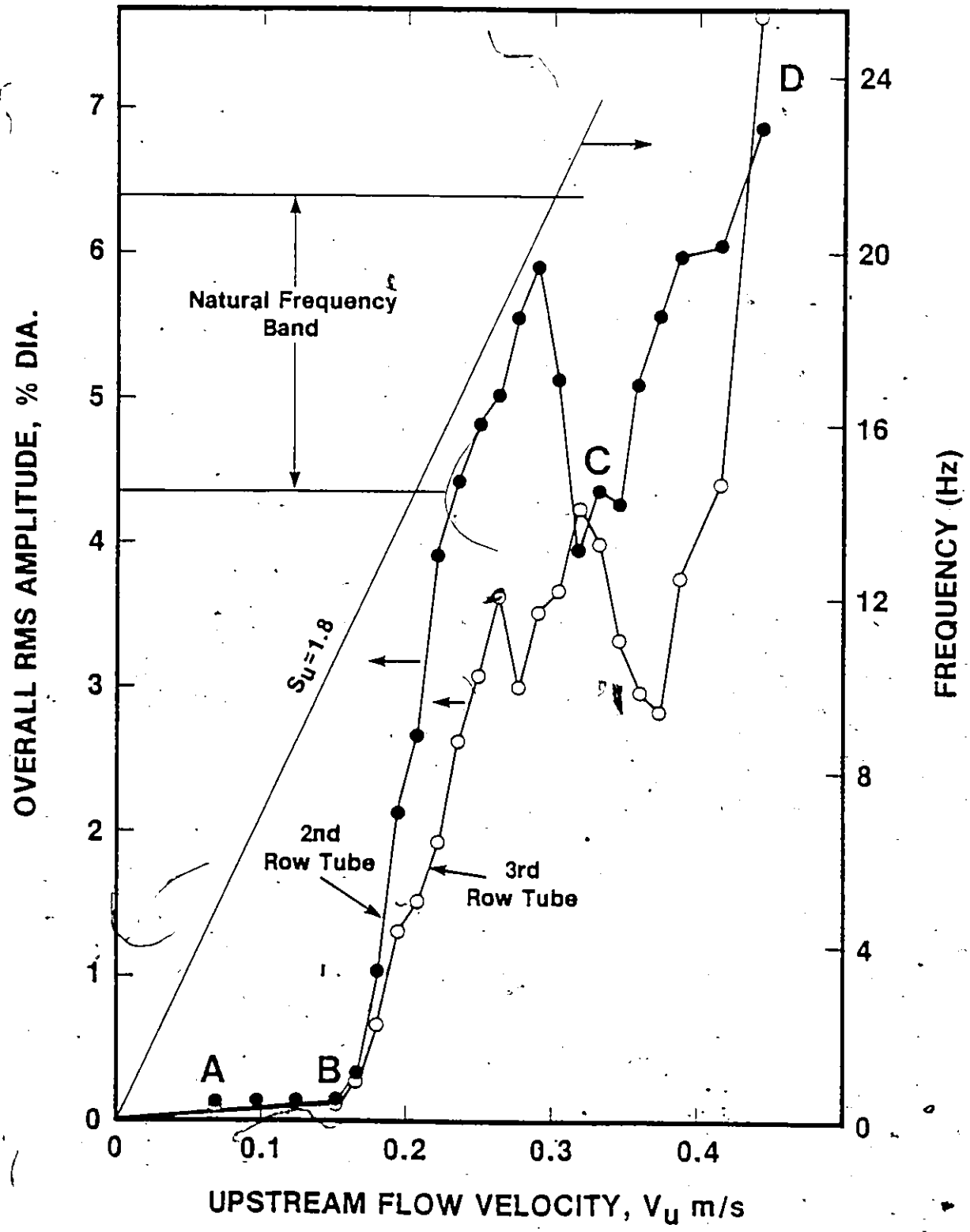

Figure 5.12 Overall RMS responses of the two monitored tubes

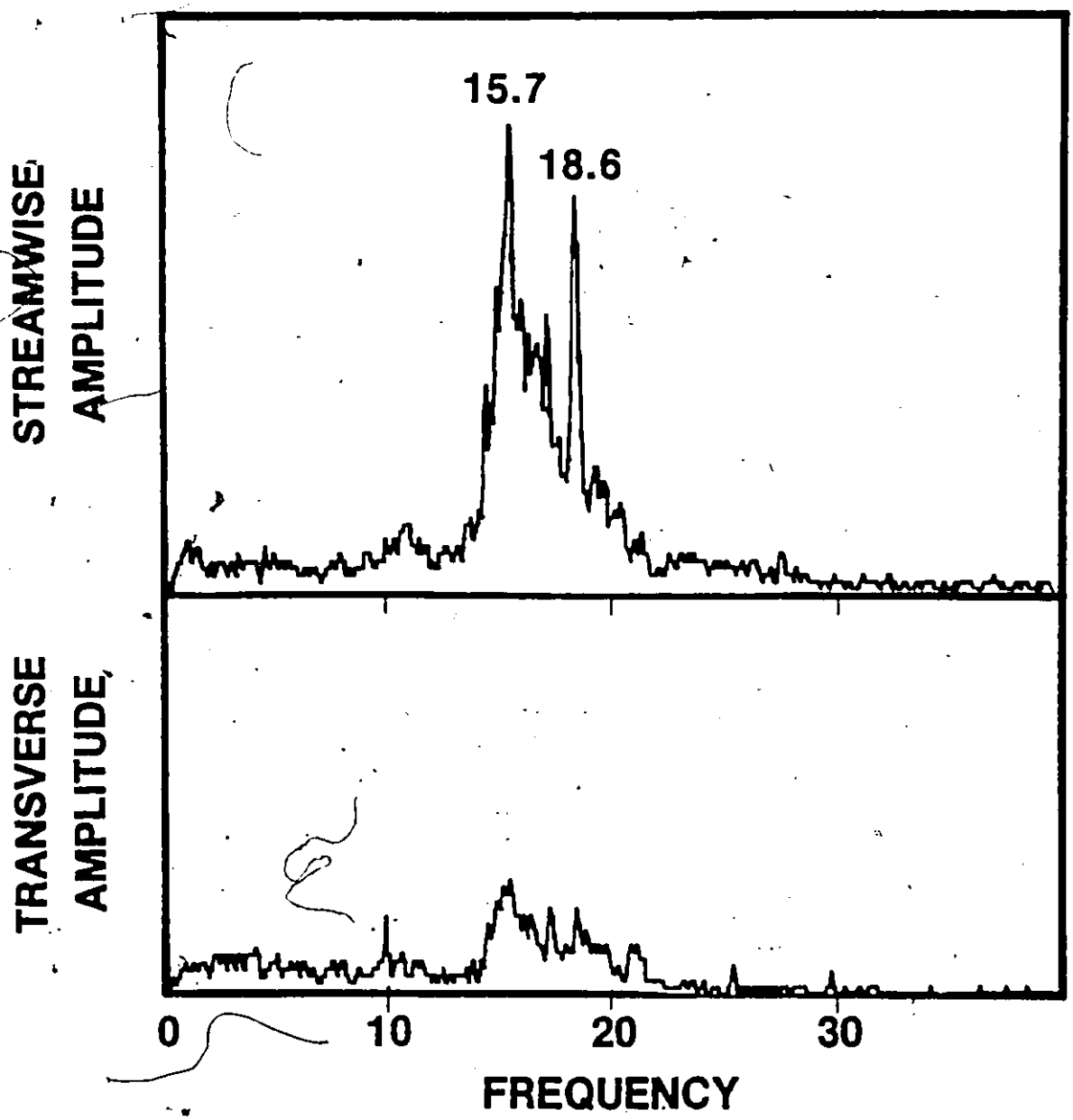

Figure 5.13 Response spectra of tube no.5 at V_u = 0.15 m/s

frequencies. The absence of vorticity generated spikes was also observed by Weaver and Yeung [114] in their investigation of a similar array.

The interstitial flow structure in this flow velocity range is exemplified by the photograph of figure 5.14 taken at a flow velocity V_u = 0.12 m/s. The corresponding Reynolds number Re_p for this figure is 9.1 x 10^3 and observations show that the interstitial flow has the same characteristics as those noted for figure 5.8 at a Reynolds number Re_p = 5.23 x 10^3. The wake flows are turbulent and no coherent wake structure is observed. The main stream flow in the flow lanes is deflected randomly by the flow entering and leaving the wakes. Thus, the coherence of the main stream flow is reduced as it travels deeper into the bundle and interacts with the turbulent wakes.

5.4 Vorticity Response of Both Monitored Tubes

In the flow velocity range 0.15 m/s < V_u < 0.29 m/s, the response amplitudes of both monitored tubes increase considerably in the streamwise direction with a small increase in the transverse direction. The spectra of tube no. 5 given in figure 5.15 were recorded at the flow velocity V_u = 0.19 m/s. These are typical of the recorded spectra for tube no. 5 in this flow velocity range. Similar spectra were recorded for tube no. 8. The random response at lower flow velocities has given way to a periodic response as indicated by the presence of discrete dominant spikes in these spectra. The frequency corresponding to the dominant spike at the flow velocity

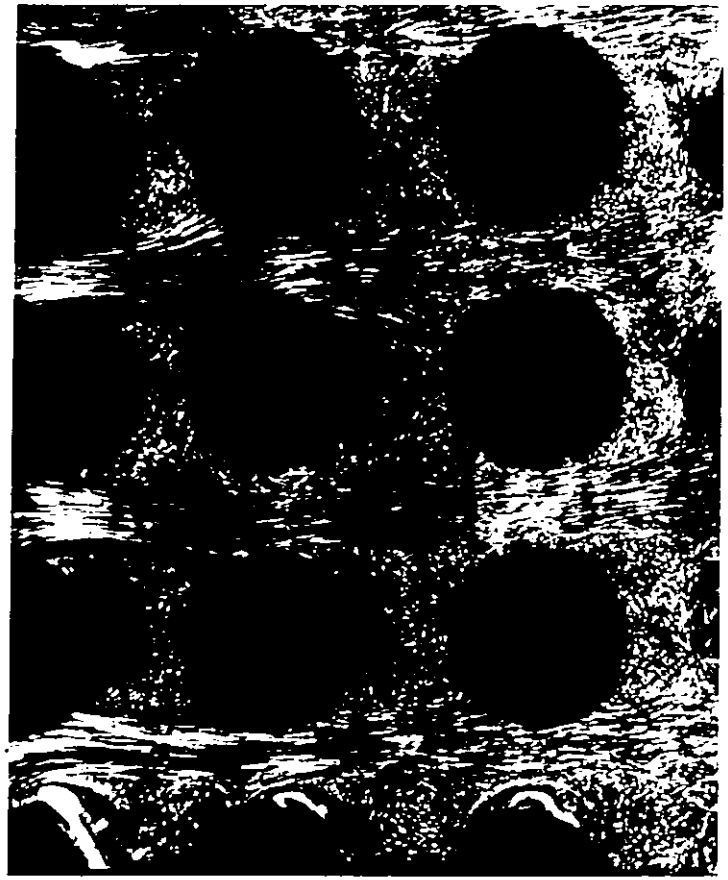

Figure 5.14 Flow visualization at $Re_p = 9.1 \times 10^3$

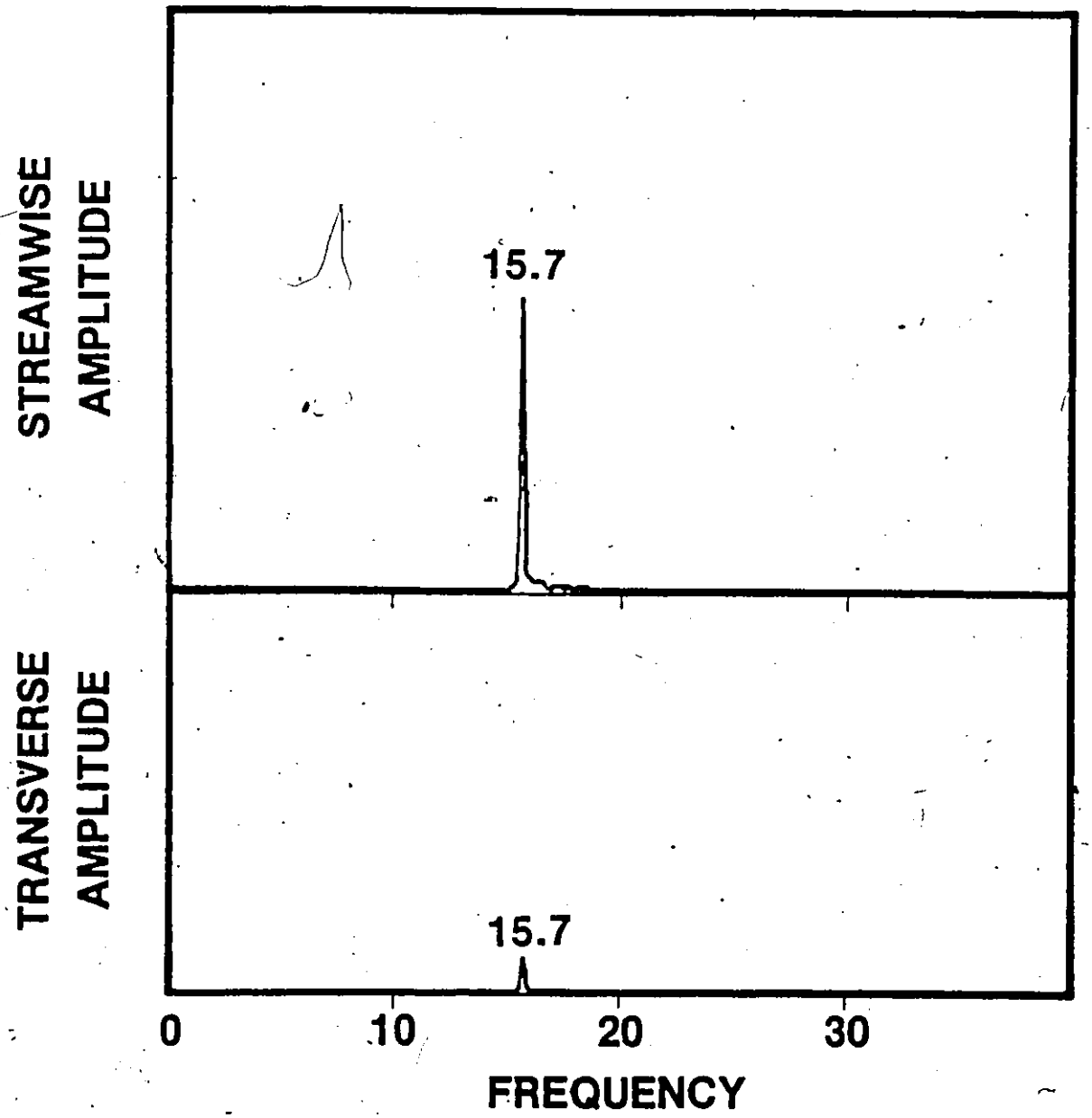

Figure 5.15 Response spectra of tube no.5 at V_u = 0.19 m/s

V_u = 0.19 m/s falls in the lower range of the fluid coupled natural frequencies of figure 5.13. Thus some interaction phenomenon is driving the tubes at one of their natural frequencies. It would appear that the streamwise oscillations were initiated by some discrete, or perhaps, narrow band excitation mechanism which was obscured by the turbulence and could not be observed using the developed flow visualization technique.

The dominant frequencies in the recorded spectra are plotted against the upstream velocity, V_u, in figure 5.16. It is seen that a straight line referred to as "the frequency response line" can be drawn through these points with very little scatter. If this line is extrapolated backward, we see that it intersects with the ordinate at a frequency which is close to the lowest frequency in the fluid coupled natural frequency range for both monitored tubes. The line does not pass anywhere near the origin. Hence while this line is a linear function of flow velocity, it is not related to a constant Strouhal number and it is not obvious why the tubes behave in this way.

As the streamwise response amplitudes of both monitored tubes continue to increase with increasing flow velocity, the spikes in the recorded spectra become more dominant as is clear from the spectra of figure 5.17 recorded at the flow velocity V_u = 0.29 m/s. Similar spectra were recorded at the same flow velocity for tube no. 8. Such developments indicate

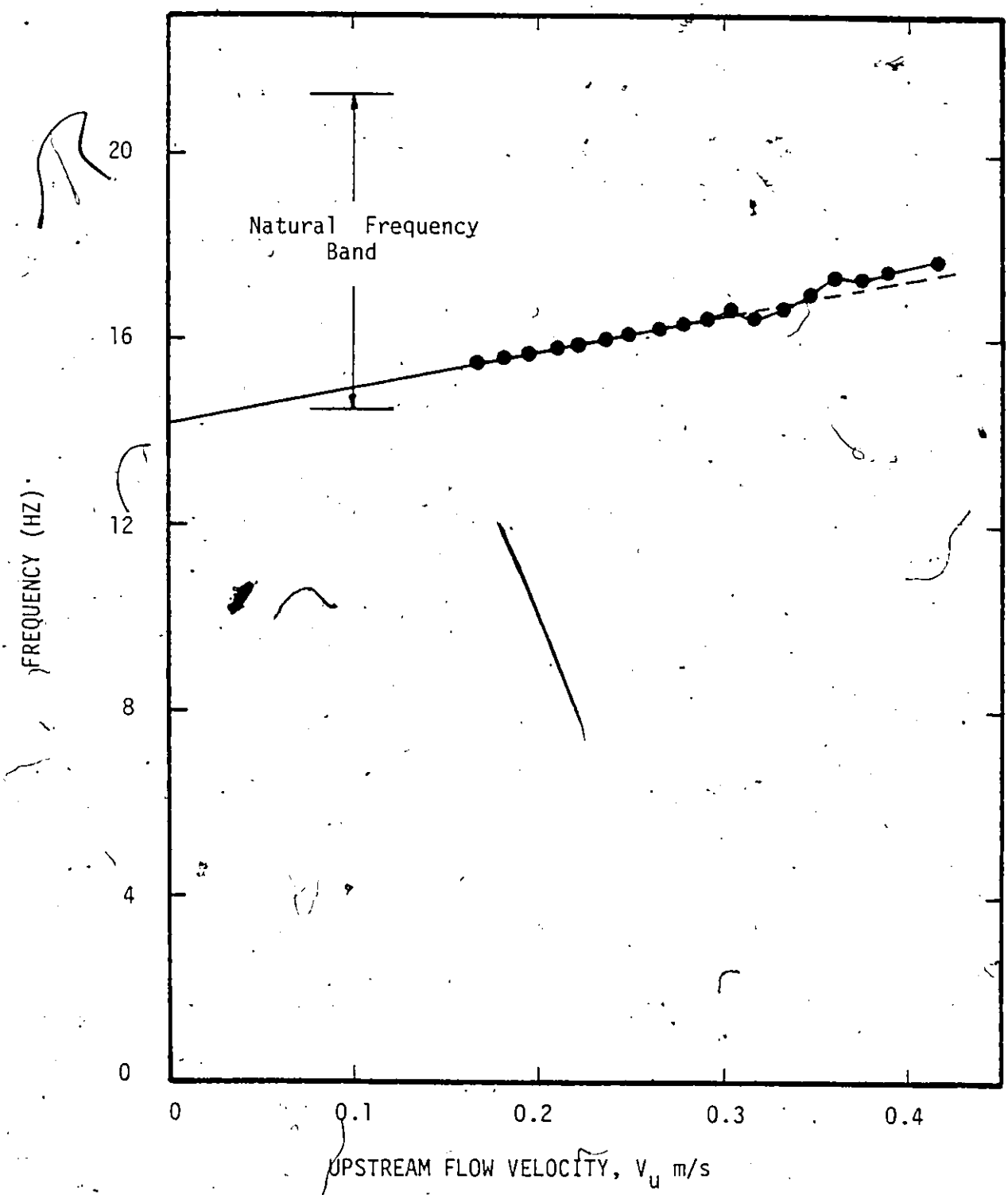

Figure 5.16 The Frequency Response Line

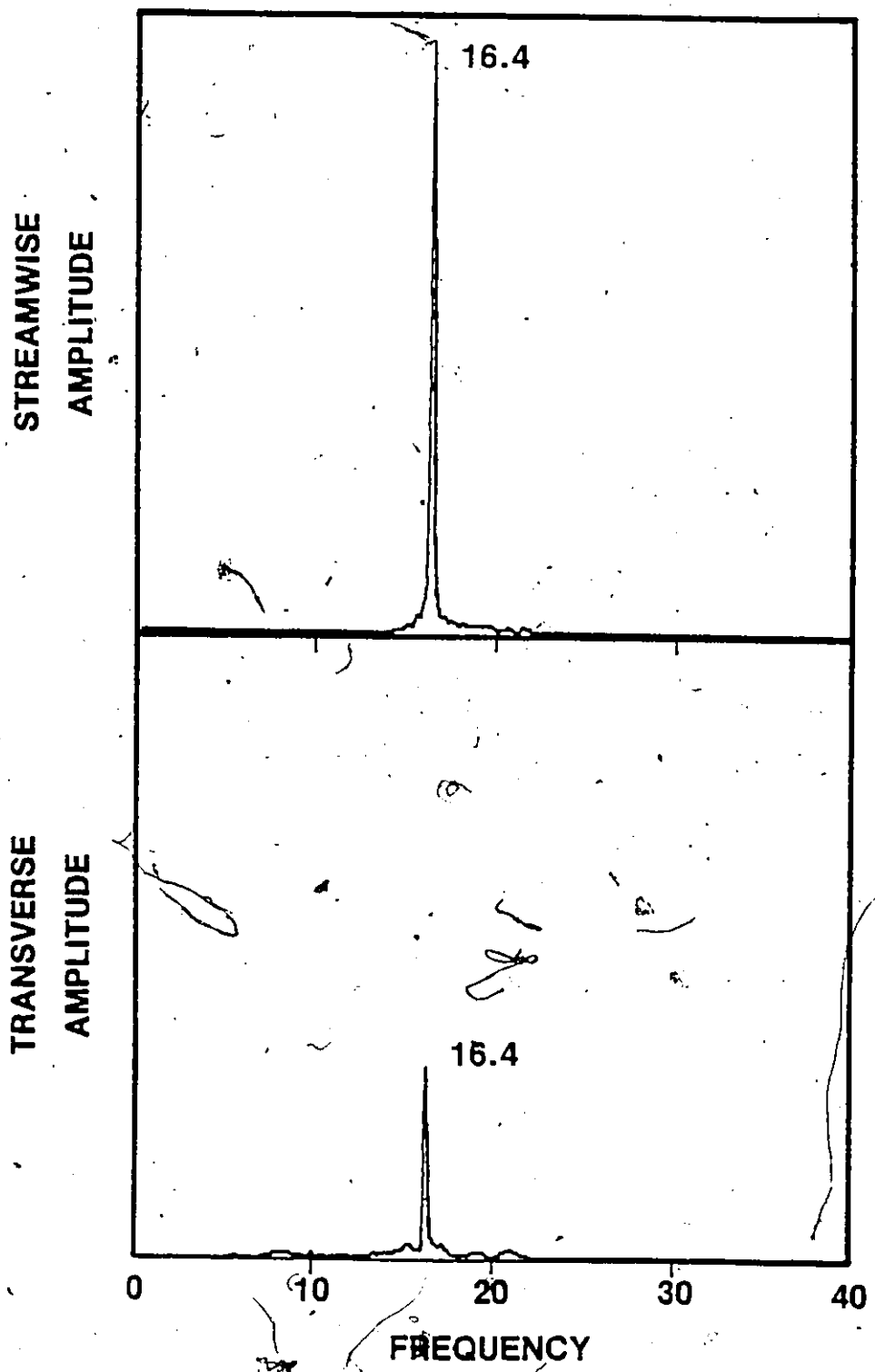

Figure 5.17 Response spectra of tube no.5 at V_u= 0.29 m/s

that the mechanism responsible for the periodic response, has gained considerable strength.

The streamwise response amplitude of tube no. 5 reaches a peak at the flow velocity V_u = 0.29 m/s after which the amplitude level decreases with increasing flow velocity. The decline in the amplitude response curve of figure 5.10 stops at a flow velocity V_u = 0.32 m/s. The streamwise response amplitude of tube no. 8 reaches a peak at the flow velocity V_u = 0.32 m/s, and a similar decline in the response curve is also observed in figure 5.11. The decline in the amplitude response curve is arrested at the flow velocity V_u = 0.37 m/s. The response spectra of both monitored tubes at the flow velocity V_u = 0.32 m/s are given in figures 5.18 and 5.19 respectively. A dominant spike at 16.5 Hz is seen in the spectra of tube no. 8 and in the streamwise spectrum of tube no. 5. The transverse spectrum of tube no. 5, however, indicates somewhat disorganized frequency response, at this flow velocity. Nevertheless, the dominant motion of both monitored tubes is in the streamwise direction as the curves of figures 5.10 and 5.11 indicate. The reason for the presence of a local peak in the response amplitude curve of tube no. 8 at the flow velocity V_u = 0.26 m/s is not understood. The recorded spectra at this local peak and the trough that followed, are not different from the spectra of figure 5.17.

Cine-films taken in this flow velocity range, reveal some additional information. Two frames in half a cycle of

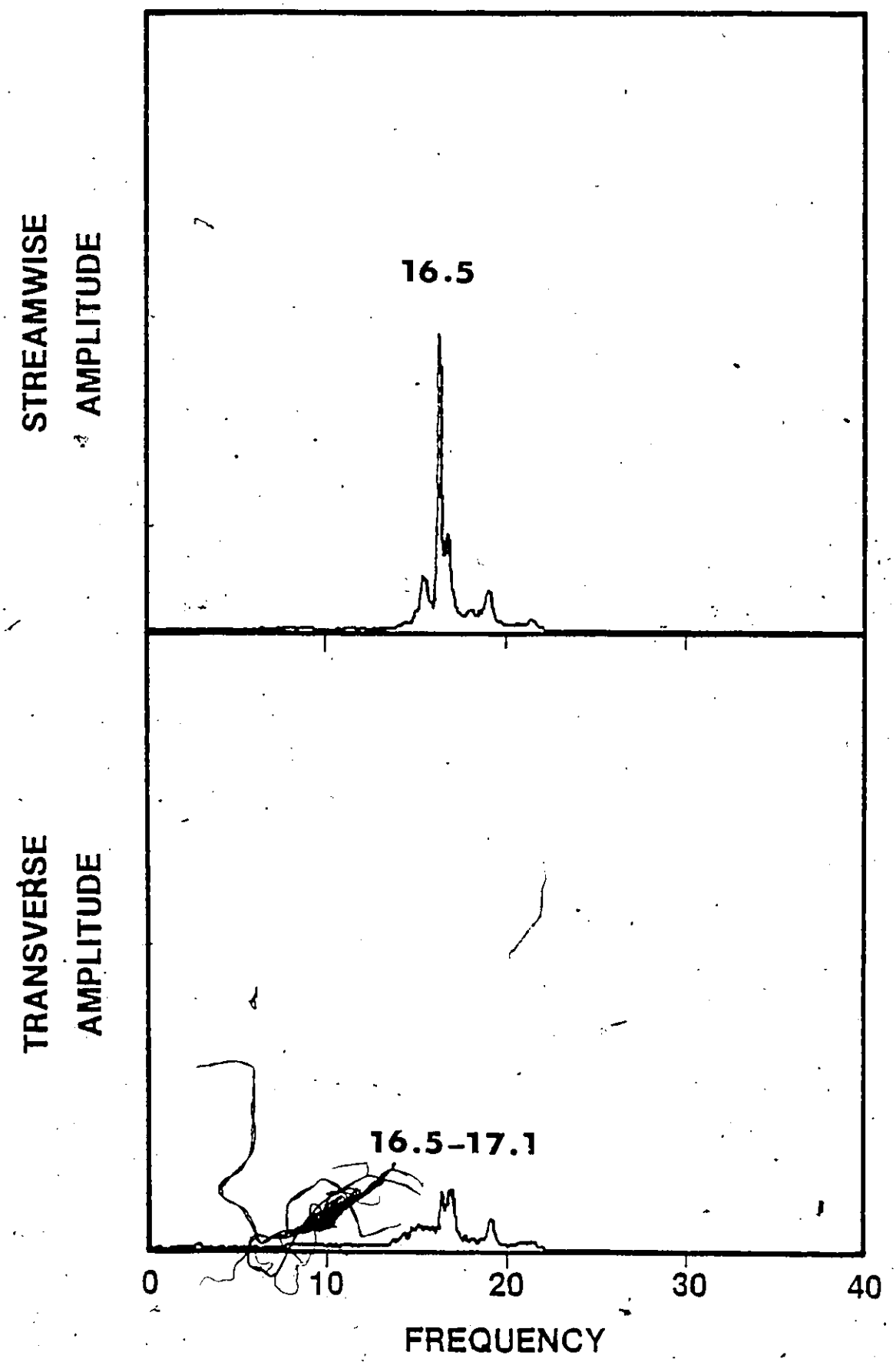

Figure 5.18 Response spectra of tube no.5 at V_u = 0.32 m/s

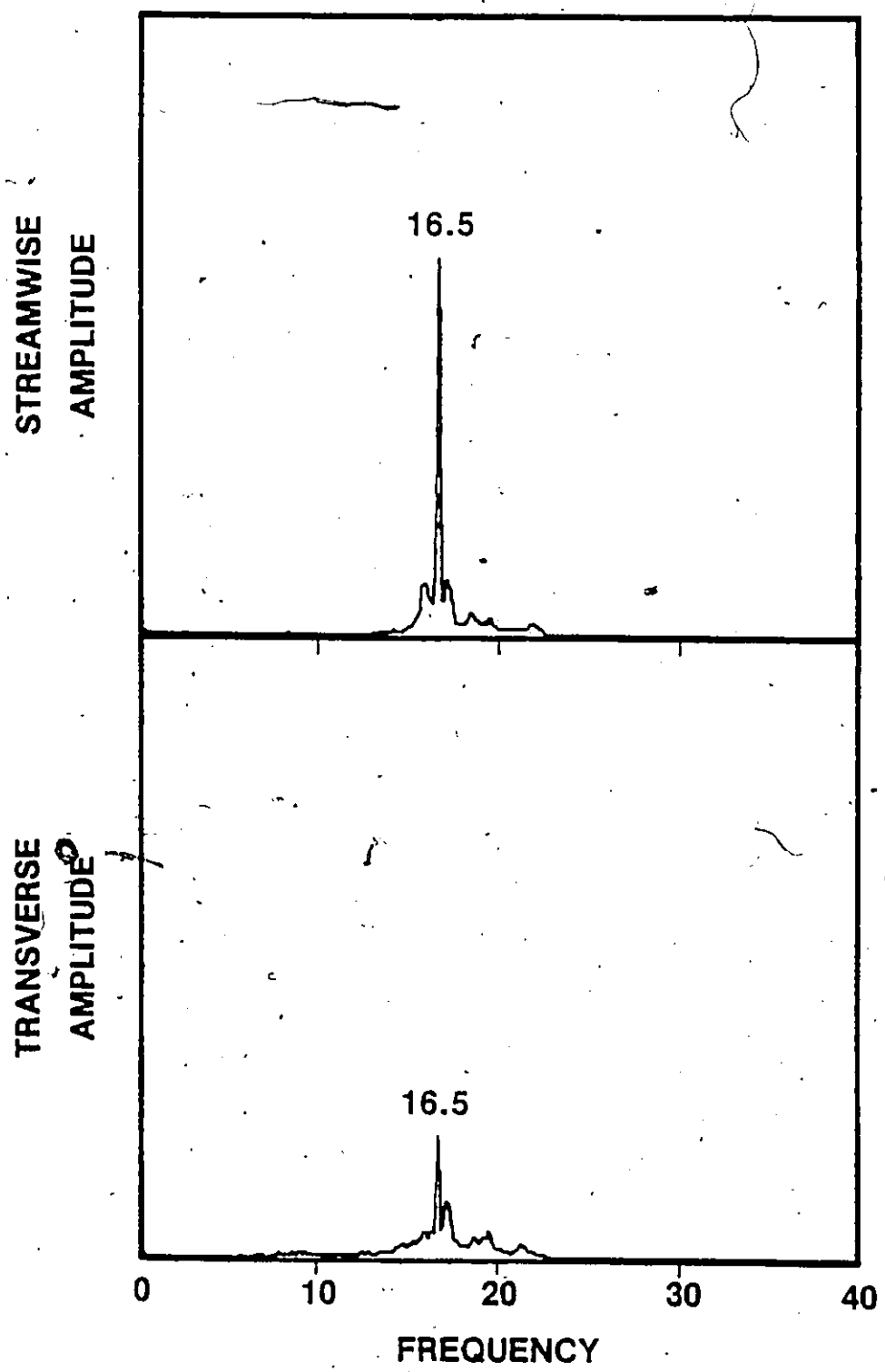

Figure 5.19 Response spectra of tube no.8 at V_u= 0.32 m/s

tube motion are reproduced in figure 5.20 from a cine-film taken at the flow velocity V_u = 0.25 m/s, the framing rate being 166 frames per second. The film was taken while a stream of tracer particles was directed towards the tubes of the second column. It is seen that the second row tubes are constantly exposed to symmetric vortices shed from the tubes of the first row. It is also seen from the film that the first and second tube rows execute in-line oscillations and, in doing so, move in opposition to each other. Tube no. 2, in the first row, sheds a pair of symmetric vortices every cycle of its motion. This occurs whenever the tube is at its extreme downstream position and reverses its direction of motion. It is an acknowledged fact that synchronization leads to spectacular magnification of fluctuating forces on the vibrating tube in comparison with those measured on a stationary one. The near constancy of the period of time available for vortex formation means that more vorticity is generated in the synchronization range with increasing flow velocity and hence stronger vortices [142]. Given also the stable mode of relative tube motion enhanced by the transverse symmetry of the square in-line array, which allowed direct communication between the wakes of the tubes in a row, the amplitude of tube motion continually increased. Under these circumstances a dynamic feed-back mechanism develops and sustains this type of self-controlled vibration [58]. The frequency of the symmetric vortex shedding from tube no. 2 was calculated from

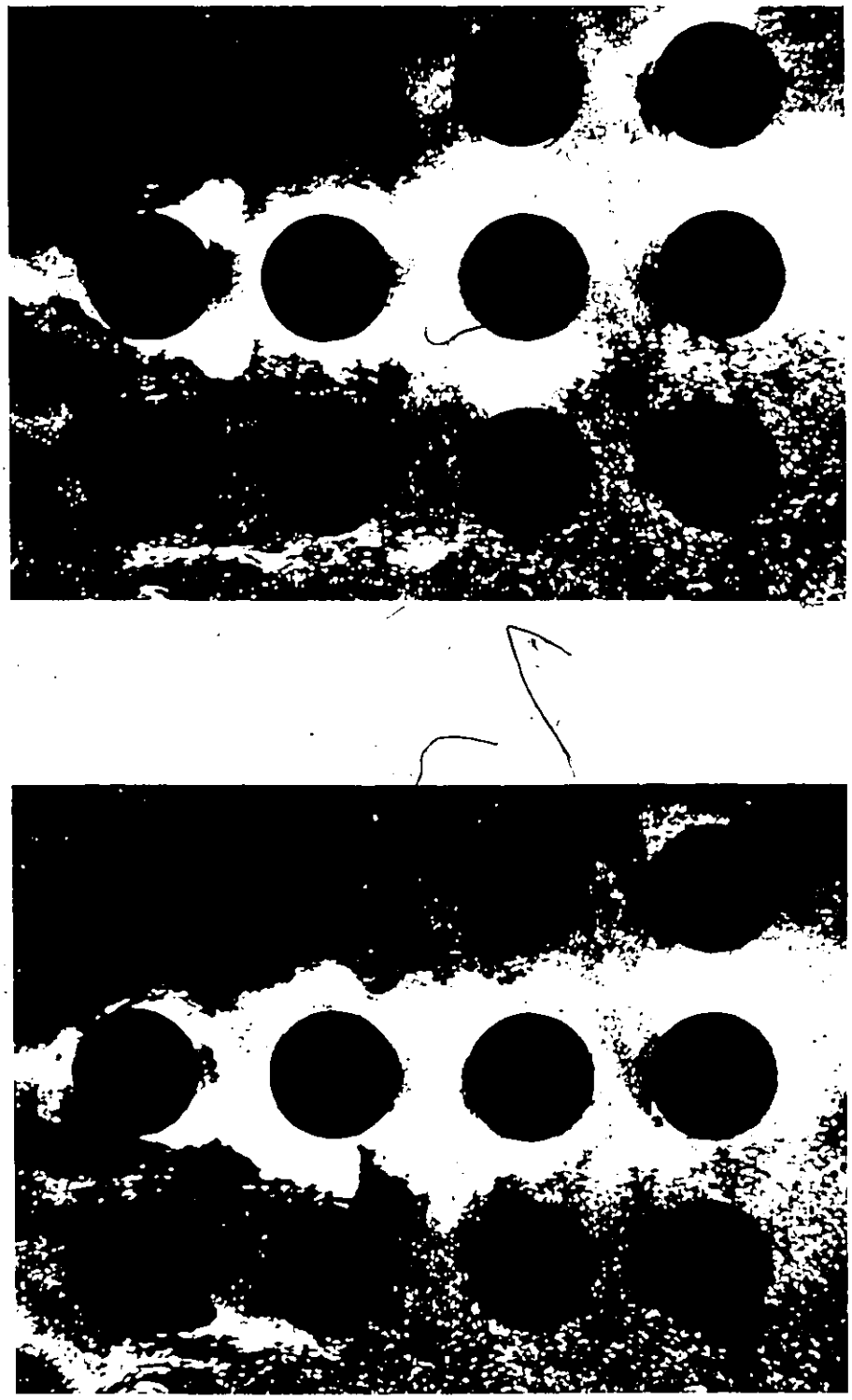

Figure 5.20 Symmetric vortex shedding at V_u = 0.25 m/s

the cine-films at three different flow velocities and is compared in table 5.1 with the frequency of vibration of tube no. 5 obtained from the recorded frequency spectra. It is evident that tube no. 5 vibrates at the same frequency as that of the symmetric vortex shedding from tube no. 2 upstream of it. The films recorded at different flow velocities in the range 0.15 m/s < V_u < 0.29 m/s showed that each tube oscillates at a constant amplitude which depends on the flow velocity and that the relative mode shape does not change with either flow velocity or time.

The still photograph of figure 5.21 shows that the symmetric vortices shed by tube no. 2 in the first row are in phase with vortex pairs shed from other tubes in the same row. Evident also in this photograph, is the effect of vortex shedding in narrowing the passages of the main stream flow in the flow lanes. Several developments in the flow structure, in the interior region of the flexible array can be seen in the photographs presented and in the films taken. These are,

a) shedding of coherent vortex pairs from the first row which diffuse through subsequent tube rows into the bundle.

b) distortion of the main stream flow with the diffused structure of these vortices.

c) interference of the tubes as they vibrate with the main stream flow and the resulting impingement of the latter on the tubes.

Table 5-1

Calculated frequency of symmetric vortex shedding from tube no. 2 and the recorded frequency of tube no. 5

V_u m/s	Tube no. 5 frequency of vibration Hz from frequency spectra	Frequency of symmetric vortex shedding from tube no. 2 Hz from cine-films
0.25	16.1	16.1
0.28	16.3	16.3
0.29	16.4	16.4

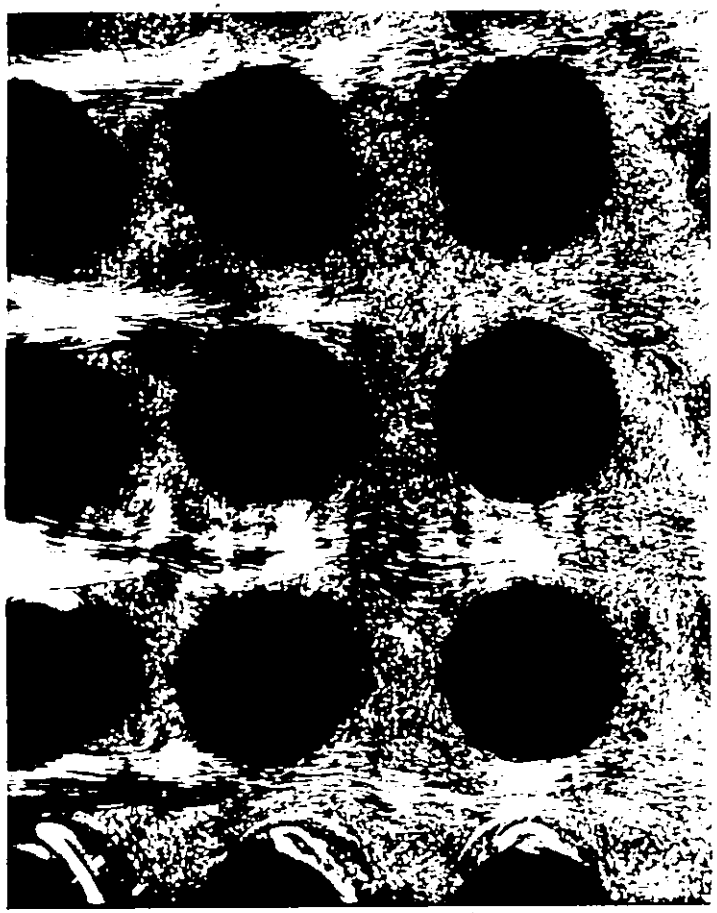

Figure 5.21 Flow Visualization at V_u = 0.22 m/s

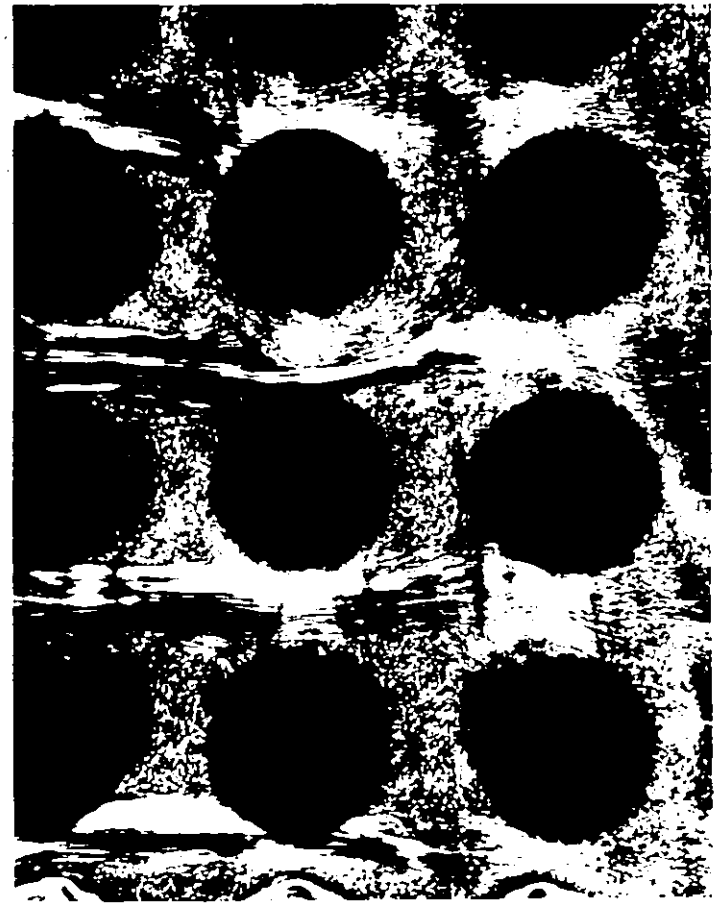

Figure 5.22 Flow Visualization at V_u = 0.29 m/s

Such developments inside the flexible bundle admit random irregularities in the main stream flow in the flow lanes. The cumulative growth of such random irregularities results in an increased level of turbulence as more tube rows are traversed by the flow. However, despite the apparent loss of coherency in the main stream flow in the flow lanes, still relatively well defined main stream flow can be identified throughout the bundle.

The rigid part of the tube bundle was filmed and photographed at the same flow velocities to compare the structure of its interstitial flow with that of the flexibly mounted bundle. The photograph of figure 5.22 was taken at the flow velocity V_u = 0.29 m/s. In contrast with the flexibly mounted tube bundle, no discernible pattern of symmetric or alternate vortex shedding has been observed in the films, or can be found in the still photograph in the wakes of any row of tubes. This shows that the coherent symmetric vortex shedding in the flexibly mounted tube bundle was generated by the streamwise motion of the tubes. This also indicates that the motion of the tubes gives rise to different phenomena and flow patterns from those observed when the tubes are rigidly mounted. The main stream flow in the flow lanes is seen to be relatively more coherent than its counterpart in the flexible tube bundle in its interior region. This can be attributed to the lack of tube motion.

The contribution to increasing turbulence in the main

stream flow in the rigid bundle comes from the unstable wake flows as they leave the wake region. This is seen in the photograph of figure 5.22. The transverse symmetry of the square array apparently leads to a greater coherence of interstitial flow phenomena in that the wakes of all tubes in a row are directly connected. This does not occur in staggered arrays since the wakes of all tubes in a row are separated by tubes in the next downstream row. Thus the regular flow patterns and relative tube motions seen in square in-line arrays are not expected in staggered arrays.

5.4.1 Discussion of the Results

The details of the interstitial flow structure behind the second and the third row of tubes are not as clear as those behind the first row of tubes. Clear identifiable vortex structures behind the second and third row of tubes are not observed. It appears that a coherent flow structure with low turbulence level, like that approaching the tubes of the first row, is required for a distinct vortex structure to be identifiable. With the advent of increasing turbulence level in the main stream flow of the flow lanes, the coherent flow structure breaks down and the distinct vortex structure is swamped by turbulence and is no longer seen. This view is held by some researchers, notably Lubin et al. [143] and Jones et al. [144]. Nevertheless, the periodic response of the second and third row tubes can be seen in the cine-films taken and can be inferred from the recorded tube response spectra. The frequency

of the periodic response coincides with the frequency of response of the first row as can be seen from table 5.1.

The response amplitude curves of tube no. 5 and tube n. 8 peaked at the flow velocities V_u = 0.29 m/s and 0.32 m/s respectively, after which the control of the mechanism was lost and the response amplitudes declined with increasing flow velocity. Accordingly, these peaks were attributed to vorticity resonance i.e. the coincidence of symmetric vorticity shedding with the fluid coupled natural frequencies of tube vibrations. Weaver and Yeung [115], investigated various types of tube arrays in water cross flow. They reported that the peaks in the amplitude response curves, attributed to vorticity response, occur at or close to the velocity range corresponding to the intersection of a constant Strouhal number line with the band of fluid coupled tube natural frequencies. Owen's turbulence excitation prediction [26] as well as vortex shedding predictions of Chen [21] and Zukauskas and Katinas [117] all suggest a Strouhal number based on upstream velocity of 0.9, for the three square arrays considered by Weaver and Yeung [115]. Such a Strouhal number line intersects the natural frequency range of the tube arrays at some point well beyond the stability threshold. However, they found that if a Strouhal number of 1.8 is taken, exactly two times the expected value, the intersection of the corresponding Strouhal line with the tube natural frequencies coincided in every case with the rise in the response curve that was attributed to vorticity shedding. Accordingly Weaver and Yeung [114, 115] deduced that

the tubes could be excited by every vortex rather than each pair of alternating vortices. Following this idea, the constant Strouhal line for $S_u = 1.8$ was drawn in figures 5.12. The peak in the response amplitude curve of tube no. 5 at the flow velocity $V_u = 0.29$ m/s falls in the flow velocity range where the Strouhal line intersects the fluid coupled natural frequency range. Similarly the first peak in the response amplitude curve of tube no. 8 at flow velocity $V_u = 0.26$ m/s falls within this flow velocity range and the second peak at $V_u = 0.32$ m/s falls just above it. The implications are that the phenomenon observed by Weaver and Yeung [115] is also observed here and that the peaks in the response amplitude curves can be attributed to the same mechanism.

It is seen that there is a disagreement between the apparent Strouhal number found in the present investigation and that found by Chen [21], Zukauskas and Katinas [117] and Owen [26]. It is to be noticed that the Strouhal number data of Owen [26] and Chen [21] were obtained by hot wire measurements. The data were viewed and interpreted by Chen as due to alternate vortex shedding and by Owen as due to turbulence. The arrangement of hot wires in the wake of the cylinder in the experiments of Chen, is intended to measure the frequency of the assumed alternate vortex shedding. Owen placed his hot wire downstream of the array, practically in the wake of a tube in the last row. Therefore, his data might have been influenced by what is happening in the free wake

of that tube and not necessarily indicative of flow deep inside the array.

In contrast with Owen's theory [26], "a state of almost complete incoherence" does not exist, at least in the four rows of the bundle considered here. The behaviour observed in the present study would not be affected by the presence of more downstream rows of tubes. The investigations of Weaver and Grover [39], Grover and Weaver [30] and Fitzpatrick and Donaldson [125] showed that the turbulence instensity has essentially reached its maximum value by the fourth row.

A great deal of our knowledge about the so-called vortex shedding in in-line and staggered tube bundles come from the work of Chen. His analysis [20, 104] is based on the assumption of alternate vortex shedding but says nothing about symmetric vortex shedding. The results of the present study showed that alternate vortex shedding was not observed. Instead we see symmetric vortex shedding and streamwise oscillations. The downstream tubes separated the symmetrically shed vortices from the upstream tubes and prevented their influence on each other. The assumption of transverse acoustic oscillations made by Chen renders the theory inapplicable in water flows since acoustic resonance is not likely for such heavy fluids. It is also clear from figure 5.20 that a vortex shed by an upstream tube will not vanish in front of the downstream tube so that a new vortex from the downstream tube will grow and become a sequel of the diminishing vortex.

The first row vortices are seen to pass the second row tubes and a sequence of three vortex pairs can be identified in the photographs.

It may be that acoustic resonance in a tube bundle subjected to a cross flow of air, is capable of producing the kind of regular vortex pattern drawn by Chen in references [21, 104]. However, this certainly does not occur in the absence of acoustic resonance as shown in the present study. It must be also stated that Chen's drawings [21, 71, 104] are highly speculative with no hard data to substantiate his arguments.

Chen's analysis was based on observations of tube arrays in air. In water flows, the range of reduced velocities and tube spacing may influence the effects of vortex shedding. King and Johns [145] experimented with two cylinders of diameter d separated by a distance G along a common centre-line in the flow direction, exposed to water flow. They found that if the ratio $\frac{G}{d} < 1.75$, symmetric vortices are shed from both cylinders in the reduced velocity range $1.25 < \frac{V}{f_n d} < 2.5$ and both cylinders will oscillate in the in-line direction. This range of reduced velocities coincides with the range of reduced velocities for an isolated cylinder executing in-line oscillations in a flowing water [79, 146]. Nevertheless, King and Johns' interpretations of the complex behaviour of the two cylinders arranged in tandem was different from that given to explain the behaviour of the isolated cylinder. In

the latter case, the upper and the lower limits of the reduced velocity range were governed by higher multiples of the Strouhal number, S = 0.2, for an isolated rigid cylinder [79, 146]. In the former case, King and Johns [145] attributed the behavior of the two cylinders to a complex mutual interference between them as they interact with the flow field. This explanation takes into consideration the fact that cylindrical bodies in the wakes of other cylinders do not conform to the pattern of behavior recorded when the cylinders are isolated.

In this regard, the work of King and Johns [145] provides an interesting comparison with the present findings. The reduced velocity range corresponding to the range of flow velocities during which the apparent lock-in persisted in the present study is

$$1.3 < \frac{V_p}{f_n d} < 2.2.$$

This agrees very well with the range found by King and Johns for two cylinders in tandem. However, in view of the paucity of information about in-line oscillations of square arrays, it is not known with certainty how significant or reliable this agreement is. More research is needed to clarify this point.

It should be noted that the theory of Lever and Weaver [147] indicates that fluidelastic instability in tube arrays is not possible in the streamwise direction. This prediction agrees quite well with the bulk of experimental data reported

in the literature. It follows that one is reluctant to attribute the response peak discussed in this section to fluidelastic instability.

In summary, it appears reasonable to conclude that vorticity shedding is the excitation mechanism in the flow velocity range $0.15 < V_u < 0.32$ m/s. The following observations lend support to this contention. Firstly, the theoretical study of Lever and Weaver [147] showed that the streamwise direction in which tube oscillations occurred is stable from fluidelastic excitation. This prediction agrees quite well with the bulk of experimental data reported in the literature [45]. Secondly, the relative mode shape is stable and the motion occurs at a single frequency, figure 5.16, rather than being modulated with changing relative mode shapes characteristic of fluidelastic excitation [39, 40]. Thirdly, the onset of the large amplitude response corresponds to a Strouhal number exactly twice that expected from the literature [21, 26, 117] and agrees well with the results of Weaver and Yeung [114]. Finally, while no coherent vortex shedding was observed in the range $0 < V_u < 0.15$ m/s, flow visualization films and photographs show unequivocally that pairs of symmetric vortices are shed in the range $0.15 < V_u < 0.32$ m/s.

5.5 Fluidelastic Response

In the flow velocity range 0.32 m/s $< V_u < 0.42$ m/s some undulations exist in the overall RMS amplitude curves of

both monitored tubes of figure 5.12. The details of these undulations in the streamwise and transverse directions are found in the response curves of figures 5.10 and 5.11. Such undulations and irregularities in the response amplitude curves were observed in the investigations of Weaver and Yeung [114, 115], Pettigrew and Gorman [32], Heilker ~~and~~ Vincent [148] and Weaver and Koroyannakis [40], for similar and different array patterns. It was suggested by Weaver and Koroyannakis [40] that the irregularities in the response curves in the fluidelastic region are due to shifts in unstable fluid coupled modes and associated frequencies.

In this flow velocity range, both monitored tubes respond essentially at the same frequencies but with different corresponding amplitudes. The difference in the resultant amplitude response of both monitored tubes is clear from figure 5.12. Also noticeable in this velocity range is that the frequencies of the dominant spikes deviate from the frequency response line of slope 0.19 drawn in figures 5.16.

The recorded spectra of both monitored tubes in the flow velocity range 0.32 m/s < V_u < 0.36 m/s indicate clearly that the frequency response is disorganized compared to that observed in the range 0.15 - 0.32 m/s. This can be seen in the spectra of figures 5.18 and 5.23 for tube no. 5 and 5.19 and 5.24 for tube no. 8. In the streamwise spectra of these figures, other less dominant spikes appear together with the dominant ones. In the transverse spectra, the sharp or

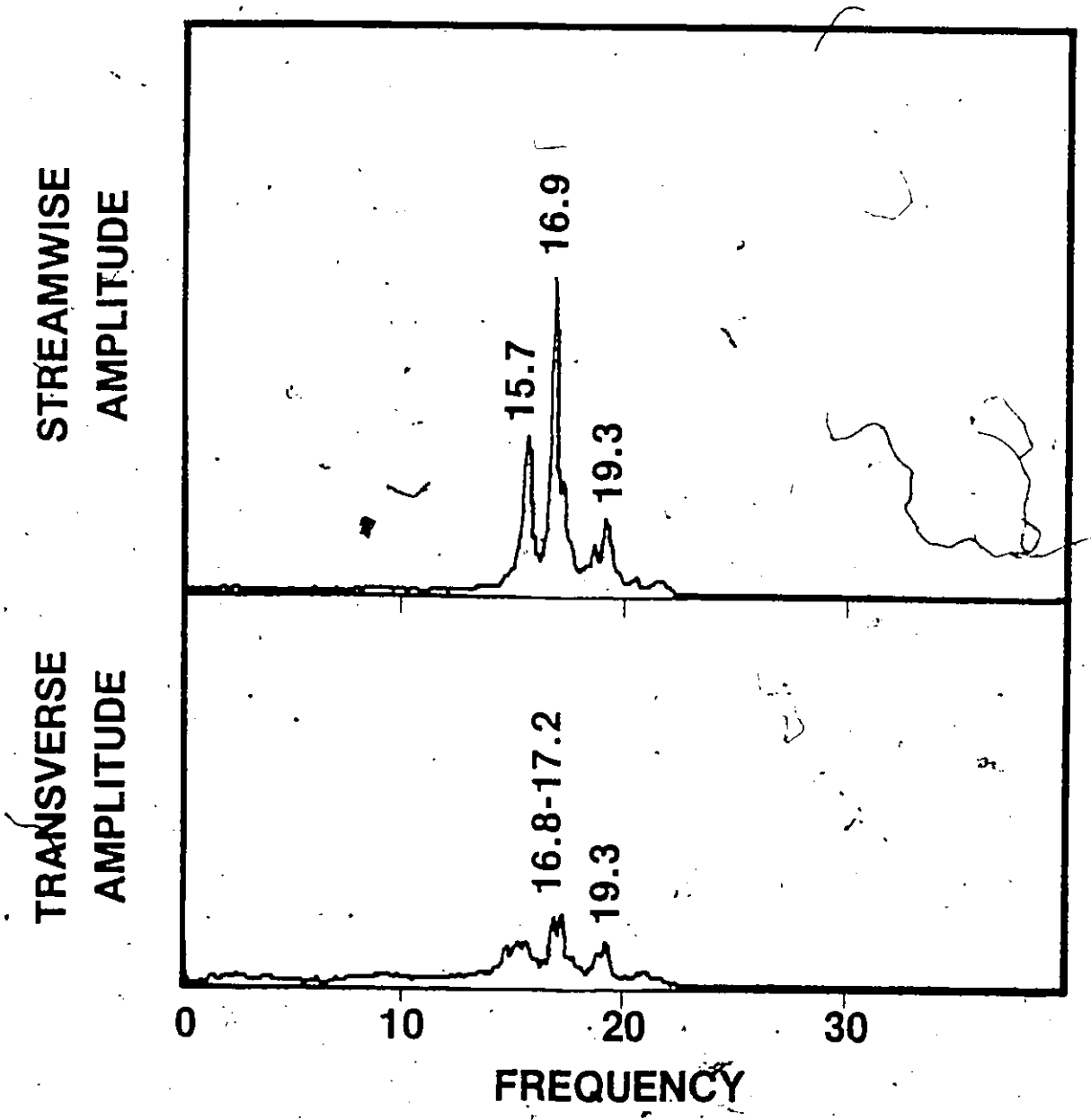

Figure 5.23 Response spectra of tube no.5 at V_u = 0.35 m/s

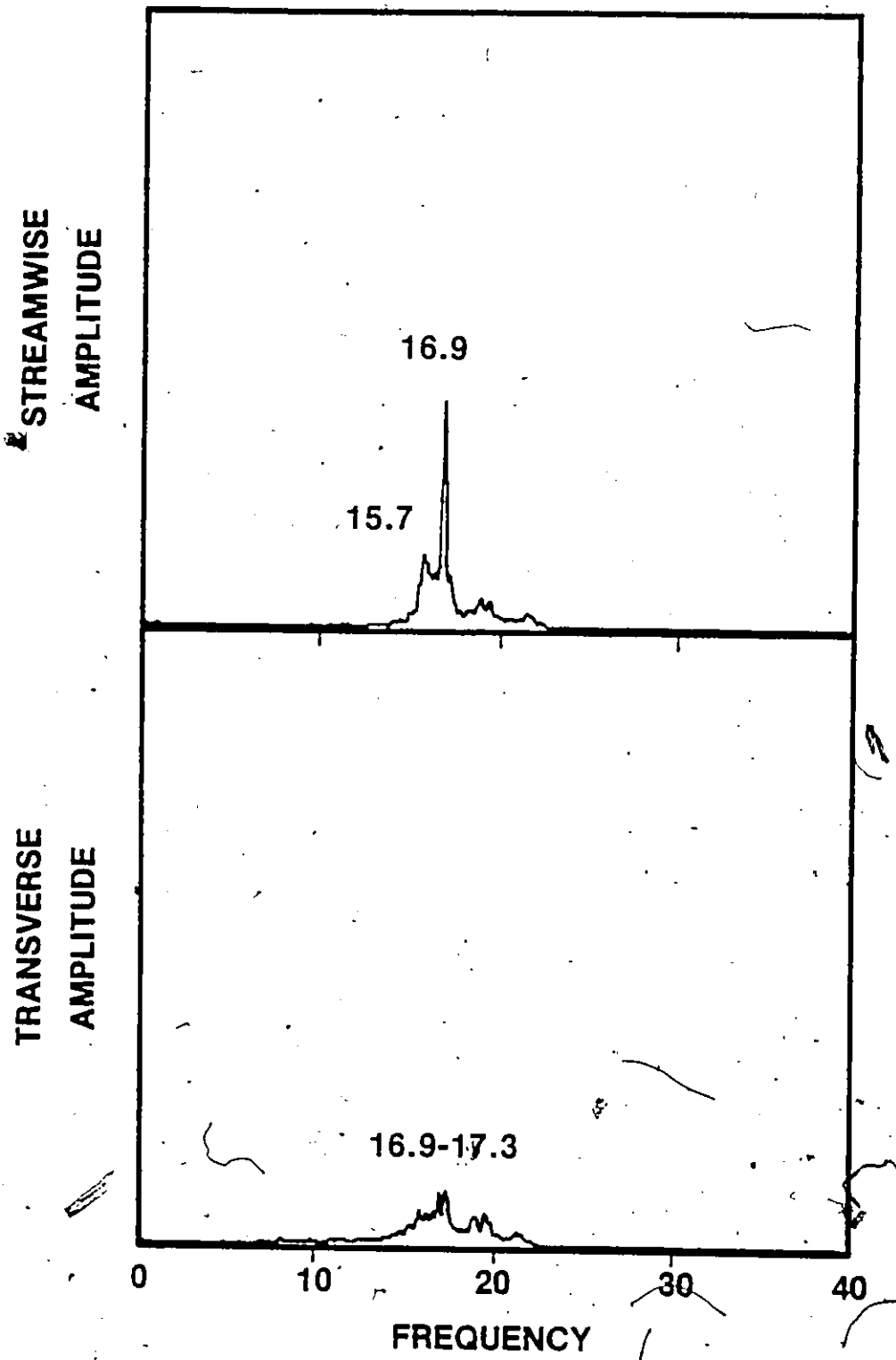

Figure 5.24 Response spectra of tube no.8 at V_u= 0.35 m/s

narrow band spikes are replaced by broader ones.

In the flow velocity range 0.36 m/s < V_u < 0.42 m/s, much better organized frequency response of both monitored tubes is seen in the spectra of figure 5.25 and 5.26 for tube no. 5 and tube no. 8 respectively. The spikes in the spectra of tube no. 5 are more pronounced than those of tube no. 8. At the flow velocity V_u = 0.35 m/s, the spectra of tube no. 5 given in figure 5.23 show that the dominant spike in the streamwise direction has a frequency of 16.9 Hz while in the transverse direction, the dominant frequencies are 16.9 and 17.3 Hz. Increasing the flow velocity to V_u = 0.37 m/s, the spectra of figure 5.25 show that the dominant spikes in the streamwise and transverse directions occur at a frequency of 17.3 Hz. The response spectra of tube no. 8 show essentially the same trends as is evident by comparing the spectra of tube no. 5 with those of tube no. 8 given in figures 5.24 and 5.26, recorded at the flow velocities V_u = 0.35 m/s and 0.37 m/s respectively.

In the amplitude response curves of tube no. 5 given in figure 5.10 a sharp upturn in the transverse response curve starts at the flow velocity V_u = 0.35 m/s. The trend towards increasing transverse response of tube no. 8 is also seen in figure 5.11 although a sudden sharp upturn in the transverse amplitude response is not evident. It may be hypothesized that the transverse response of tube no. 8, as the flow velocity increases beyond V_u = 0.35 m/s, is affected by the

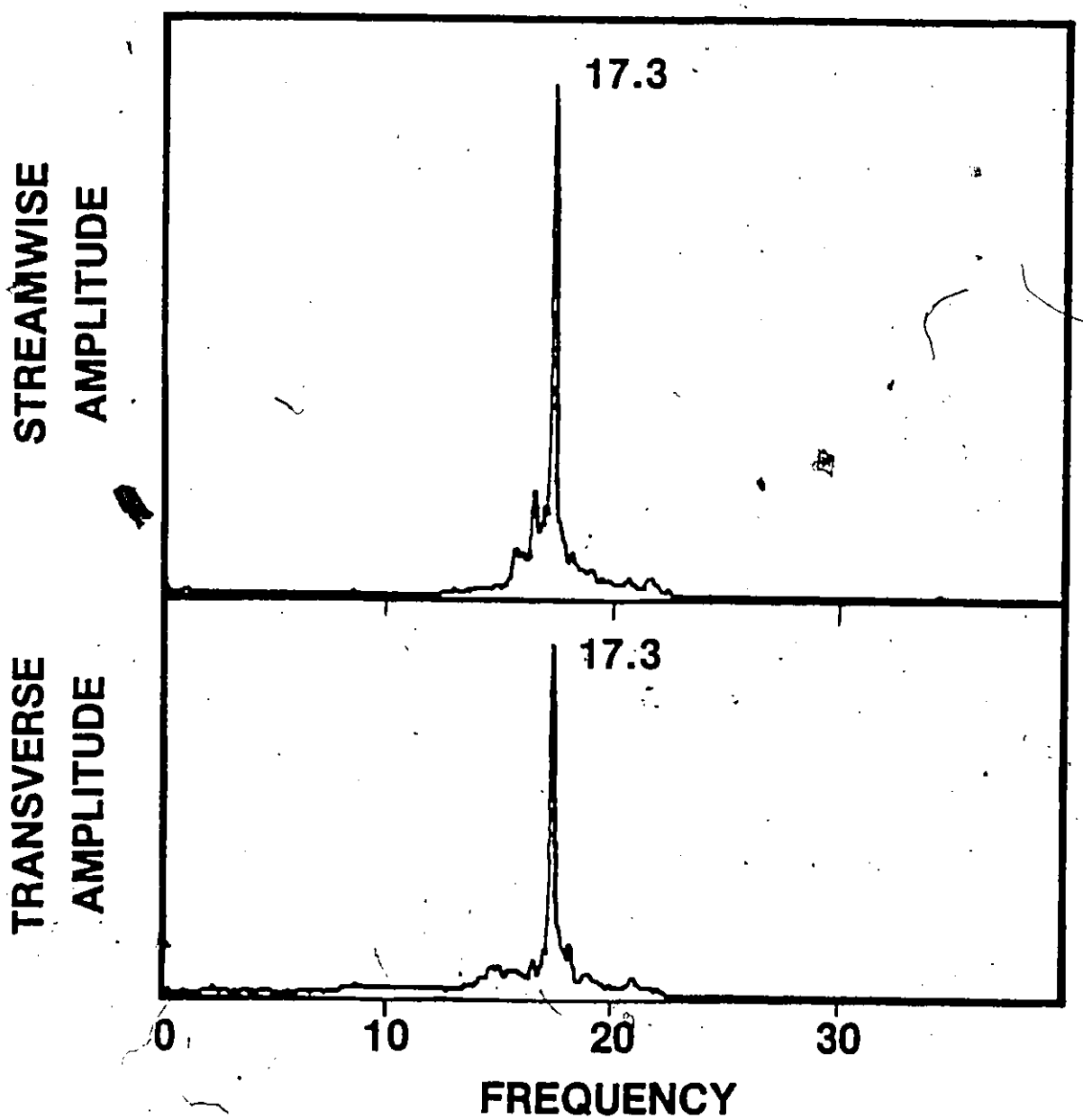

Figure 5.25 Response spectra of tube no.5 at $V_u = 0.37$ m/s

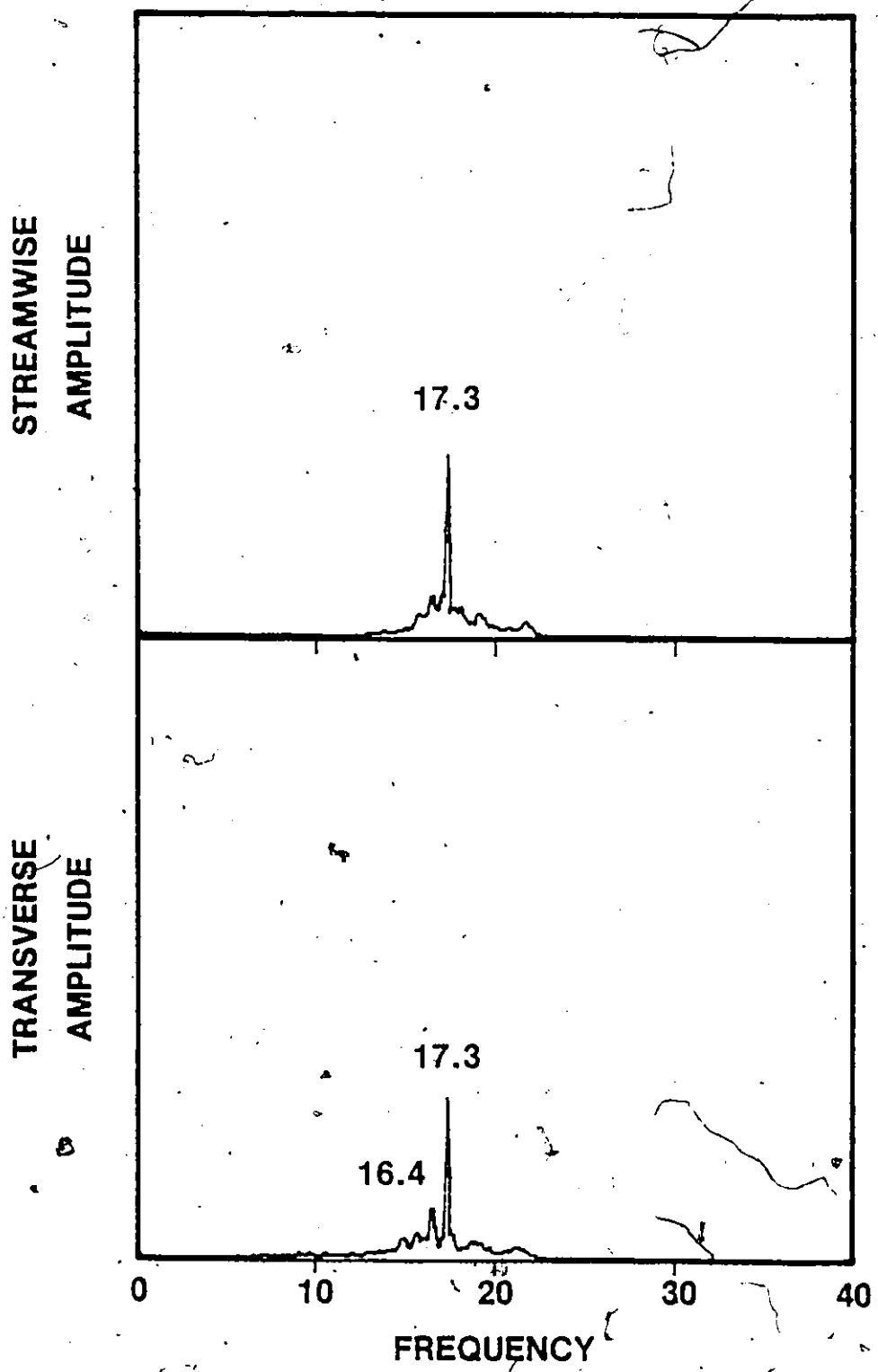

Figure 5.26 Response spectra of tube no.8 at V_u = 0.37 m/s

increasing levels of turbulence in the main stream flow from the second to the third tube row. Several other factors may also influence the response amplitude of this tube. The unstable time dependent relative mode between tubes, the interaction of this tube with the wake of tube no. 5 upstream of it as well as its own wake and, the strong fluid coupling are factors to be also considered.

It is seen from figure 5.12 that at the flow velocity V_u = 0.29 m/s, the overall RMS amplitude of tube no. 5 has reached a value of about 6 percent of a tube diameter. This response was attributed to "vorticity resonance" in section 5.4. In this regard, Weaver and Yeung [114] compared the stability thresholds as given by the "2 1/2% diameter amplitude" and "the sudden upturn" in the response curves definitions. It is clear from their plot of stability thresholds that the "2 1/2% diameter amplitude" criterion has yielded very low stability thresholds as compared with that given by the "sudden upturn" in the response curves definition for a square array. The results of the present investigation presented above, lend support to Weaver and Yeung's argument in favour of the latter definition of stability threshold. This further supports the contention that the excitation mechanisms in these two flow regions are different. Vorticity resonance is always associated with regular motions while fluidelastic instability has generally been observed to be associated with significant amplitude modulations. However, several contemporary theories suggest that the transverse response amplitude curve is more

important than the resultant amplitude curve in defining the critical velocity. Tanaka and Takahara [45, 46] demonstrated that, in an in-line array, the tubes lose their stability in the transverse direction. Very recently, Lever and Weaver [146] introduced a theoretical model for the prediction of fluidelastic instability in tube banks. Their theory is based on the premise that a tube in an array first loses stability in the direction transverse to the free stream. Lever [149] has shown that fluidelastic instability cannot be initiated in the streamwise direction. In view of this, the stability threshold in the present study is defined as the flow velocity at which

1 - a sudden upturn, or a trend of increasing amplitude with increasing flow velocity, occurs in the transverse response amplitude curve, and

2 - the disorganized frequency response gives way, with increasing flow velocity, to a more periodic one at the prevailing fluid coupled natural frequency.

According to this definition, it is reasonable to consider that the onset of fluidelastic instability is established at the flow velocity $V_u = 0.35$ m/s. At this flow velocity a sudden sharp upturn in the transverse amplitude response of tube no. 5 and a sustained trend towards increasing transverse response of tube no. 8 with increasing flow velocity beyond $V_u = 0.35$ m/s is observed. The disorganized

frequency response in the flow velocity range 0.32 m/s < V_u < 0.35 m/s has given way to a more periodic frequency response in the velocity range 0.35 m/s < V_u < 0.42 m/s as the spectra of figures 5.23 to 5.26 illustrate.

In support of this argument, Tanaka and Takahara [45, 46] demonstrated the dependence of the stability boundary on the reduced velocity. For similar in-line arrays, Weaver and Yeung [114, 115] reported that the critical reduced velocity at the onset of fluidelastic instability

$$\left(\frac{V_p}{f_n d}\right)_{cr} = 2.38.$$

In the present investigation, the calculated reduced velocity at instability based on the pitch velocity V_p = 3 x 0.35 m/s and the observed frequency of 17.3 Hz has a value of 2.36. This value compares very well with that reported by Weaver and Yeung.

In the post stable region, V_u > 0.35, cine films and photographs show that the amplitudes of vibration and the relative mode shape between tubes are both flow velocity and time dependent. At times the tube motion is primarily in the transverse direction with the tubes in a column in phase with one another and 180° out of phase with the neighbouring tube column. The photographs of figure 5.27 taken at V_u = 0.44 m/s depicts such relative mode between tubes and the flow redistribution which accompanies this motion. However, the large amplitude oscillations are highly modulated and at different times the relative mode shape between tubes changes

(a)

(b)

Figure 5.27 Flow Visualization at $V_u = 0.44$ m/s

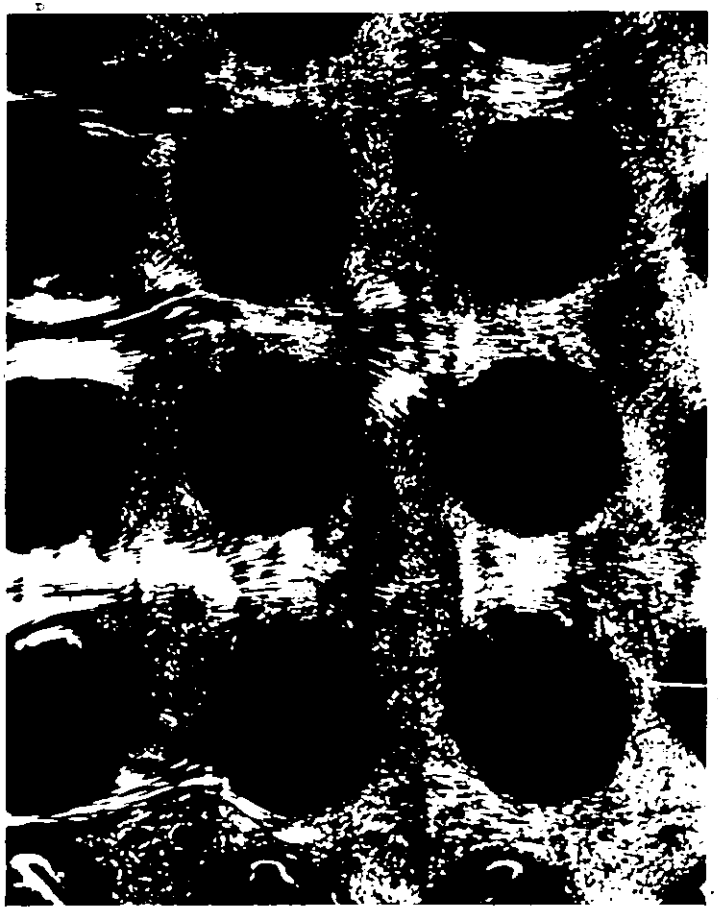

(a)

(b)

Figure 5.28 Flow Visualization at V_u = 0.44 m/s

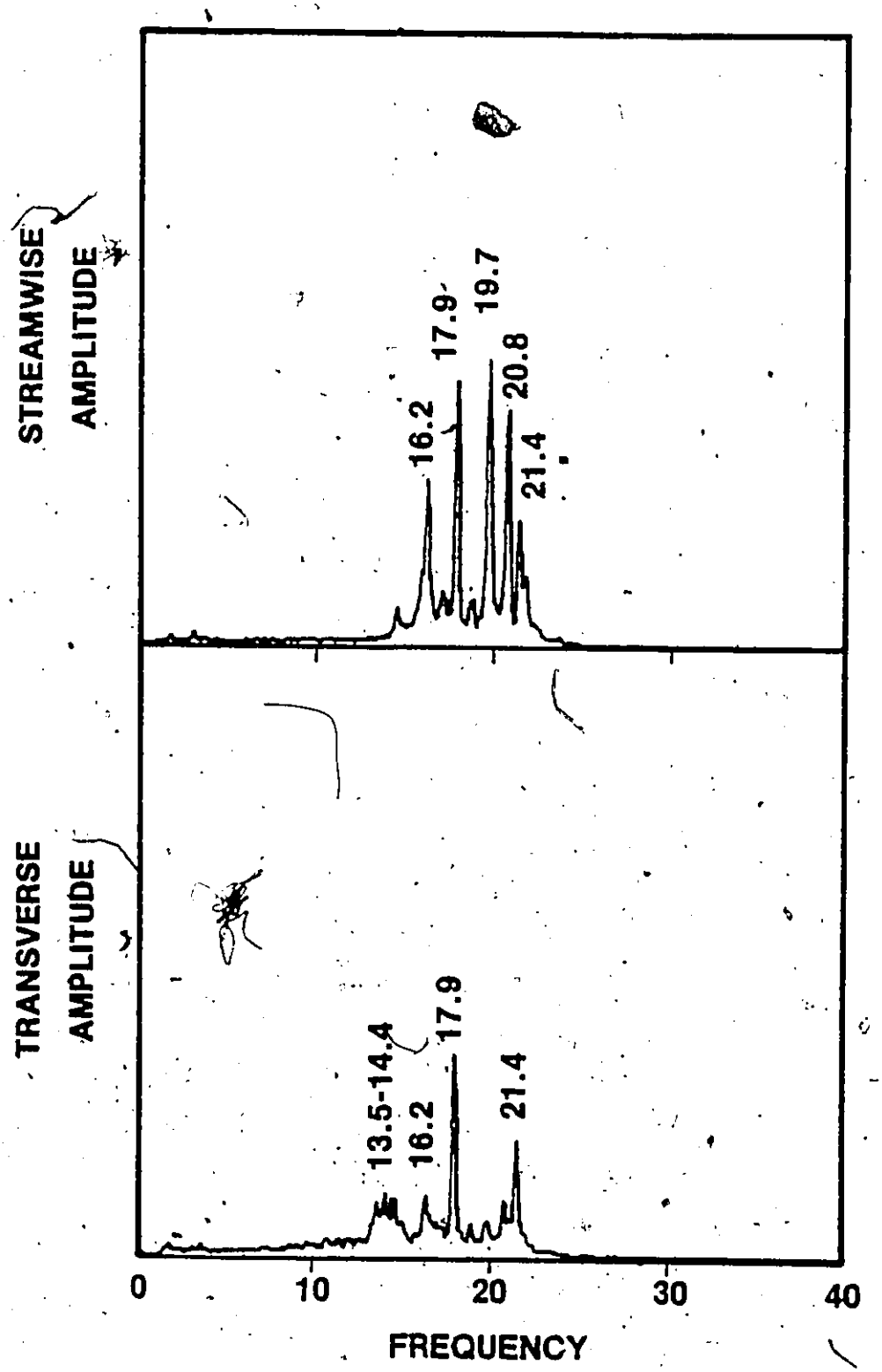

Figure 5.29 Response spectra of tube no.5 at 0.44 m/s

entirely. The tubes whirl in a less regular relative pattern with a notably different interstitial flow between tube rows and columns. Such a circumstance is illustrated in the photograph of figure 5.28(a) taken at the same flow velocity of 0.44 m/s. The spectra of figure 5.29, recorded at V_u = 0.44 m/s for tube no. 5, show that several spikes of variable strength appear at different frequencies as a result of the highly unstable relative mode shapes.

The rigidly mounted tube bundle was filmed and photographed at the same flow velocities. The photograph of figure 5.28(b), taken at V_u = 0.44 m/s depicts the interstitial flow structure and behaviour. Regular and relatively coherent main stream flow in the flow lanes is clearly seen which is attributed to the absence of tube motion. The only interference with the main stream flow comes from the turbulent wake flows as they leave the wakes and deflect the main stream flow randomly. The turbulent wake structure is clearly evident and the nature of flow behaviour is essentially the same as that seen earlier at lower flow velocities presented in figure 5.22 at V_u = 0.29 m/s.

CHAPTER 6

ROTATED SQUARE ARRAY RESPONSE

6.1 Introduction

In this chapter, the results obtained in investigating the rotated square array will be presented, discussed and compared with the results of other independent investigations. The overall RMS amplitude response curves of the two monitored tubes, tube no. 4 in the second row and tube no. 6 in the third row, are shown in figure 6.13. With reference to this figure, three different flow regimes are identified and discussed in separate sections. The interstitial flow structure in the flow velocity range $V_T < 0.14$ m/s, part OA of the response curves, is examined in section 6.2. Measurements of the RMS amplitude responses were not attempted, since the response is negligible. Flow regimes that developed with increasing Reynolds number are identified, the mechanics of vortex formation and shedding are established, and Strouhal numbers are calculated based on data obtained from the interstitial flow. In section 6.3, the resonant responses in the flow velocity range 0.14 m/s $< V_T <$ 0.83 m/s part AB of the curves, are discussed. Strouhal numbers are calculated based on data obtained from the response spectra of both monitored tubes. The undulatory nature of the stream-

wise and transverse response curves is explained in accordance with the calculated Strouhal numbers. Fluidelastic response in the flow velocity range 0.83 m/s < V_T < 1.02 m/s, part BC of the response curves, is then presented in section 6.4. Threshold velocities and critical reduced velocities, are calculated and nature of the excitation mechanism is explored.

The interstitial flow structure in a relatively rigidly mounted bundle is also investigated in the flow velocity range 0.48 m/s < V_T < 1.02 m/s using the developed flow visualisation technique. The interstitial flow structures of the flexibly and rigidly mounted bundles are compared, to illustrate the important effects of relative tube motions.

The important case of a single flexible tube in an otherwise rigid bundle is examined in section 6.5. The results are then compared with those of the same tube in the flexibly mounted tube bundle.

Three flow velocities can be identified for this array in figure 3.4. The upstream flow velocity V_u, the velocity in the gap between two tubes in the first row V_T, and the velocity in the minimum gap between two tubes V_g. The velocity V_T is calculated as,

$$V_T = \frac{2P \cos 45}{2P \cos 45 - d} \quad V_u$$

where

P is the pitch 35.9 mm

d is the diameter 25.4 mm

Accordingly,

$$V_T = 2V_u$$

The velocity V_g is calculated as

$$V_g = \frac{1}{2} \frac{2P \cos 45}{P-d} V_u$$

Accordingly,

$$V_g = \frac{P \cos 45}{P-d} V_u$$

$$V_g = 2.415 V_u$$

Both velocities V_T and V_g will be used in discussing the results of the rotated square array. In the square, in-line array, we had only one velocity to contend with, namely,

$$V_T = V_p = 3V_u$$

It is therefore expected that the main stream flow velocity in the flow lanes of a rotated square array will be lower than that in the square in-line array at the same V_u, since $V_g < V_p$.

6.2 Flow Developments at Low Reynolds Numbers

Despite the closeness of pitch to diameter ratio of the rotated square array and the square, in-line array, being 1.414 and 1.5 respectively, the different pattern of tube arrangement played an important role in shaping the developed flow pattern. The distance between two tubes in the same

column of the rotated square array, is twice as large compared with that distance in the square, in-line array. This means that the wake of a tube in the former array has twice as large a distance to develop than in the latter array. However, the presence of two tubes in close proximity on the opposite sides of the wake region of a tube in the rotated square array, alter the straight flow lanes of the square in-line array to S-shaped flow lanes. The main stream flow in the S-shaped flow lanes greatly influence the width of a tube wake in the rotated square array.

To identify the developing flow regimes in this array, the same procedure described in Chapter 5 was followed here. Up to a Reynolds number, based on the velocity in the minimum gap between two tubes, $Re_g \approx 40$, a regime of nearly unseparated flow develops. The laminar flow in the flow lanes follows the contour of the tubes and the streamlines close behind the tubes. The photograph of figure 6.1, taken at a flow velocity corresponding to a Reynolds number $Re_g \approx 20$, shows the essential features of this flow regime. This unseparated flow regime was not observed in the square in-line array and for an isolated circular cylinder it is expected up to a Reynolds number, $Re < 5$. A comparison between the flow regimes found in the rotated square array and those formed in the wake of an isolated circular cylinder is given in figure 6.8.

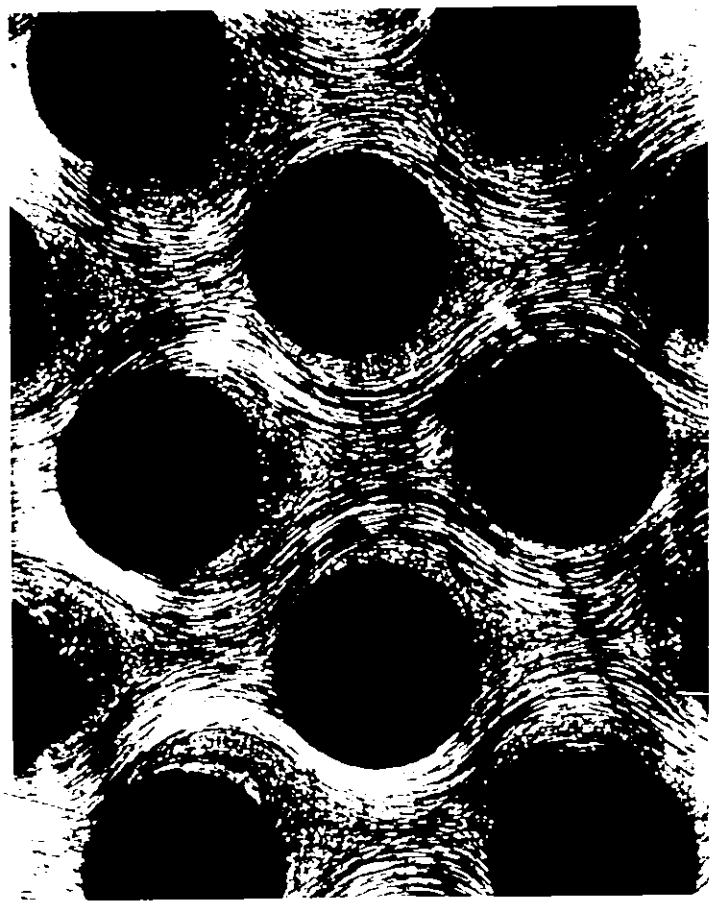

Figure 6.1 Flow Visualization at $Re_g = 20$

Figure 6.2 Flow Visualization at $Re_g = 120$

In the Reynolds number range $40 < Re_g < 150$ the boundary layers separate from the tubes in the successive rows. Wakes that vary in size are formed behind the first three rows as can be seen from the photograph of figure 6.2 taken at the Reynolds number $Re_g = 120$. The near wake behind a tube in the first row is about 13 mm long and the stream lines close together downstream of the wake. The wakes behind the second and third row tubes extend all the way to the downstream rows. A pair of stable elongated vortices, similar to the Foppl vortices formed behind an isolated circular cylinder in the Reynolds number range $5 < Re < 40$, are seen to develop in the wakes of the first three row tubes.

In the Reynolds number range $150 < Re_g < 250$, larger stable vortices are seen in the wakes of the first row tubes with the stream lines closing behind them. The wakes of the second and third row become unstable, the instability being manifested by the periodic oscillations of these wakes. The amplitude of wake oscillation behind a third row tube is larger than that of a second row tube. Consequently the instability of a third row tube wake is more pronounced than that of a second row tube. The photograph of figure 6.3, taken at a Reynolds number $Re_g \approx 240$, illustrates the features of this flow regime. Three separate vortex structures can be identified in the wake of tube no. 7, whose centers lie above and below the wake axis, as a result of vigorous wake oscillations. The wake flows do not interfere significantly up to this point with

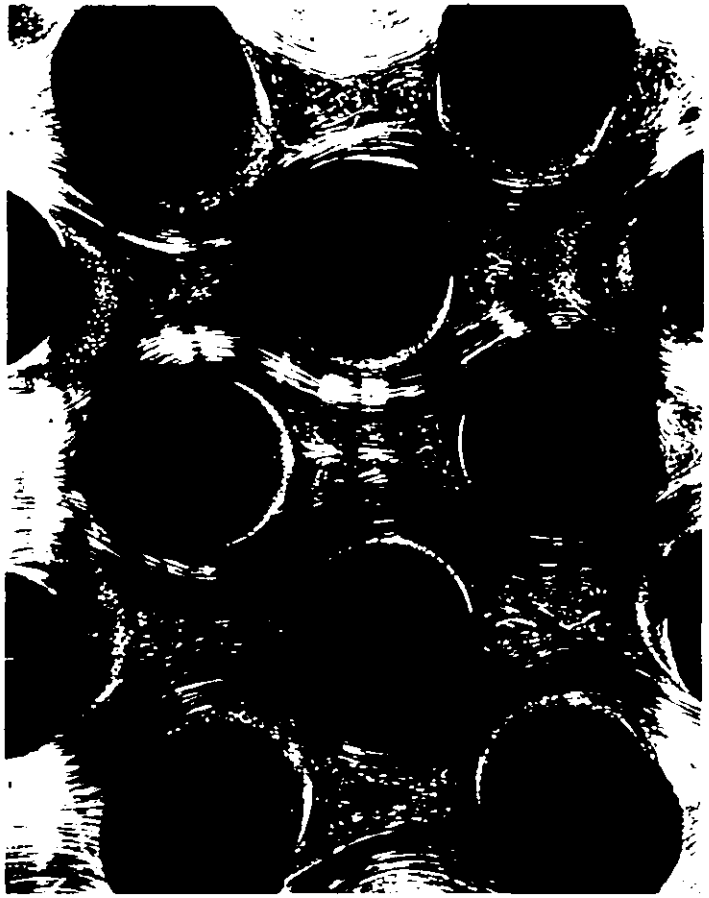

Figure 6.3 Flow Visualization at $Re_g = 240$

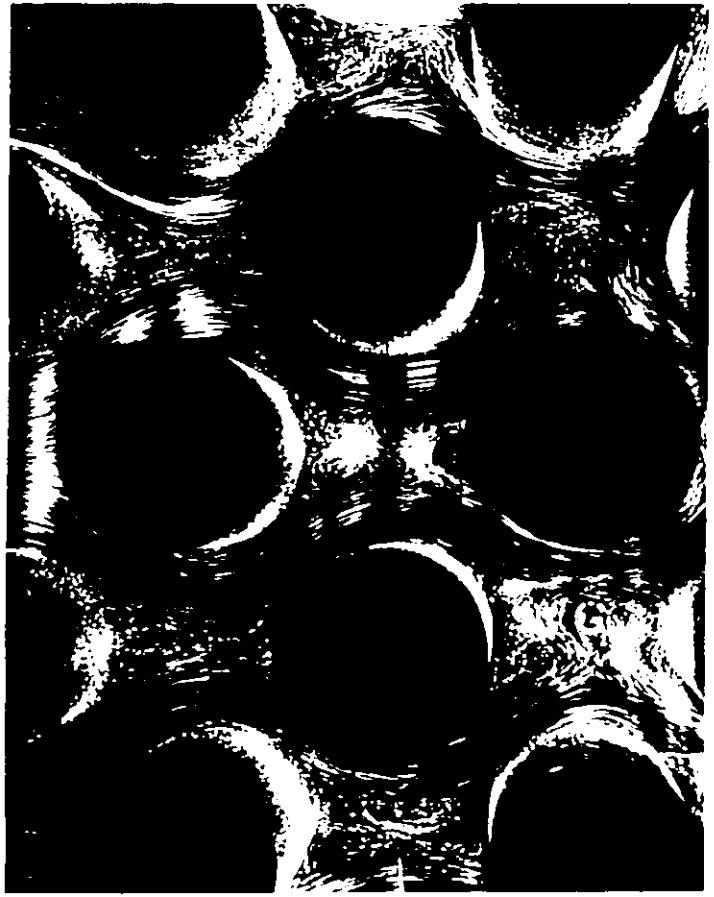

Figure 6.4 Flow Visualization at $Re_g = 320$

the main stream flow on either side of the tube. Only a small amount of flow crosses the wakes at their downstream ends, in front of the tubes of the downstream row, from one flow lane to the other and the wakes of the tubes widen with increased flow velocity, thereby narrowing to a certain extent the flow lanes. For an isolated circular cylinder, a regime of laminar vortex shedding in which the periodicity is governed by the wake instability, develops in the Reynolds number range $40 < Re < 90$.

In the Reynolds number range $250 < Re_g < 350$, the wake behind a first row tube extends all the way to the third row and continues to maintain stable vortices. The instability of a second row tube wake is more pronounced as the wake oscillation amplitude becomes larger, and alternate vortex shedding is established in the wakes of the third row tubes. The photograph of figure 6.4 taken at the Reynolds number $Re_g \approx 320$ illustrates the flow development in this Reynolds number range. Three vorticies can be identified in the wake of tube no. 4 similar to those observed in the wake of tube no. 7 in the previous flow regime. In the wakes of tube no. 6 and tube no. 7, two full size vortices can be seen. Each of these vortices will leave the wake, after its structure has been deformed, and enter the main stream flow as a newly formed vortex begins to grow. In doing so, the vortex leaving the wake region directly interferes with the main stream flow as is evident in the photograph. For an isolated circular cylinder, a laminar vortex street is established in the Reynolds number

range $90 < Re < 150$ whose periodicity is governed by the vortex shedding frequency.

In the Reynolds number range $350 < Re_g < 550$ alternate vortex shedding is observed in the wakes of the second and third row tubes. Unstable vortex shedding develops in the wakes of the first row tubes. Two photographs of the alternate vortex shedding process inside the tube bundle, taken at the Reynolds number $Re_g = 480$, are given in figure 6.5. It can be seen that the new born vortices at the tube shoulders advance into the wakes of the second and third row tubes while the old vortices are deformed by contact with the downstream tube and ultimately are smeared into the flow lanes. It can also be seen by comparing the photographs of figure 6.5 with those of figures 6.1 and 6.2, the extent of deformity of the main stream flow in the flow lanes. This is the result of vortex shedding in the wakes of the tubes and the subsequent interference of the wake flows with the main stream flow in the flow lanes. Cine-films taken in this Reynolds number range indicate that no obvious phase relationship exists between the vortices shed from the tubes of any row. The non-existence of such relationship is a direct consequence of the influence of the tube pattern on the flow development inside the tube bundle. The presence of the next row tubes prevents the establishment of direct communication between the wakes of the former row. For an isolated circular cylinder the laminar vortex shedding process continues in the Reynolds number range

(a)

(b)

Figure 6.5 Flow Visualization at $Re_q = 480$

$150 < Re < 300$, with a transition to turbulence in the vortex filaments.

Further developments in the main stream flow and the wakes of the tubes take place in the Reynolds number range $550 < Re_g < 2.1 \times 10^3$. At a Reynolds number $Re_g = 600$, a separation bubble is seen to form on the lower sides of tube no. 6 and tube no. 7 in the third row as a result of flow separation and reattachment to the tube surface. After formation it travels downstream with the flow, close to the surface of the tube and is discharged in its wake. The cine film taken shows that the fluid contained within the separation bubble performs a circulatory motion during its travel. Two close up photographs for tube no. 6 and tube no. 7 are given in figure 6.6 where the separation bubble can be easily identified. This phenomenon has never been reported in the published literature at such low Reynolds numbers.

The photographs of figure 6.7 were taken at a slightly higher Reynolds number of $Re_g = 670$. The photographs show the essential features of flow and wake developments behind the first three successive rows. It can be seen that turbulent small wakes exist behind the tubes of the third row, and that part of the main stream flow crosses diagonally from one flow lane on either side of the tube to the other. Turbulent vortices are shed in the wakes of the second row tubes and relatively more coherent vortex structures can be identified in the wakes of the first row tubes. For an isolated circular

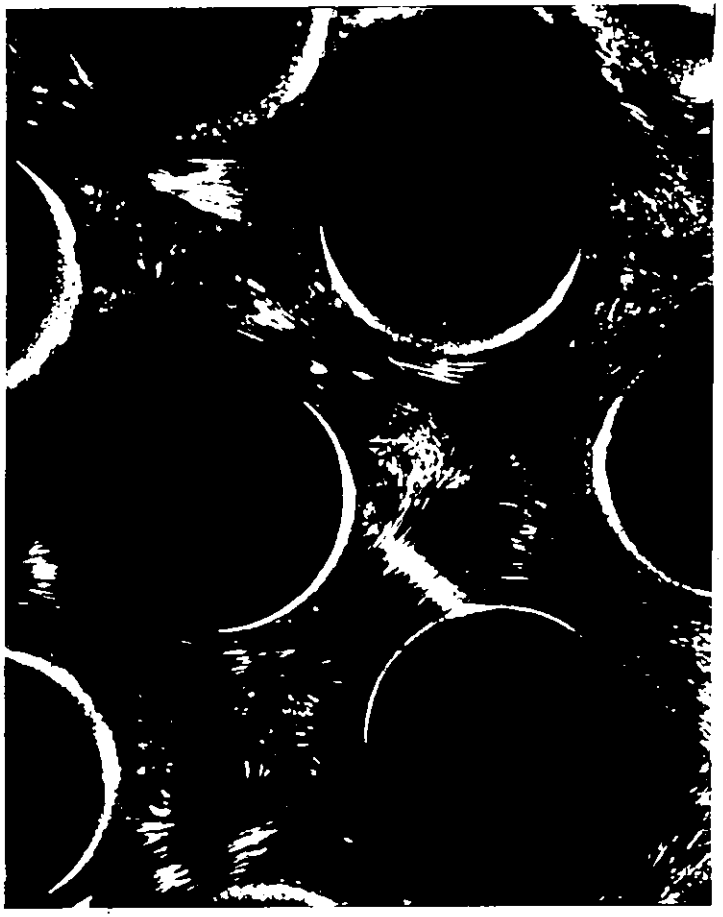

(a)

(b)

Figure 6.6 Flow Visualization at $Re_g = 600$

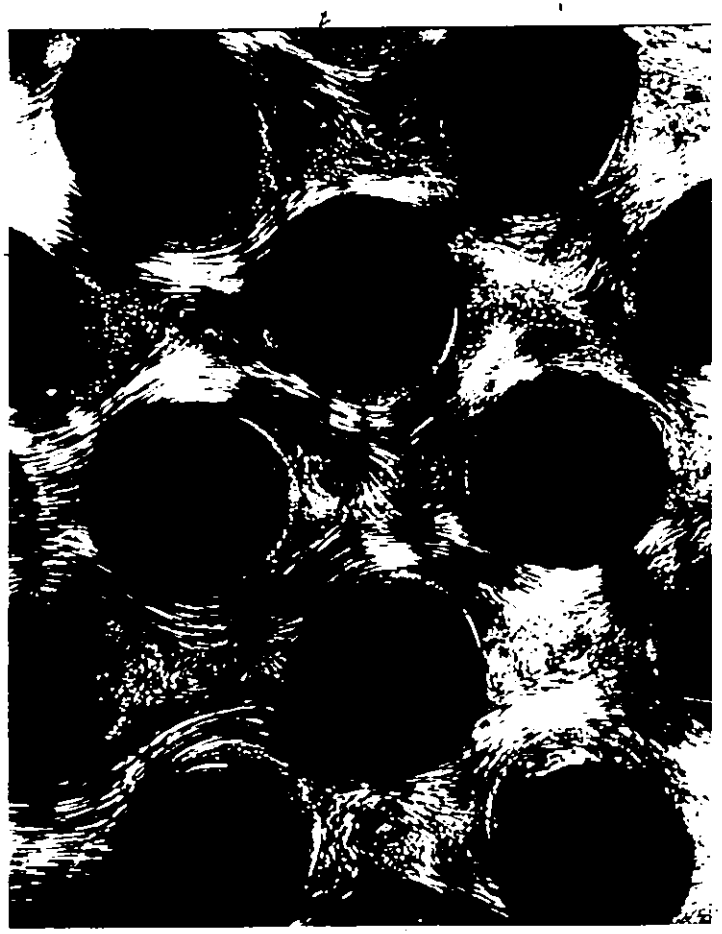

(a)

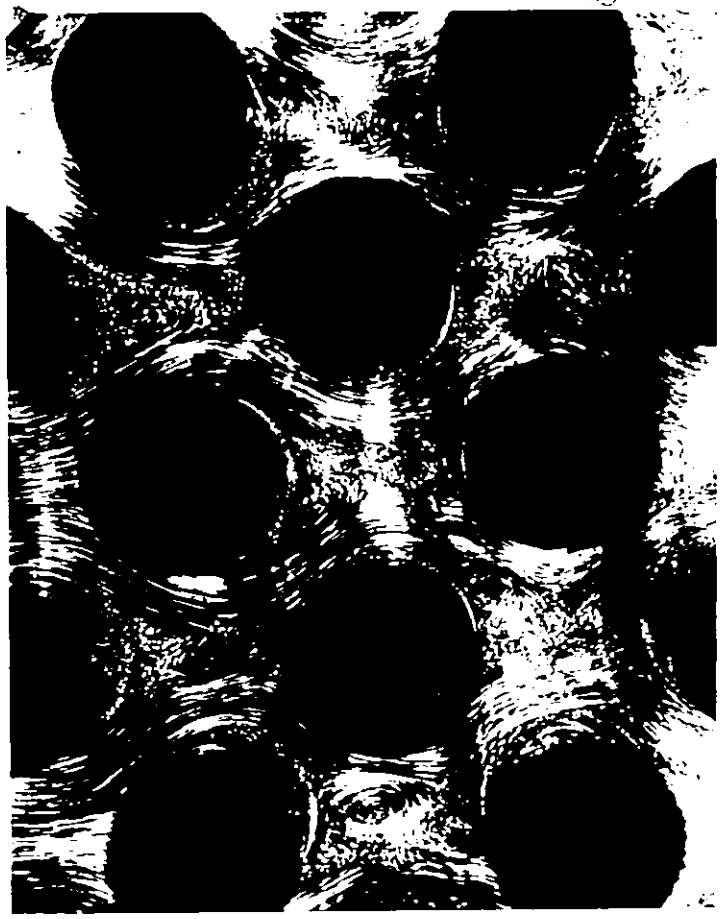

(b)

Figure 6.7 Flow Visualization at $Re_g = 670$

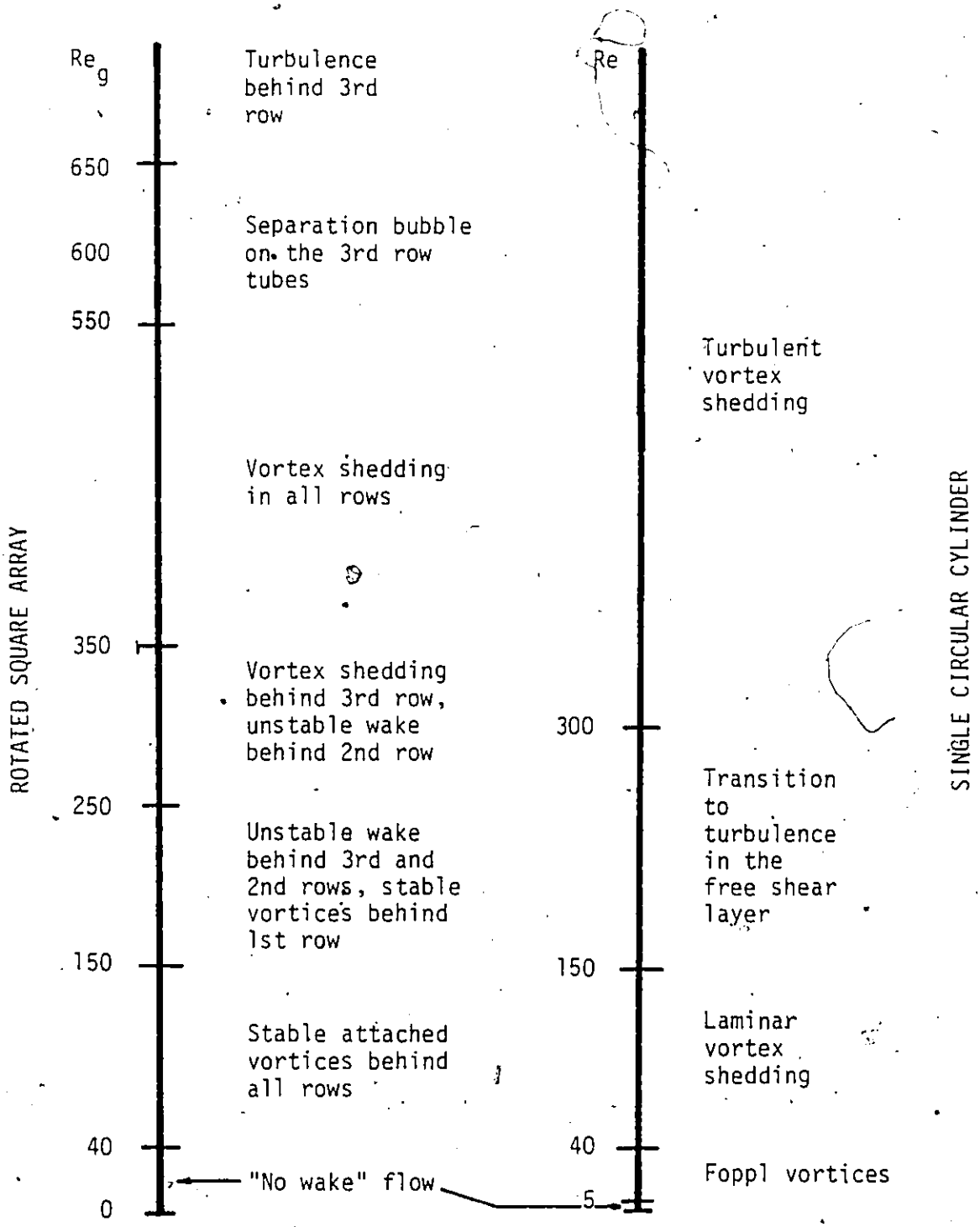

Figure 6.8 Comparison between the flow regimes behind an isolated cylinder and those found in the rotated square array

cylinder a fully turbulent vortex street is established in the Reynolds number range $300 < Re < 2 \times 10^5$. Such a turbulent vortex street is not observed in the rotated square array due to close proximity of the downstream rows, i.e., while the transition to turbulence in the wake of an isolated cylinder produces a turbulent periodic vortex street, transition to turbulence in the wake of tubes in an array apparently produces no such regular wake structure.

In summary, the structure of the interstitial flow in the first three rows of the rotated square array is found to depend on the row depth and the Reynolds number range. Within a given Reynolds number range, the wake size and structure behind the first three rows are different. Flow regimes behind a tube in a given row change with different Reynolds number ranges. The flow regimes formed in the wake of an isolated circular cylinder in a cross flow are found to develop behind the third row of tubes at comparable Reynolds numbers. Nevertheless, small wakes are found behind the third row tubes when the Reynolds number Re_g exceeds 550, in contrast with a fully turbulent vortex street behind an isolated circular cylinder in the range $300 < Re < 2 \times 10^5$. Although the same flow regimes eventually develop in the wake of a second row tubes the correlation with the Reynolds number ranges reported for the isolated circular cylinder generally decreases. This suggests that nearly fully developed main stream flow in the flow lanes is established at about the third row of tubes. Except in the

narrow range of Reynolds numbers $350 < Re_p < 550$ where large vortices are formed and shed and in the absence of tube motion, the flow lanes are strongly sinusoidal in shape and almost constant in width. The geometrical characteristics suggest that in the interior of the rotated square array considered here where a fully developed main stream flow is established, similar flow fields encircle each individual tube. Therefore, the tube bundle behaviour can be studied by considering only one tube in such a flow field whose dynamical characteristics are related to its geometrical characteristics stated above.

The results presented so far, although at low Reynolds numbers agree in principle with the results of Zdravkovich and Namork [48, 49]. Neither the first nor the second rows of tubes, typically represent the tube bank. The interstitial flow structure within the first two rows is different from that behind the third row. Only the main stream flow approaching the third row can be considered as nearly fully developed and therefore approaching that of deep inside a tube bundle. The investigation of Grover and Weaver]30] indicated that turbulence intensity reaches a maximum value after about four rows of tubes.

6.2.1 The Mechanics of Vortex Formation and Shedding

The flow separation from a stationary isolated cylinder and the ensuing vortex formation, growth and motion have been extensively studied. The phenomenon of an alternating vortex

street is intrinsic to the flow itself and results from the interaction between the shear layers, base pressure, diffusion and dissipation of vorticity and the far wake, i.e., a consequence of the particular velocity distribution throughout the field [78]. Gerrard [74], based on Bloor's investigation [150] of the formation region, proposed a physical model that describes the process of vortex shedding from an isolated stationary cylinder. The vortex itself was assumed to be formed by rolling-up of the shear layer. An irrotational flow from outside the wake, crosses the wake axis bringing with it the fluid from the other shear layer, which bears vorticity of opposite sign to that of the entraining layer. The fluid from the opposite shear layer is partly entrained by (a) the growing vortex and (b) partly by the shear layer upstream from the vortex. The rest of the flow will find its way into the interior of the formation region adjacent to the cylinder base. The part (b) of the entrained fluid, bearing vorticity of opposite sign, cuts off further circulation from the separated shear layer that feeds the vortex. The mature vortex is then shed and moves downstream. The proposed physical model is devised for the Reynolds number range $10^3 < Re < 5 \times 10^4$ where transition to turbulence moves upstream in the shear layer. Griffin and Ramberg [151] forced a cylinder to vibrate in a transverse direction at 85% of the Strouhal frequency with an amplitude of 0.5 of the tube diameter. They reported, and substantiated their findings by photographs, that the wake

patterns and the entrainment process behind the vibrating cylinder support in detail, Gerrard's model. Sarpkaya [78, 152] proposed a mechanism, exhibited by numerical experiments that is quite similar but not identical to that suggested by Gerrard [74]. According to this mechanism, instabilities begin to develop in one of the shear layers, which is drawn across the wake in response to reduction in the base pressure initiated by the action of the vortex growing on the other side of the wake. This nearly corresponds to a time when the shear layer drawn in has least circulation or is most permeable, and the vortex growth has already been reduced to a minimum. The break up of further supply to the vortex is attributed to stretching, diffusion and dissipation action of vorticity that breaks up the deforming turbulent vortex sheet. The first vortex is then shed while the other vortex is growing at a decreasing rate. It entrains part of the oppositely signed vorticity left in the wake by the cut sheet and the irrotational fluid drawn from outside through the opening created by the shedding of the first vortex. When the circulation in the feeding sheet decreases to its minimum, the sheet deforms, diffuses and is drawn across the wake by the reduction of the base pressure due to the action of another vortex growing on the other side of the wake and the shedding cycle repeats itself. Shedding of a vortex in the models of Gerrard and Sarpkaya is initiated by cutting off further supply of circulation from its sheet. The two models differ in the way by which further supply

of circulation is cut off.

These detailed observations regarding vortex formation behind a single cylinder are very helpful in studying and interpreting the vortex shedding phenomenon observed in the rotated square tube array. The insight gained of the shedding process from the cine-films, taken particularly in the Reynolds number range $350 < Re_p < 550$, permitted the drawing of the idealized sketches of figure 6.9 to illustrate the process of vortex formation and shedding. As the shear layer springing from the lower shoulder of the tube enters the wake region it rolls up into a small vortex adjacent to the tube aided by the circulation of the flow into the already separated one, figure 6.9(a). The shear layer continues feeding the vortex as it grows and advances into the wake region, figure 6.9(b). The old vortex being squeezed against the downstream tube, begins to deform. The shear layer springing from the upper shoulder of the tube rolls up into a small vortex adjacent to the cylinder in the same manner. Figure 6.9(c) depicts the new born, the fully detached, and the deformed vortices as the latter joins the main stream in the upper flow lane. This constitutes half a cycle of vortex shedding and is repeated for the second half.

It is important to note that the process just described is a laminar vortex shedding process which takes place in the Reynolds number range $350 < Re_g < 550$ whereas Gerrard's model is devised for the Reynolds number range $10^3 < Re < 5 \times 10^4$,

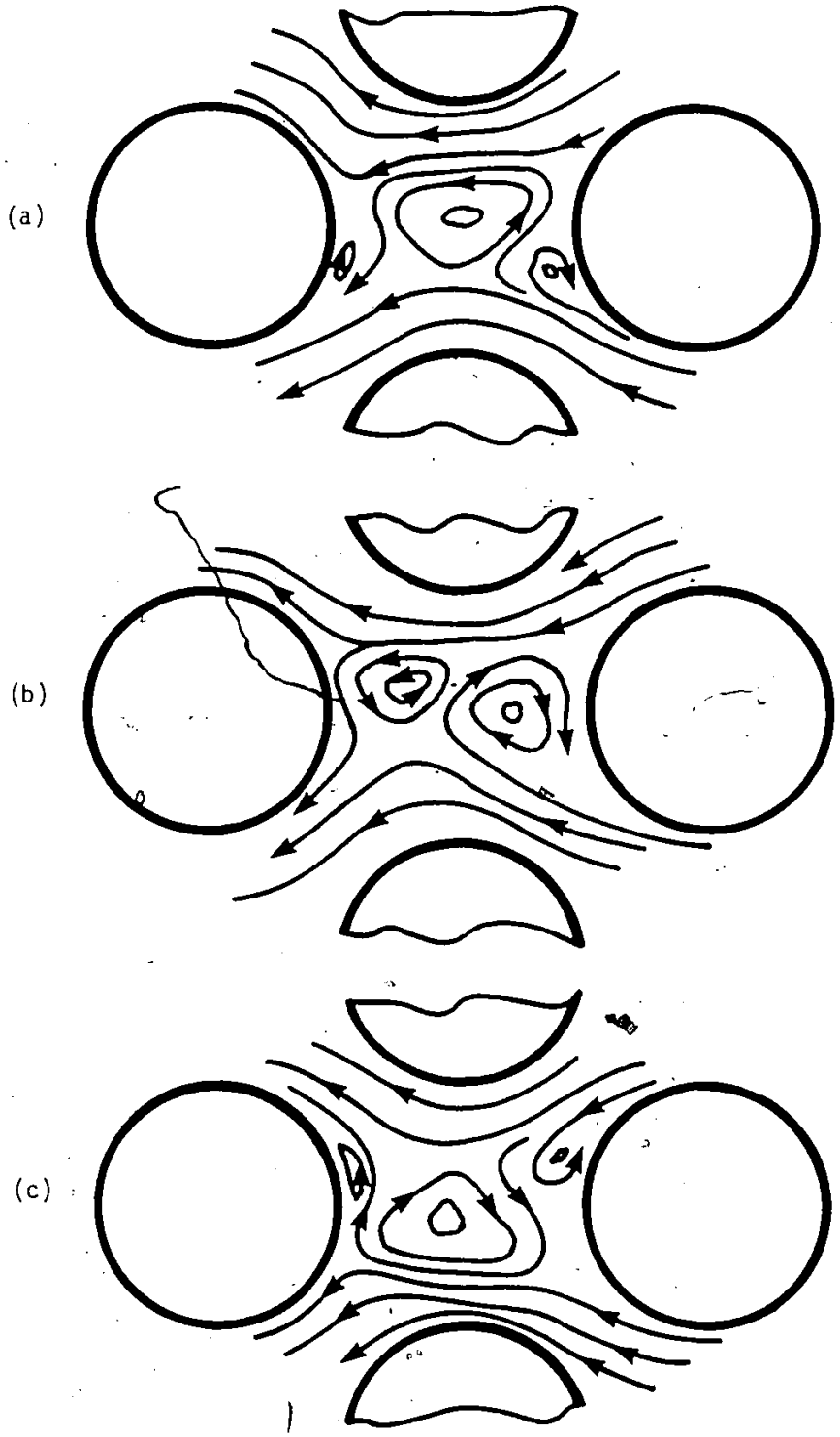

Figure 6.9 Vortex formation and shedding

where transition to turbulence moves upstream in the shear layer. The laminar vortex shedding process occurs within the confinement of the rotated square array and therefore is subject to the influence of the wing tubes on either side of the wake and the proximity of the downstream cylinder. On the other hand Gerrard and Sarpkaya's models were suggested for a free wake of an isolated circular cylinder in a uniform cross flow.

6.2.2 Strouhal Number Calculations

From the cine-films taken for the tube bundle it was possible to determine Strouhal numbers for the discrete vortex shedding process that took place in the wakes of tube no. 4 and tube no. 6. The vortex shedding process as seen in these cine-films is not stationary. The shedding process continues for a period of time after which the regular shedding of vortices is interrupted and either irregular vortex shedding takes place or no vortex shedding occur at all. This lasts for a short period of time after which the regular vortex shedding process resumes again. The number of vortex cycles and the number of frames containing these cycles were counted. The frequency f_c of vortex shedding was calculated as

$$f_c = \frac{\text{number of vortex cycles}}{\text{number of frames}} \times \text{framing rate}$$

A Strouhal number S_T was then determined based on the flow velocity V_T in the gap between two tubes in the first row, since

most Strouhal data reported in the literature are based on this flow velocity. The Strouhal numbers S_g and S_u based on V_g and V_u respectively can be obtained directly from the relations

$$S_g = 0.83\ S_T, \quad \text{and}$$

$$S_u = 2\ S_T$$

The calculated frequency, f_c, of discrete vortex shedding, is drawn against the transverse velocity V_T in figure 6.10. Points A and B correspond to the frequency of vortex shedding behind tube no. 6 at two different flow velocities. A straight line is drawn through these two points and as can be seen, the relationship is linear. The calculated Strouhal number for this line is $S_T = 1.1$. Points C and D correspond to the frequency of vortex shedding behind tube no. 4 at higher flow velocities. A straight line is drawn for these points but, as can be seen, the fit is not as good as for the 3rd row tube. This may be the result of the higher Reynolds number and tendency toward greater turbulence. The calculated Strouhal number for this line is $S_T = 1.3$. The two average Strouhal number lines are redrawn in figures 6.11 and 6.12 for comparison purposes. Such Strouhal numbers are calculated for the flow velocity range $0 < V_T < 0.02$ m/s. The Strouhal numbers reported in the literature are based on detected periodicities recorded at higher flow velocity ranges.

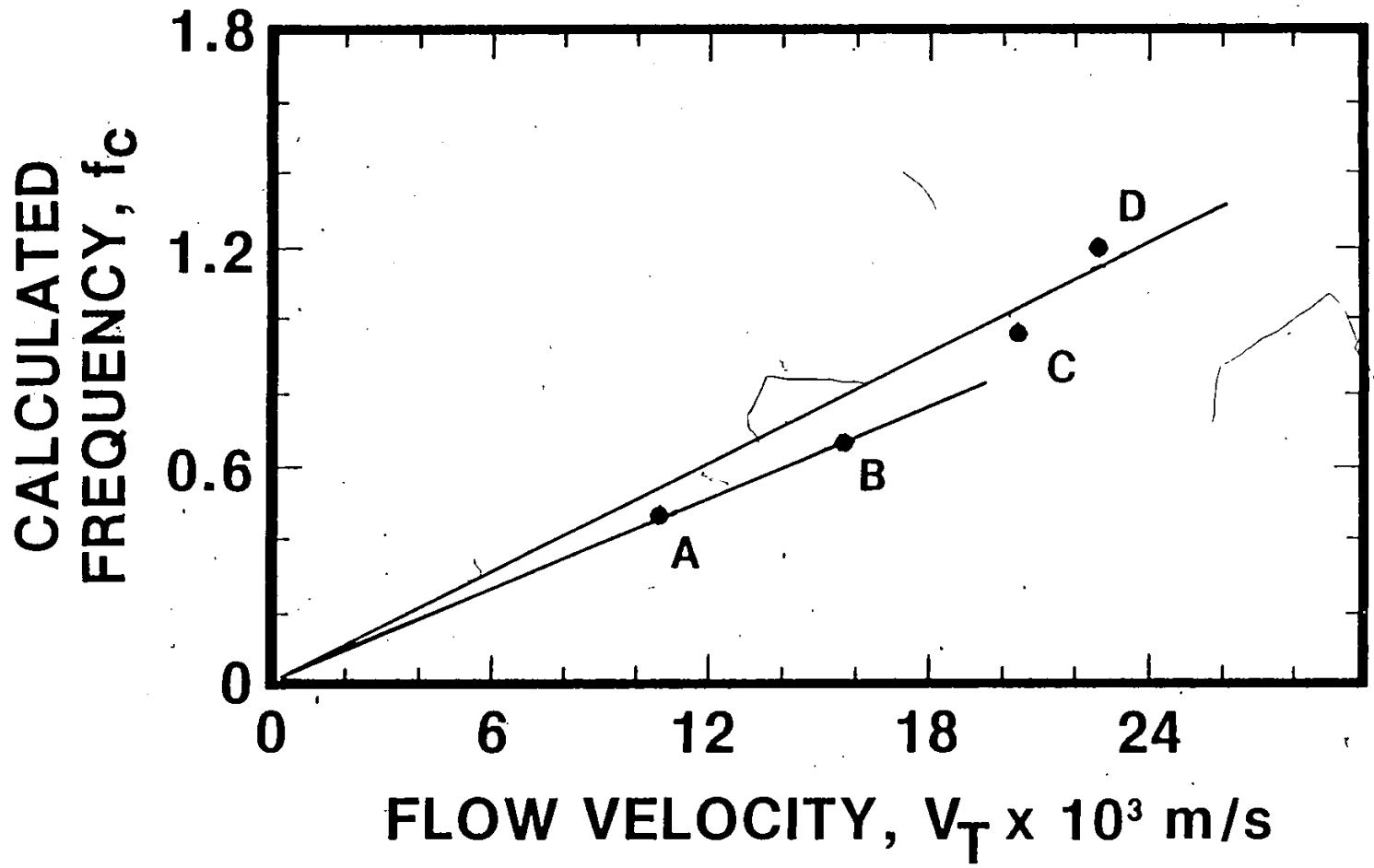

Figure 6.10 Strouhal lines for the observed vortex shedding process

6.3 Resonant Response of Both Monitored Tubes

The streamwise and transverse response curves of tube no. 4 and tube no. 6 are given in figures 6.11 and 6.12 respectively. The overall RMS amplitude response curves of both monitored tubes are given in figure 6.13. The velocity V_T in these figures denotes the flow velocity between two adjacent tubes in the first row and is equal to twice the upstream flow velocity. The choice of V_T permits direct comparison with the pertinent data reported in the technical literature. While the responses of the two tubes differ in some details, the excitation mechanisms involved are essentially the same. In the flow velocity range $0.14 < V_T < 0.55$ m/s, the response amplitudes greadually increase with increasing flow velocity and the response is random in nature. Two noticeable events are observed in the response curves of figures 6.11 and 6.12 at higher flow velocities. The first occurs at 0.66 m/s where a peak and a kink in the streamwise and transverse responses respectively are seen in figures 6.11 and 6.12. Such an event is passed undetected in the overall RMS response curves of figure 6.13. The second takes place at 0.80 m/s where two peaks can be seen in the transverse response curves of both monitored tubes. The dominance of the third row tube transverse response over that in the streamwise direction rendered this peak visible in the corresponding curve of figure 6.13. The peak is followed by a trough at the flow velocity $V_T = 0.83$ m/s after which the response amplitudes rise again

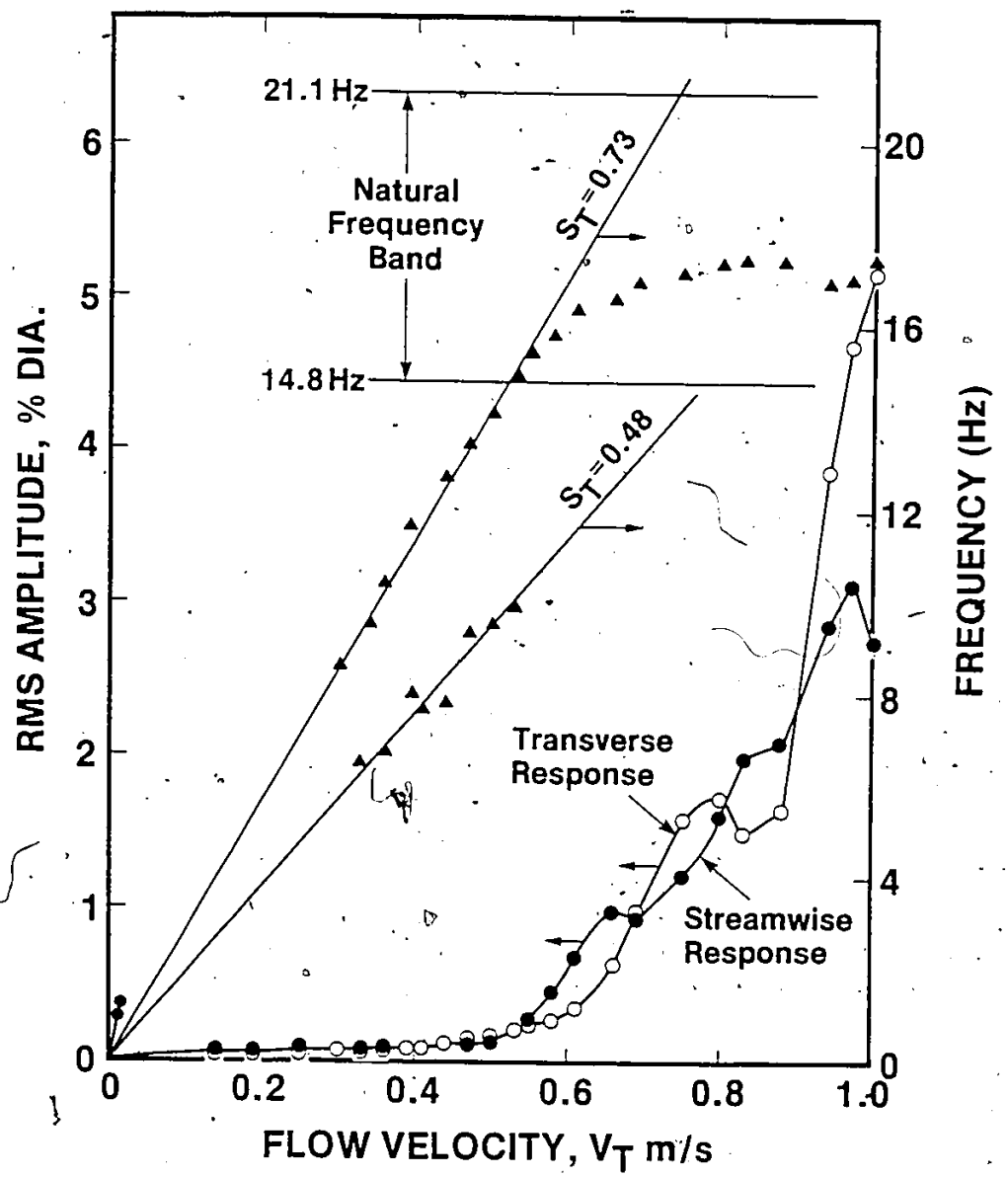

Figure 6.11 Response of tube no.4 in the second row

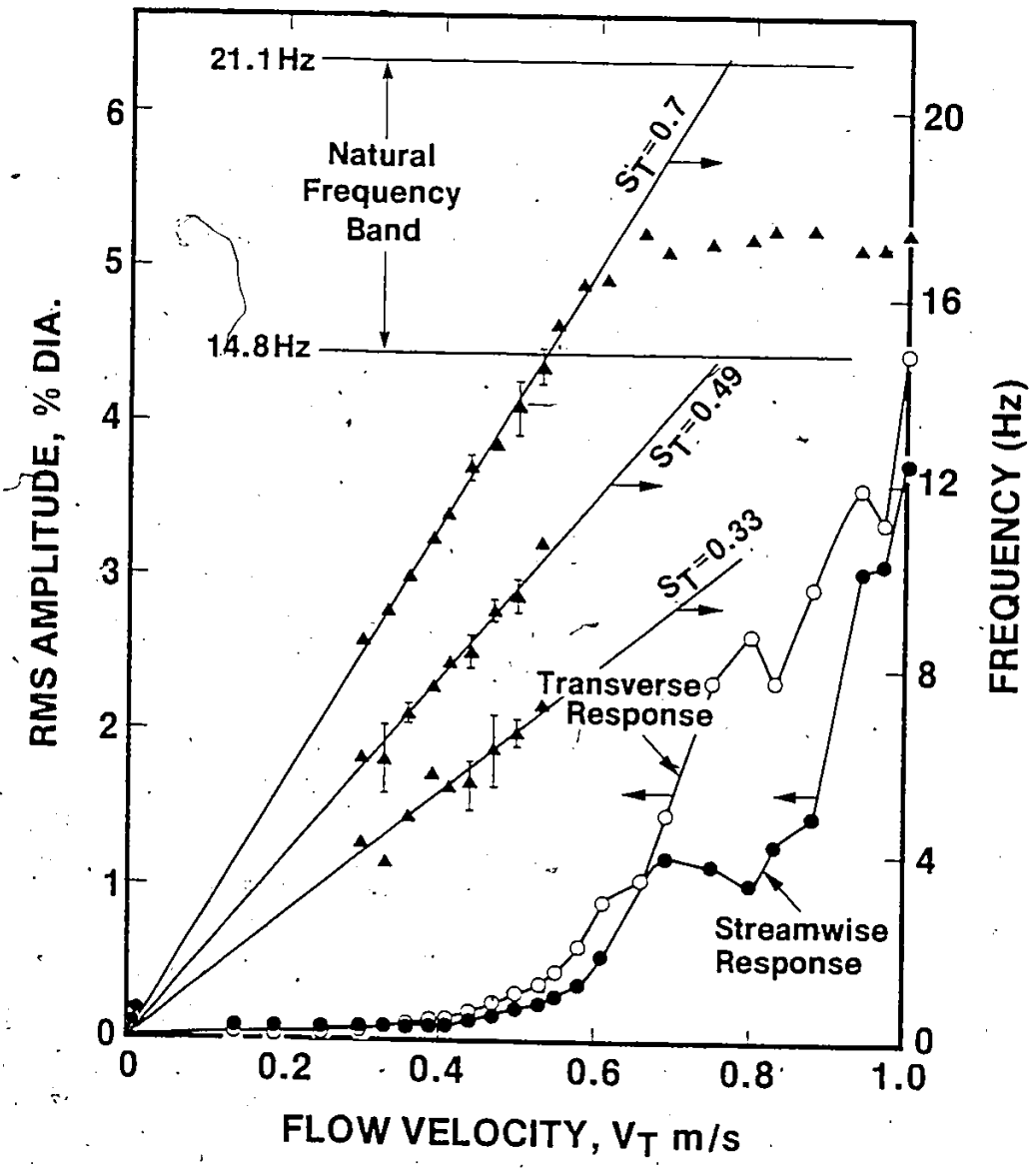

Figure 6.12 Response of tube no.6 in the third row

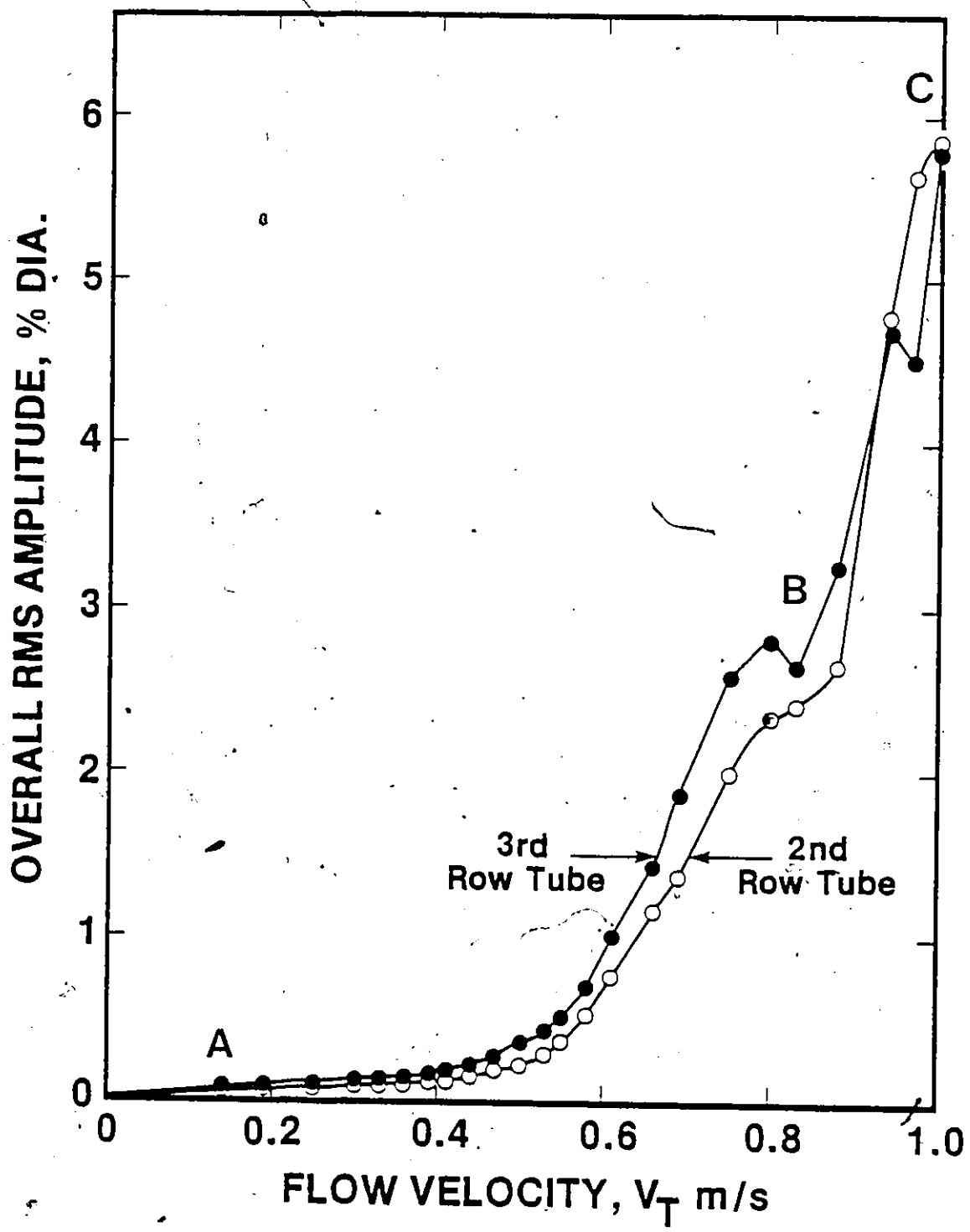

Figure 6.13 Overall RMS responses of the two monitored tubes

sharply with a small increase in the flow velocity.

In the present investigation, the smallest flow velocity at which different flow periodicities were detected is $V_T = 0.30$ m/s. In the range $0.02 < V_T < 0.30$ m/s turbulence dominates so that no coherent vortex structure can be seen and the flow periodicity is too weak to be detected. Thus, uncertainty regarding the relationship between the frequency of flow periodicity and the flow velocity reigns over this range.

Frequency spectra, taken at different flow velocities above 0.30 m/s, are given in figures 6.14 to 6.16 for tube no. 6 and 6.17 for tube no. 4. Figure 6.14, recorded at $V_T = 0.36$ m/s, depicts the cluster of fluid coupled natural frequencies in the range of about 14.8 to 21.1 Hz. In these and other spectra a dominant spike appears at 16.7 Hz in the lower range of the fluid coupled natural frequency band. The frequency of this spike weakly depends on flow velocity and tube location. At the same flow velocity, the frequency at which the spike appears in the spectra of tube no. 6 is slightly different from that at which the spike appears in the spectra of tube no. 4. With increasing flow velocity, the frequency at which the spike appears in the fluid coupled natural frequency band, in the spectra of both monitored tubes, slightly changes.

The transverse response spectra of figures 6.14 to 6.16 illustrate that two kinds of response coexist at lower

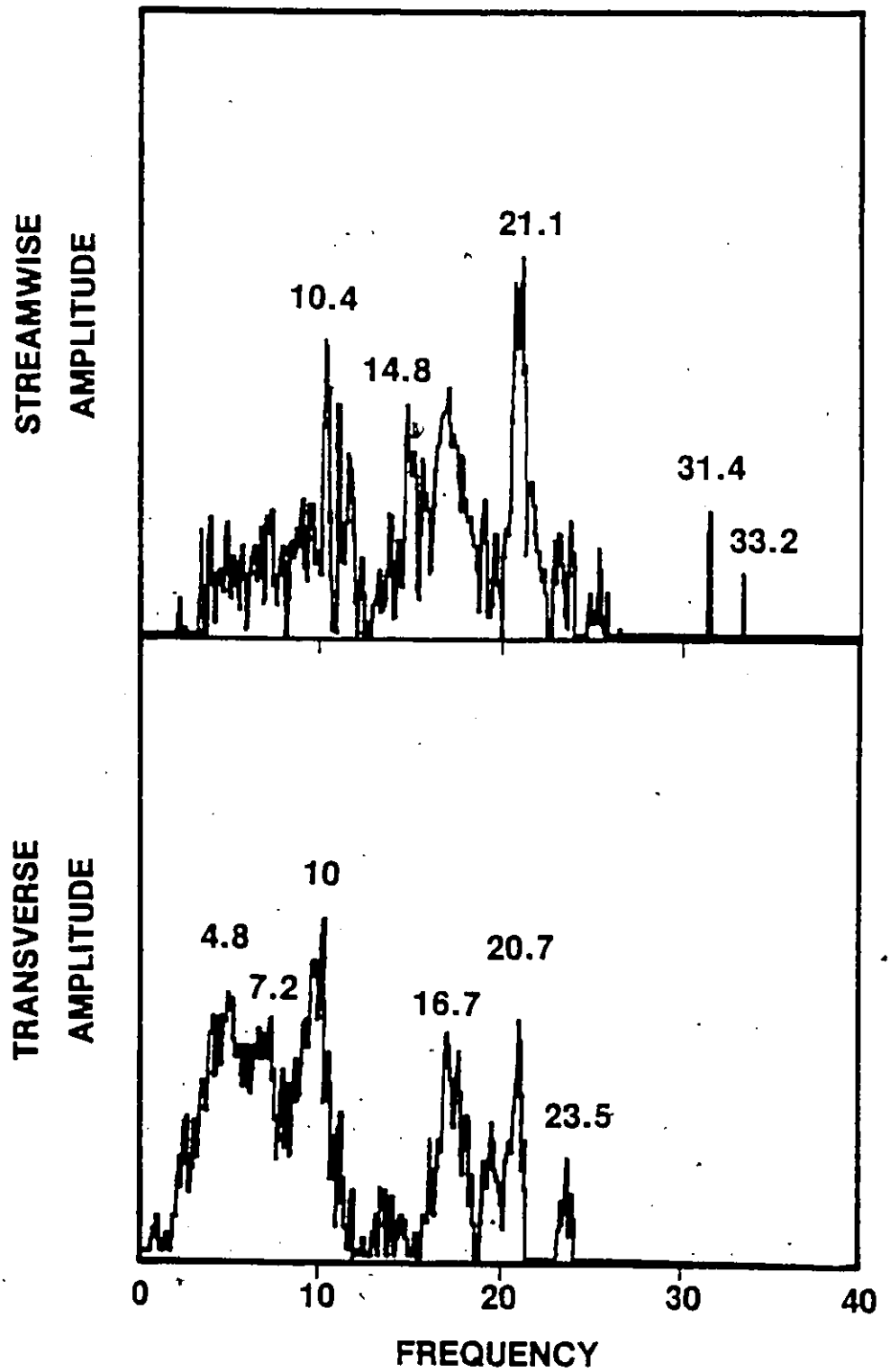

Figure 6.14 Response spectra of tube no.6 at V_T= 0.36 m/s

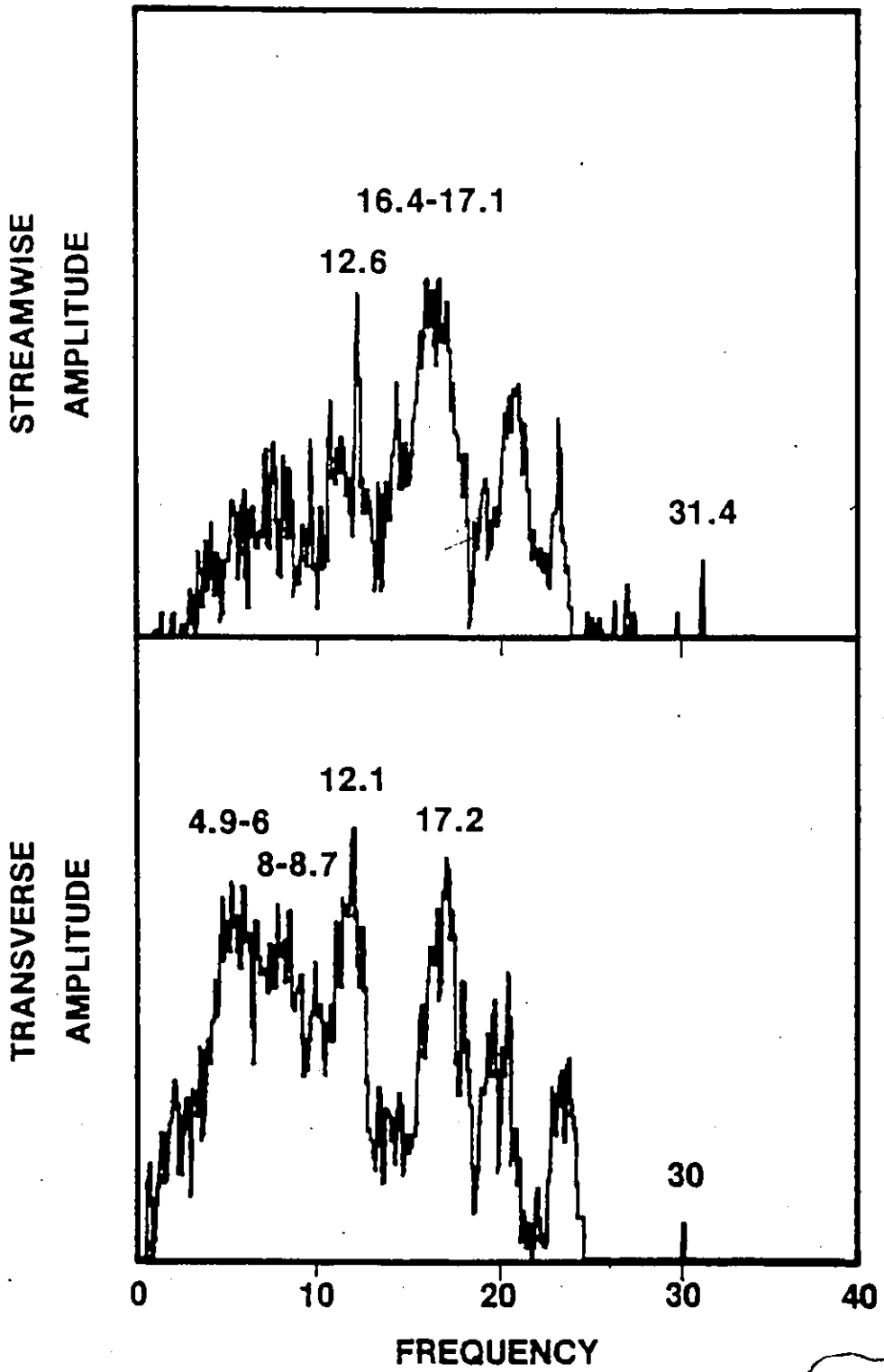

Figure 6.15 Response spectra of tube no.6 at V_T= 0.44 m/s

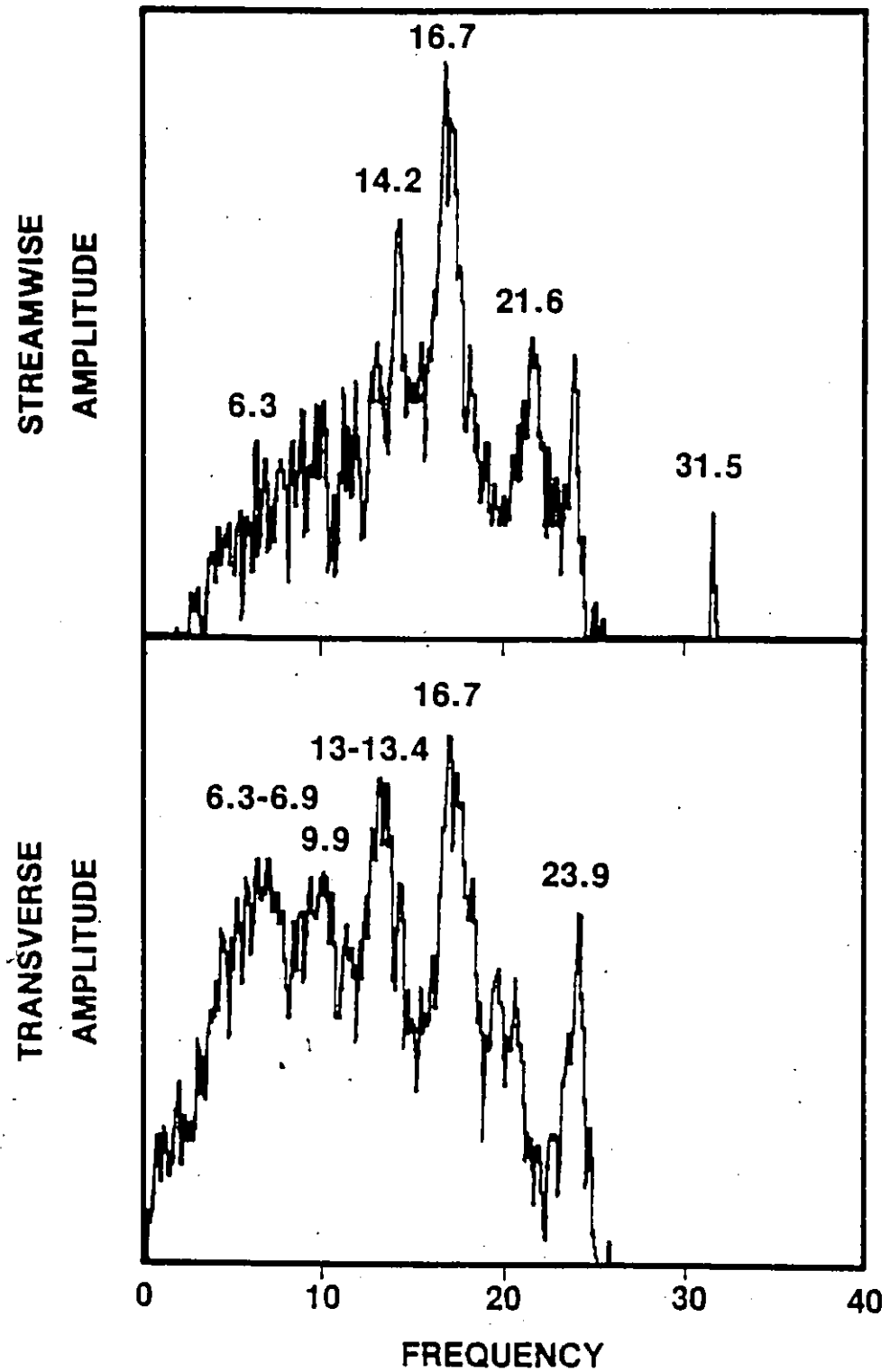

Figure 6.16 Response spectra of tube no.6 at V_T= 0.50 m/s

frequencies and reveal some of their characteristics. The first response corresponds to the broadband double peaked hump and is termed here "turbulence response". The band of frequencies of this response widens with increasing flow velocity until it ultimately overlaps the fluid coupled natural frequency band. The second response corresponds to the narrow band peak and is termed here "vorticity response". The peaks in the turbulence and vorticity responses shift linearly to higher frequencies with increasing flow velocity. The frequencies of these and other similar peaks found at different flow velocities are drawn against the flow velocity V_T in figure 6.12. The lines drawn through these points correspond to the average Strouhal numbers S_T of 0.70 for vorticity shedding and 0.49 and 0.33 for turbulence responses. The same kinds of response can be identified in the transverse spectra of the second row monitored tube however, the turbulence response is characterized by a single peaked hump as shown in figure 6.17. The peak at 3.3 Hz is apparently a random response as it does not appear in other spectra and is not a constant Strouhal number phenomenon. The average Strouhal numbers for vorticity shedding and turbulence responses for the lines drawn through the corresponding frequency points in figure 6.11 are found to be 0.73 and 0.48 respectively. At a flow velocity $V_T = 0.61$ m/s the vorticity response peak coincides with the natural frequency peak at 16.4 Hz. Nevertheless a background turbulence can be seen in the spectra of figure 6.18. In the flow velocity range $0.66 < V_T < 0.83$ m/s a single frequency dominates the recorded spectra of both monitored

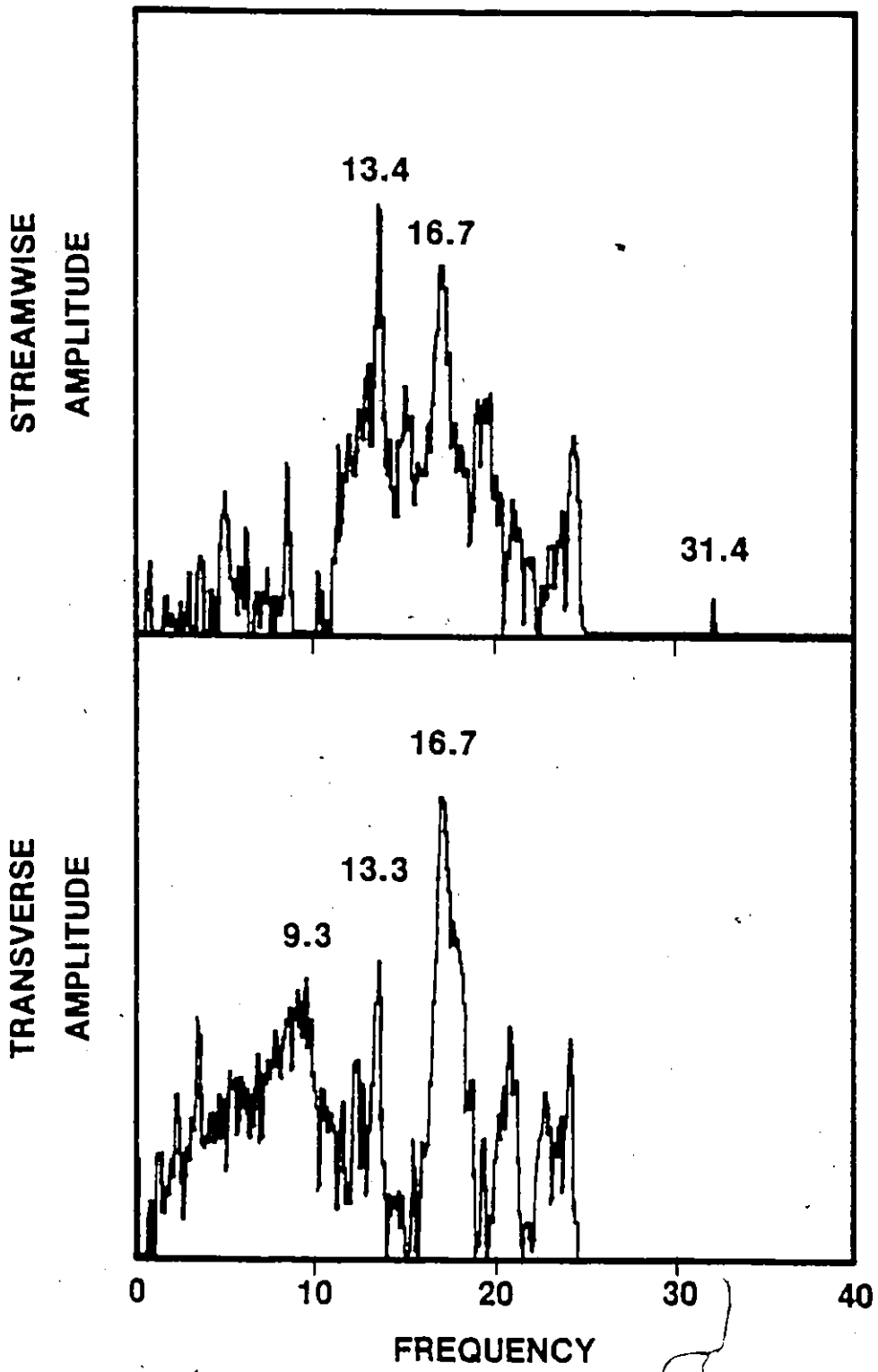

Figure 6.17 Response spectra of tube no.4 at V_T= 0.47 m/s

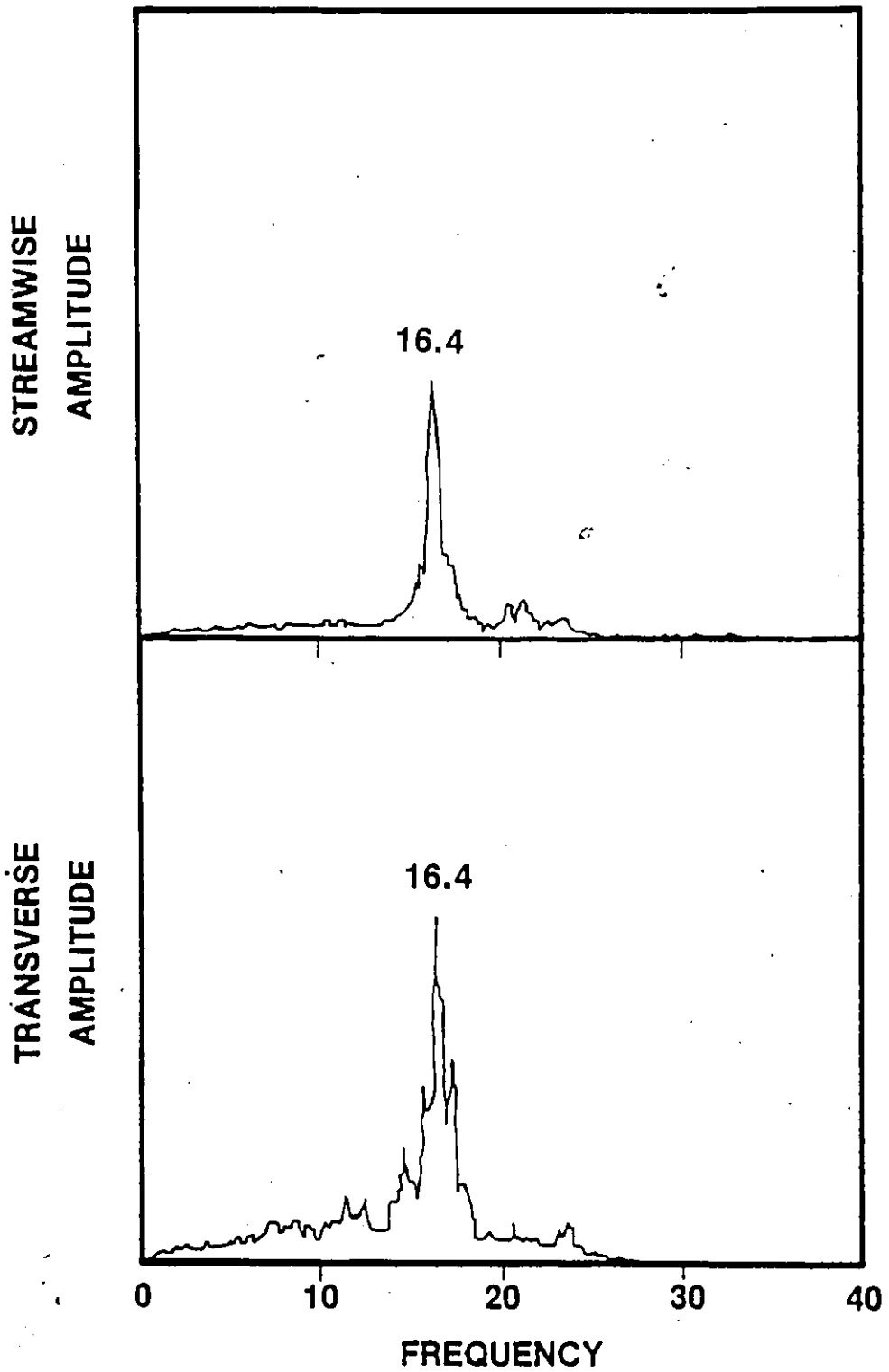

Figure 6.18 Response spectra of tube no.6 at V_T= 0.61 m/s

tubes. This frequency shifts upwards with increasing flow velocity and the turbulence background is greatly reduced. This is illustrated by the spectra of figure 6.19 recorded at the flow velocity of 0.80 m/s. The trough at V_T = 0.83 m/s in the transverse response curve of figure 6.12 is characterized by a much less well organized behaviour as can be seen in the spectra of figure 6.20.

These results suggest that vorticity shedding and turbulence coexist as separate phenomena as the spectra of figure 6.14 to 6.17 indicate. The vorticity shedding peak approaches the dominant peak in the natural frequency band and coincides with it at the flow velocity V_T = 0.61 m/s. The flow velocity V_T = 0.66 m/s, at which the first irregularity occurs in the response curves of figures 6.11 and 6.12, is within the flow velocity range where the vorticity shedding Strouhal lines of S_T = 0.73 and 0.70 intersect the fluid coupled natural frequency band. Consequently, this irregularity in the response curves is attributed to vorticity shedding. Weaver and Yeung [114, 115] reported vorticity shedding Strouhal numbers S_T = 0.63 and 0.69 respectively for a rotated square array with a pitch ratio of 1.5. Pettigrew and Gorman [32] reported vorticity shedding Strouhal numbers, based on the flow velocity at resonance, S_T = 0.85 and 0.81 for tubes in the first and in an interior row of a rotated square array with a pitch ratio of 1.3. The latter Strouhal numbers may be somewhat low since the flow velocities at resonace are usually

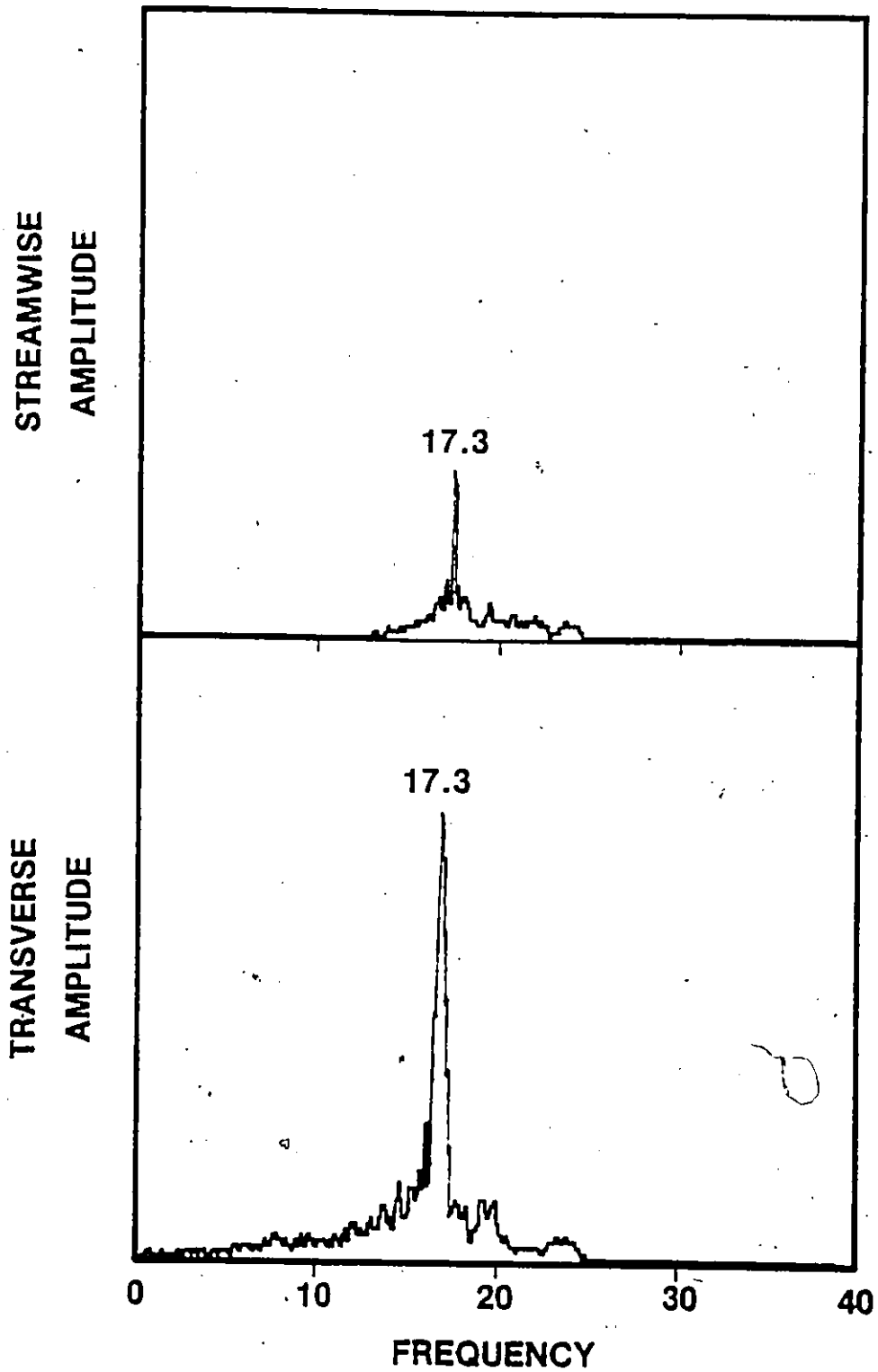

Figure 6.19 Response spectra of tube no.6 at $V_T = 0.80$ m/s

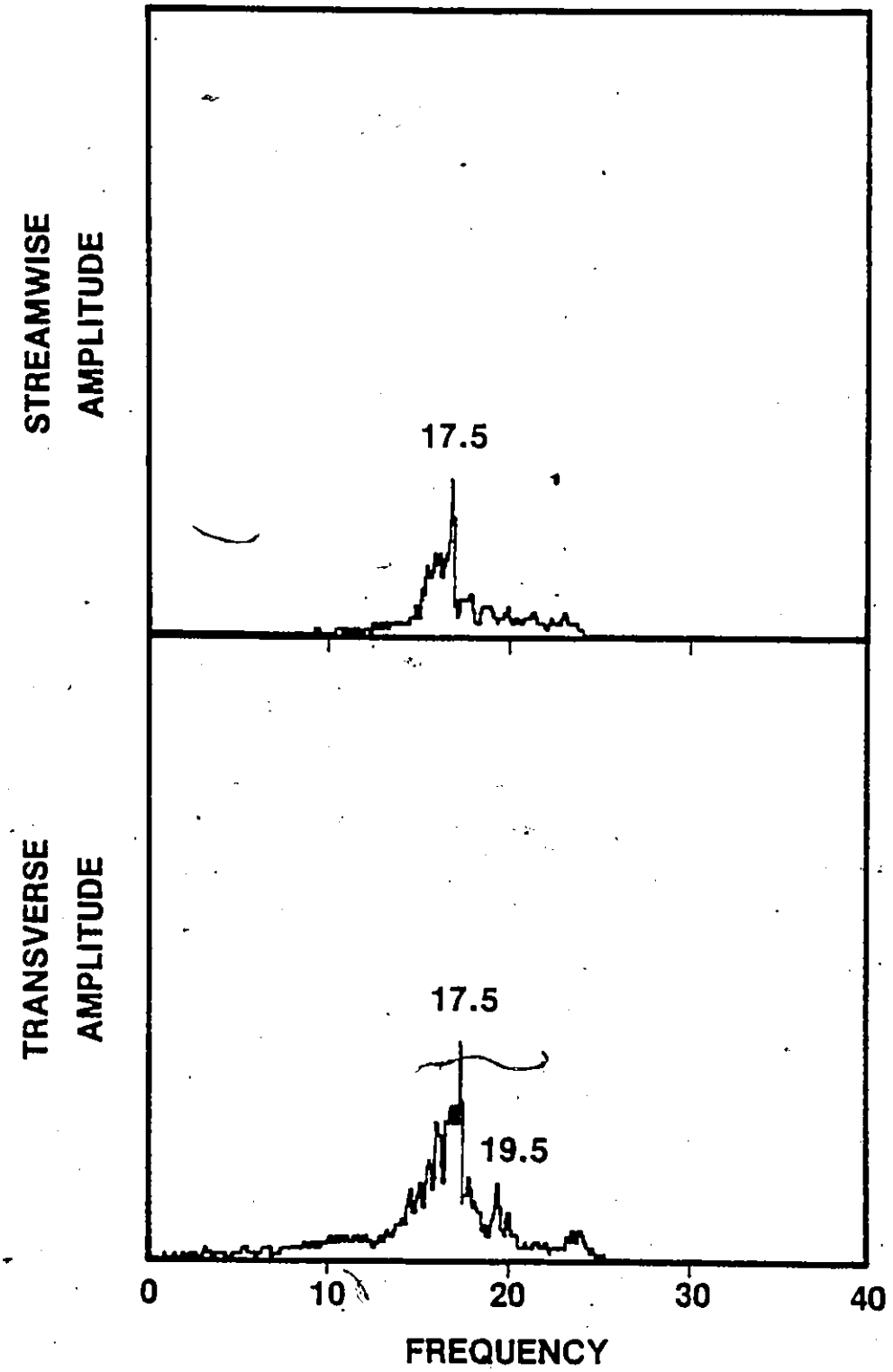

Figure 6.20 Response spectra of tube no.6 at V_T= 0.83 m/s

higher than the velocities at which the frequency of vorticity shedding is captured by the prevailing fluid coupled natural frequency of the tube. Note that the vorticity response spike coincided with the natural frequency spike in the recorded spectra at 0.61 m/s which corresponds to Strouhal number $S_T = 0.69$. The kink and the peak in the response curves occurred at 0.66 m/s and correspond to Strouhal number $S_T = 0.64$. The alternate approach followed here and in the investigation of Weaver and Yeung [115] of determining the Strouhal data from tube response measurements at flow velocities removed from resonance seems to be the most reliable. Nevertheless, the vorticity shedding Strouhal numbers found in the present investigation conform with those reported and are consistent with the trend of increasing Strouhal numbers with decreasing pitch ratios.

That the second event observed in the transverse response curves of figures 6.11 and 6.12, i.e. the peaks at $V_T = 0.80$ m/s, was caused also by vorticity shedding is perhaps more argumentative. However, the following observations support this contention. Firstly, synchronization occurred at $V_T = 0.61$ m/s where a peak at 16.4 Hz dominates the spectra of both monitored tubes. Secondly, at the flow velocity of 0.66 m/s, where the first event occurred in the response curves of figures 6.11 and 6.12, the overall RMS amplitude is about 1.5% of the tube diameter as can be seen from figure 6.13. This amplitude is large enough to increase the strength

of vorticity shedding and the span-wise correlation which leads to increased flow organization. In fact, flow visualization films showed that at the flow velocity of 0.66 m/s the amplitude and the relative mode shape are time invariant. Thirdly, a single dominant spike appears in the spectra of both monitored tubes in the flow velocity range $0.66 < V_T < 0.83$ m/s and the background turbulence is greatly reduced as can be seen from the spectra of figure 6.19 recorded at 0.80 m/s. The overall RMS response amplitude continues to increase and reaches 3% of tube diameter at 0.80 m/s thereby imposing even greater organization on the flow. Fourthly, at 3% of a tube diameter amplitudes and $V_T = 0.80$ m/s, the control exercised by the motion of the tubes on vorticity shedding is lost, the amplitudes are reduced and the response curves exhibit a trough at 0.83 m/s. Such behaviour is consistent with that of an isolated cylinder in water cross-flow in the lock-in region [58]. Lastly, Pettigrew and Gorman [32] noted that resonance peaks can occur in the streamwise and the transverse directions and two resonance peaks can also occur in the same direction. Therefore, it should not come as a surprise that the two events observed in the response curves are attributed here to vorticity shedding resonance. Owen's turbulence excitation predictions [26] for this array suggest a Strouhal number $S_T = 0.52$. Putnam [101] and Chen [21] reported a Strouhal number $S_T = 0.56$ for this array and attributed it to vortex shedding. The Strouhal numbers calculated using the

flow velocity 0.80 m/s at the peak and the recorded frequencies for the second and the third row monitored tubes remarkably agree with that reported by Putnam and Chen, being $S_T = 0.55$. This emphasizes the distortion in Strouhal numbers obtained from resonance data.

The close agreement between the Strouhal numbers found by Putnam [101] and Chen [21] on one hand and those predicted by Owen's equation [26] on the other for this particular array, justifies Paidoussis's observation [18] that from the practical viewpoint, Chen's and Owen's predictions lead to essentially the same Strouhal numbers. This is to be expected since most of the data used to establish the value of the constant K in Owen's equation are in fact due to vortex shedding as was discussed in Chapter 2. So, it should not come as a surprise that Chen's and Owen's Strouhal numbers are in close agreement. It is important, however, to recognize that Chen's analysis and Owen's theory treat two different phenomena. Whether or not the two phenomena exist in reality and whether or not the origin of flow periodicity is but one mechanism, treated in terms of vortex shedding by Chen and in terms of turbulence by Owen, have been controversial open-ended questions. Any attempt to answer such questions has involved accepting one model or the other without hard experimental evidence. A significant contribution to the present state of knowledge is advanced here which demonstrates that vorticity shedding and turbulence coexist as separate phenomena. However,

vorticity shedding is the mechanism responsible for the observed resonance peaks in the response curves.

Flow visualization films taken at different flow velocities and studied in slow motion revealed that bundle oscillations became barely visible at V_T = 0.41 m/s. At a higher flow velocity V_T = 0.48 m/s the oscillations are seen to be random in nature. The photograph of figure 6.21 is a frame of a cine film taken at V_T = 0.55 m/s with a stream of tracer particles released upstream from the first row. Diffusion of the tracer particles illustrates the nature of the flow and the increasing turbulence as the flow progresses through the bundle. The photograph of figure 6.22 was taken at a flow velocity V_T = 0.66 m/s which falls within the synchronization range and corresponds to the first observed peak in the response curves of figures 6.11 and 6.12. Despite the observed well organized tube response and the coincidence of the vorticity shedding frequency with the prevailing tube natural frequency, coherent vortex structures presumably responsible for the detected periodicity in the response spectra are not observed. Cine films taken at this flow velocity revealed that the amplitude response and the relative mode shape between tubes are velocity dependent but regular and, at a given flow velocity, time invariant. As a result of the tube's relative motions, the sizes of the gaps between tubes vary and some flow redistribution takes place between these gaps. The photograph of figure 6.23, taken at the same flow

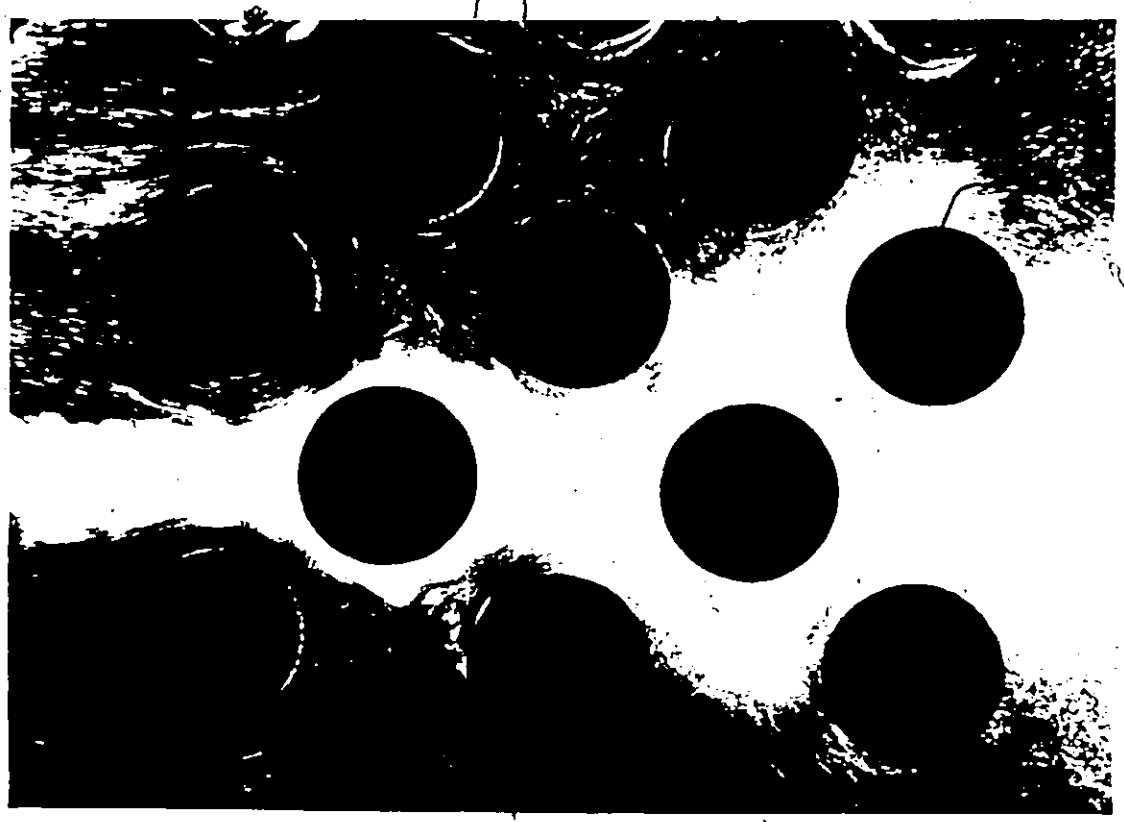

Figure 6.21 Flow Visualization at V_T = 0.55 m/s

Figure 6.22 Flow Visualization at $V_T = 0.66$ m/s (Flexible Array)

Figure 6.23 Flow Visualization at $V_T = 0.66$ m/s (Rigid Array)

velocity, 0.66 m/s, for the rigidly mounted tube bundle, indicate a better definition of the main stream flow and the wake regions than in the flexibly mounted bundle of figure 6.22. The relative loss of coherency in the main stream flow in the latter is attributed partly to the disturbances created in the local flow fields around the individual tubes at the frequency of tube motion, and partly to the flow redistribution due to the relative mode shape. Despite the loss of coherency in the main stream flow of the flexibly mounted bundle, the main stream flow persists and can be traced to the last tube row. Similarly, cine films were taken at V_T = 0.80 m/s which correspond to the second peak in the amplitude response curves of figures 6.11 and 6.12. No coherent vortex structure can be identified at this flow velocity either. However, the response amplitudes and the relative mode shape between tubes are seen to be velocity and time dependent.

6.4 Fluidelastic Response

At the flow velocity V_T = 0.83 m/s, a trough is seen in the transverse response curves of figures 6.11 and 6.12 for both monitored tubes. A less well organized behaviour was seen in the spectra of figure 6.20 recorded for the third row monitored tube at 0.83 m/s. A similar frequency response behaviour is seen in the spectra of figure 6.24 recorded for the second row monitored tube at the same flow velocity. The flow velocity 0.83 m/s also marks a sudden upturn in the

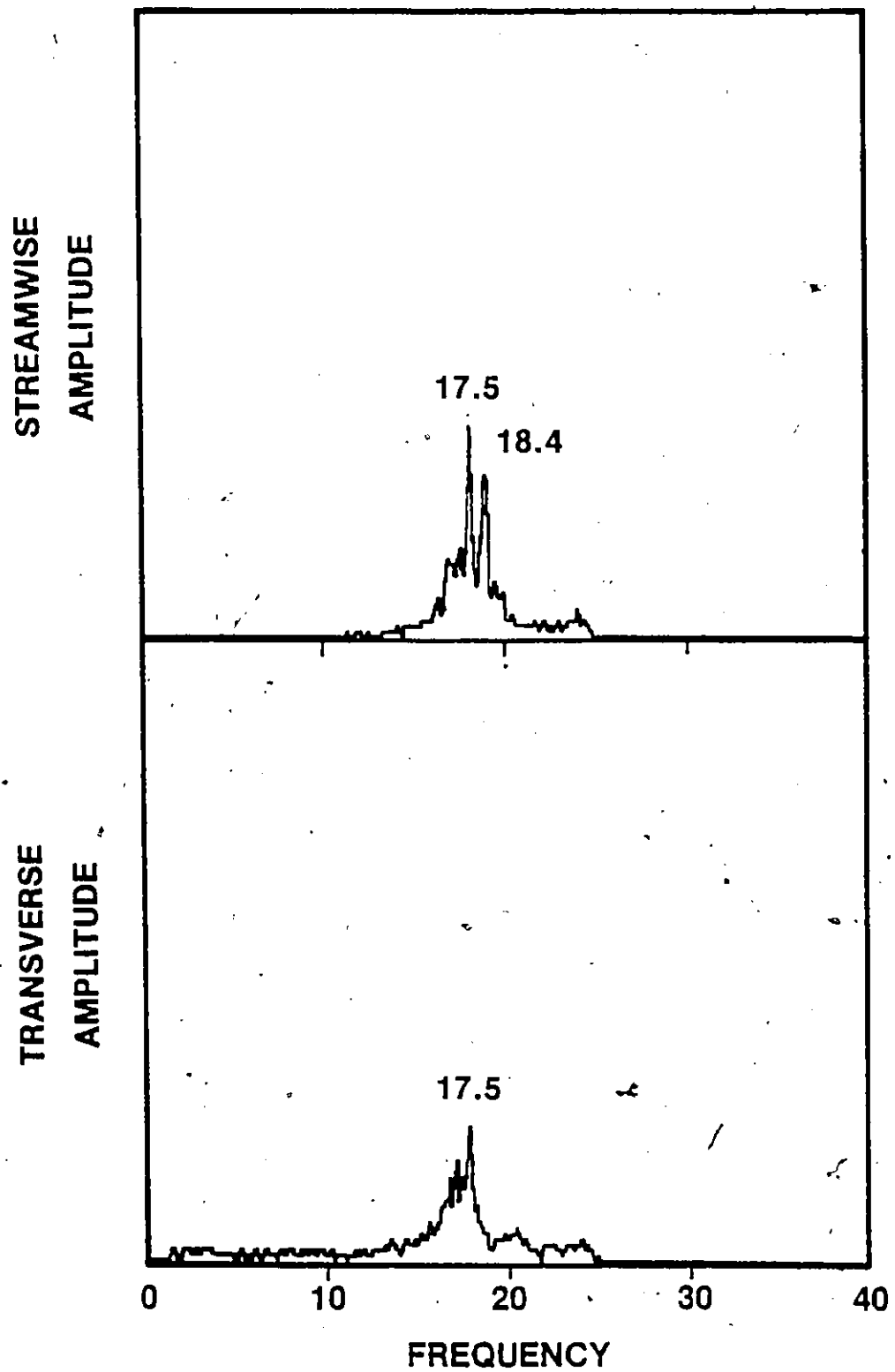

Figure 6.24 Response spectra of tube no.4 at V_T= 0.83 m/s

transverse response amplitude of the third row monitored tube, figure 6.12. The sudden upturn in the transverse amplitude response curve of the second row monitored tube, figure 11, is delayed until a flow velocity V_T = 0.88 m/s is reached. Increasing the flow velocity beyond 0.88 m/s, a better organized frequency response develops in the spectra of both monitored tubes. Figures 6.25 and 6.26 recorded at V_T = 0.94 m/s for the second and the third row monitored tubes respectively illustrate a better organization in the transverse response. Note that the transverse spectrum of the second row monitored tube is better organized than that of the third row tube, a circumstance that may suggest a fluid coupling dependence on the row depth. The spectra of figures 6.27 and 6.28 recorded at V_T = 1.02 m/s where the largest amplitudes developed before terminating the experiment for fear of tube-to-tube clashing, further support that observation. A single spike dominates the transverse spectrum of tube no. 4, figure 6.27 while two spikes can be seen in the transverse spectrum of tube no. 6, figure 6.28.

Yeung and Weaver [122] discussed several ways used by researchers [32, 148, 153] to define the threshold velocity that marks the onset of fluidelastic instability. The difficulty encountered in determining the stability threshold is attributed in part to vorticity resonance preceding fluidelastic instability. Vorticity resonance may partially mask, by being nearly superimposed, or somewhat alter the stability threshold,

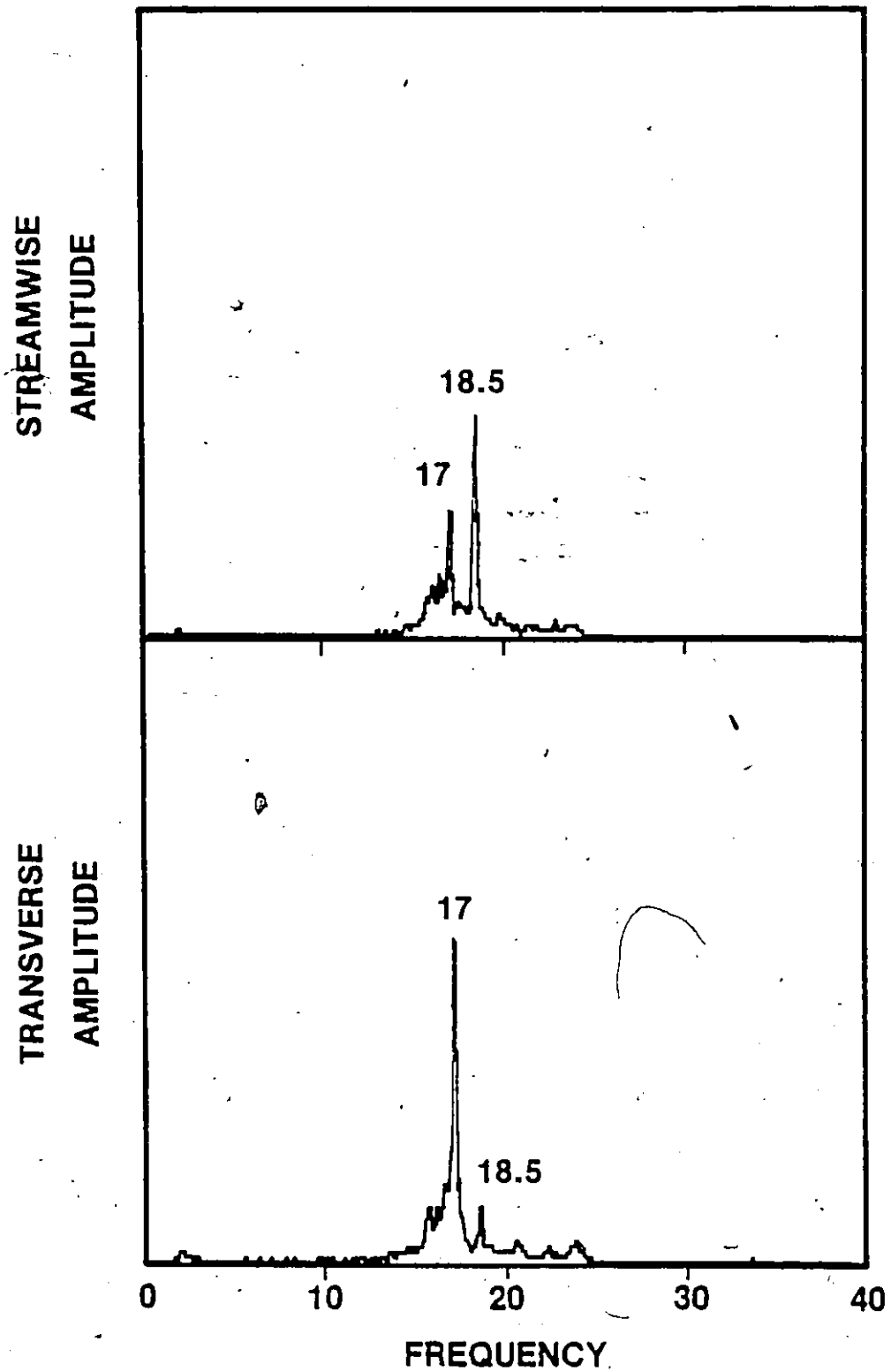

Figure 6.25 Response spectra of tube no.4 at V_T= 0.94 m/s

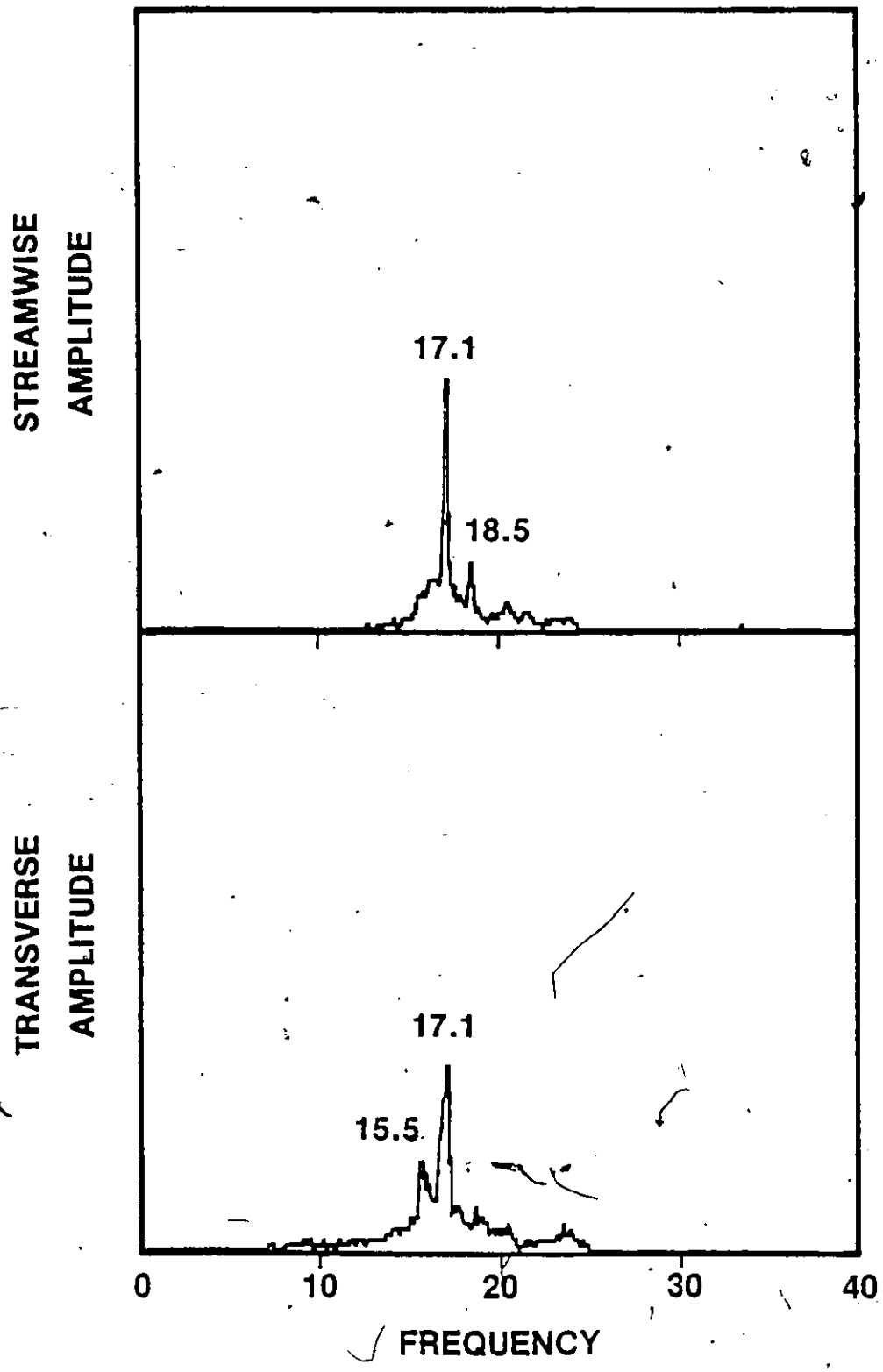

Figure 6.26 Response spectra of tube no.6 at V_T= 0.94 m/s

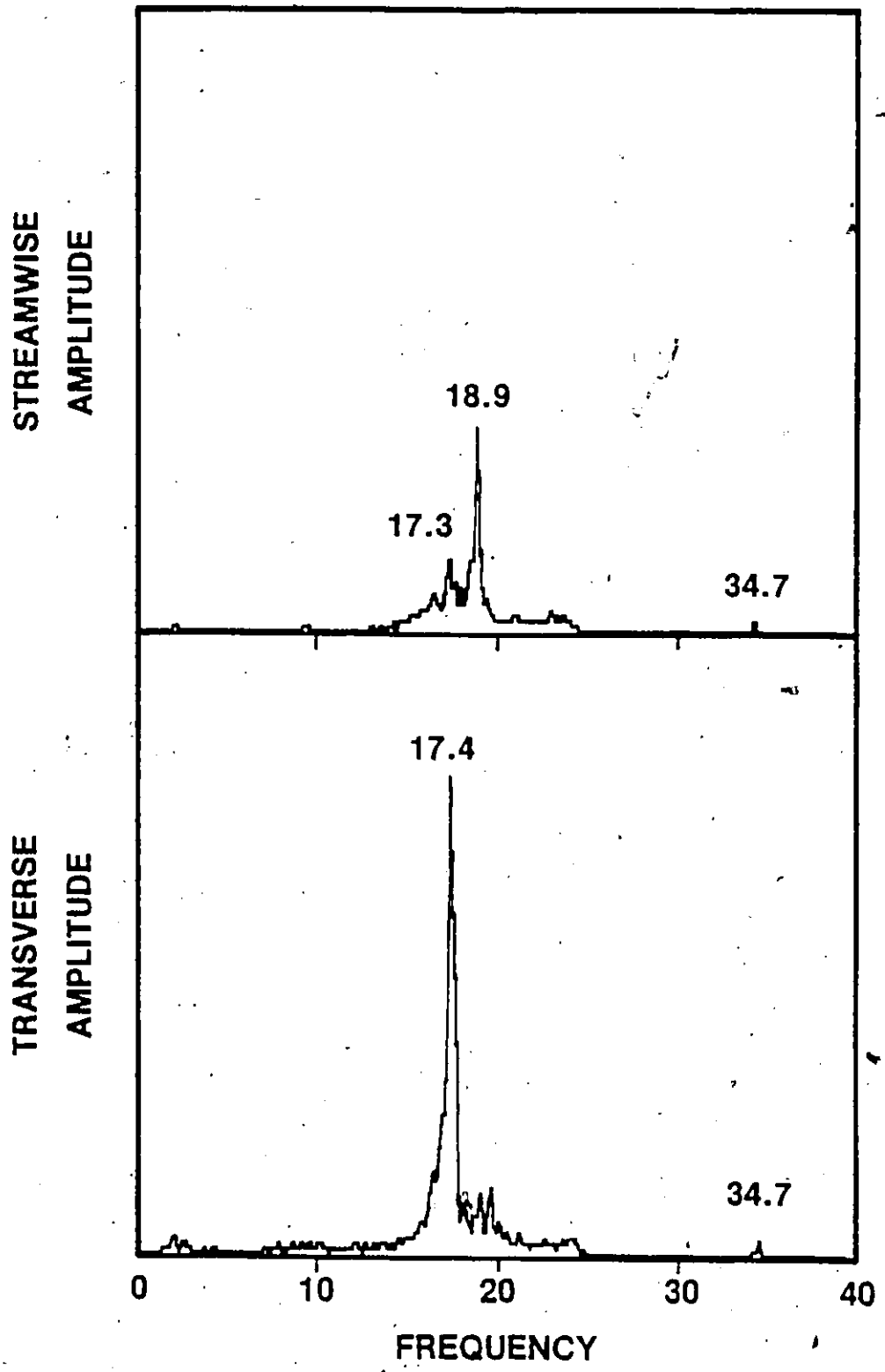

Figure 6.27 Response spectra of tube no.4 at V_T= 1.02 m/s

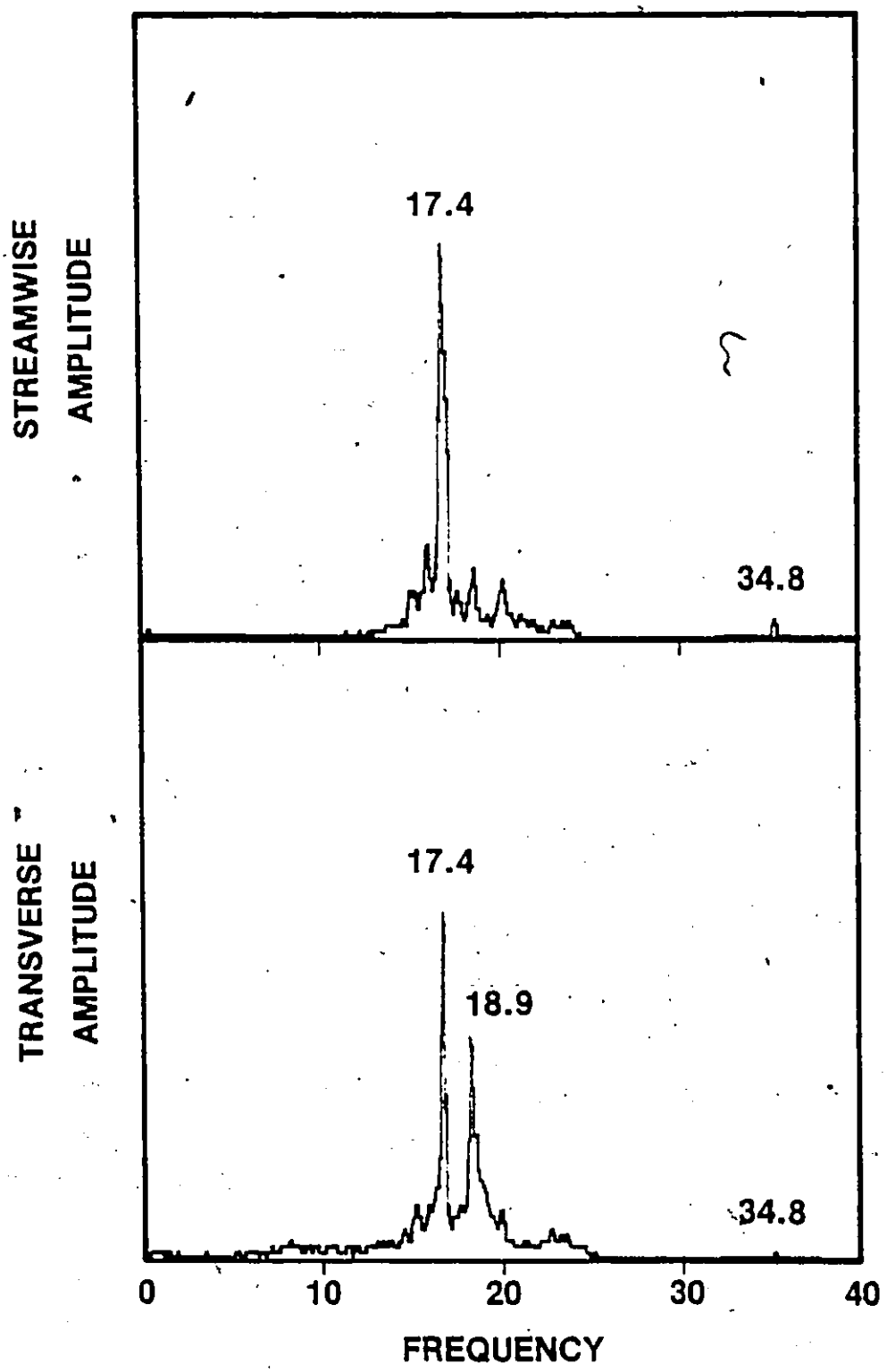

Figure 6.28 Response spectra of tube no.6 at V_T= 1.02 m/s

by causing larger response amplitudes before V_{cr} thereby having a nonlinear and unknown effect on the velocity at which instability would have occurred in the absence of vorticity resonance. It is not known with any degree of certainty what the effect of vorticity resonance is on the stability threshold other than the fact that it makes precise determination of V_{cr} a difficult task. In Chapter 5, the stability threshold was defined as the flow velocity at which a sudden upturn or a trend of increasing amplitude with increasing flow velocity occurs in the transverse response curve associated with organized periodic response at the prevailing fluid coupled natural frequency. According to this definition the critical flow velocity for tube no. 4 is V_T = 0.88 m/s and that for tube no. 6 is V_T = 0.83 m/s. The critical reduced velocity, based on the observed frequency at instability of 17.5 Hz and the upstream velocity V_u, is 0.99 for tube no. 4 and 0.93 for tube no. 6. These values of critical reduced velocity agree reasonably well with the value of 0.94 reported by Weaver and Yeung [115] and the value of 0.89 reported by the same authors [114] for a rotated square array of a pitch ratio 1.5.

Differences in vibrations of tube arrays in air and in water flows are due to the effects of significant added mass and strong fluid coupling. Chen [154], in a theoretical study of tube banks restricted to vibrate in a stationary fluid, has shown that a natural frequency of a tube in the

bank is associated with a frequency band that corresponds to the relative modes of the neighbouring tubes. He extended his method to include the effect of flowing fluid, assuming that his potential flow theory was valid as long as the ratio of tube displacement to tube diameter is small. In a later experimental investigation, Chen et al. [155] showed that the theory [154] predicted the added mass effects very well. Information about the effect of flowing fluid on the added mass coefficients are nonexistent with the exception of the trends established experimentally in references [115, 40]. The results of the present investigation add to and substantiate these established trends. The added mass coefficient may be determined from the relation,

$$C_m = \frac{\gamma_t}{\gamma_w} \left[\left(\frac{f_a}{f_w}\right)^2 - 1 \right]$$

The added mass coefficients for both monitored tubes, calculated accordingly, are given in table 6.1. It can be seen that the added mass coefficient of a single tube vibrating in still water within the rigid bundle C_{ms} is considerably smaller than C_{ml}, calculated when all tubes are free to vibrate in a flowing fluid.

Once the fluidelastic instability takes over and becomes the dominant excitation mechanism, the amplitude of the whirling tube motion increases considerably with a small increase in the flow velocity. The flow velocity in real heat exchangers

Table 6-1

Calculation of the Added Mass Coefficient of Both Monitored Tubes

	Tube no. 4	Tube no. 6
f_a Hz	27.75	27.50
f_w Hz all tubes rigid but one	19.50	19.25
γ_t specific gravity of the tube material (plexiglass) kg/m^2	1140	1140
γ_w specific gravity of water kg/m^2	1000	1000
Lowest frequency in the turbulence induced response F_ℓ Hz	14.8	15.1
Observed frequency at resonance F_r Hz	16.4	16.4
Observed frequency at instability F_i Hz	17.5	17.5
C_{ms} added mass coefficient in still water (only monitored tube flexible)	1.17	1.19
$C_{m\ell}$ added mass coefficient based on F_ℓ	2.87	2.64

must not exceed the threshold velocity that marks the onset of fluidelastic instability, otherwise rapid damage of tubes should be expected. Several theoretical and experimental investigations using different approaches were carried out to probe the nature of this destructive mechanism and to develop criteria by which the critical flow velocity can be predicted, [33, 36, 37, 44-46, 68, 149, 156-161]. However, Yeung and Weaver [122] remarked that the fluidelastic instability mechanism is not clearly understood and current design practice relies heavily on experience and empirical coefficients. The present study is a step in the direction of understanding the complex nature of the excitation mechanism. Of particular interest here is to study the influence of the neighbouring tubes, the contribution of the wake flows, and the state of the main stream flow surrounding a given unstable tube.

Tanaka and Takahara [45], forced a tube to vibrate at an amplitude of 0.1d in a square array. It can be concluded from their measurements that the unsteady fluid dynamic forces acting on the tube caused by its own motion are significantly larger than those acting on the tube due to the vibration of its closest neighbours. The overall RMS amplitudes of tube no. 4 and tube no. 6 at instability are much smaller than 0.1d as figure 6.13 indicates. Therefore the influence of the surrounding tubes on the monitored ones, at these much smaller amplitude levels must be very small at instability.

It was shown in section 6.3 that as a result of the tube's relative motions the sizes of the gaps between tubes vary

and some flow redistribution takes place between these gaps as illustrated by the photograph of figure 6.22 taken at the flow velocity V_T = 0.66 m/s. The photographs of figures 6.29 and 6.30 taken at a flow velocity V_T = 0.97 m/s for the flexibly and rigidly mounted tube bundles further illustrate this point. At the higher flow velocity of 0.97 m/s the response amplitudes are bigger and more vigorous flow redistribution can be seen in the photograph of figure 6.29. The photograph of figure 6.30 taken for the rigidly mounted tube bundle at the same flow velocity V_T = 0.97 m/s indicates that significant flow redistribution is absent in the absence of tube motion. In fact, this photograph is similar in the essential details, to that presented in figure 6.23 taken at a much lower flow velocity.

Furthermore, the photograph of figure 6.29 illustrates the extent to which the orientation of the wakes behind the first and the second tube rows can change with respect to the downstream rows and the impingement of the deflected main stream flow emerging from the gaps on the downstream tubes. A tube in the third row, for example, can see an upstream approaching pattern of flow that varies with time and velocity. Similarly, the velocity profile seen by a second row tube will be velocity and time dependent as the gaps between the upstream first row tubes vary with time and velocity. The photographs of figures 6.29 and 6.30 illustrate that a second and a third row tubes develop apparently quite different wakes

Figure 6.29 Flow Visualization at V_T = 0.97 m/s (Flexible Array)

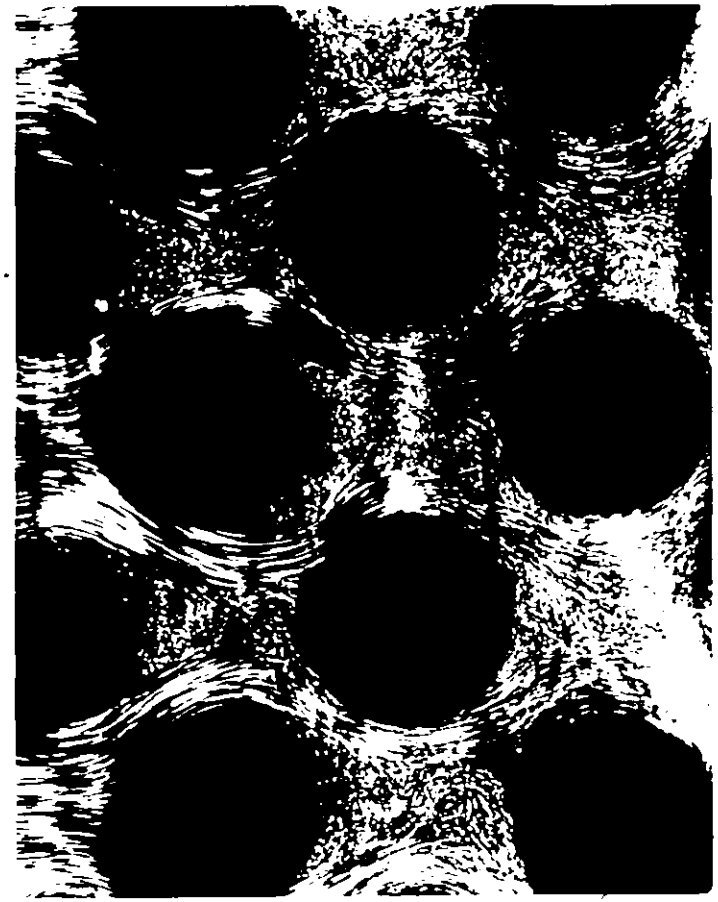

Figure 6.30 Flow Visualization at V_T = 0.97 m/s (Rigid Array)

yet they have close stability thresholds as was shown earlier. From this, one can conclude that wake details, at least for the rotated square array studied here, do not seem to be very important. This conclusion supports an important assumption made by Lever and Weaver in their theoretical treatment [147].

The investigations of Zdravkovich and Namork [48, 49] of the interstitial flow structure inside a normal triangular array having $x_t = 1.375$ and $x_\ell = 1.1875$, depicted in figure 6.31a, have shown that wide wakes are formed behind the first row tubes, and narrow wakes are formed behind the second and the third row tubes. The details of these investigations were discussed in Chapter 2. The results were inferred from time average pressure distribution curves measured around a stationary tube and confirmed by fluctuating pressure curves together with the results of traversing a miniature hot wire probe across the wake. In view of the results of Achenbach [108] and Batham's [109] investigations Zdravkovich and Namork [48] attributed the narrow wakes formed behind the second row tubes in their bank to the close proximity of the tubes. To illustrate the effect of pitch and pattern on the wake shape inside a bundle a parallel triangular array is depicted in figure 6.31b. The wing tubes are farther apart in this case while the downstream tube is closer to the upstream tube than in the case of figure 6.31a. This implies that the interference of the wing tubes with the flow past the upstream tube is reduced while the close proximity of the downstream

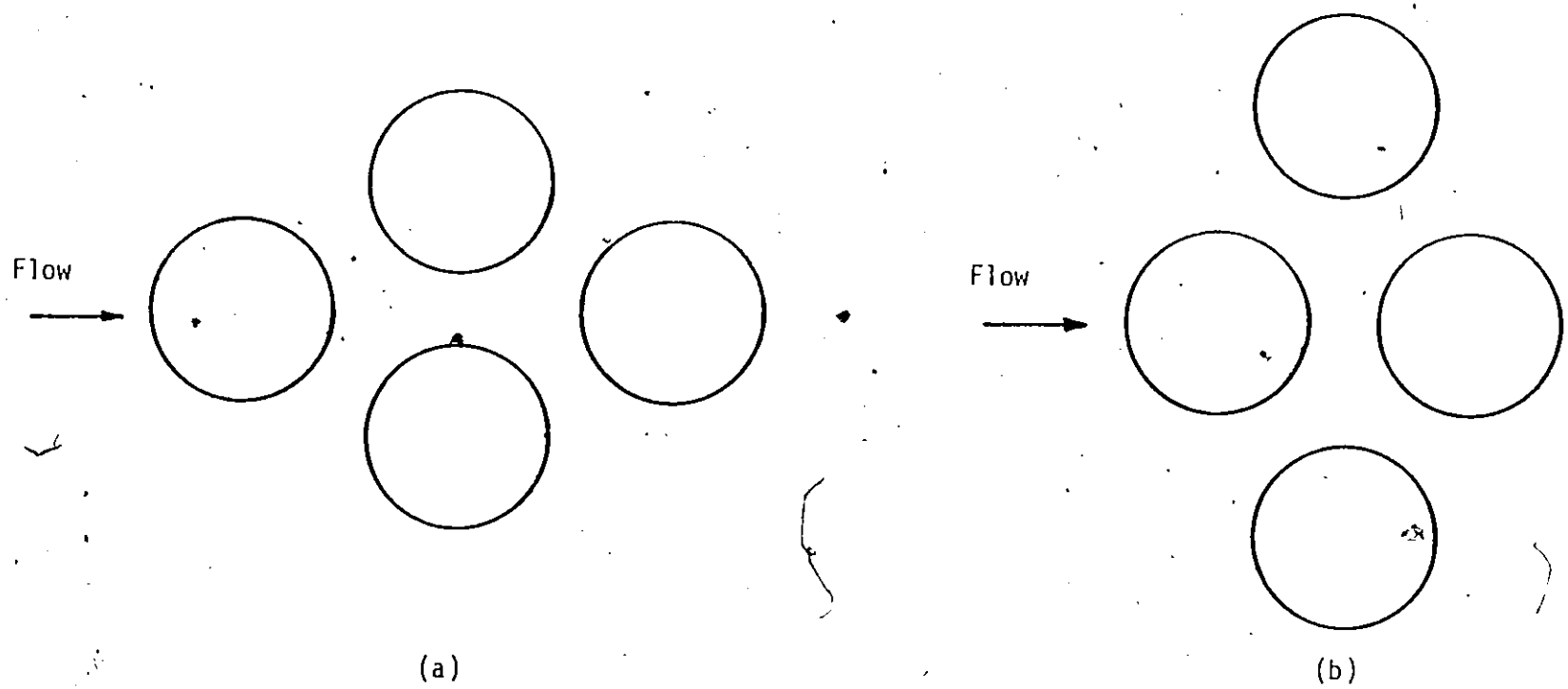

Figure 6.31 Normal and parallel triangular arrangements

tube will be more pronounced. The result is that a wide wake between the upstream and the downstream tubes may be formed in this case. The rotated square array is an intermediate case between the normal triangular array of Zdravkovich and Namork depicted in figure 6.31a and the parallel triangular array of figure 6.31b. The normal triangular array of Zdravkovich and Namork is compared with the presently considered rotated square array in figure 6.32. The wake shapes, therefore, are expected to conform basically to the pattern inferred by Zdravkovich and Namork yet the pattern should also be influenced to a degree with the particular rotated square configuration considered. The resulting wake pattern in the first three rows of the rigidly mounted rotated square array investigated here can be seen in the photograph of figure 6.30. The instantaneous wake shapes and sizes appear to be greatly affected by the redistributed flow between the gaps as the photograph of figure 6.29 for the flexibly mounted bundle indicates.

Having said that, it is not difficult to see the advantages of the developed flow visualization technique, the potential of its application and the insight that can be gained by its utilization in investigating the complex problem of flow induced vibration. In multi-row tube arrays with different pitches and patterns, flow visualization is a direct, relatively easy method to use which does not interfere physically with the system under investigation. The whole flow field, the

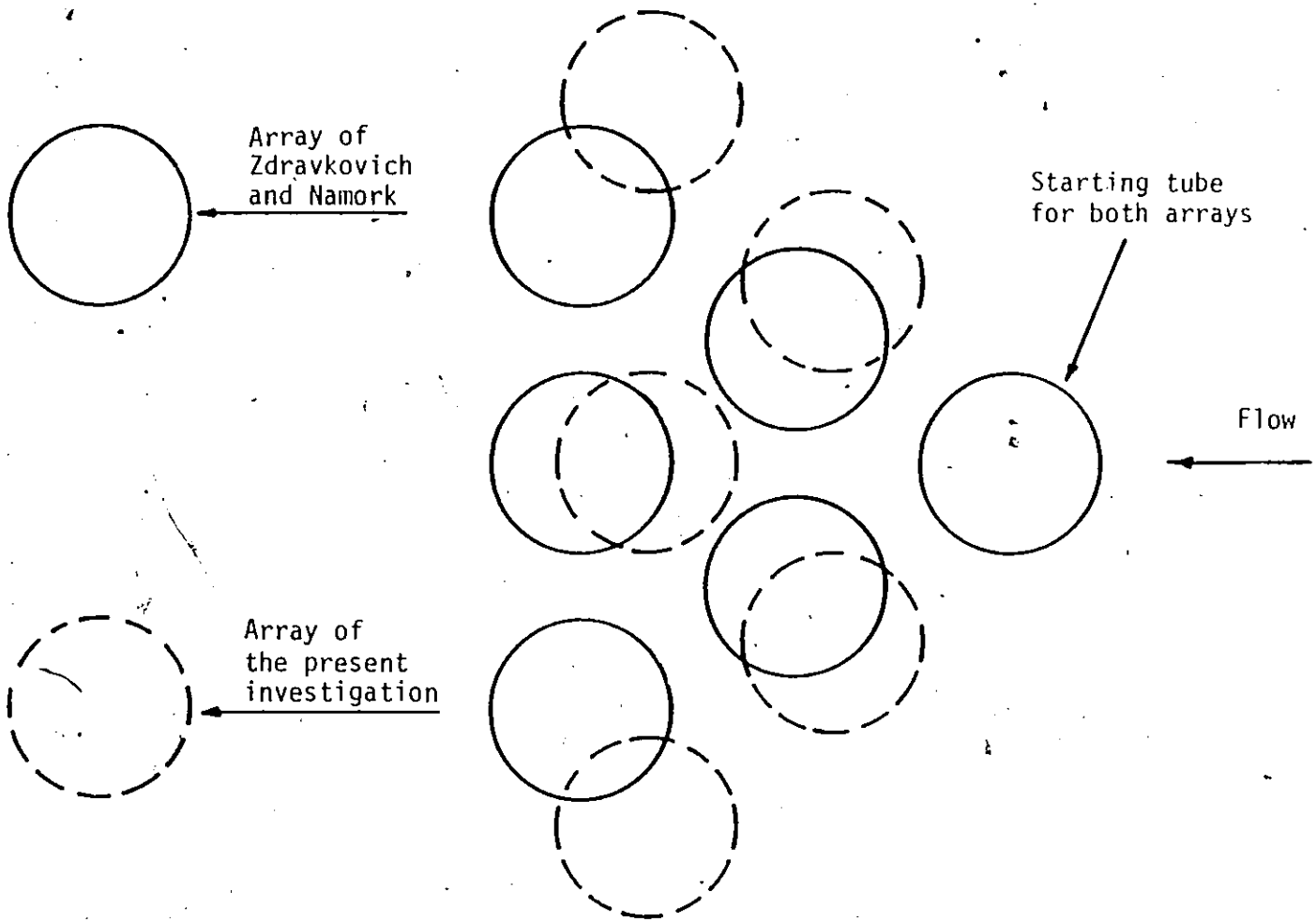

Figure 6.32 Comparison between the array of Zdravkovich and Namork and the array of the present investigation

amplitudes and relative mode shapes of flexibly mounted tubes, and their variation with velocity and time can be permanently recorded on cine-films. These can be studied later in slow motion to gain insight in the elusive nature of the excitation mechanisms. Methods based on time averaging cannot provide information that are related in any obvious way to a mechanism of energy transfer. By examining the instantaneous flow behaviour using a flow visualization technique, such as the one developed here, one can see how the flow pattern changes from one instant to another and therefore develop the insight into energy exchange mechanisms.

The results of the present investigation, which pointed out the importance of flow redistribution and the relatively negligible effect of neighbouring tubes and wake flows on the instability of a given tube in water flow, are in contrast with Chen's inference of how fluidelastic instability is initiated [29] in staggered tube bundles. Chen's analysis was presented in detail in Chapter 2. The flow patterns constructed by Chen [29] are not supported by physical evidence and are speculative in nature. However, the results of the present investigation, supported by cine-films and photographs, indicate that the flow pattern envisaged by Chen for tube bundles in air flows do not occur for these arrays in water. The photograph of figure 6.29 indicates that coherent vortex structures or any other wake phenomena are nonexistent. Given Reynolds number similarity, the possible explanations are that either

these patterns do not exist at all or that they only exist in the presence of acoustic resonance. It follows that Chen's observations are not valid for tube bundles in water.

In section 6.5 the effects of the surrounding tubes on the critical velocity of tube no. 6, the main stream flow in the flow lanes and flow redistribution, will all be examined in detail for the case where a single tube is allowed to vibrate in an otherwise rigid bundle.

6.5 Response of a Single Flexible Tube in a Rigid Bundle

A given phase relationship with the same frequency between a tube and its closest neighbours is necessary for tube instability in the theories of Connors [33] and Blevins [36, 37]. Based on this assertion, Blevins [36] predicted that frequency detuning of adjacent tube rows should prevent fluidelastic instability. Weaver and Lever [38] reported that a 3 percent difference in tube row frequencies could produce an increase in the critical flow velocity up to 40 percent. However, they also found that the effect of frequency detuning of greater than about 10 percent has no effect on the stability threshold. Therefore, one must be suspicious of any theory which depends on relative tube motion for instability. Soper [153], for a single flexible tube in a single row, and Southworth and Zdravkovich [162] for a single flexible tube in a rigid two row array, have shown that the flexibly mounted tube can become unstable, although the stability threshold

was significantly delayed. Weaver and Grover [39] demonstrated that a flexible tube in an otherwise rigid parallel triangular array of pitch ratio 1.375 in an air flow can indeed become unstable. The instability occurs at essentially the same threshold velocity if all tubes were allowed to vibrate. The same bundle was tested in water flow [40] with a single flexible tube surrounded by rigid ones. It was found that the flexibly mounted tube also became unstable in the water flow and that the reduced velocity at instability was somewhat lower than that for the same tube in a flexible bundle. Weaver and Yeung [114] compared the response of a single flexible tube in an otherwise rigid array, with that of a flexibly mounted one. The array had a rotated square configuration with a pitch ratio of 1.5. They showed that the stability threshold in both cases was essentially the same. The theoretical model of Lever and Weaver [147] was based on the assumption that a single tube in an array becomes unstable independent of the motion of its neighbouring tubes. It is clear from all this that the flow behaviour and tube stability characteristics of a single tube in a rigid array are of fundamental importance.

In the present investigation, it was decided to study the response of a single flexible tube in the rotated square array. An acrylic plate 1/8 inch thick, with suitable holes of 1 inch diameter to accommodate all the tubes of the bundle, was prepared. A larger diameter hole was drilled in the plate

around the location of tube no. 6. The plate was then forced down the tubes to a height of two inches above the floor of the water tunnel. In this way, all the tubes except tube no. 6 became effectively rigid. The experimental procedure, previously outlined for the case of the flexibly mounted array, was also followed here.

The streamwise and transverse response curves are given in figure 6.33. Up to V_T = 0.41 m/s the response is small and the amplitudes increase practically linearly with increasing flow velocity. In the range $0.41 < V_T < 0.80$ m/s a gradual upturn in the transverse response curve is noticeable, nevertheless at 0.80 m/s the transverse response amplitude does not exceed one percent of the tube diameter. Beyond V_T = 0.80 m/s, a sudden upturn in the transverse response curve can be identified and the transverse response amplitude reaches about 4 percent of the tube diameter at V_T = 0.88 m/s. These features can also be identified in figure 6.34 where the overall RMS response amplitude curve is compared with that of the same tube in a full flexibly mounted bundle. The peak at 0.80 m/s in the latter curve cannot be found in the former one although the trend of rising transverse amplitude with increasing flow velocity is present.

Frequency spectra of the tube response, recorded at different flow velocities, are given in figures 6.35 to 6.40. The cluster of fluid coupled natural frequencies observed in the spectra of the full flexibly mounted bundle has been reduced

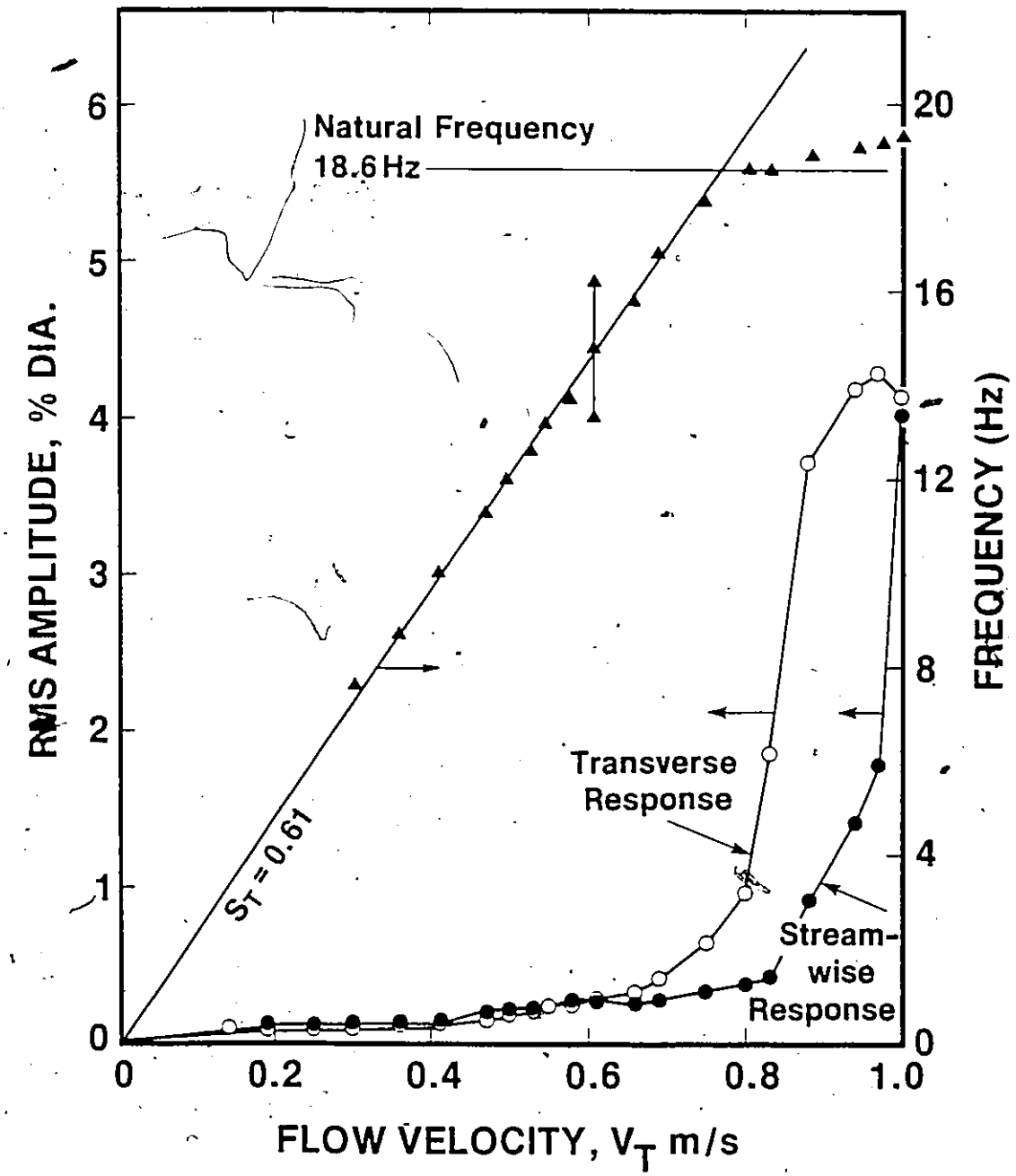

Figure 6.33 Response of the flexible tube in the rigid bundle

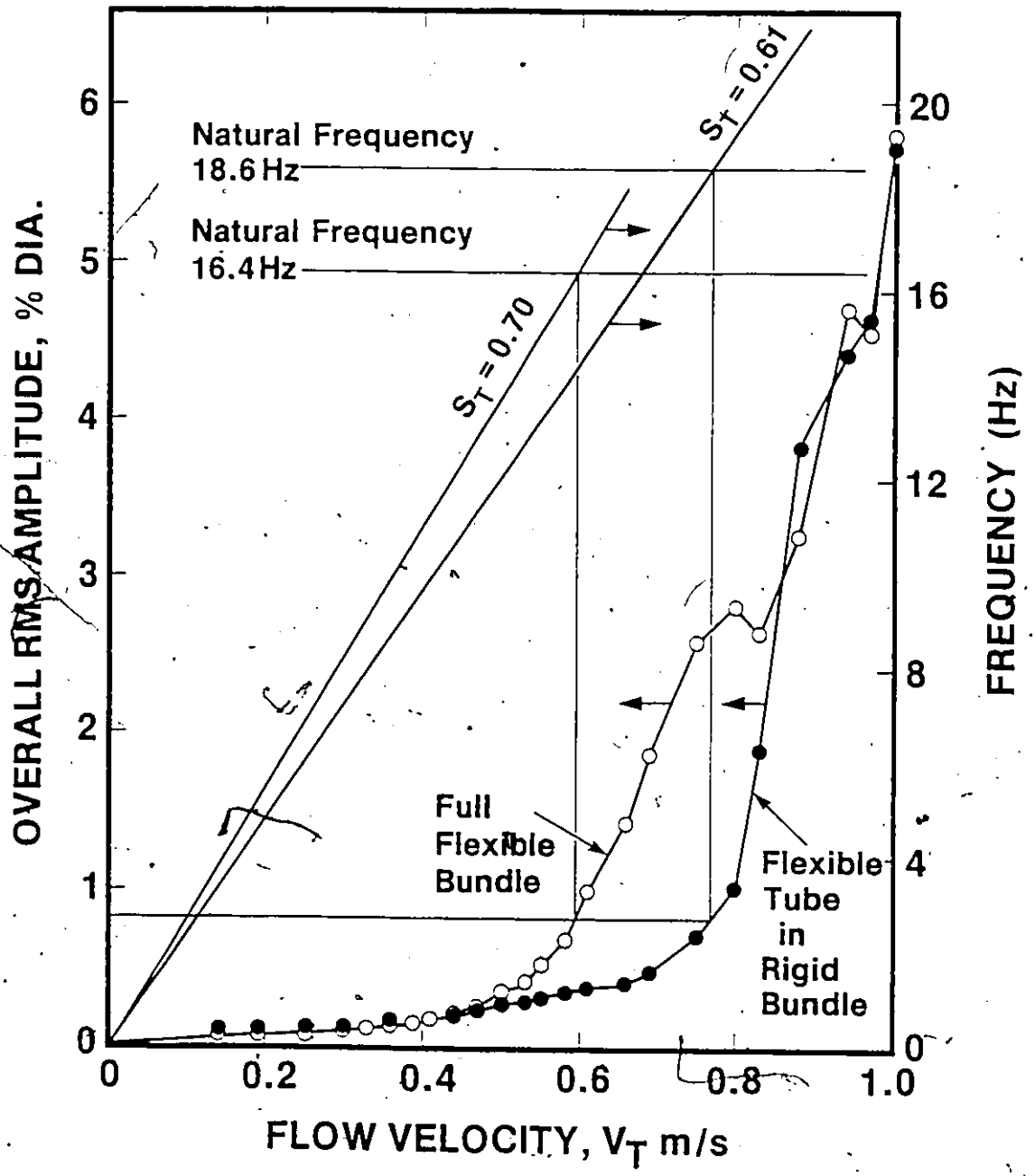

Figure 6.34 Overall RMS responses of the flexible tube in the flexible and the rigid bundles

to a single frequency of 19.6 Hz as is evident from figure 6.35 recorded at V_T = 0.30 m/s. This natural frequency remains fairly constant with increasing flow velocity and corresponds to that value found in quiescent fluid. Periodicity at the lower frequencies which corresponds to narrow band peaks at about 7.7 and 11.3 Hz can be identified in figures 6.35 and 6.36, the latter being recorded at V_T = 0.47 m/s. These frequency peaks shift to higher frequencies linearly with increasing flow velocity. Such frequencies are plotted against V_T in figure 6.33 and a straight line drawn through these points corresponds to an average Strouhal number S_T = 0.61. In view of the characteristics just outlined of this flow periodicity, it is reasonable to conclude that it has its origin in vorticity shedding. At a flow velocity V_T = 0.69 m/s, a new dominant spike at 18.5 Hz appears in the transverse spectrum of figure 6.37 between the frequency of vorticity shedding at 16.8 Hz and the natural frequency of 19.5 Hz. The closeness of vorticity shedding frequency and the natural frequency indicates imminent synchronization between the two. The gradual increase in the transverse amplitude may be attributed to this synchronization. The new peak at 18.6 Hz constitutes a slight downward shift in the natural frequency so that the resonance frequency is 18.6 Hz rather than the frequency of 19.6 Hz observed in quiescent fluid. On the other hand, these larger amplitudes could be the result of fluidelastic instability. It would appear that the two events occurred nearly simultaneously and

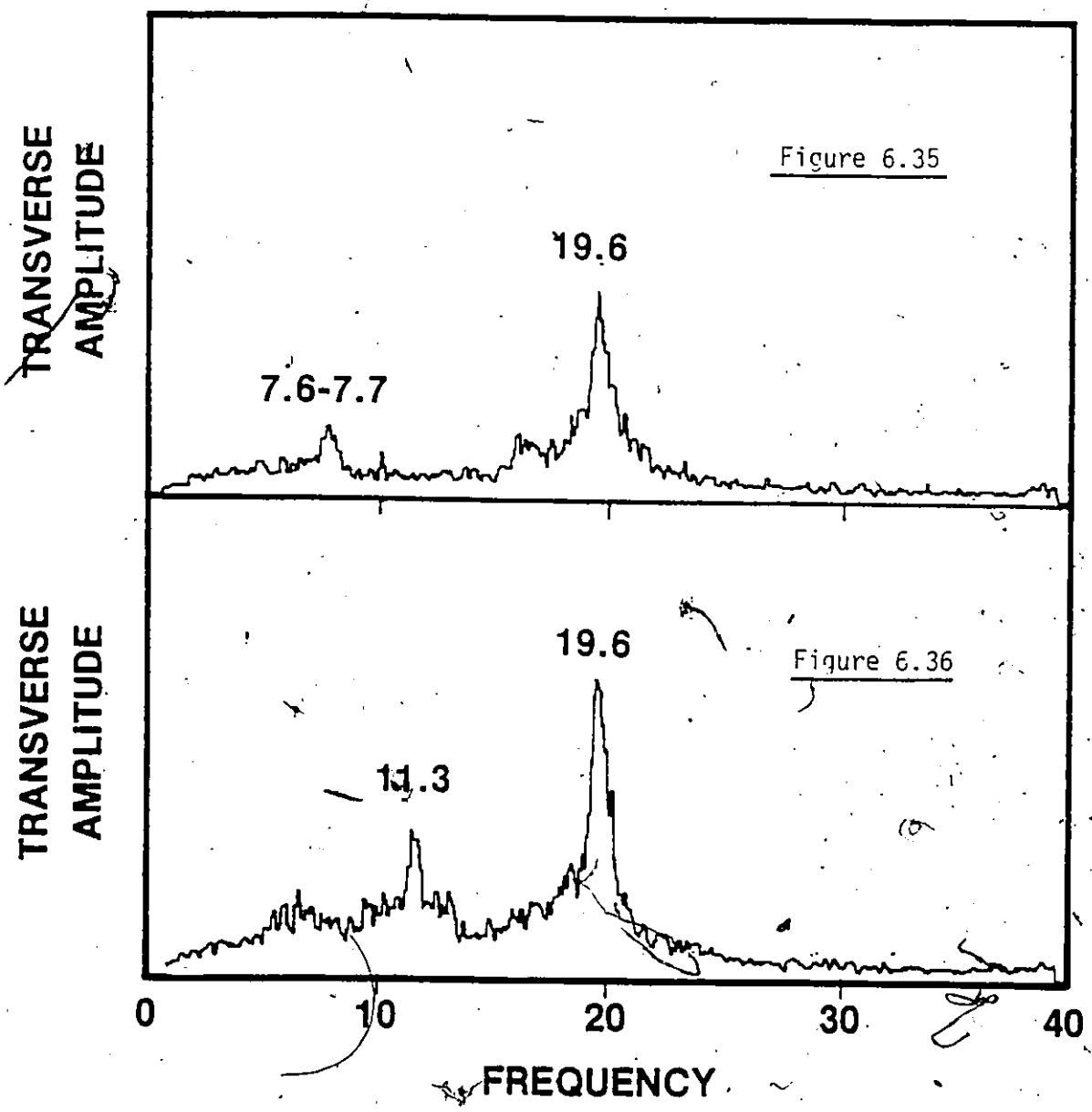

Figure 6.35 Transverse response spectrum at V_T= 0.30 m/s

Figure 6.36 Transverse response spectrum at V_T= 0.47 m/s

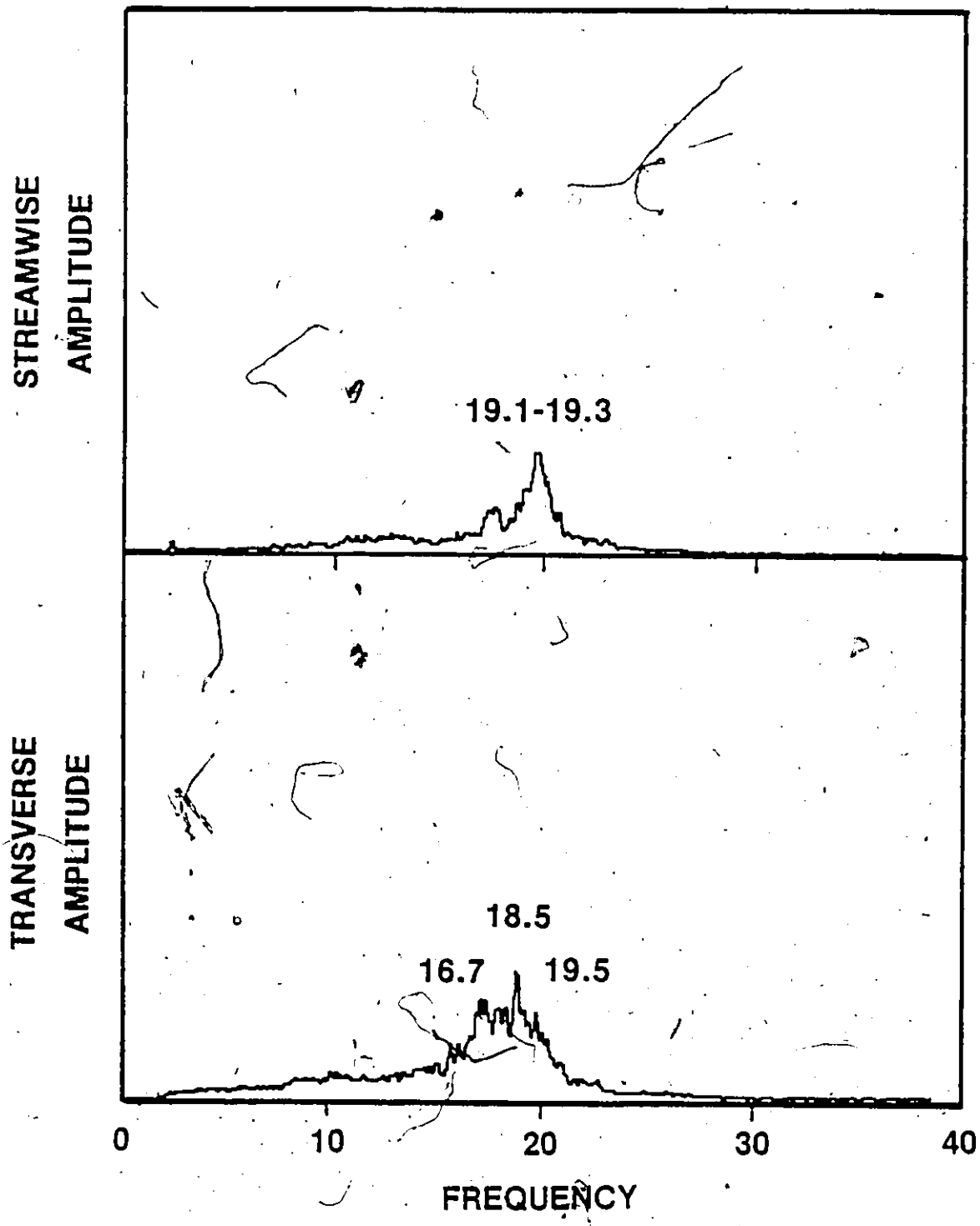

Figure 6.37 Response spectra at V_T= 0.69 m/s

were superimposed on each other. At V_T = 0.80 m/s a single peak at 18.6 Hz dominates the transverse spectrum of figure 6.38. Beyond V_T = 0.80 m/s a single spike dominates the streamwise and transverse response spectra and its frequency increases slightly with increasing flow velocity. Typical spectra of those recorded in the range $0.80 < V_T < 1.02$ m/s are given in figures 6.39 and 6.40. Other less dominant peaks in the response spectra of the post stable region found for the same tube in a full flexible bundle do not appear in the spectra of the post stable region for the case at hand. This is evident from comparing figures 6.39 and 6.40 with figures 6.26 and 6.28 recorded at the same flow velocities for the same tube in the full flexible bundle. It would appear that the purer frequency response observed in figures 6.39 and 6.40 is due to the fact that the neighbouring tubes are effectively rigid.

It is seen in figure 6.34, where the overall RMS responses of the flexible tube in the flexible and rigid bundles are compared, that the responses are practically identical in the velocity ranges $0 < V_T < 0.55$ m/s and $0.83 < V_T < 1.02$ m/s. However, the responses differ substantially in the range $0.55 < V_T < 0.83$ m/s. The difference in the amplitude levels can be explained in terms of the prevailing natural frequencies at resonance and the Strouhal numbers found in the two cases. The flexible tube in the full flexible bundle has a Strouhal number S_T = 0.7, a natural frequency of 16.4 Hz and hence the

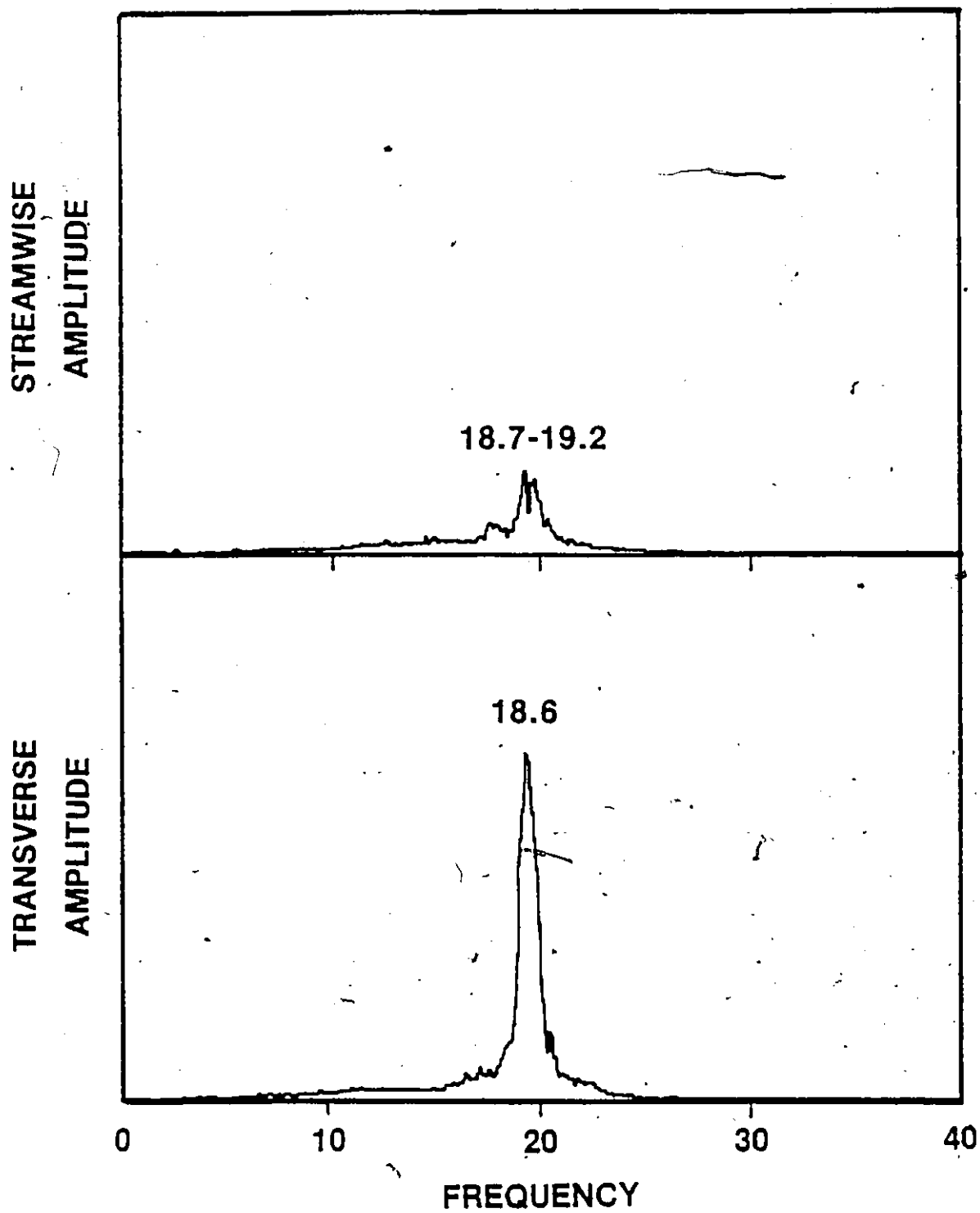

Figure 6.38 Response spectra at V_T= 0.80 m/s

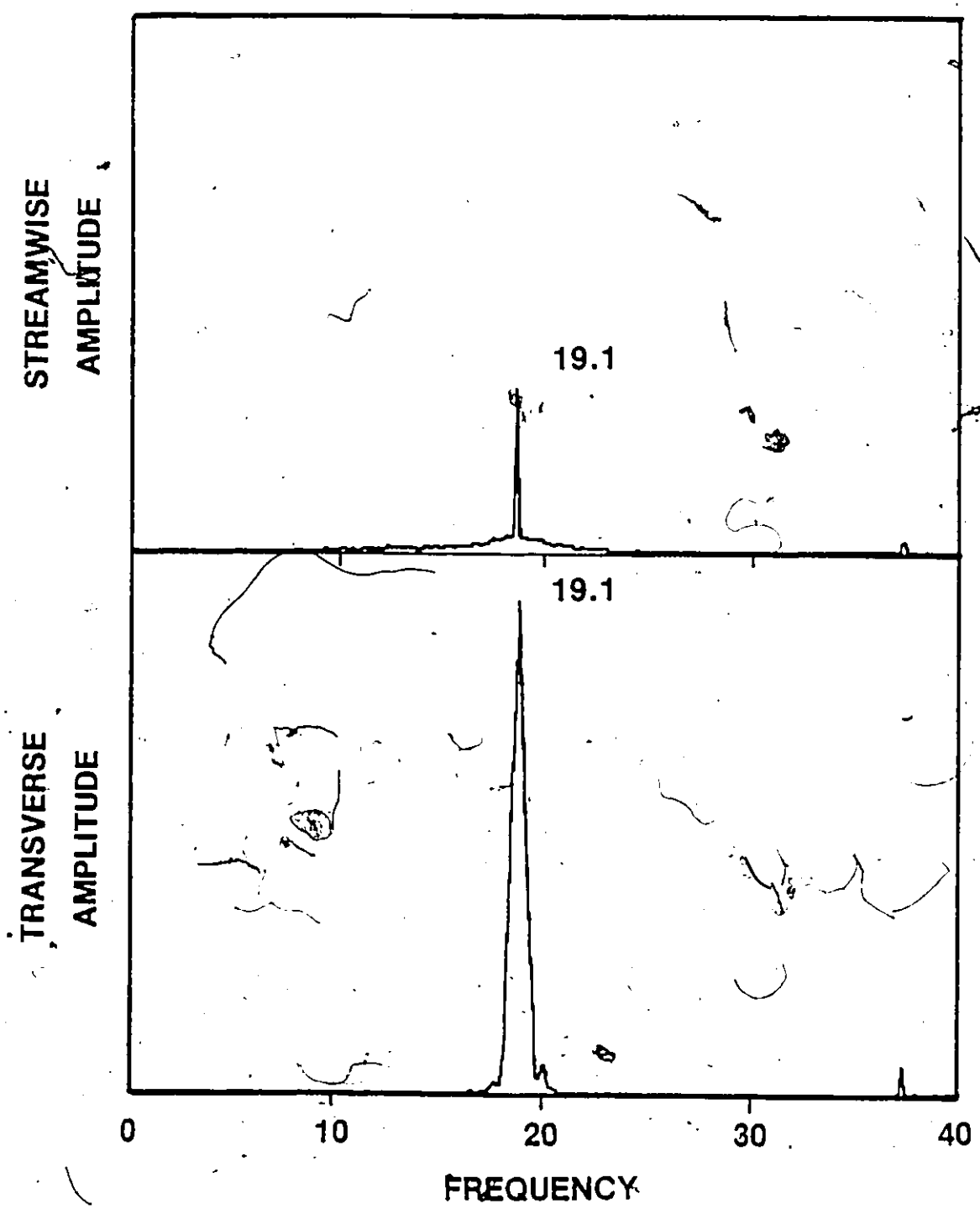

Figure 6.39 Response spectra at V_T= 0.94 m/s

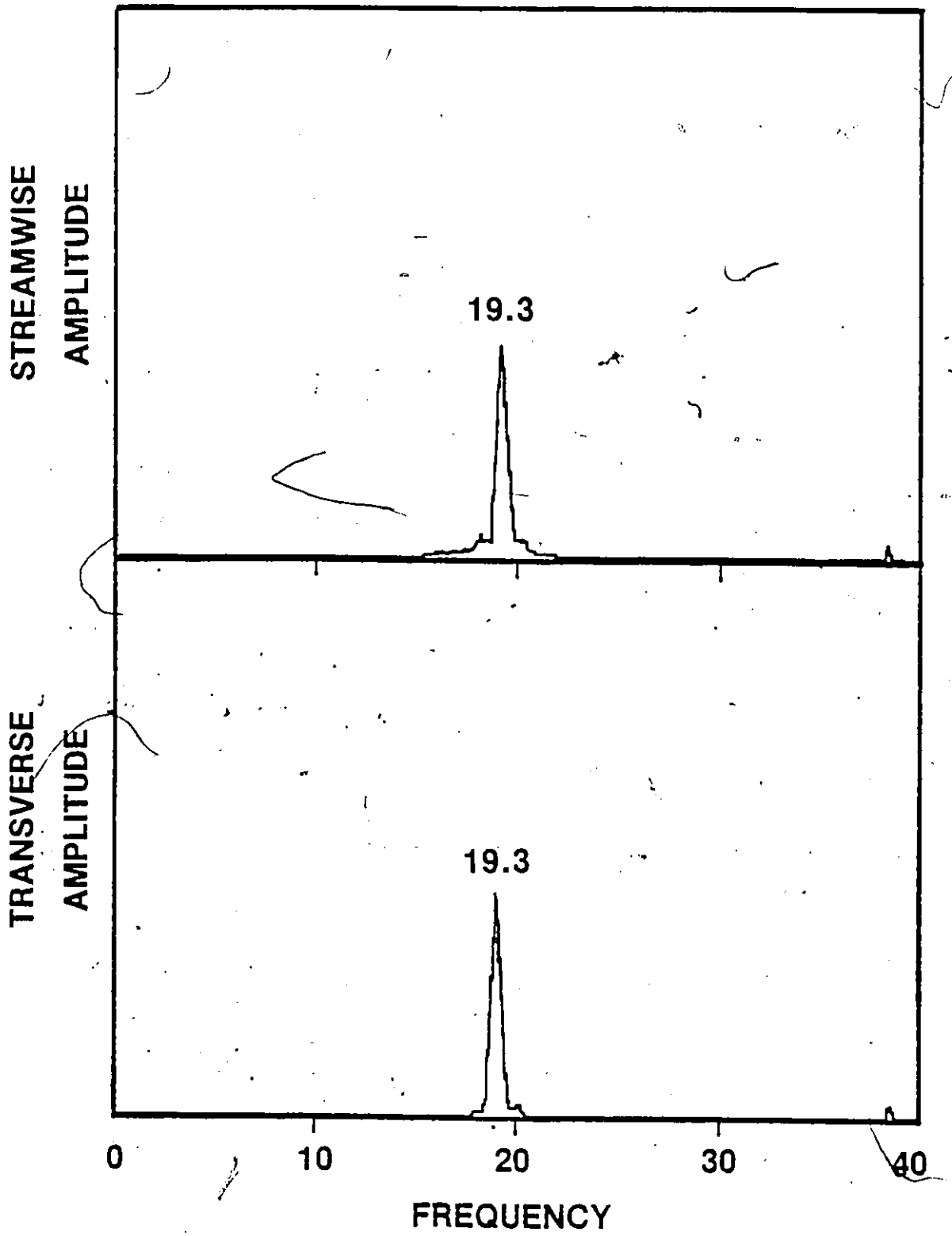

Figure 6.40 Response spectra at V_T= 1.02 m/s

resonance velocity V_T = 0.61 m/s. Therefore an early rise in its overall RMS response amplitude curve should be expected. The flexible tube in the rigid bundle however indicated a Strouhal number S_T = 0.61 and a natural frequency of 18.6 Hz. The flow velocity at resonance is expected, therefore, to be 0.77 m/s and the rise in its overall RMS response amplitude curve should be delayed accordingly. It is clear from figure 6.34 that the amplitude levels of the flexible tube in the full flexible bundle and that in the rigid bundle at the flow velocities 0.61 m/s and 0.77 m/s respectively are practically the same.

There seems to be no doubt that the flow velocity V_T = 0.80 m/s marks the instability threshold for the flexible tube in the rigid bundle. From a practical point of view, therefore, a single flexible tube in a rigid bundle becomes unstable essentially at the same flow velocity if all the surrouding tubes were flexibly mounted. This implies that the relative motion of the neighbouring tubes has a little effect on the critical velocity. The underlying observation here is that at the stability threshold, the response is predominantly in a transverse direction and a sharp increase in the transverse response occurs with a small increase in the flow velocity. This lends support to the theoretical treatment of Lever and Weaver [147] which proceeded on the assumption that the tube looses stability first in the transverse direction.

The critical reduced velocity and the added mass

coefficients for tube no. 6 in a rigid bundle are less than those for tube no. 6 in a flexibly mounted bundle. This is evident from the comparison given in table 6.2. These results are also in agreement with those reported in reference [40] for a triangular array.

Flow visualization show clearly the vigorous response above 0.80 m/s and reveal its nature as well as the flow behaviour in the fluidelastic region. The response is predominantly in the transverse direction as can be seen from the photographs of figures 6.41 to 6.43 taken at V_T = 0.97 m/s. The monitored tube reaches its uppermost position thereby narrowing the gap upstream of it. As a result, the approaching flow does not enter the upper flow lane but proceeds in the direction of the diagonal, figure 6.41. The tube, moving transversally downward in figure 6.42, has passed the midway point of its stroke. The flow is beginning to be established in the upper flow lane while that in the lower flow lane is being cut in response to the narrowing of the gap and is one the point of changing its direction. In figure 6.43 the tube reaches the lower most point of its stroke, the width of the gap is minimum and the lower main flow is moving now in a diagonal direction. It is clear that the main stream flow approaching the flexibly mounted tube cannot respond instantaneously to the variations in the width of the gaps and hence its motion must lag behind the motion of the tube. Such phase lag between the tube motion and the flow redistribution is seen

Table 6-2

Comparison between the critical reduced velocities and the added mass coefficients of tube no. 6 in a rigid bundle and in a flexible bundle

	tube no 6 flexible	
	In a Rigid bundle	In a Flexible bundle
V_T cr	0.80 m/s	0.83 m/s
V_u cr	0.40 m/s	0.415 m/s
$f_{obs.}$	18.6 Hz	17.5 Hz
critical reduced velocity ($V_u/f_{obs.}d$)	0.85	0.93
added mass coefficient	1.35	1.73

Figure 6.41 Flow Visualization at $V_T = 0.97$ m/s
Flexible Tube Near Uppermost Position

Figure 6.42 Flow Visualization at $V_T = 0.97$ m/s
Flexible Tube Near Mid-way Position

Figure 6.43 Flow Visualization at $V_T = 0.97$ m/s

Flexible Tube Near Lowermost Position

very clearly in the cine-films when studied at lower projection velocities. This phase lag must also occur in the flexibly mounted tube bundle but is obscured by the motion of neighbouring tubes as each tube is independently unstable, the relative tube motion is highly modulated and irregular. Thus, the flow redistribution observed appears random.

CHAPTER 7

CONCLUSIONS AND RECOMMENDATIONS

The intent of the present investigation was to study flow phenomena in heat exchanger tube arrays in water cross flow. A flow visualization technique was developed for this purpose which was suitable for studying the interstitial flow over a wide range of Reynolds numbers. A sheet of light was used at an interior plane normal to the tube axes and the flow was seeded with fine aluminum particles. This permitted observations to be made in the lighted plane and eliminated flow distortion by the boundary layer or free surface effects often found in flow visualization studies. The details of the observed flow phenomena were captured using still and high speed motion photographs. Simultaneously with detailed flow observations, tube response data were obtained so that they could be related directly with the fluid excitation phenomena. It was hoped that such studies would provide insights into the various excitation mechanisms.

Two tube bundle configurations were considered in the present study. The first was an in-line square array of tubes having a pitch to diameter ratio of 1.5. The array was four rows deep with eight tubes per row. The second array was a rotated square configuration with a pitch to diameter ratio of 1.414. This array was five rows deep with six tubes in each

row. In both cases, twelve tubes were flexibly mounted on one side of the array while the remaining tubes were rigidly mounted. This permitted comparing the structures of the interstitial flow in identical flexibly mounted and rigidly mounted tube bundles to deduce the effect of the motion of the tubes.

The principal conclusions drawn from investigating the square in-line array are as follows:

1. Up to a Reynolds number based on upstream flow velocity of about $Re_u \doteq 150$, straight laminar flow lanes exist between the tube columns with trapped stable symmetric vortices in the wakes of the tubes.
2. A transition to turbulence takes place at a Reynolds number of about $Re_u = 150$ and the transition is complete by about $Re_u \doteq 400$, beyond which no coherent wake phenomena are visible in the absence of tube motion.
3. Turbulence development in the interior of the tube bundle rendered the flow pattern around the third and subsequent rows different from that around the first and the second tube rows as the flow visualization results indicated. This implies that one and two tube row models are not representative of full heat exchanger arrays.
4. Vorticity shedding resonance in the array considered resulted in large amplitude response in the streamwise direction. Symmetric pairs of vortices are shed from

the first row tubes and persist up to at least the third tube row. The response of the second tube row is the largest and reaches about 6% of the tube diameter. Such behaviour may not occur for in-line tube arrays with pitch ratios significantly different from 1.5.

5. Fluidelastic instability is associated with significant flow redistribution and large transverse response amplitudes as the results of flow visualization have shown. It occurs at a critical reduced velocity based on the gap velocity of 2.36.

The principal conclusions drawn from investigating the rotated square array are as follows:

1. Up to a Reynolds number, based on the upstream flow velocity, of about $Re_u = 230$ the flow regimes found to develop for the tube array closely resemble those for an isolated circular cylinder in a cross flow. In particular, regimes of unseparated "potential" flow, stable attached vortex pairs and alternate vortex shedding were found within the confinement of the tube bundle. For the first time, alternate shedding of vortices was observed in a closely packed array. The possible existence of such phenomena has been the subject of much controversy in recent years.
2. At a Reynolds number of about $Re_u = 230$, the laminar vortex behaviour behind the third row becomes unstable

as transition to turbulence develops in the wake regions. This transition to turbulence occurs first behind the third row, because of the disturbances born in the flow by the first and second row tubes, then moves upstream as one would expect. The flow visualization clearly shows that turbulence is essentially fully developed by the third row of tubes and hence the flow around tubes in the first and second rows is not typical of that inside the tube bundle. This has important implications in terms of modelling heat exchanger tube dynamics as one and two row models have often been employed and such results must be considered questionable.

3. No coherent wake flow behaviour was observed above the Reynolds number of $Re_u = 230$. This would appear contradictory as a clear periodic excitation is indicated in the spectra of tube response. It is possible that turbulent vortices are being shed but are obscured from visibility by the high ambient turbulence level.

4. It would appear that, at least for this array, vorticity shedding and turbulence coexist as independent phenomena. Observations and computations show that numerous errors of attribution exist in the literature. Confusion has been created by inferring excitation mechanisms from observed response behaviour.

5. Fluidelastic instability is associated with large amplitude transverse oscillations and occurs approximately at a critical reduced velocity based on the upstream flow velocity of 0.99. This value compares favourably with the values of 0.89 and 0.94 reported in the literature for a rotated square array of pitch ratio equal to 1.5. Flow visualization showed significant flow redistribution but appeared random due to the motion of the neighbouring tubes.

6. The turbulence response, characterized by a wide band hump in the response spectra of the monitored tubes, observed in a flexibly mounted tube bundle has disappeared when all tubes except the monitored one were effectively rigid. This implies that the basic turbulence characteristics in a flexibly mounted array of tubes are greatly influenced by the motion of the tubes.

7. Fluidelastic instability of a flexibly mounted third row tube in an otherwise rigid bundle is associated with a predominantly transverse response with significantly clear flow redistribution as flow visualization has shown. Fluidelastic instability in this case occurs at essentially the same flow velocity as that when the surrounding tubes were free to move. This indicates that fluid coupled motion of adjacent tubes is not necessary for instability. The critical reduced velocity and the added mass coefficient are found to be

less than those found in the flexibly mounted tube array.

The results thus obtained illustrate the effect of array pattern on the flow phenomena that develop inside a tube array. In the rotated square array where the distance between two successive tubes in a column is large compared with that in the square in-line array, alternate vortex shedding is observed at low Reynolds numbers. The square in-line array pattern investigated permits synchronization of the wakes of the adjacent tubes in a row, in-line oscillations of the tubes, synchronized symmetric vortex shedding, and admits large amplitude resonant oscillations. Such global phenomena and flow organization were not observed in the rotated square array. This may be due to the staggered arrangement and the existence of a tube between the wakes of tubes in adjacent rows which effectively prevent communication between wakes. It appears also that the rotated square array is more stable than the square in-line array. The monitored third row tube in the former becomes unstable at a flow velocity $V_u = 0.42$ m/s while a monitored third row tube in the latter becomes unstable at $V_u = 0.35$ m/s.

Recommendations for Future Research

The present investigation provided some new insights into the nature of the excitation mechanisms associated with two different array patterns and given pitch ratios. In

addition, it paved the way for further insights to be made in the nature of the excitation mechanisms associated with other array patterns. The rotated square array is an intermediate case between the parallel and normal triangular array configurations and it is expected that vortex shedding, turbulence and stability boundary to be affected by the geometrical pattern of the array. Such excitation mechanisms are also affected by variations in the pitch ratio. The behavior of a tube in the interior of a given array is expected to resemble that of an isolated cylinder. At large pitch ratios the Strouhal number decreases to a value of 0.2 and thus stronger vortices with more coherent structure will be shed and vortex streets will be established. Fluidelastic excitation will disappear and tube resonance will be the phenomenon of main concern. At small pitch ratios the interference effects will be more pronounced and the close proximity of tubes will have its signature on the excitation mechanisms. Flow visualization combined with tube response spectra can be utilized to study these cases of interest and to show how smooth the transition is between excitation mechanisms in different array patterns at large and small pitch ratios.

In the rotated square array investigated here, periodicity of a discrete nature has been detected in the response spectra of the monitored tubes. While this periodicity was attributed to vorticity shedding, the cause of this periodicity remains obscure. A stroboscopic study, where a

stroboscope held at the top of the test section and driven at the frequency of the periodicity or multiple integrals of this frequency, may help detect the origin of this periodicity in the seeded flow.

Once the wake regions and the main stream flows are defined by flow visualization, hot film anemometer studies can be undertaken to further investigate the problem of turbulent vortex shedding. It is known that for an isolated circular cylinder the formation region length varies with the Reynolds number. Accordingly the anemometer can be positioned in the wake of the monitored tube at variable distances from it to investigate the existence of turbulent vortex street in the interior of the tube bundle. Of particular interest is how the turbulent vortex street, if it exists, is affected by the main stream flows, crossing of flow from one flow lane to another and the point in the wake beyond which the turbulent vortices disintegrate into turbulence.

BIBLIOGRAPHY

1. Nelms, H. A. and Segaser, C. L. "Survey of Nuclear Reactor System Primary Circuit Heat Exchangers", ORNL - 4399, Oak-Ridge, Apl. 1969.

2. Hartlen, R. T. "Recent Field Experience with Flow Induced Vibration of Heat-Exchanger Tubes" Int. Symp. on Vib. Problems in Industry, Paper No. 611, Keswick, England, 1973.

3. Shin, Y. S. and Wambsganss, M. W. "Flow Induced Vibration in LMFBR Steam Generators", ANL-75-16, A. N.L., Argonne.

4. Dueck, D. G. "Major Heat Exchanger Performance in Ontario Hydro Operated CANDU Nuclear Generating Stations" Presented at the Canadian Nuclear Association Heat Exchanger Reliability Seminar, Toronto, May 1st, 1980.

5. Flow Induced Vibration in Heat Exchangers Ed. D. D. Reiff, ASME, New York, 1970.

6. Proceedings of UKAEA/NPL International Symposium on Vibration Problems in Industry, Keswick, England, 1973.

7. Proceedings of IUTAM/IAHR Symposium on Flow Induced Vibrations, Karlsruhe, Germany, Aug. 1972, "Flow Induced Structural Vibrations", Ed. E. Naudascher Springer-Verlag, Berlin, 1974.

8. Fluid-Structure Interaction Phenomena in Pressure Vessel and Piping Systems, Ed. M. K. Au-Yang and S. J. Brown, ASME, New York, 1977.

9. Transactions of the 4th International Conference on Structural Mechanics in Reactor Technology (SMIRT), San Francisco, 1977.

10. Proceedings of BNES International Conference on Vibration in Nuclear Plant, Keswick, England, May 1978.

11. Flow Induced Vibrations, Ed. S. S. Chen and M. D. Bernstein, ASME, New York, 1979.

12. Dynamics of Fluid-Structure Systems in the Energy Industry, Ed. M. K. Au-Yang, S. J. Brown and J. R. McDermott, ASME, New York, 1979.

13. Proceedings of IAHR/IUTAM Symposium on Practical Experiences with Flow-Induced Vibrations, Karlsruhe, Sept. 1979, Ed. E. Naudascher and D. Rockwell, Springer Verlag, Berlin, 1980.

14. Savkar, S. D. "A Survey of Flow Induced Vibrations of Cylindrical Arrays in Cross-Flow", ASME Winter Annual Meeting, New York, N.Y. 1976, Paper No. 76-WA/FE-21.

15. Chenoweth, J. M. and Kistler, R. S. "Flow Induced Tube Vibrations in Shell-and-Tube Heat Exchangers" HTRI Report SAN/1273-I-UC-93, 1977.

16. Chen, S. S. "Flow Induced Vibrations of Circular Cylindrical Structures, Part II: Cross Flow Considerations", Schock and Vibration Digest, vol. 9(11), 1977, pp. 21-27.

17. Blevins, R. D. "Flow Induced Vibrations in Nuclear Reactors: A Review Progress in Nuclear Energy, vol. 4, 1979, pp. 25-49.

18. Paidoussis, M. P. "Flow Induced Vibrations in Nuclear Reactors and Heat Exchangers, Practical Experience and State of Knowledge". Proceedings IUTAM/IAHR Symposium on Practical Experiences with Flow Induced Vibrations, Karlsruhe, 1979, Springer-Verlag, pp. 1-80, 1980.

19. Paidoussis, M. P. "Fluidelastic Vibrations of Cylinder Arrays in Axial and Cross Flow - State of the Art" Session 40 ASME Energy Technology Conference, San Francisco, Aug. 1980.

20. Pettigrew, M. J. "Flow Induced Vibration Phenomena in Nuclear Power Station Components", Power Industry Research, vol., 1981, pp. 97-133.

21. Chen, Y. N. "Flow Induced Vibration and Noise in Tube Bank Heat Exchangers Due to Von Karman Streets", J. Eng. Ind. 90(1), Feb. 1968, pp. 134-146.

22. Funakawa, M. and Umakoshi, R. "The Acoustic Resonance in Tube Bank", Bull. JSME, 13(57), March 1970, pp. 348-355.

23. Morse, P. M. "Vibration and Sound", McGraw Hill, 2nd ed., p. 398, 1968.

24. Zdravkovich, M. M. and Nuttall, J. A. "On the Elimination of Aerodynamic Noise in Staggered Tube Bank", J. Sound and Vibration, 34(2), 1974, pp. 173-177.

25. Baylac, G. and Gregoire, J. P. "Etude des Ecoulements et des Phenomenes Acoustiques dans un Faisceau de Tubes". In "Aero-Hydro-elasticite", Eyrolles, Paris, 1973, pp. 279-379.

26. Owen, P. R. "Beffeting Excitation of Boiler Tube Vibration", J. Mechanical Engineering Science, vol. 7, 1965, pp. 431-439.

27. Grotz, B. J. and Arnold, F. R. "Flow Induced Vibrations in Heat Exchangers", Stanford University, California, Dept. Mech. Engng. Tech. Rep. No. 31, 1956.

28. Chen, Y. N. "Excitation Sources of the Flow Induced Vibrations and Noise in Tube Bank Heat Exchangers" Symposium on Noise and Fluids Engineering, ASME Winter Annual Meeting, Atlanta, Georgia, Nov. 27-Dec. 2, 1977.

29. Chen, Y. N. "The Sensitive Tube Spacing Region of Tube Bank Heat Exchangers for Fluid-Elastic Coupling in Cross-Flow", ASME Winter Annual Meeting, Atlanta, Georgia, Nov. 27-Dec. 2, 1977.

30. Grover, L. K. and Weaver, D. S. "Cross Flow Induced Vibrations in a Tube Bank Vortex Shedding", J. Sound and Vibrations, 59(2), 1980, pp. 225-237.

31. Pettigrew, M. J., Sylvester, Y. and Campagna, A. O. "Vibration Analysis of Heat Exchanger Tube Arrays" Nuclear Engineering and Design, 48, 1978, pp. 97-115.

32. Pettigrew, M. J. and Gorman, D. J. "Vibration of Heat Exchanger Components in Liquid and Two Phase Cross Flow", B.N.E.S. Vibration in Nuclear Plant, Keswick, 1978.

33. Connors, H. J. "Fluidelastic Vibration of Tube Arrays Excited by Cross-Flow", ASME Symposium on Flow Induced Vibration in Heat Exchangers, 1970.

34. Livesey, J. L. and Dye, R. C. F. "Vortex Excited Vibrations of a Heat Exchanger Tube Row", J. Mechanical Engineering Science, vol. 4, 1962, pp. 349-352.

35. Zdravkovich, M. M., Singh, S., Nuttall, J. A. and Causon, D. M. "Flow Induced Vibrations in Staggered Tube Banks", Proceedings 6th Thermo and Fluid Mechanics Convention, Durham, 1976, pp. 237-243.

36. Blevins, R. D. "Fluidelastic Whirling of a Tube Row", ASME J. of Pressure Vessel Technology, vol. 96, 1974, pp. 263-267.

37. Blevins, R. D. "Fluidelastic Whirling of Tube Rows and Tube Arrays", ASME J. of Fluid Engineering, Sept. 1977, pp. 457-461.

38. Weaver, D. S. and Lever, J. "Tube Frequency Effects on Cross Flow Induced Vibrations in Tube Arrays", Proceedings of the fifth Biennial Symposium on Turbulence, University of Missouri-Rolla, Missouri, Science Press, Princeton, N.J., 1977, pp. 323-331.

39. Weaver, D. S. and Grover, L. K. "Cross Flow Induced Vibrations in a Tube Bank - Turbulent Buffeting and Fluidelastic Instability", J. Sound and Vibration, vol. 59, no. 2, 1978, pp. 277-294.

40. Weaver, D. S., and Koroyannakis, D. "The Cross Flow Response of a Tube Array in Water A Comparison with the Same Array in Air", ASME J. Pressure Vessel Technology, vol. 104, 1982, pp. 139-146.

41. Zdravkovich, M. M. "Flow Induced Vibrations in Irregularly Staggered Tube Bundles and Their Suppression", UKAEA/NPL International Symposium, Vibration Problems in Industry, Keswick, 1973, Paper No. 413.

42. Gorman, D. J. "Experimental Study of Peripheral Problems Related to Liquid Flow Induced Vibration in Heat Exchangers and Steam Generators", Paper F4/g, SMIRT, San Francisco, 1977.

43. Chen, Y. N. "The Orbital Movement and the Damping of the Fluidelastic Vibration of Tube Banks Due to Vortex Formation. Part 2 - Criterion for the Fluidelastic Orbital Vibration of Tube Arrays" ASME Paper No. 73-DET-146.

44. Connors, H. J. "Fluidelastic Vibration of Heat Exchanger Tube Arrays", Transactions of the ASME, J. Mechanical Design, Paper No. 77-DET-90.

45. Tanaka, H. and Takahara, S. "Unsteady Fluid Dynamic Force on Tube Bundle and its Dynamic Effect on Vibration", Flow Induced Vibrations of Power Plant Component, ASME Special Publication PVP - 41, 1980, pp. 77-92.

46. Tanaka, H. and Takahara, S. "Fluidelastic Vibration of Tube Arrays in Cross Flow", J. Sound and Vibration, 77(1), 1981, pp. 19-37.

47. Zdravkovich, M. M. and Namork, J. E. "Excitation, Amplification and Suppression of Flow-Induced Vibrations in Heat Exchangers", IAHR/IUTAM Symposium on Practical Experiences with Flow Induced Vibrations, Karlsruhe, Germany, Sept. 3-6, 1979.

48. Zdravkovich, M. M. and Namork, J. E. "Flow Structure within both Stationary and Vibrating Tube Banks with Triangular Pitch", B.N.E.S. Vibration in Nuclear Plant, Keswick, U.K., May 1978, Paper 2:5.

49. Zdravkovich, M. M. and Namork, J. E. "Structure of Interstitial Flow between Closely Spaced Tubes in Staggered Array", The Third National Congress on Pressure Vessel and Piping Technology, San Francisco, Calif., 1979.

50. Collar, A. R. "The Expanding Domain of Aeroelasticity" J. of the Royal Aeronautical Society, London, England, vol. 50, no. 428, 1946.

51. Bisplinghoff, R. L., Ashley, H. and Halfman, R. L. "Aeroelasticity", Addison Wesley, Cambridge, Mass., 1955.

52. Fung, Y. C. "The Theory of Aeroelasticity" John Wiley & Sons Inc., New York, 1957.

53. Flax, A. H. "Aero and Hydro-Elasticity", Proc. of the First Symp. on Naval Structural Mechanics, Pergamon Press, New York, 1960.

54. Heller, S. R., and Abramson, H. N. "Hydroelasticity - A New Naval Science", J. of the American Society of Naval Engineers, vol. 71, no. 2, 1959.

55. Heller, S. R. "Hydroelasticity", Advances in Hydroscience, vol. 1, Academic Press, New York, N.Y. 1964, pp. 94-160.

56. Abramson, H. N. "Dydroelasticity - Some Problems and Some Solutions", ASME Symp. Fluid Solid Interaction, 1967, pp. 187-222.

57. Toebes, G. H. "Flow Induced Structural Vibrations", ASCE J. Eng. Mech. Div., 91 (EM6), 1965, pp. 39-66.

58. Weaver, D. S. "On Flow Induced Vibrations in Hydraulic Structures and their Alleviations", Canadian Journal of Civil Engineering, vol. 3, no. 1, 1976, pp. 126-137.

59. Weaver, D. S. "Special Topics in Mechanics", Course notes, Mechanical Engineering Course no. 736 Winter 1980-1981, McMaster University Mechanical Engineering Department.

60. Bolotin, V. V. Nonconservative Problems of the Theory of Elastic Stability, Pergamon Press, New York, N.Y., 1963.

61. Leipholz, H. H. E. Stability Theory, Academic Press, New York, N.Y., 1970.

62. Baker, W. E., Westine, P. S. and Dodge, F. T. "Similarity Methods in Engineering Dynamics", Hayden Book Co., New Jersey.

63. Marris, A. W. "A Review on Vortex Streets, Periodic Wakes, and Induced Vibration Phenomena", J. Basic Engineering, 86(2), 1964, pp. 185-196.

64. Batchelor, G. K. An Introduction to Fluid Dynamics, Cambridge University Press, 1977.

65. Kovasznay, L. S. G. "Hot Wire Investigations of the Wake Behind Cylinders at Low Reynolds Numbers", Proceedings, Royal Society (London), Series A, vol. 198, 1949, p. 174.

66. Tritton, D. J. "Experiments on the Flow Past a Circular Cylinder at Low Reynolds Numbers", J. Fluid Mechanics, vol. 6, Part 4, 1959, p. 547.

67. Roshko, A. "On the Development of Turbulent Wakes from Vortex Streets", NACA Report 1191, 1954, p. 801.

68. Blevins, R. D. Flow Induced Vibrations, Van Nostrand Reinhold Company, 1977.

69. Bishop, R. E. D. and Hassan, A. Y. "The Lift and Drag Forces on a Circular Cylinder in a Flowing Liquid", Proceedings of the Royal Society A277, 1964, pp. 32-51.

70. Surry, D. "The Effect of High Intensity Turbulence on the Aerodynamics of a Rigid Circular Cylinder at Subcritical Reynolds Number", University of Toronto Institute for Aerospace Studies, UTIAS Report no. 142, 1969.

71. Chen, Y. N. and Weber, M. "Flow Induced Vibrations in Tube Bundle Heat-Exchangers with Cross and Parallel Flow. Part two Cross Flow", Proceedings of the Symposium on Flow Induced Vibrations in Heat Exchangers; ASME, Winter Annual Meeting, New York, Dec. 1, 1970, pp. 57-74.

72. Keefe, R. T. "An Investigation of the Fluctuating Forces Acting on a Stationary Circular Cylinder", University of Toronto, UTIA Report no. 76, 1961.

73. Lienhard, J. H. "Synopsis of Lift, Drag and Vortex Frequency Data for Rigid Circular Cylinders", Bulletin 300, College of Engineering, Washington State University, 1966.

74. Gerrard, J. H. "The Mechanics of the Formation Region of Vortices behind Bluff Bodies", J. Fluid Mechanics, 25, 1966, pp. 401-413.

75. Griffin, O. M. and Vataw, C. W. "The Vortex Street in the Wake of a Vibrating Cylinder", J. Fluid Mechanics, 51, 1972, pp. 31-48.

76. Koopmann, G. H. "The Vortex Wakes of Vibrating Cylinders at Low Reynolds Numbers", J. Fluid Mechanics, 28, 1967, pp. 501-512.

77. Toebes, G. H. "The Unsteady Flow and Wake near an Oscillating Cylinder", Trans. Amer. Soc. Mech. Eng., J. Basic Engineering, 91, Sept. 1969, pp. 493-505, Discussion pp. 859-862.

78. Sarpkaya, T. "Vortex-Induced Oscillations - A Selective Review", Trans. Amer. Soc. Mech. Eng., J. Appl. Mech., 46, 1979, pp. 241-258.

79. King, R. "A Review of Vortex Shedding Research and its Application", Ocean Engng., vol. 4, 1977, pp. 141-171.

80. Scruton, C. "On Wind Excited Oscillations of Stacks, Towers and Masts", Proc. Conf. on Wind Effects on Buildings and Structures, Teddington, 1963.

81. Walshe, D. E. "Wind Excited Oscillations of Structures" H.M.S.O. Publications S.B.N. 114800162, 1972.

82. Auger, A. "Wind Induced Vibration in a Space Frame Structure", Symp. on Wind Effects on Buildings and Structures, Loughborough, 1968.

83. King, R. and Prosser, M. J. "Criteria for Flow Induced Oscillations of a Cantilevered Cylinder in Water", IUTAM/IAHR. Symp. on Flow Induced Structural Vibrations, Karlsruhe, 1972.

84. Karman, Th. V. "On the Mechanics of Resistance Experienced by a Body Moving through a Fluid", Gottinger Nach., 13, 1912, pp. 547-562.

85. Walshe, D. E. and Wootton, L. R. "Preventing Wind-Induced Oscillations of Structures of Circular Section.

86. Hartlen, R. T. and Currie, I. G. "Lift Oscillator Model of Vortex Induced Vibration", J. Engineering Mechanics Division of ASCE, vol. 96, 1970, EMS, pp. 577-591.

87. Laudl, R. "Theoretical Model for Vortex-Excited Oscillations", Proceedings of the International Symposium on Vibration Problems in Industry, Keswick, England, 1973.

88. Currie, I. G., Hartlen, R. T. and Martin, W. W. "The Response of Circular Cylinders to Vortex Shedding", Flow Induced Structural Vibrations, ed. Naudascher, E., Springer-Verlag, Berlin, 1974, pp. 128-142.

89. Griffin, O. M., Skap, R. A., and Ramberg, S. E. "The Resonant Vortex Excited Vibrations of Structures and Cable Systems", Proceedings of the Offshore Technology Conference, Paper no. 2319, Houston, Texas, 1975.

90. Iwan, W. D. and Blevins, R. D. "A Model for Vortex-Induced Oscillations of Structures", ASME J. Applied Mechanics, vol. 41, 1974, pp. 581-586.

91. Blevins, R. D., and Burton, T. E. "Fluid Forces Induced by Vortex Shedding", ASME J. Fluids Engineering, vol. 95, 1976, pp. 19-24.

92. Paidoussis, M. P. "A Review of Flow Induced Vibrations in Reactors and Reactor Components", Nuclear Engineering and Design, vol. 74, 1982, pp. 31-60.

93. Sarpkaya, T. "Fluid Forces on Oscillating Cylinders", J. Waterway, Port, Costal and Ocean Division, ASCE, vol. 104, 1978, pp. 275-290.

94. Savkar, S. D. and So, R. M. C. "On the Buffeting Response of a Cylinder in Turbulent Cross Flow", General Electric Report GEAP 24149, Sept. 1978.

95. So, R. M. C. and Savkar, S. D. "Buffeting Forces on Rigid Circular Cylinders in Cross Flows", J. Fluid Mechanics, vol. 105, 1981, pp. 397-425.

96. Spivak, H. M. "Vortex Frequency and Flow Pattern in the Wake of Two Parallel Cylinders at Varied Spacing Normal to an Air Stream", J. of the Aeronautical Sciences, June 1946, pp. 289-301.

97. Thomas, D. G. and Kraus, K. A. "Interaction of Vortex Streets", J. Applied Physics, vol. 35, no. 12, Dec. 1964, pp. 3458-3459.

98. Bearman, P. W. and Wadcock, A. J. "The Interaction Between a Pair of Circular Cylinders Normal to a Stream", J. Fluid Mech., vol. 61, Part 3, 1973, pp. 499-511.

99. Zdravkovich, M. M. "Review-Review of Flow Interference between Two Circular Cylinders in Various Arrangements", J. Fluids Engineering, Dec. 1977, pp. 618-633.

100. Putnam, A. A. "Flow Induced Noise in Heat Exchangers", J. Engineering for Power, Oct. 1959, p. 417.

101. Putnam, A. A. "Flow Induced Noise and Vibration in Heat Exchangers", ASME Publication, Paper no. 64-WA/HT-21.

102. Wieghardt, K. E. G. "On the Resistance of Screens", Aero Quart., vol. 4, 1953, p. 186.

103. Hill, R. S. and Armstrong, C. "Aerodynamic Sound in Tube Banks", Proc. Phys. Soc., vol. 79, Part 1, 1962, p. 225.

104. Chen, Y. N. "Frequency of the Karman Vortex Streets in Tube Banks", J. of the Royal Aeronautical Society, London, vol. 71, 1967, pp. 211-214.

105. Tung, C. "Instability of Three-Row Vortex Streets", AIAA Journal, vol. 2, 1964, pp. 1143-1144.

106. Chen, Y. N. "Fluctuating Lift Forces of the Karman Vortex Streets on Single Circular Cylinders and in Tube Bundles Part 3 Lift Forces in Tube Bundles", ASME J. Engineering for Industry, 94(2), 1972.

107. Gross, H. G. Untersuchung Aeroelastischer Schwingungs mechanismen Und Duren Berucksichtigung Bei Der Auslegung Von Rohrbundelwarmetauschern. Dissertation, Technical University of Hanover, 1975.

108. Achenbach, E. "Investigations on Flow through a Staggered Tube Bundle at Reynolds Numbers up to 10^7. Warme und Stoffubertragung 1969, 2, 47-52.

109. Batham, J. P. "pressure Distributions on In-Line Tube Arrays in Cross Flow", Proc. Int. Symp. Vibration Problems in Industry, Keswick, 1973, Paper 4b1.

110. Chen, Y. N. "Fluctuating Lift Forces of the Karman Vortex Streets on Single Circular Cylinders and in Tube Bundles. Part 1 - The Vortex Street Geometry of the Single Circular Cylinder", ASME J. Engineering for Industry, 94(2), 1972.

111. Chen, Y. N. "Fluctuating Lift Forces of the Karman Vortex Streets on Single Circular Cylinders and in Tube Bundles, Part 2 - Lift Forces of Single Cylinders", ASME J. Engineering for Industry, 94(2), 1972.

112. "Hydraulic Institute Standards for Centrifugal Rotary & Reciprocating Pumps", Thirteenth Edition, Hydraulic Institute, 1975. Cleveland, Ohio. Library of Congress Card No. A56-4036.

113. Koroyannakis, D. "Liquid Cross-Flow-Induced Vibrations of a Tube-Array", Master of Engineering Thesis, Mechanical Engineering Department, McMaster University, Hamilton, Ontario, 1980.

114. Weaver, D. S. and Yeung, H. C. "Approach Flow Direction Effects on the Cross-Flow-Induced Vibrations of a Square Array of Tubes, J. Sound and Vibration, 78(3), 1983, pp. 469-482.

115. Weaver, D. S. and Yeung, H. C. "The Effect of Tube Mass on the Flow Induced Response of Various Tube Arrays in Water", J. Sound and Vibration, vol. 93(3), 1984, pp. 409-425.

116. Fitz-Hugh, J. S. "Flow Induced Vibrations in Heat Exchangers", Proceedings of UKAEA/NPL International Symposium on Vibration Problems in Industry, Keswick, 1973, Paper 427.

117. Zukaukas, A. and Katinas, V. "Flow Induced Vibrations in Heat Exchanger Tube Banks", Proceedings of the IUTAM-IAHR Symposium on Practical Experiences with Flow Induced Vibrations, Karlsruhe, pp. 188-196 (Editor E. Naudasher and D. Rockwell), Berlin, Springer-Verlag, 1980.

118. Hartlen, R. T. "Wind Tunnel Determination of Fluid-Elastic-Vibration Thresholds for Typical Heat Exchanger Tube Patterns, Mechanical Research Department Report 74-309-K, Ontario Hydro Research Division, Toronto, Ontario.

119. Weaver, D. S. and ElKashlan, M. "On the Number of Tube Rows Required to Study Cross-Flow Induced Vibrations in Tube Banks", J. Sound and Vibration, 75, 1981, pp. 265-273.

120. Gorman, D. J. "Experimental Development of Design Criteria to Limit Liquid Cross-Flow-Induced Vibration in Nuclear Heat Exchange Equipment", Nuclear Science and Engineering, 61, 1876, pp. 324-336.

121. Southworth, P. J. and Zdravkovich, M. M. "Effect of Grid-Turbulence on the Fluid-Elastic Vibrations of In-Line Tube Banks in Cross Flow", J. Sound and Vibration, 39(4), 1975, pp. 461-469.

122. Yeung, H. C. and Weaver, D. S. "The Effect of Approach Flow Direction on the Flow Induced Vibrations of a Triangular Tube Array", ASME J. Vibration, Acoustics, Stress and Reliability, vol. 105, no. 1, 1981, pp. 76-82.

123. Fitzpatrick, J. A. and Donaldson, I.S. "Row Depth Effects on Turbulence Spectra and Acoustic Vibrations in Tube Banks", J. Sound and Vibration, 73(2), 1980, pp. 225-237.

124. Merzkirch, W. "Flow Visualization", Academic Press Inc., New York, 1974.

125. Clayton, B. R. and Massey, B. S. "Flow Visualization in Water: A Review of Techniques", J. Scientific Instruments, vol. 44, 1967, pp. 2-11.

126. Morris, R. E. and Haythornthwaite, B. "Water Flow Analogues for Gas Dynamics", Engineering, London, vol. 190, 1960, pp. 261-263.

127. Chesters, J. H., Halliday, I. M. D. and Howes, R. S. "Some Aspects of Fluid Flow", London: Arnold, 1951, pp. 176-193.

128. McEachern, N. V. and Bowker, A. J. "Water Tunnel Flow Visualization Experiments in a 2" Square Duct", NRC, NAE Laboratory Memo AE-117, National Research Council of Canada, Ottawa, Apl. 1960.

129. Winter, E. F. "Flow Visualization Techniques Applied to Combustion Problems", J. Royal Aeronautical Society, vol. 62, 1958, pp. 268-276.

130. Schraub, F. A., Kline, S. J., Jenry, J., Runstadler, P. W., and Littell, A. "Use of Hydrogen Bubbles for Quantitative Determination of Time Dependent Velocity Fields in Low-Speed Water Flows". J. Basic Eng., vol. 87, 1965, pp. 429-444.

131. Clutter, D. W., Smith, A. M. O. and Brazier, J. G. "Techniques of Flow Visualization using Water as the Working Medium", Report of Douglas Aircraft Co., No. ES29075, 1959.

132. Dobrodzicki, G. A. "Flow Visualization in the NAE Water Tunnel", NRC, Aeronautical Report LR-557, Feb. 1972.

133. Weaver, D. S. and Adubi, F. A. "Flow Visualization Studies of Check Valve Vibrations", Proceedings of the Fourth Biennial Symposium on Turbulence in Liquids, University of Missouri-Rolla, Missouri, 1975.

134. Prandtl, L. and Tietjens, O. G. "Applied Hydro and Aeromechanics", McGraw Hill, 1934 (Translated from German Edition, Springer, 1931).

135. Wallis, R. P. and White, C. M. "Resistance to Flow through Nests of Tubes", Engineering, 1938, vol. CXL VI.

136. Wallis, R. P. "Photographic Study of Fluid Flow between Banks of Tubes", Engineering, vol. 148, 1939, pp. 423-426.

137. Rouse, H. "Fluid Mechanics for Hydraulic Engineers", Dover Publication, New York, 1961, p. 375.

138. Morsi, S. A. and Alexander, A. J. "An Investigation of Particle Trajectories in Two-Phase Flow Systems", J. Fluid Mech., vol. 55, 1972, pp. 193-208.

139. Chen, C. J. and Emrich, R. J. "Investigation of the Shock-Tube Boundary Layer by a Tracer Method", Phys. Fluids, vol. 6, 1963, pp. 1-9.

140. Somerscales, E. F. C. "Fluid Velocity Measurement by Particle Tracking", 1st Symposium on Flow - Its Measurement and Control in Science and Industry, 1971, Paper no. 1-4-163. The Instrument Society of America, Pittsburgh, Pennsylvania.

141. Hyzer, W. G. Engineering and Scientific High-Speed Photography, The MacMillan Company, New York, 1962.

142. Zdravkovich, M. M. "Modification of Vortex Shedding in the Synchronization Range", ASME Paper No. 81-WA/FE-25.

143. Lubin, B. T., Guerrero, H. N., and Kantayya, R. C. "Response of a Tube Bank to Cross Flow Induced Excitation at Trans and Supercritical Reynolds Numbers", Symposium on Practical Experiences with Flow Induced Vibrations, Karlsruhe, Germany, 1979.

144. Jones, G. W. et al. "Aerodynamic Forces on Stationary and Oscillating Circular Cylinders at High Reynolds Numbers", NASA-TR-R-300.

145. King, R. and Johns, D. J. "Wake Interaction Experiments with Two Flexible Circular Cylinders in Flowing Water", J. Sound and Vibration, 45(2), 1976, pp. 259-283.

146. King, R., Prosser, M. J. and Johns, D. J. "On Vortex Excitation of Model Piles in Water", J. Sound and Vibration, vol. 29, 1972, pp. 169-188.

147. Lever, J. H. and Weaver, D. S. "A Theoretical Model for Fluidelastic Instability in Heat Exchanger Tube Bundles", J. Pressure Vessel Technology, vol. 104, Aug. 1982, pp. 147-157.

148. Heilker, W. J. and Vincent, R. Q. "Vibration in Nuclear Heat Exchangers due to Liquid and Two-Phase Flow", ASME Century 2 Nuclear Engineering Conference, San Francisco, Paper No. 80-C2/NE-4, 1980.

149. Lever, J. H. "A Theoretical Model for the Cross-Flow Induced Fluid-Elastic Instability in Heat Exchanger Tube Bundles", Ph.D. Thesis, Mech. Engng. Dept., McMaster University, 1983.

150. Bloor, M. S. "The Transition to Turbulence in the Wake of a Circular Cylinder", J. Fluid Mechanics, vol. 19, 1964, p. 290.

151. Griffin, O. M. and Ramberg, S. E. "The Vortex Street Wakes of Vibrating Cylinders", J. Fluid Mechanics, vol. 66, Part 3, 1974, pp. 553-576.

152. Sarpkay, T. and Shoaff, R. L. "An Inviscid Model of Two-Dimensional Vortex Shedding for Transient and Asymptotically Steady Separated Flow over a Cylinder", AIAA, 17th Aerospace Science Meeting, New Orleans, 1979, Paper no. 79-0281, Jan. 15-17.

153. Soper, B. M. H. "The Effect of Tube Layout on the Fluid-elastic Instability of Tube Bundles in Cross Flow", ASME Symposium HTD, 1980, vol. 9, Flow Induced Heat Exchanger Tube Vibration.

154. Chen, S. S. "Dynamics of Heat Exchanger Tube Banks", ASME J. of Fluids Engineering, vol. 99, 1977, pp. 462-467.

155. Chen, S. S., Jendrzejczyk, J. A. and Wambsganss, M. W., "Experiments on Fluidelastic Vibrations of Tube Arrays", Technical Memorandum, ANL-CT-77, Argonne National Lab., Argonne, Ill., 1977.

156. Goyder, H. G. D. "Unstable Vibrations of a Bundle of Cylinders due to Cross Flow", Int. Conf. on Recent Advances in Structural Dynamics, Inst. of Sound and Vibration Research, University of Southampton, England, July 7-11, 1980.

157. Price, S. J. and Paidoussis, M. P. "Fluidelastic Instability of an Infinite Double Row of Circular Cylinders subjected to a Uniform Cross Flow", ASME J. of Mechanical Design, 1981, Paper no. 81-DET-24.

158. Chen, S. S. "A Mathematical Model for Cross-Flow Induced Vibrations of Tube Rows", 3rd Intl. Conf. Pressure Vessel Technology, Part 1, 1977, pp. 415-426.

159. Chen, S. S. "Cross Flow Induced Vibrations of Heat Exchanger Tube Banks", Nucl. Eng. Des., vol. 47, 1978, pp. 67-86.

160. Chen, S. S. "instability Mechanisms and Stability Criteria of a Group of Circular Cylinders subjected to Cross-Flow, Part I: Theory", ASME Journal of Mechanical Design, 1981, Paper No. 81-DET-21.

161. Chen, S. S. "Instability Mechanisms and Stability Criteria of a Group of Circular Cylinders subjected to Cross-Flow. Part II: Numerical Results and Discussions", ASME Journal of Mechanical Design, Paper no. 81-DET-22, 1981.

162. Southworth, P. J. and Zdravkovich, M. M. "Cross Flow Induced Vibrations of Finite Tube Banks in an In-Line Arrangement", J. Mechanical Engineering Science, vol. 17, 1975, pp. 190-198.

APPENDIX A

STRAIN GAUGES

CALIBRATION CURVES

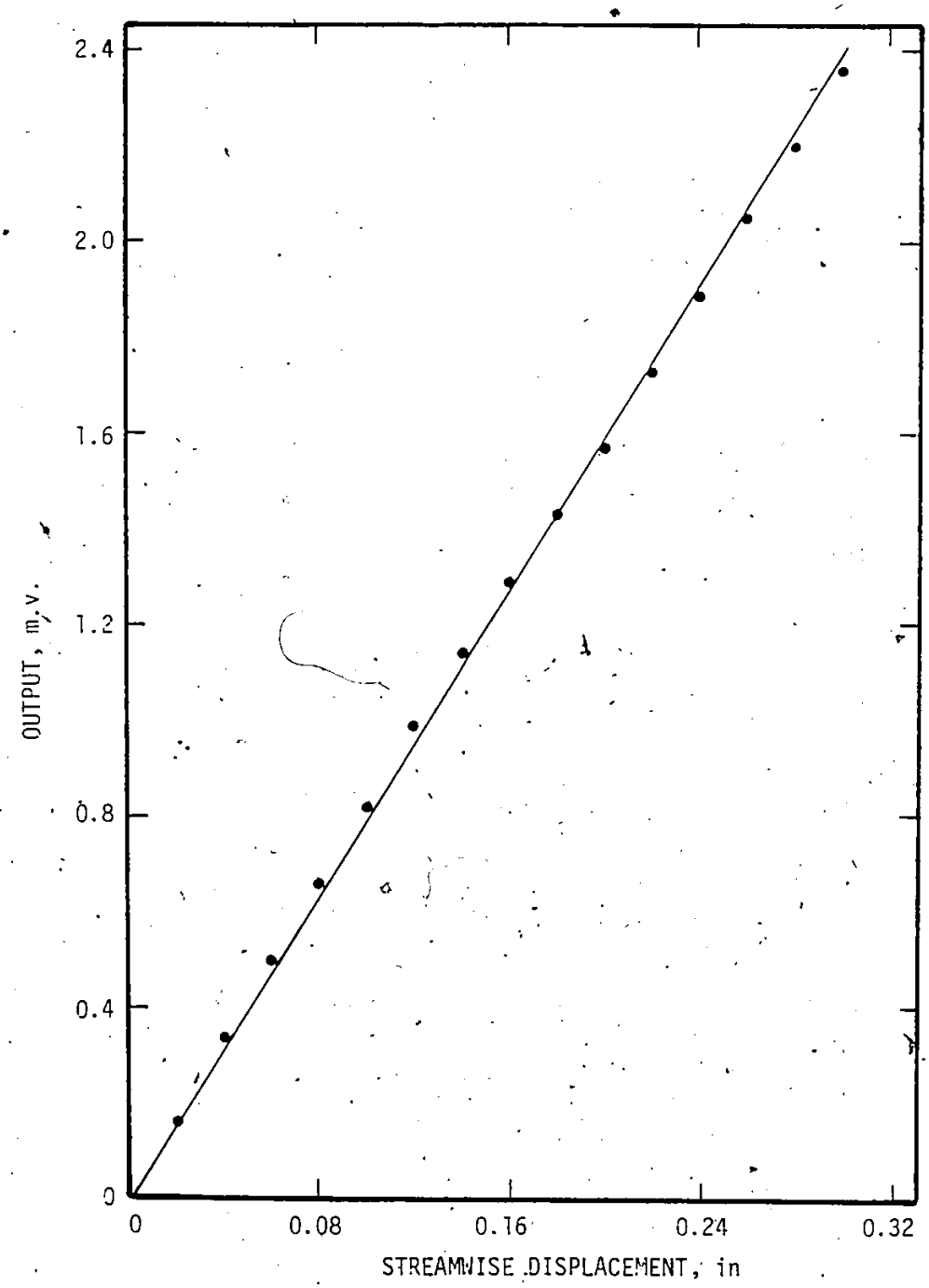

Figure A1 Calibration curve of a second row tube strain gauge in the streamwise direction

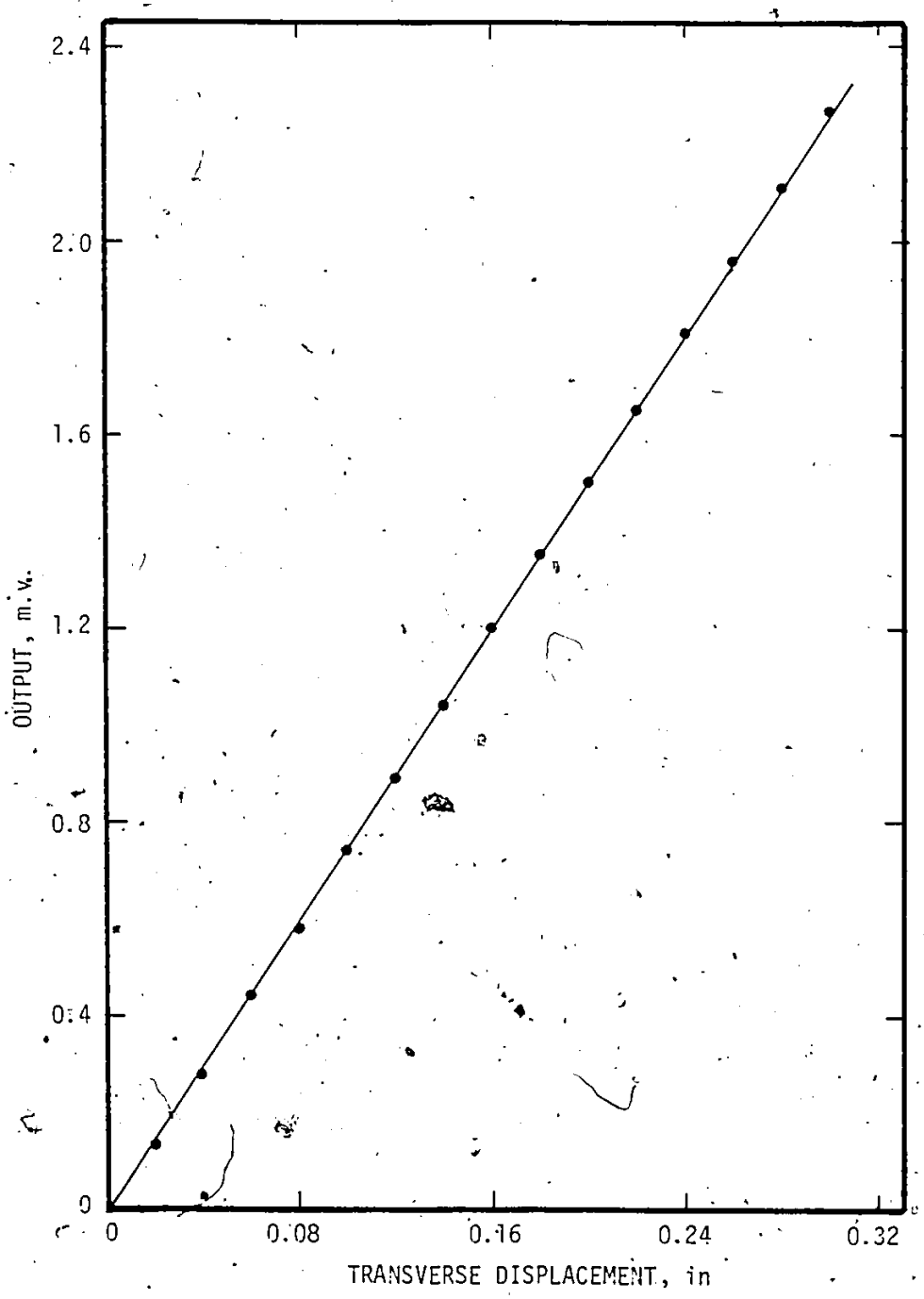

Figure A2 Calibration curve of a second row tube strain gauge in the transverse direction

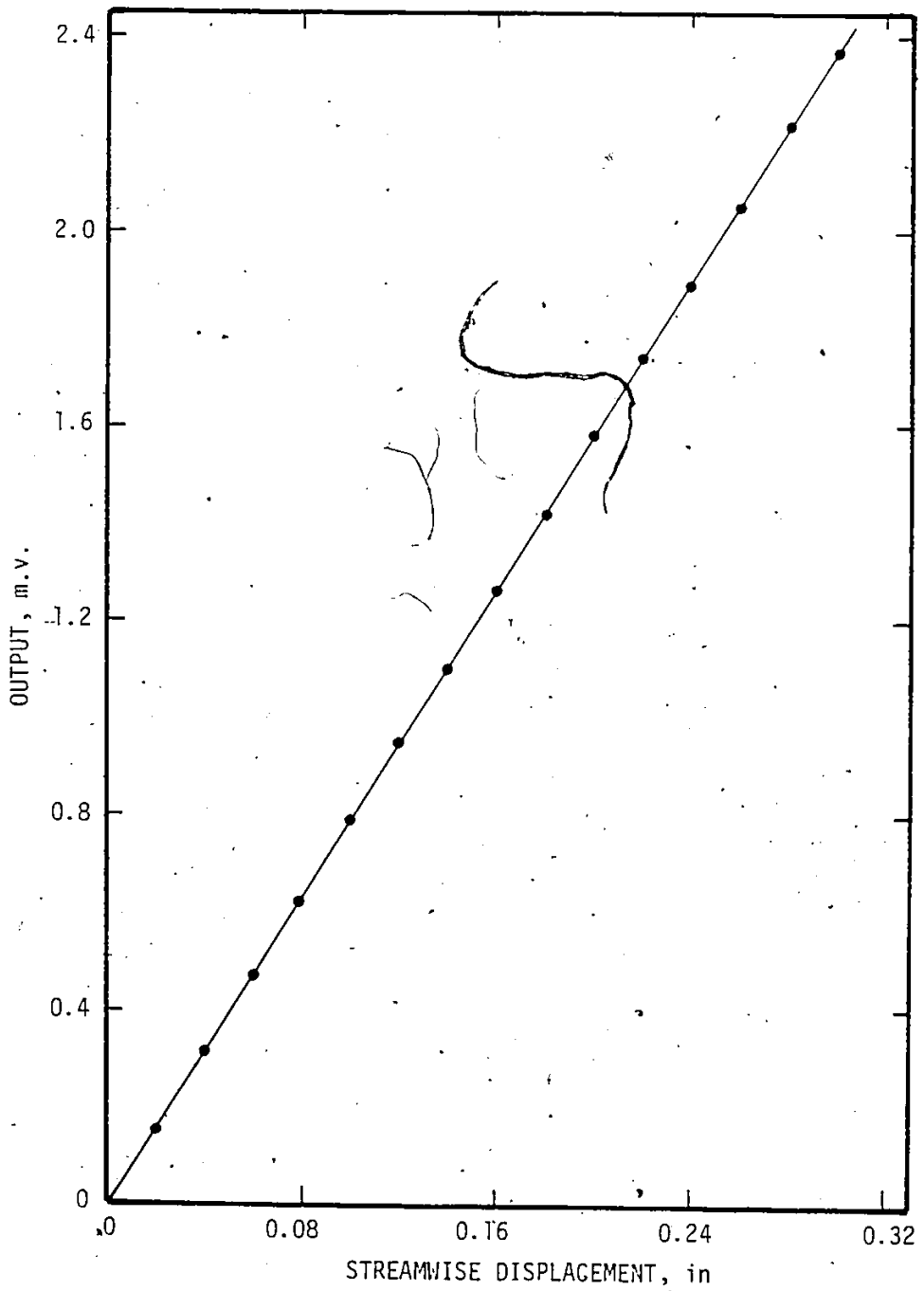

Figure A3 Calibration curve of a third row tube-strain gauge in the streamwise direction

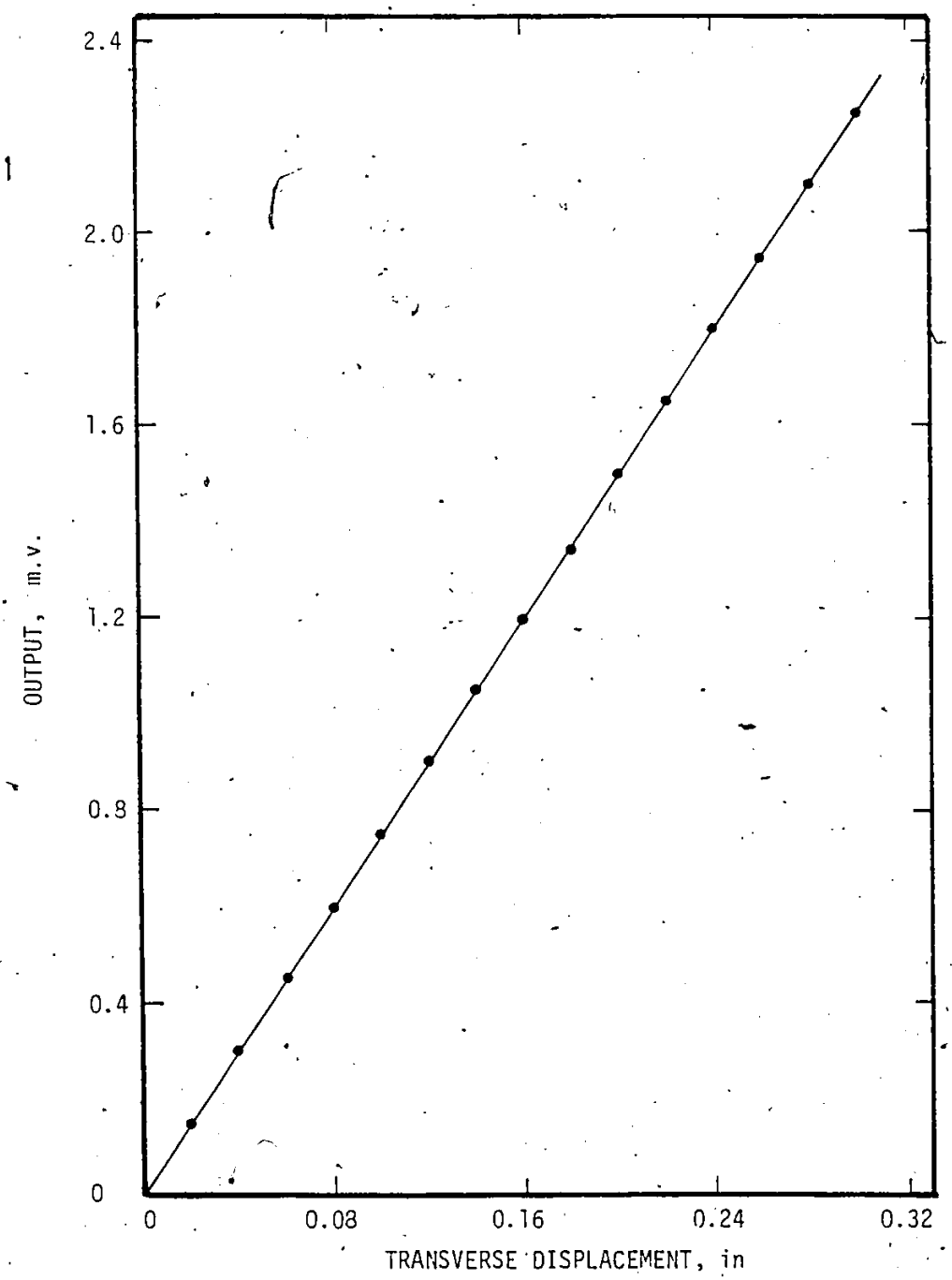

Figure A4 Calibration curve of a third row tube strain gauge in the transverse direction

APPENDIX B

THE PHOTOGRAPHIC METHOD FOR TAKING STILL PHOTOGRAPHS

Still photographs were taken using the Graflex camera and 4x5 Plus-X-Pan negative sheets. The following steps summarize the photographic method.

1. The camera is mounted above the test section on its stand and is securely bolted so that no movement occurs during the taking of pictures.
2. The light source (projector bulbs) must be exposed to a stream of cooling air before the lights are turned on. Failure to do so drastically shortens the life of the projector bulbs.
3. The image is focused as sharply as possible using the ground glass of the Graflex camera.
4. The film holder, loaded with the 4x5 sheets, is inserted in its place. The camera is now ready for taking photographs.
5. The SIXTOMAT electronic light meter is adjusted for film sensitivity by turning the film speed dial until the required ASA number appears opposite the indicating marks in the appropriate window.
6. With the light meter close to the camera and in the direction of camera view, push the diffusing sphere to the left or right as far as it will go.

7. Press the operating switch on the meter and turn the calculator ring until the circular reference window is totally green. Now, the shutter speed and aperture scales are set for the selection of a suitable exposure combination. (See Appendix C for further details).
8. It must be noted that no light meter entirely eliminates the need for personal judgement.

APPENDIX C

THE PHOTOGRAPHIC METHOD FOR TAKING CINE-FILMS

Cine-films were taken using LOCAM model 51 high speed camera and 16 mm Plus-X-negative film. The film loading procedure is outlined in the LOCAM instruction manual and must be followed very closely to avoid destroying the film and unwanted delays. Operating and focusing information are also included in the manual. Having completed the necessary measurements and observations of a tested tube bundle, the tube response behaviour is then studied in order to determine the flow velocities at which flow visualization might provide insights into the excitation mechanisms. These flow velocities are established in the test section and cine films, as well as still photographs, are taken of the developing flow patterns. An important factor to be considered at the outset is the length of the tracer particle streaks. These should not be too long or too short otherwise important features of the flow details will be lost. Knowing the mean flow velocity at the point of interest and the preferred streak length, the shutter speed can then be determined. Experience has shown that streak lengths between 6 mm and 12 mm are most instructive. The framing rate can be calculated from the relation

$$\frac{\text{Shutter opening in degrees}}{\text{frames/second} \times 360} = \text{shutter speed in seconds}$$

as given in the LOCAM instruction manual. The light meter reading will then give the aperture required for the chosen shutter speed.

In the actual process of taking films at a certain flow velocity, it is advisable to take films at the predetermined, slightly higher and slightly lower framing rates. The amount of trial and error required to produce quality flow visualization photographs reduces with experience and the development of better judgement. In the work reported in this thesis, the process was:

(a) with all nine illumination lights on, the tracer particle quantity in the flow was increased until the light meter index showed between 11.5 and 12.5.

(b) a film was taken at the selected shutter speed with additional films taken at those speeds required for apertures at least one full stop higher and lower than that indicated for the preferred shutter speed.